Advancing prostate cancer therapies through integrative multi-omics

Advancing prostate cancer therapies through integrative multi-omics

It's about time

Simon Linder

Advancing prostate cancer therapies through integrative multi-omics

It's about time

Simon Linder

Advancing prostate cancer therapies through integrative multi-omics
It's about time

Simon Linder

ISBN: 978-94-6483-062-0

About the cover: The cover of this thesis illustrates how small pieces – when properly arranged and combined – can come together to form something much bigger. The integrative multi-omics approaches described in this dissertation use exactly the same strategy to ultimately help us better understand how best to advance prostate cancer therapies.

Cover design and layout: © www.evelienjagtman.com
Printing: Ridderprint | www.ridderprint.nl

Advancing prostate cancer therapies through integrative multi-omics

It's about time

PROEFSCHRIFT

ter verkrijging van
de graad van doctor aan de Technische Universiteit Eindhoven,
op gezag van de rector magnificus prof. dr. S.K. Lenaerts,
voor een commissie aangewezen door het College voor Promoties,
in het openbaar te verdedigen op vrijdag 30 juni 2023 om 11:00 uur

door

Simon Linder

geboren te Ludwigshafen am Rhein,
Duitsland

Dit proefschrift is goedgekeurd door de promotoren en de samenstelling van de promotiecommissie is als volgt:

Voorzitter:	prof. dr. M. Merkx
Promotor:	prof. dr. W. Zwart
Copromotor:	dr. A.M. Bergman (Nederlands Kanker Instituut)
Promotiecommissieleden:	prof. dr. ir. L. Brunsveld
	prof. dr. S. Fröhling (University of Ulm, German Cancer Research Center, National Center for Tumor diseases)
	prof. dr. C. Bevan (Imperial College London)
	prof. dr. H. Verheul (Erasmus Medisch Centrum)
	prof. dr. J. Kind (Radboud Universiteit Nijmegen, Hubrecht Instituut)

Het onderzoek of ontwerp dat in dit thesis wordt beschreven is uitgevoerd in overeenstemming met de TU/e Gedragscode Wetenschapsbeoefening.

"The two most powerful warriors
are patience and time."

– Leo Tolstoy –

Table of contents

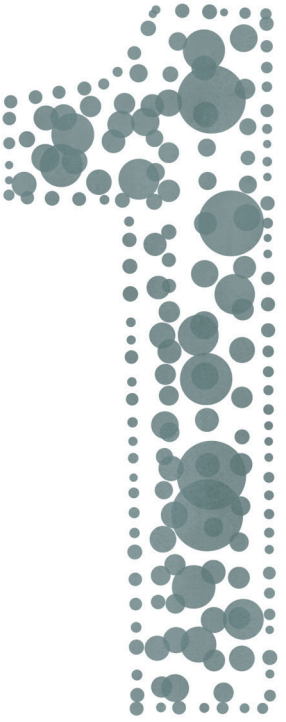

General introduction

Prostate cancer

Diagnosis and grading

Each year, more than 1.4 million men are diagnosed with prostate cancer. This makes prostate cancer the second most common cancer in men and, with 375,000 deaths annually, also one of the most common causes of cancer-related death[1]. At present, prostate cancer diagnosis is primarily based on histological assessment of tissue biopsies and determination of serum levels of prostate-specific antigen (PSA), but advanced imaging techniques, such as magnetic resonance imaging (MRI), are also being used to enhance diagnostic performance[2]. If prostate cancer is detected on biopsy, a so-called Gleason score is determined, which helps predict the prognosis of these patients[3]. The Gleason score is a histological assessment, which describes the differentiation status of the two most predominant cellular growth patterns in a biopsy, and for prostate cancer ranges from low-grade (International Society for Urological Pathology grade group 1, GG1 = Gleason ≤ 6) to intermediate-grade (GG2-3 = Gleason 7) to high-grade (GG4-5 = Gleason 8-10).

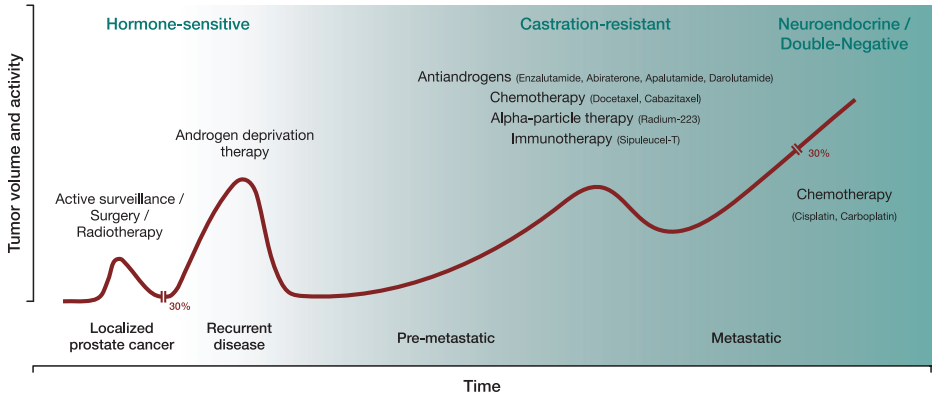

Figure 1: Natural history of prostate cancer and available therapeutic options. Most patients present with localized prostate cancer, which is treated with either active surveillance (low-grade tumors only), radical prostatectomy (surgery), or radiation therapy with curative intent. Approximately 30% of patients experience a biochemical relapse characterized by an increase in serum PSA levels, after which they are treated with chemical castration (ADT). Despite initial efficacy, tumors evolve into lethal castration-resistant disease that is treated with antiandrogens, chemotherapy, alpha-particle therapy, or immunotherapy. As a result of sustained AR-directed interventions, approximately 30% of castration-resistant tumors lose AR expression and evolve into very aggressive neuroendocrine (NE^+/AR^-) or double-negative (NE^-/AR^-) cancers for which platinum-based chemotherapeutic agents are the only therapeutic option.

Natural history and treatment options

Most patients present with organ-confined, localized disease whose risk of metastasis is assessed by Gleason score, serum PSA level, and tumor stage. Depending on the associated risk, patients can either be monitored without intervention through active surveillance (mostly low-grade GG1) or can potentially be cured through locoregional therapies, such as radical prostatectomy (surgical removal of the prostate) or radiotherapy[4] (**Fig. 1**). However, approximately 30% of these patients will experience a biochemical recurrence – a rise in serum PSA levels – which indicates prostate cancer relapse (**Fig. 1**). At this stage, patients can be treated with androgen deprivation therapy (ADT) which is the mainstay therapy ever since the direct critical connection between male sex hormones (androgens) and prostate cancer progression has first been described by Huggins and Hodges in 1941[5]. ADT aims at suppressing the biosynthesis of androgens in the testis in order to inactivate the androgen receptor (AR) – the key driver of prostate cancer development and progression[6]. Although initially very effective, resistance to ADT inevitably develops, and the disease progresses to metastatic castration-resistant prostate cancer (mCRPC) for which there is no cure (**Fig. 1**). Most mCRPC tumors acquire molecular features that allow them to activate AR signaling and proliferate even in an environment with very low circulating androgen levels[7,8]. Therefore, several highly effective AR-targeting antiandrogens (enzalutamide, abiraterone darolutamide, apalutamide) have been developed, which are widely used for the clinical management of mCRPC, but there are also non-AR-targeting therapies available, including chemotherapy (docetaxel, cabazitaxel), alpha-particle therapy (radium-223), immunotherapy (Sipuleucel-T), or combinations thereof – all of which are elaborately discussed in **Chapter 2**[9]. However, due to inter-patient heterogeneity, treatment responses to these lines of therapy vary between patients, and *de novo* or acquired resistance represent major medical challenges[10,11]. In addition to genetic alterations, lineage plasticity by epigenetic rewiring is a reported mechanism of resistance[12], leading to AR-independent forms of prostate cancer that develop as an adaptive response under the pressure of prolonged AR-targeted therapies (**Fig. 1**). Approximately 30% of mCRPC tumors escape their epithelial lineage confinement[13] and enter a highly plastic state, ultimately trans-differentiating into either neuroendocrine prostate cancer (NEPC; NE^+/AR^-) or double-negative prostate cancer (NE^-/AR^-). Although AR expression is eventually lost in these tumors, AR reprogramming and transcriptional rerouting in response to AR-targeted intervention – in combination with reprogramming of epigenetic regulators – have been found to play an important role in the transition to more lineage-plastic phenotypes[14-16]. Despite progress in the identification of molecular mechanisms underlying NEPC, such as genomic alterations[17-20], deregulation of epigenetic regulators[21-23], transcription factors[19,24-27], and other molecular signaling pathways[28], the survival rate of patients with NEPC remains very low, and the only

available therapeutic option is platinum-based chemotherapy[29]. This indicates that new therapeutic targets are urgently needed, not only for NEPC but for almost all prostate cancer stages, and the identification of targetable drivers that would prevent the transition to treatment-resistant disease after castration would be very attractive.

Androgen receptor

Androgen receptor signaling axis in prostate cancer

The androgen receptor (AR) is a nuclear receptor of the steroid hormone receptor subfamily that resides in the absence of ligands in the cytoplasm (**Fig. 2**), where it is stabilized by molecular chaperones such as heat-shock protein 90 (HSP90) and maintained in an inactive but high-affinity hormone-binding state[30,31]. Upon binding of androgens (**Fig. 2**), like testosterone or its more potent metabolite dihydrotestosterone (DHT), AR undergoes a series of conformational changes, leading to its dissociation from heat shock proteins and activation[32,33]. The activated receptor then homodimerizes and translocates to the nucleus (**Fig. 2**), where it binds to thousands of sites throughout the human genome at specific AR-response elements (AREs), which are primarily located in intronic or distal intergenic *cis*-regulatory elements – also known as enhancers[34,35]. AR binds to these elements with the help of pioneer factors such as FOXA1 and HOXB13, and recruits nuclear receptor cofactors (NRCs), like coactivators or corepressors[36,37]. Through long-range chromatin interactions in three-dimensional genomic space[38], these coregulators can control the expression of directly responsive target genes involved in various cellular processes, such as proliferation, survival, and stress response pathways like the unfolded protein response (UPR).

Androgen receptor cofactor repertoire

As shown in **Figure 2**, AR does not operate in isolation, but rather recruits a large spectrum of other transcription factors and NRCs. While some of these factors are critical for AR chromatin interactions others boost AR's transcriptional output. FOXA1 and HOXB13 are pioneer factors capable of remodeling compacted chromatin in part through recruiting histone acetyltransferases and other chromatin remodelers to render their target loci accessible to transcription factors such as AR[39-42]. *FOXA1* is among the most-frequently mutated genes in prostate cancer[17,43,44], which was reported to not only alter its pioneering function, but also perturb epithelial differentiation programs, and promote tumor progression[45,46]. *HOXB13* on the other hand, is not a frequent target of somatic mutations in prostate cancer, but a germline variant (G84E) has been identified, which is associated with a significantly increased risk of hereditary prostate cancer[47]. In addition to pioneer factors, AR also interacts with a plethora of

other proteins involved in various molecular processes[48], such as chromatin remodeling (SWI/SNF), transcriptional repression, and cell cycle, most of which are essential for AR-driven prostate cancer cell proliferation , and thus represent promising therapeutic targets[49].

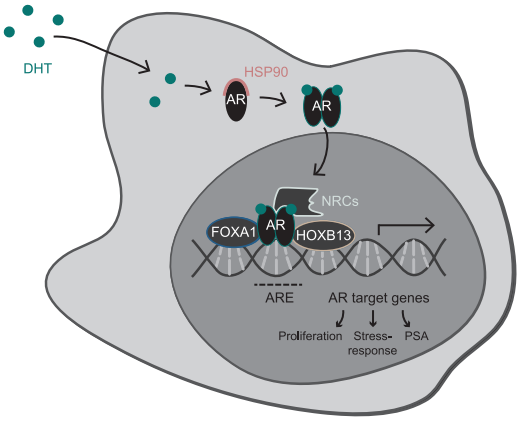

Figure 2: The androgen receptor signaling axis in prostate cancer. Upon dihydrotestosterone (DHT) binding, the AR dissociates from heat-shock protein 90 (HSP90), dimerizes and translocates to the nucleus, where it binds to AR-response elements (ARE) with the help of pioneer factors, such as FOXA1 and HOXB13, and recruits nuclear receptor coregulators (NRCs), coactivators or corepressors, to regulate transcription of directly responsive genes involved diverse biological processes, such as cell proliferation and stress-response. Also highlighted is the AR target gene prostate-specific antigen (PSA), a well-known biomarker for prostate cancer progression and treatment response.

Androgen receptor cistrome

The cistrome refers to the genome-wide landscape of transcription factor binding sites or histone modifications, which basically maps all genomic locations of *cis*-acting targets (*cis*-regulatory elements such as enhancers or promoters) of *trans*-acting factors (such as transcription factors). AR cistromic regulation is tightly regulated in a cell/tissue type- and context-dependent manner, leading to the expression of distinct AR-driven transcriptional programs implicated in many different biological processes[35]. In normal prostate epithelial cells (**Fig. 3A**), AR primarily binds to genomic regions containing canonical AR binding motifs to regulate genes that induce terminal differentiation and suppress growth[50]. However, in prostate cancer (**Fig. 3B**), the AR pathway stimulates cell proliferation and survival, which is based on massive cistromic reprogramming of AR during tumorigenesis. This cistromic plasticity away from normal AR binding sites (N-ARBS) toward primary tumor-specific AR binding sites (T-ARBS) is in part facilitated through overexpression of AR pioneer factors FOXA1 and HOXB13, which can

reprogram AR binding to genomic regions enriched for forkhead and homeodomain motifs[51]. During metastatic progression, the AR binding landscape changes once more (**Fig. 3C**). In contrast to T-ARBS, reprogrammed AR sites in metastatic disease (Met-ARBS) are not created *de novo*, but rather prepopulated by FOXA1 and HOXB13 during prostate organogenesis and now commissioned by AR during metastatic outgrowth, demonstrating how metastatic prostate cancer can reactivate developmental epigenomic programs[52].

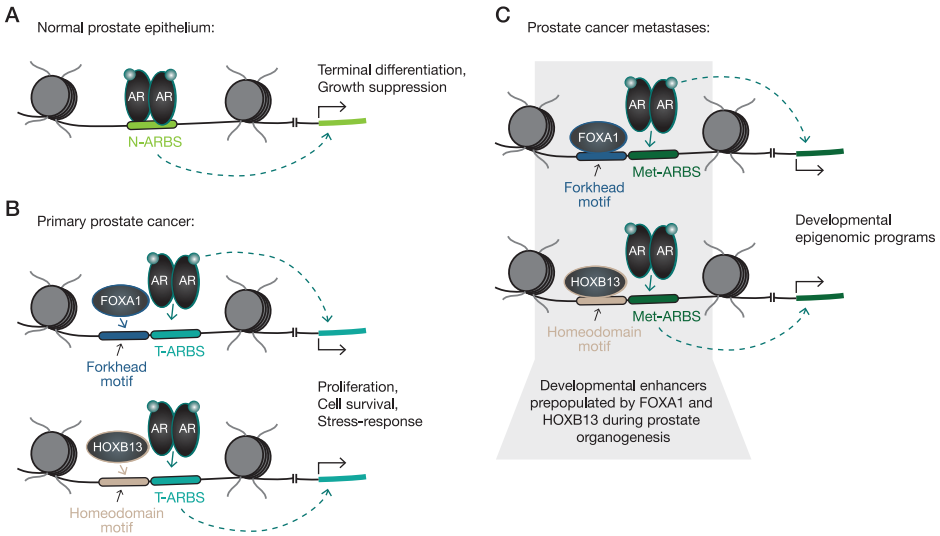

Figure 3: Androgen receptor cistromic reprogramming. (**A**) AR binding sites enriched in normal prostate epithelium (N-ARBS) contain canonical AR binding motifs and regulate genes that induce terminal differentiation and suppress growth. (**B**) Overexpression of AR pioneer factors FOXA1 and HOXB13 during tumorigenesis, reprograms the AR cistrome toward primary tumor-specific AR binding sites (T-ARBS), which, in contrast to N-ARBS, stimulate both cell proliferation as well as cell survival, for example by activating stress-response pathways. (**C**) During metastatic progression AR occupies metastasis-specific AR binding sites (Met-ARBS) that are prepopulated by FOXA1 and HOXB13 during prostate organogenesis to reactivate developmental epigenomic programs.

Transcription factor charting through integrative multi-omics

The human body is composed of several trillion cells[53], all carrying identical genomic information that encodes ~25,000 different protein-coding genes[54]; yet it is made up of a variety of different cell types and lineages with diverse biological functions. This highlights the importance of transcription factors and epigenetic modifiers in assigning

distinct cell identities that lead to organ development and function by temporally dictating and regulating tissue- and context-dependent gene expression programs, Transcription factors (such as AR) can achieve this by binding to regulatory elements located primarily in the non-coding genome, which makes up 98% of the DNA in the mammalian nucleus (only 2% of all human DNA is protein-coding), and thus mediating long-range interactions between such enhancer elements and the promoter regions of their respective target genes[55]. Therefore, genome-wide transcription factor profiling through chromatin immunoprecipitation followed by massive parallel sequencing (ChIP-seq) is widely used to identify the precise genomic locations where transcription factors bind the DNA[56] (**Fig. 4A**). Although very informative, chromatin interaction of transcription factors alone fails to describe how the activity of *cis*-regulatory elements is modulated upon binding and how this affects gene regulation. Consequently, integrating ChIP-seq datastreams with one or more additional omics approaches helps to shed light on the mechanism behind differential chromatin occupancy and its downstream effects. Integration of transcription factor ChIP-seq data with epigenomic profiles of histone modifications – which can be either active (such as H3K27ac, $H3K4me_3$) or repressive (such as $H3K27me_3$) – allows investigation of possible effects of transcription factor binding on the epigenetic environment and chromatin state of regulatory element and provides clues to enhancer activity[57,58] (**Fig. 4B**). In addition, massive parallel reporter assays for enhancer activity (such as self-transcribing active regulatory region sequencing[59], STARR-seq) enable to functionally assess the ability of certain DNA sequences to enhance transcriptional output (**Fig. 4C**). AR STARR-seq experiments in androgen-stimulated prostate cancer cells, for instance, have shown that the vast majority of AR binding sites are not inducible by androgens but rather are constitutively inactive, and thus have increased our understanding of why there are 10-100 times more AR binding sites throughout the genome than differentially expressed genes[60]. Furthermore, combining cistromic data with copy-number variation sequencing (CNV-seq) helps to untangle whether differential binding events are due to transcription factor reprogramming or rather based on copy-number alterations (**Fig. 4D**). This is particularly useful when analyzing samples that have been treated for an extended period of time, which may have resulted in drug-induced clonal expansion. Most importantly, ChIP-seq experiments are usually integrated with gene expression (RNA-seq) data to study how transcription factor binding to regulatory elements influences the expression of downstream responsive genes (**Fig. 4E**). Therefore, distal binding sites need to be coupled to their respective target genes, which was historically done using a genomic window of 20-50 kb[61,62]. This simple approach is, however, not necessarily well-suited for enhancer-binding transcription factors, since most enhancer-promoter interactions go far beyond a linear distance of 20-50 kb, as has been shown for a developmental enhancer of the AR gene (650 kb) in prostate cancer

cells[35,63]. Recent advances in chromosome conformation detection methods, such as Hi-C or HiChIP, allow more robust and precise identification of enhancer-promoter pairs without restriction to a maximum linear distance[64]. Finally, by combining ChIP-seq experiments with orthogonal proteomic methods such as rapid immunoprecipitation mass spectrometry of endogenous proteins (RIME), context-dependent changes in the composition of the transcriptional complex can be identified (**Fig. 4F**), allowing simultaneous profiling of the cistrome and interactome of a given transcription factor, and thus identification of crucial coregulators which may serve as therapeutic targets[48,65].

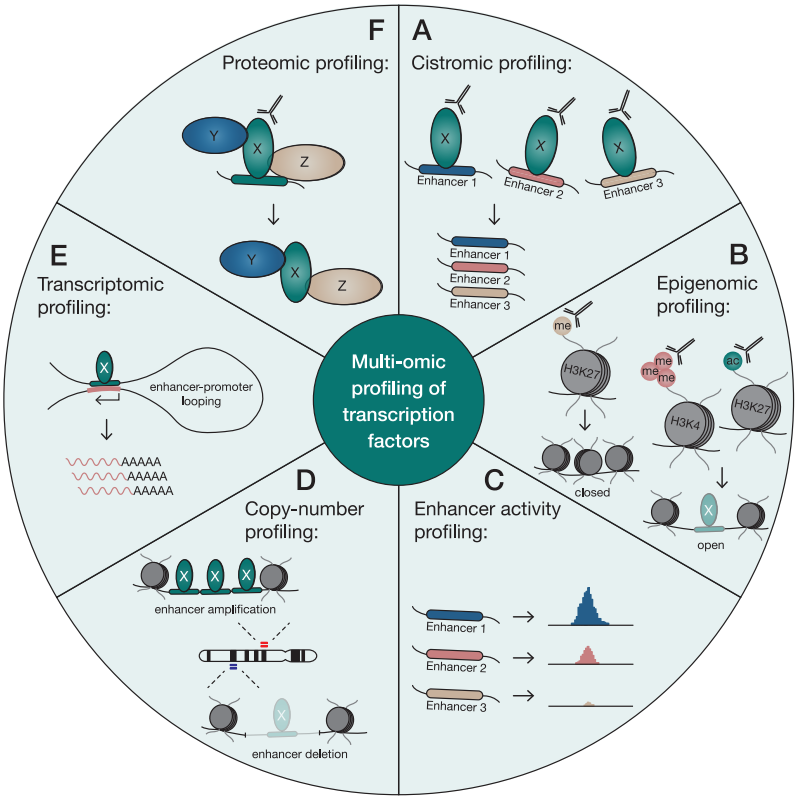

Figure 4: Integrative multi-omic profiling of transcription factors. Integrating transcription factor chromatin immunoprecipitation sequencing (ChIP-seq) experiments (**A**) with epigenomic profiling (**B**) by histone mark ChIP-seq, enhancer activity profiling (**C**) by massive parallel reporter assays, copy-number profiling (**D**) by copy-number sequencing (CNV-seq), transcriptomic profiling (**E**) by RNA-seq, and/or proteomic profiling (**F**) by rapid immunoprecipitation mass spectrometry of endogenous proteins (RIME), allows for much more insightful characterizations of the gene regulatory potential of a transcription factor and its downstream effects on enhancer activity, chromatin state, and target gene expression.

Thesis outline

The scope of this thesis is to improve our current understanding of hormonal signaling in prostate cancer, and to gain more insights into the cellular adaptation mechanisms that lead to acquired hormone therapy resistance using integrative multi-omics approaches.

In **Chapter 2**, the clinical history of enzalutamide – one of the most frequently used AR-targeting agents – is reviewed, providing a concise overview of its preclinical development, use and efficacy in the treatment of advanced prostate cancer. Furthermore, we describe translational research on biomarkers of enzalutamide response, highlight potential new combination therapies, and conclude with the clear need for biomarkers for optimal treatment sequencing and new therapeutic targets in the enzalutamide-resistant setting.

Understanding how prostate cancers adapt to AR-targeted interventions is critical for identifying novel drug targets to improve the clinical management of treatment-resistant disease. Therefore, in **Chapter 3**, we performed integrative multi-omics analyses on tissues isolated before and after three months of AR-targeted enzalutamide monotherapy from patients with high-risk prostate cancer enrolled in a neoadjuvant clinical trial. These analyses included tissue ChIP-seq for our drug target AR, pioneer factor FOXA1, and the active histone modification H3K27ac, which we subsequently integrated with CNV-seq, STARR-seq, RNA-seq, and tissue microarray immunohistochemistry data generated from the same tumor specimens. This revealed an enzalutamide-induced epigenomic plasticity toward prosurvival signaling and uncovered the circadian regulator ARNTL as an acquired vulnerability after AR inhibition, presenting a novel lead for therapeutic development.

In **Chapter 4**, we set out to characterize the AR chromatin binding landscape and associated transcriptional programs in a specific subset of low-risk grade group 1 (GG1) prostate cancer with a pathological Gleason score 6 to answer the long-standing question in the field of whether these lesions are truly cancerous or rather benign, given their overall negligible risk to metastasize. We show that the gene regulatory potential of AR in low-grade GG1 lesions is very similar to higher-grade tumors and distinctly different from normal prostate epithelium, which positions these lesions as *bona fide* cancers from an epigenetic perspective.

Previously, we identified a prognostic 9-gene classifier, which can stratify prostate cancer patients on outcome[62]. In **Chapter 5**, we further characterized the prognostic value and biological function of one of these 9 genes: XBP1; a key player in the unfolded

protein response (UPR) pathway. In primary prostate cancer, low expression of XBP1 was consistently associated with biochemical recurrence in five independent cohorts. Through integrative cistromic and transcriptomic analyses, we could demonstrate that AR activation triggers UPR signaling through the ERN1/XBP1 axis leading to elevated XBP1 transcriptional activity, which not only results in expression of UPR genes but also functionally drives part of the AR transcriptional program.

Finally, **Chapter 6** provides a general discussion of the work presented in this thesis, with a clear focus on how well-designed multi-omics studies can help address the dilemma of drug resistance in prostate cancer and what outstanding questions remain to be addressed.

References

1 Sung, H. *et al.* Global Cancer Statistics 2020: GLOBOCAN Estimates of Incidence and Mortality Worldwide for 36 Cancers in 185 Countries. *CA Cancer J Clin* **71**, 209-249 (2021). https://doi.org:10.3322/caac.21660

2 Litwin, M. S. & Tan, H. J. The Diagnosis and Treatment of Prostate Cancer: A Review. *JAMA* **317**, 2532-2542 (2017). https://doi.org:10.1001/jama.2017.7248

3 Gleason, D. F. & Mellinger, G. T. Prediction of prognosis for prostatic adenocarcinoma by combined histological grading and clinical staging. *J Urol* **111**, 58-64 (1974). https://doi.org:10.1016/s0022-5347(17)59889-4

4 Mottet, N. *et al.* EAU-EANM-ESTRO-ESUR-SIOG Guidelines on Prostate Cancer-2020 Update. Part 1: Screening, Diagnosis, and Local Treatment with Curative Intent. *Eur Urol* **79**, 243-262 (2021). https://doi.org:10.1016/j.eururo.2020.09.042

5 Huggins, C. & Hodges, C. V. Studies on prostatic cancer. I. The effect of castration, of estrogen and androgen injection on serum phosphatases in metastatic carcinoma of the prostate. *CA Cancer J Clin* **22**, 232-240 (1972). https://doi.org:10.3322/canjclin.22.4.232

6 Harris, W. P., Mostaghel, E. A., Nelson, P. S. & Montgomery, B. Androgen deprivation therapy: progress in understanding mechanisms of resistance and optimizing androgen depletion. *Nat Clin Pract Urol* **6**, 76-85 (2009). https://doi.org:10.1038/ncpuro1296

7 Karantanos, T., Corn, P. G. & Thompson, T. C. Prostate cancer progression after androgen deprivation therapy: mechanisms of castrate resistance and novel therapeutic approaches. *Oncogene* **32**, 5501-5511 (2013). https://doi.org:10.1038/onc.2013.206

8 Robinson, D. *et al.* Integrative clinical genomics of advanced prostate cancer. *Cell* **161**, 1215-1228 (2015). https://doi.org:10.1016/j.cell.2015.05.001

9 Linder, S., van der Poel, H. G., Bergman, A. M., Zwart, W. & Prekovic, S. Enzalutamide therapy for advanced prostate cancer: efficacy, resistance and beyond. *Endocr Relat Cancer* **26**, R31-R52 (2018). https://doi.org:10.1530/ERC-18-0289

10 Prekovic, S. *et al.* Molecular underpinnings of enzalutamide resistance. *Endocr Relat Cancer* **25**, R545-R557 (2018). https://doi.org:10.1530/ERC-17-0136

11 Seruga, B., Ocana, A. & Tannock, I. F. Drug resistance in metastatic castration-resistant prostate cancer. *Nat Rev Clin Oncol* **8**, 12-23 (2011). https://doi.org:10.1038/nrclinonc.2010.136

12 Zou, M. *et al.* Transdifferentiation as a Mechanism of Treatment Resistance in a Mouse Model of Castration-Resistant Prostate Cancer. *Cancer Discov* **7**, 736-749 (2017). https://doi.org:10.1158/2159-8290.CD-16-1174

13 Bluemn, E. G. *et al.* Androgen Receptor Pathway-Independent Prostate Cancer Is Sustained through FGF Signaling. *Cancer Cell* **32**, 474-489 e476 (2017). https://doi.org:10.1016/j.ccell.2017.09.003

14 Davies, A. *et al.* An androgen receptor switch underlies lineage infidelity in treatment-resistant prostate cancer. *Nat Cell Biol* **23**, 1023-1034 (2021). https://doi.org:10.1038/s41556-021-00743-5

15 Su, W. *et al.* The Polycomb Repressor Complex 1 Drives Double-Negative Prostate Cancer Metastasis by Coordinating Stemness and Immune Suppression. *Cancer Cell* **36**, 139-155 e110 (2019). https://doi.org:10.1016/j.ccell.2019.06.009

16 Eickhoff, N., Bergman, A. M. & Zwart, W. Homing in on a Moving Target: Androgen Receptor Cistromic Plasticity in Prostate Cancer. *Endocrinology* **163** (2022). https://doi.org:10.1210/endocr/bqac153

17 Abida, W. *et al.* Genomic correlates of clinical outcome in advanced prostate cancer. *Proc Natl Acad Sci U S A* **116**, 11428-11436 (2019). https://doi.org:10.1073/pnas.1902651116

18 Ku, S. Y. *et al.* Rb1 and Trp53 cooperate to suppress prostate cancer lineage plasticity, metastasis, and antiandrogen resistance. *Science* **355**, 78-83 (2017). https://doi.org:10.1126/science.aah4199

19 Mu, P. *et al.* SOX2 promotes lineage plasticity and antiandrogen resistance in TP53- and RB1-deficient prostate cancer. *Science* **355**, 84-88 (2017). https://doi.org:10.1126/science.aah4307

20 Beltran, H. *et al.* Divergent clonal evolution of castration-resistant neuroendocrine prostate cancer. *Nat Med* **22**, 298-305 (2016). https://doi.org:10.1038/nm.4045

21 Clermont, P. L. *et al.* Polycomb-mediated silencing in neuroendocrine prostate cancer. *Clin Epigenetics* **7**, 40 (2015). https://doi.org:10.1186/s13148-015-0074-4

22 Cyrta, J. *et al.* Role of specialized composition of SWI/SNF complexes in prostate cancer lineage plasticity. *Nat Commun* **11**, 5549 (2020). https://doi.org:10.1038/s41467-020-19328-1

23 Dardenne, E. *et al.* N-Myc Induces an EZH2-Mediated Transcriptional Program Driving Neuroendocrine Prostate Cancer. *Cancer Cell* **30**, 563-577 (2016). https://doi.org:10.1016/j.ccell.2016.09.005

24 Bishop, J. L. *et al.* The Master Neural Transcription Factor BRN2 Is an Androgen Receptor-Suppressed Driver of Neuroendocrine Differentiation in Prostate Cancer. *Cancer Discov* **7**, 54-71 (2017). https://doi.org:10.1158/2159-8290.CD-15-1263

25 Berger, A. *et al.* N-Myc-mediated epigenetic reprogramming drives lineage plasticity in advanced prostate cancer. *J Clin Invest* **129**, 3924-3940 (2019). https://doi.org:10.1172/JCI127961

26 Kim, S. *et al.* PEG10 is associated with treatment-induced neuroendocrine prostate cancer. *J Mol Endocrinol* **63**, 39-49 (2019). https://doi.org:10.1530/JME-18-0226

27 Rotinen, M. *et al.* ONECUT2 is a targetable master regulator of lethal prostate cancer that suppresses the androgen axis. *Nat Med* **24**, 1887-1898 (2018). https://doi.org:10.1038/s41591-018-0241-1

28 Beltran, H. *et al.* Molecular characterization of neuroendocrine prostate cancer and identification of new drug targets. *Cancer Discov* **1**, 487-495 (2011). https://doi.org:10.1158/2159-8290.CD-11-0130

29 Aparicio, A. M. *et al.* Platinum-based chemotherapy for variant castrate-resistant prostate cancer. *Clin Cancer Res* **19**, 3621-3630 (2013). https://doi.org:10.1158/1078-0432.CCR-12-3791

30 Fang, Y., Fliss, A. E., Robins, D. M. & Caplan, A. J. Hsp90 regulates androgen receptor hormone binding affinity in vivo. *J Biol Chem* **271**, 28697-28702 (1996). https://doi.org:10.1074/jbc.271.45.28697

31 Echeverria, P. C. & Picard, D. Molecular chaperones, essential partners of steroid hormone receptors for activity and mobility. *Biochim Biophys Acta* **1803**, 641-649 (2010). https://doi.org:10.1016/j.bbamcr.2009.11.012

32 Brinkmann, A. O. *et al.* Mechanisms of androgen receptor activation and function. *J Steroid Biochem Mol Biol* **69**, 307-313 (1999). https://doi.org:10.1016/s0960-0760(99)00049-7

33 Gao, W., Bohl, C. E. & Dalton, J. T. Chemistry and structural biology of androgen receptor. *Chem Rev* **105**, 3352-3370 (2005). https://doi.org:10.1021/cr020456u

34 Wang, Q. *et al.* Androgen receptor regulates a distinct transcription program in androgen-independent prostate cancer. *Cell* **138**, 245-256 (2009). https://doi.org:10.1016/j.cell.2009.04.056

35 Stelloo, S., Bergman, A. M. & Zwart, W. Androgen receptor enhancer usage and the chromatin regulatory landscape in human prostate cancers. *Endocr Relat Cancer* **26**, R267-R285 (2019). https://doi.org:10.1530/ERC-19-0032

36 Heinlein, C. A. & Chang, C. Androgen receptor (AR) coregulators: an overview. *Endocr Rev* **23**, 175-200 (2002). https://doi.org:10.1210/edrv.23.2.0460

37 Shang, Y., Myers, M. & Brown, M. Formation of the androgen receptor transcription complex. *Mol Cell* **9**, 601-610 (2002). https://doi.org:10.1016/s1097-2765(02)00471-9

38 Zhang, Z. *et al.* An AR-ERG transcriptional signature defined by long-range chromatin interactomes in prostate cancer cells. *Genome Res* **29**, 223-235 (2019). https://doi.org:10.1101/gr.230243.117

39 Hankey, W., Chen, Z. & Wang, Q. Shaping Chromatin States in Prostate Cancer by Pioneer Transcription Factors. *Cancer Res* **80**, 2427-2436 (2020). https://doi.org:10.1158/0008-5472.CAN-19-3447

40 Cirillo, L. A. *et al.* Opening of compacted chromatin by early developmental transcription factors HNF3 (FoxA) and GATA-4. *Mol Cell* **9**, 279-289 (2002). https://doi.org:10.1016/s1097-2765(02)00459-8

41 Lupien, M. *et al.* FoxA1 translates epigenetic signatures into enhancer-driven lineage-specific transcription. *Cell* **132**, 958-970 (2008). https://doi.org:10.1016/j.cell.2008.01.018

42 Sahu, B. *et al.* Dual role of FoxA1 in androgen receptor binding to chromatin, androgen signalling and prostate cancer. *EMBO J* **30**, 3962-3976 (2011). https://doi.org:10.1038/emboj.2011.328

43 Barbieri, C. E. *et al.* Exome sequencing identifies recurrent SPOP, FOXA1 and MED12 mutations in prostate cancer. *Nat Genet* **44**, 685-689 (2012). https://doi.org:10.1038/ng.2279

44 Cancer Genome Atlas Research, N. The Molecular Taxonomy of Primary Prostate Cancer. *Cell* **163**, 1011-1025 (2015). https://doi.org:10.1016/j.cell.2015.10.025

45 Adams, E. J. *et al.* FOXA1 mutations alter pioneering activity, differentiation and prostate cancer phenotypes. *Nature* **571**, 408-412 (2019). https://doi.org:10.1038/s41586-019-1318-9

46 Parolia, A. *et al.* Distinct structural classes of activating FOXA1 alterations in advanced prostate cancer. *Nature* **571**, 413-418 (2019). https://doi.org:10.1038/s41586-019-1347-4

47 Ewing, C. M. *et al.* Germline mutations in HOXB13 and prostate-cancer risk. *N Engl J Med* **366**, 141-149 (2012). https://doi.org:10.1056/NEJMoa1110000

48 Stelloo, S. *et al.* Endogenous androgen receptor proteomic profiling reveals genomic subcomplex involved in prostate tumorigenesis. *Oncogene* **37**, 313-322 (2018). https://doi.org:10.1038/onc.2017.330

49 Xiao, L. *et al.* Targeting SWI/SNF ATPases in enhancer-addicted prostate cancer. *Nature* **601**, 434-439 (2022). https://doi.org:10.1038/s41586-021-04246-z

50 Isaacs, J. T. Resolving the Coffey Paradox: what does the androgen receptor do in normal vs. malignant prostate epithelial cells? *Am J Clin Exp Urol* **6**, 55-61 (2018).

51 Pomerantz, M. M. *et al.* The androgen receptor cistrome is extensively reprogrammed in human prostate tumorigenesis. *Nat Genet* **47**, 1346-1351 (2015). https://doi.org:10.1038/ng.3419

52 Pomerantz, M. M. *et al.* Prostate cancer reactivates developmental epigenomic programs during metastatic progression. *Nat Genet* **52**, 790-799 (2020). https://doi.org:10.1038/s41588-020-0664-8

53 Bianconi, E. *et al.* An estimation of the number of cells in the human body. *Ann Hum Biol* **40**, 463-471 (2013). https://doi.org:10.3109/03014460.2013.807878

54 International Human Genome Sequencing, C. Finishing the euchromatic sequence of the human genome. *Nature* **431**, 931-945 (2004). https://doi.org:10.1038/nature03001

55 Palstra, R. J. & Grosveld, F. Transcription factor binding at enhancers: shaping a genomic regulatory landscape in flux. *Front Genet* **3**, 195 (2012). https://doi.org:10.3389/fgene.2012.00195

56 Mundade, R., Ozer, H. G., Wei, H., Prabhu, L. & Lu, T. Role of ChIP-seq in the discovery of transcription factor binding sites, differential gene regulation mechanism, epigenetic marks and beyond. *Cell Cycle* **13**, 2847-2852 (2014). https://doi.org:10.4161/15384101.2014.949201

57 Kron, K. J. *et al.* TMPRSS2-ERG fusion co-opts master transcription factors and activates NOTCH signaling in primary prostate cancer. *Nat Genet* **49**, 1336-1345 (2017). https://doi.org:10.1038/ng.3930

58 Stelloo, S. *et al.* Integrative epigenetic taxonomy of primary prostate cancer. *Nat Commun* **9**, 4900 (2018). https://doi.org:10.1038/s41467-018-07270-2

59 Arnold, C. D. *et al.* Genome-wide quantitative enhancer activity maps identified by STARR-seq. *Science* **339**, 1074-1077 (2013). https://doi.org:10.1126/science.1232542

60 Huang, C. F. *et al.* Functional mapping of androgen receptor enhancer activity. *Genome Biol* **22**, 149 (2021). https://doi.org:10.1186/s13059-021-02339-6

61 Sharma, N. L. *et al.* The androgen receptor induces a distinct transcriptional program in castration-resistant prostate cancer in man. *Cancer Cell* **23**, 35-47 (2013). https://doi.org:10.1016/j.ccr.2012.11.010

62 Stelloo, S. *et al.* Androgen receptor profiling predicts prostate cancer outcome. *EMBO Mol Med* **7**, 1450-1464 (2015). https://doi.org:10.15252/emmm.201505424

63 Takeda, D. Y. *et al.* A Somatically Acquired Enhancer of the Androgen Receptor Is a Noncoding Driver in Advanced Prostate Cancer. *Cell* **174**, 422-432 e413 (2018). https://doi.org:10.1016/j.cell.2018.05.037

64 Giambartolomei, C. *et al.* H3K27ac HiChIP in prostate cell lines identifies risk genes for prostate cancer susceptibility. *Am J Hum Genet* **108**, 2284-2300 (2021). https://doi.org:10.1016/j.ajhg.2021.11.007

65 Mohammed, H. *et al.* Rapid immunoprecipitation mass spectrometry of endogenous proteins (RIME) for analysis of chromatin complexes. *Nat Protoc* **11**, 316-326 (2016). https://doi.org:10.1038/nprot.2016.020

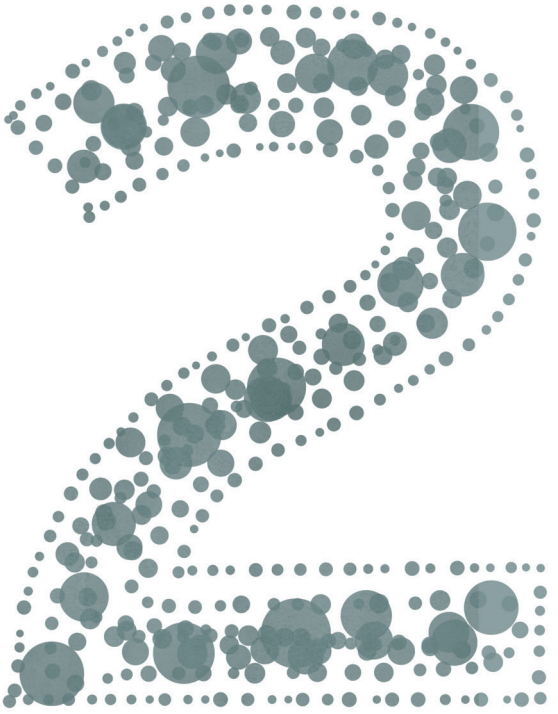

REVIEW

Enzalutamide therapy for advanced prostate cancer: efficacy, resistance and beyond

Simon Linder, Henk van der Poel, Andries M. Bergman, Wilbert Zwart, and Stefan Prekovic

Adapted from *Endocrine-Related Cancer* 26, R31–R52 (2019).

Abstract

The androgen receptor drives the growth of metastatic castration-resistant prostate cancer. This has led to the development of multiple novel drugs targeting this hormone-regulated transcription factor, such as enzalutamide – a potent androgen receptor antagonist. Despite the plethora of possible treatment options, the absolute survival benefit of each treatment separately is limited to a few months. Therefore, current research efforts are directed to determine the optimal sequence of therapies, discover novel drugs effective in metastatic castration-resistant prostate cancer and define patient subpopulations that ultimately benefit from these treatments. Molecular studies provide evidence on which pathways mediate treatment resistance and may lead to improved treatment for metastatic castration-resistant prostate cancer. This review provides, firstly a concise overview of the clinical development, use and effectiveness of enzalutamide in the treatment of advanced prostate cancer, secondly it describes translational research addressing enzalutamide response vs resistance and lastly highlights novel potential treatment strategies in the enzalutamide-resistant setting.

Introduction

Ever since the discovery that prostate cancer (PCa) growth after androgen deprivation therapy (ADT) remains dependent on androgen receptor (AR) signaling, researchers have been looking for new effective ways to block the action of this hormone-dependent transcription factor[1-3]. Upon stimulation with androgens, the AR dissociates from its molecular chaperones and translocates to the nucleus, where it binds to thousands of sites throughout the human genome to regulate transcription of directly responsive genes, including pro-mitotic genes involved in tumor cell proliferation[4-6] (**Fig. 1A**). Inhibiting androgen signaling through ADT initially results in tumor regression in the vast majority of cases, but inevitably the tumor cells adapt to low androgen levels, leading to disease progression which is known as castration-resistance[7-9]. Potent antiandrogens, that either target the AR directly through physical competition with the receptor's natural ligand dihydrotestosterone (DHT) or indirectly via inhibition of androgen biosynthesis, are among the treatment options for metastatic castration-resistant prostate cancer (mCRPC)[10]. At the moment, enzalutamide (MDV-3100) is the most-frequently prescribed compound for treatment of mCRPC [11]. This drug belongs to the class of direct androgen receptor inhibitors and tackles the AR pathway at multiple nodes: by preventing ligand binding, by blocking AR nuclear translocation and by inhibiting DNA transactivation; ultimately abrogating the expression of androgen-responsive genes[1,12] (**Fig. 1B**). The multiple stage actions of enzalutamide on AR signaling are considered the main reason for its superior clinical activity over other direct AR inhibitors, such as flutamide, bicalutamide and nilutamide[13]. However, due to inter-patient heterogeneity of PCa, which is widely recognized as a major drawback for therapy efficacy, treatment responses to enzalutamide vary between patients[14]. Whereas some patients do not have a substantial clinical benefit from enzalutamide therapy, others who do benefit, start progressing after a certain period of time, which is also dependent on therapy sequencing[2,15,16].

This review, of which the content is illustrated in **Figure 2**, will firstly provide a comprehensive insight into the use of enzalutamide in the treatment of advanced PCa – spanning from treatment options in the pre-enzalutamide era (**1**) to its preclinical development and the landmark studies that led to its FDA approval for mCRPC (**2**). Thereupon, we discuss translational research directed at tackling unmet clinical needs in the treatment of advanced PCa using enzalutamide. This includes having on-treatment and predictive biomarkers for treatment response (**3**); a better understanding of molecular mechanisms underlying enzalutamide resistance (**4**); and lastly the development of novel therapeutic approaches aimed to overcome therapy resistance (**5**).

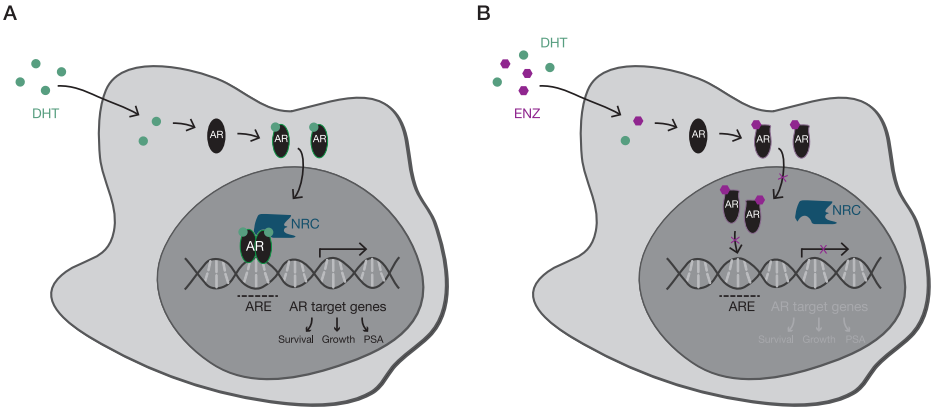

Figure 1: AR signaling axis and mechanism of action of enzalutamide. (**A**) Upon dihydrotestosterone (DHT) binding, the AR dimerizes and translocates to the nucleus, where it binds to AR-response elements (ARE) and recruits nuclear receptor coregulators (NRC), so called coactivators or corepressors, to regulate transcription of directly responsive genes involved in cell proliferation and survival. (**B**) Enzalutamide (ENZ) binding to the ligand-binding pocket of the AR results in a conformational change, rendering the receptor incapable of forming an active transcriptional complex. Further, enzalutamide blocks AR nuclear translocation and the enzalutamide-bound AR is impaired in its DNA-binding ability, ultimately preventing AR-dependent gene expression.

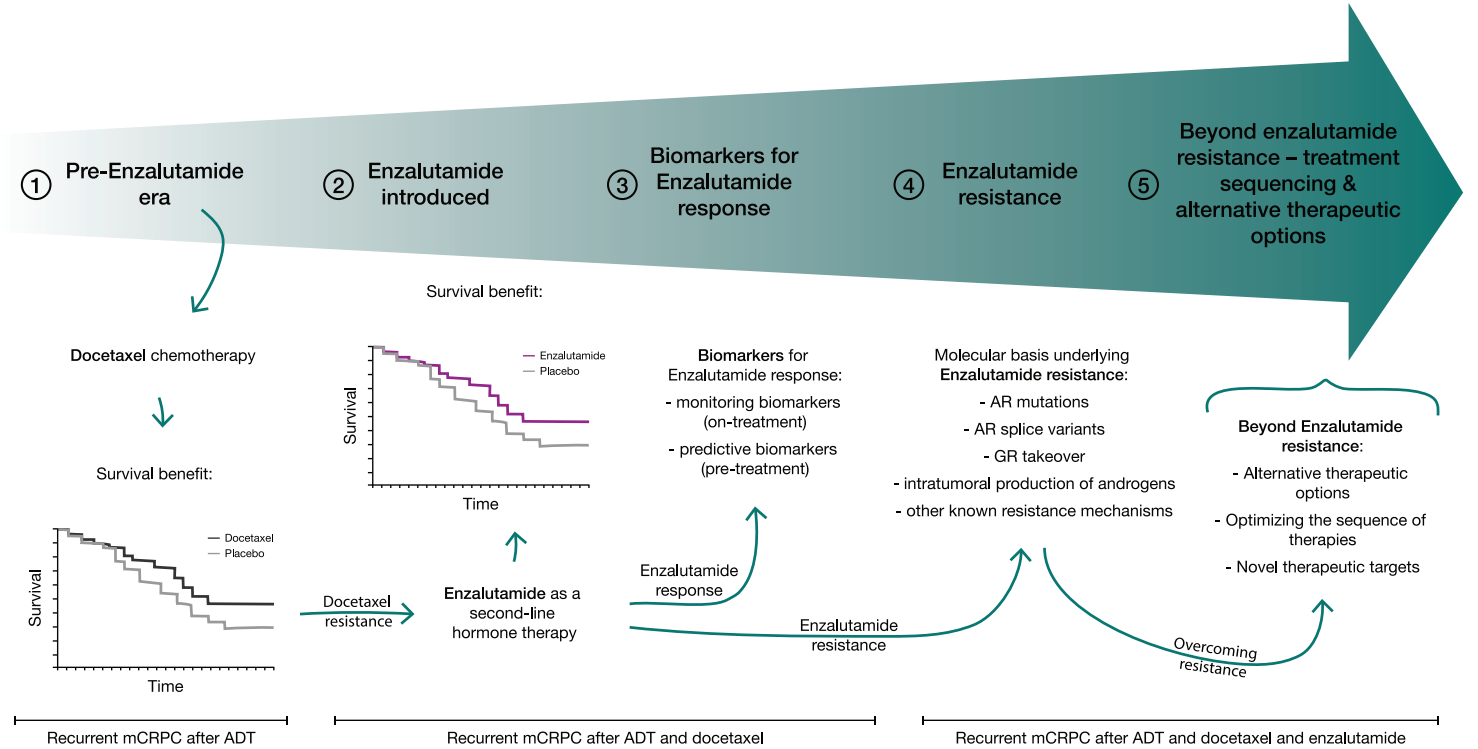

Figure 2: Graphical summary capturing the topics discussed in this review. Docetaxel has been the first agent showing a survival benefit in mCRPC patients (**1**). Despite initial responses upon docetaxel chemotherapy, patients eventually progress, whereby enzalutamide has been shown to be effective in such a docetaxel-resistant mCRPC setting (**2**). Current translational research efforts are aimed at developing biomarkers for enzalutamide response (**3**), understanding molecular underpinnings of enzalutamide-resistant mCRPC (**4**) and optimizing treatment strategies to overcome enzalutamide resistance (**5**).

The pre-enzalutamide era

Androgen deprivation therapy

ADT has been the standard of care for patients with symptomatic metastatic PCa since the forties of the last century[17]. However, despite initial response to ADT, eventually resistance emerges in practically every patient which is mediated by AR-dependent or -independent pathways[18,19]. Initially, two retrospective studies have shown a limited survival benefit of continued androgen suppression with luteinizing hormone-releasing hormone (LHRH) analogues in the mCRPC setting[20,21]. Based on these findings, all mCRPC patients enrolled in the trials discussed further below continue androgen suppression therapy. Although data is limited, the benefits of continuing androgen deprivation outweighed the potential risks of discontinuing the therapy.

Chemotherapy

In 2004, the TAX-327 trial initiated a transition in systemic mCRPC treatment[22]. In this phase III study, 1006 patients with mCRPC were randomized to receive prednisone either in combination with mitoxantrone (a chemotherapy that provides palliation, but does not lead to an improvement in survival for patients with castration-refractory PCa[23]) or with docetaxel (a chemotherapy that has been reported in phase II studies to successfully reduce serum PSA levels[24,25]). Whereas mitoxantrone, as a type II topoisomerase inhibitor that intercalates between DNA bases and thereby disrupts DNA synthesis and repair[26,27], is not directly linked to AR biology, docetaxel is. It belongs to the taxane class of chemotherapeutic agents that bind to tubulin and hyperstabilize microtubules, which ultimately leads to impairments of the mitotic cell cycle and AR signaling by preventing its nuclear translocation[28-31]. The TAX-327 study

Table 1: Clinical trials of systemic treatments for mCRPC that improve overall survival.‡

	Trial (Registration Number)	Study Intervention	
		Treatment	Control
Chemotherapy	TAX-327*	Docetaxel + Prednisone	Mitoxantrone + Prednisone
Hormonal Therapy	PREVAIL (NCT01212991)	Enzalutamide	Placebo
	AFFIRM (NCT00974311)	Enzalutamide	Placebo

‡ CI, confidence interval; ADT, androgen-deprivation therapy.

* No trial registration number available for TAX-327.

identified docetaxel as the first chemotherapeutic drug that showed a modest overall survival (OS) benefit compared to mitoxantrone (**Table 1**)[32]. Based on these results, docetaxel was established as a first-line therapy option for both, symptomatic as well as asymptomatic mCRPC.

Docetaxel resistance

As described above, mCRPC patients treated with docetaxel-based chemotherapy have a modest OS benefit implying most patients will progress rather rapidly. In patients with a good initial response to docetaxel therapy, re-challenging with the same chemotherapeutic agent results in a PSA response in up to 60% of patients with a median time to progression of 6 months[33]. As this response is less profound as compared to the therapeutic effect in the first round, it could also be hypothesized that the efficacy of docetaxel re-challenge will keep decreasing until its effect becomes negligible. Mechanisms underlying this docetaxel resistance in the mCRPC setting can be diverse[34]. On the one hand, those include rather general mechanisms associated with resistance to taxanes, including an altered microtubule composition affecting docetaxel binding (such as upregulation of certain isotypes[35] or mutations[36]), a reduced intracellular drug accumulation due to overexpression of drug efflux pumps (such as P-glycoprotein[37]) or an impaired drug distribution due to aberrant angiogenesis[38]. On the other hand, resistance can also develop due to mechanisms intrinsic to the biology of mCRPC like continued AR signaling which stimulates PCa growth and inhibits apoptosis[34] or due to the activation of compensatory oncogenic pathways (such as PI3K/AKT or MAPK/ERK[39]) which are themselves associated with proliferation and survival. As a result of taxane resistance, new therapeutic approaches tackling docetaxel-resistant mCRPC were needed and much sought-after.

Median Overall Survival (95% CI)		**Hazard Ratio (95% CI; *P*-value)**	**References**	**Sequence**
Treatment	Control			
19.2 months (17.5-21.3)	16.3 months (14.3-17.9)	0.76 (0.62-0.94; *P* = 0.009)	Tannock, et al. [22], Berthold, et al. [32]	Progression after ADT without chemotherapy
35.3 months (32.2-not yet reached)	31.3 months (28.8-34.2)	0.77 (0.67-0.88; *P* = 0.0002)	Beer, et al. [15], Beer, et al. [40]	
18.4 months (17.3-not yet reached)	13.6 months (11.3-15.8)	0.63 (0.53-0.75; *P* < 0.001)	Scher, et al. [2]	Progression after ADT and docetaxel

Enzalutamide as a second-line hormone therapy

Preclinical development

Ever since molecular profiling studies have revealed that many CRPC tumors remain AR-driven, there has been great interest in identifying novel and potent strategies to better block the AR signaling axis[41]. Such next generation antiandrogens should – unlike their first-generation counterparts (e.g., bicalutamide and flutamide) – preferably possess greater AR binding affinities without any agonistic effects[41,42]. In their search for such improved antiandrogens, Tran, et al. [1] screened nearly 200 thiohydantoin derivatives of RU59063 – a non-steroidal AR agonist with a relatively high affinity and selectivity over other nuclear hormone receptors – for retained activity in human PCa cells that overexpressed the AR protein, which is also clinically observed in the castration-resistant disease setting. RD162 and MDV3100 (now enzalutamide) were selected as the lead compounds for additional biological validation, and importantly, both antiandrogens led to tumor regression in xenograft models[1]. Due to its favorable drug-like properties, such as oral bioavailability and longer serum half-life, enzalutamide was selected for further clinical development[42].

Clinical testing

The preclinically-demonstrated antitumor activity of enzalutamide was subsequently validated in a phase I/II trial, in which patients with progressive mCRPC were enrolled in dose-escalation cohorts, ultimately demonstrating its safety and tolerability, along with antitumor effect at all tested doses[43]. In 2012, the preliminary analysis of the AFFIRM trial was published, being the first phase III study on enzalutamide in the mCRPC setting[2]. In this trial, 1199 mCRPC patients who progressed on docetaxel therapy were randomized to receive either enzalutamide or placebo. Enzalutamide treatment significantly improved patient outcome after docetaxel therapy compared to the placebo control group (**Table 1**). The efficacy of enzalutamide and its limited toxicity as compared to chemotherapy could not only be achieved in mCRPC patients who were previously treated with docetaxel, but also in the chemotherapy-naïve setting, as addressed by the PREVAIL study[15]. This was a randomized phase III trial including 1717 chemo-naïve mCRPC men comparing enzalutamide therapy to a placebo. Again, enzalutamide therapy resulted in a significant improvement in OS and radiographic progression-free survival (rPFS) (**Table 1**)[40]. Moreover, the results of the randomized phase III PROSPER trial were recently published. Therein, the addition of enzalutamide or placebo to continued ADT was tested with regards to its potential to delay metastasis formation in men with non-metastasized CRPC who are at high risk for developing distant lesions. In this setting, enzalutamide therapy led to a 71% lower risk of metastasis or death compared to placebo[44]. Based on these results, enzalutamide is now a primary treatment option for metastasis-free CRPC and asymptomatic mCRPC, whereas docetaxel is mainly used in men with symptomatic metastasized disease and acquired resistance to first-line therapeutics[15,44,45].

Biomarkers for enzalutamide response

The readout of prostate specific antigen (PSA) levels as a diagnostic biomarker was already introduced in the 1980's, but has also been questioned since then, mainly due to its non-specificity as a marker for cancerous lesions[46,47]. However, PSA measurements as a monitoring biomarker for either treatment response or resistance following PCa diagnosis and corresponding interventions, are routinely used in the clinic. PSA declines of at least 30% after 4 weeks and > 30% or > 50% after 12 weeks of treatment have been shown to correlate with a survival advantage especially in patients treated with AR-targeting compounds, whereas stable or increased PSA levels correlated with poorer outcome[48-51]. Moreover, circulating tumor cells (CTCs) seem to be a promising tool to predict a treatment-induced survival benefit. It has been observed that patients with a decline in number of CTCs (> 30%) after 4 weeks of therapy have a better prognosis[52-55]. Consequently, CTCs could be a better marker for treatment resistance in tumors progressing without an obvious PSA rise, taking into account that further validation is warranted before it can be recommended in daily clinical practice. These on-treatment readouts, however, solely allow monitoring of a patient's response to e.g., enzalutamide therapy. Whereas some men do respond exceptionally well and continue treatment for several years, others progress within months or even do not show any response at all[56]. Thus, biomarkers that enable the identification of patient subpopulations that benefit from enzalutamide treatment are urgently needed to improve the management of PCa patients.

Especially in the primary disease setting, tissue biopsies have proved to be highly informative. Besides classification systems based on clinical parameters (such as Gleason score, PSA and clinical staging)[57], genomic analyses may provide risk-assessment biomarkers that stratify patients with PCa on outcome[58-60]. However, the bone-predominant metastatic landscape of CRPC renders them rather impractical in routine clinical practice and current approaches almost exclusively focus on minimally invasive biomarkers from blood[61]. Until now, several studies have shown that the profiling of CTCs or cell-free tumor DNA (cfDNA) in liquid biopsies enables the detection of AR splice variants, *AR* copy-number gains and *AR* mutations, all of whom are at least associated with enzalutamide resistance and poorer prognosis[61-66]. Nonetheless, no such biomarker is implemented and routinely used in the clinic thus far, and further studies that robustly validate each biomarker in a prospective fashion are required for a potential practice change[56].

Molecular basis underlying enzalutamide resistance

The AFFIRM and PREVAIL trials clearly demonstrated the advantages of enzalutamide treatment. However, 46% (AFFIRM) and 22% (PREVAIL) of patients with mCRPC did not respond to second- or first-line treatment with enzalutamide, meaning that their PSA levels did not decline ≥ 50% from baseline. The remaining 54% and 78% of enzalutamide-treated patients responded initially, but PSA progression could be observed after a median time of 8.3 months (AFFIRM) and 11.2 months (PREVAIL)[2,15]. The mechanisms underlying this pre-existent or acquired resistance to enzalutamide are still not fully elucidated, but several possible mechanisms have been proposed[67]. In the next section, we will briefly discuss such potential mechanisms, which are elaborately discussed in Prekovic, et al. [19].

AR mutations

Gain-of-function mutations in the *AR* gene, especially within the exon 7 (encoding for the ligand-binding domain), have been found in 5-30% of CRPC patients[68-72]. These genomic alterations do not only permit receptor activation by various circulating steroids next to testosterone (such as H875Y or T878A) but may also alter the responsiveness of the AR to antiandrogens, resulting in antagonist-to-agonist switching[52,73,74]. This is exemplified by the F877L/T878A and M896V/S889G double mutants, which were associated with resistance[75,76] and have recently been found in cfDNA extracted from plasma of mCRPC patients progressing on enzalutamide therapy[61,77].

AR splice variants

Alternatively spliced AR variants, especially AR-V7, have been reported to be implicated in resistance to AR-targeting drugs, including enzalutamide. AR-V7 is an AR isoform that lacks the ligand-binding domain (LBD), causing the variant to be constitutively active and resistant to LBD-targeting inhibitors[78-80]. Multiple studies have demonstrated that AR-V7 expression is a biomarker for resistance to AR-targeting drugs in CRPC[81-86], but it remains to date unclear whether AR-V7 is driving the resistance or whether it merely is a manifestation of treatment-induced selective pressure without being the key-driver to therapy failure.

Glucocorticoid receptor takeover

The glucocorticoid receptor (GR) has been reported to be upregulated or re-expressed after AR blockade, indicating a complex crosstalk between AR and GR biology. Due to great similarities in the mechanism of action between nuclear receptors, GR is suggested to take over the role of AR by driving the expression of a subset of androgen-responsive genes, thus enabling the tumor to progress even in presence of the AR-selective antagonist enzalutamide[87-91].

Intratumoral production of androgens

In addition, reactivation of the AR can occur via intratumoral production of androgens, enabling the prostate cancers to progress despite ongoing androgen deprivation[92]. The expression of one of the essential enzymes in androgen biosynthesis, AKR1C3, was significantly increased in enzalutamide-resistant cells and xenograft tumors as well as in clinical specimens of advanced PCa, making it an attractive therapeutic target[93-97]. Inhibition of AKR1C3 as a novel therapeutic strategy is currently under investigation in a clinical trial (NCT02935205) studying its potential benefit in combination with enzalutamide therapy in mCRPC[98].

Other known resistance mechanisms

Next to the aforementioned AR-related underpinnings of enzalutamide resistance, several additional mechanisms have been described to give rise to therapy resistance but are not within the scope of this review. Among those are very diverse adaptations, such as metabolic changes (e.g. shifting to aerobic glycolysis[99] or alterations in the hexosamine biosynthetic pathway[100]), but also autophagy[101] or activation of certain signaling pathways (such as WNT[102] or IL-6[103]) – all of whom are addressed in depth in Prekovic, et al. [19].

Beyond enzalutamide resistance – therapy sequencing and alternative therapeutic options

Scheduling of enzalutamide treatment in mCRPC patients can differ greatly, depending on a patient's PCa stage, overall health status, treatment history and personal preference (**Fig. 3**). The mechanisms behind enzalutamide resistance (or other AR antagonists) may therefore also differ as these may depend on the settings in which the drug was administered. Over the last decade, several treatments have been developed, even though the optimal sequence of therapies still remains to be determined. This is especially the case, since none of the available therapeutic options described in **Table 2** have yet been compared head-to-head in clinical trials[104].

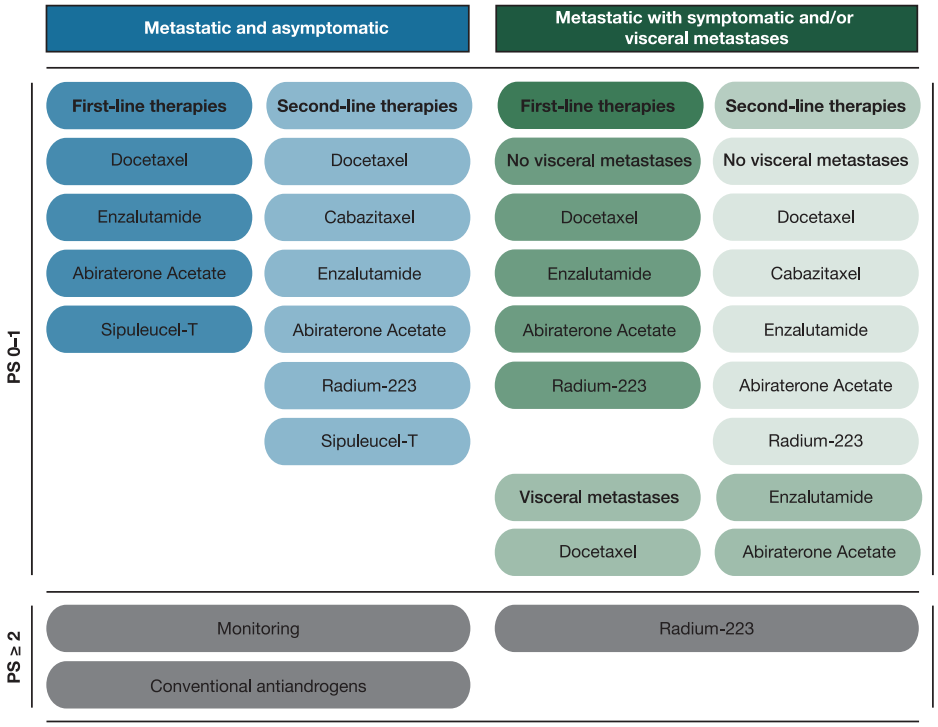

Figure 3: Schematic representation of treatment options in the mCRPC setting according to current standards of care. Therapeutic options are subdivided in first- and second-line therapies based on the clinical setting of the disease (asymptomatic versus symptomatic or visceral metastases). Treatment options are also determined by the overall performance status (PS) of the patient (PS 0-1: normal activity or some symptoms, but almost entirely ambulatory; PS ≥ 2: symptomatic patients < 50% of daytime in bed up until completely bedridden).

Available therapeutic options in clinical practice

For mCRPC patients responding to enzalutamide, there is no doubt that outcomes have improved significantly. Nevertheless, despite the survival benefits, patients are still progressing and improvements in absolute survival rates are rather disappointing. Besides enzalutamide, several other therapeutic options with proven benefit for mCRPC patients have been developed in the past 10 years, which are summarized in **Table 2** and will be briefly discussed hereafter.

Cabazitaxel

Cabazitaxel is – like docetaxel – a taxane, which stabilizes microtubules and consequently impairs mitotic cell division[28,113] (**Fig. 4A**). However, the drug shows antitumor activity in docetaxel-resistant models, potentially due to the fact that cabazitaxel is a poor substrate for the drug-efflux pump P-glycoprotein, which is reported to contribute to docetaxel resistance[114]. In line with this, cabazitaxel has been shown to improve overall survival in mCRPC patients with progressive disease on or after docetaxel-based intervention[109,110].

Abiraterone acetate

Abiraterone acetate (hereafter referred to as abiraterone) is targeting the AR signaling axis by inhibiting cytochrome P450 17A1 (CYP17A1) – an enzyme involved in intracellular biosynthesis of androgens that enables prostate cancer cells to bypass androgen deprivation (**Fig. 4B**)[3,10,115]. In addition, it has been demonstrated that abiraterone and one of its metabolic derivatives are able to directly bind to the AR and thereby inhibit the signaling of this ligand-dependent transcription factor[12,116-118]. Several large clinical trials have shown its efficacy in the hormone-naïve metastatic PCa setting[119,120] as well as in the chemo-naïve[106] and post-docetaxel[108] mCRPC setting.

Table 2: Multiple large clinical trials of alternative therapies that improve survival of patients with mCRPC.[‡]

	Trial (Registration Number)	Study Intervention	
		Treatment	Control
Hormonal Therapy	COU-AA-302 (NCT00887198)	Abiraterone + Prednisone	Placebo + Prednisone
	COU-AA-301 (NCT00638690)	Abiraterone + Prednisone	Placebo + Prednisone
Chemo-therapy	TROPIC (NCT00417079)	Cabazitaxel + Prednisone	Mitoxantrone + Prednisone
Immuno-therapy	IMPACT (NCT00065442)	Sipuleucel-T	Placebo
Alpha-particle Therapy	ALSYMPCA (NCT00699751)	Radium-223	Placebo

[‡] CI, confidence interval; ADT, androgen-deprivation therapy.

Sipuleucel-T

Sipuleucel-T is an autologous cell-based cancer immunotherapy, in which the patient's immune system is reprogrammed to recognize and eradicate cancer cells[121]. During the procedure, antigen-presenting cells are isolated from blood and primed *ex vivo* to recognize prostatic acid phosphatase – an enzyme overexpressed in prostate cancers – after which the activated immune cells are reinfused into the patient[122,123] (**Fig. 5A**). In a phase III trial, this therapeutic cancer vaccine has prolonged overall survival of mCRPC patients with asymptomatic or minimally symptomatic disease, making it the first immunotherapeutic approach shown to improve survival in PCa[111]. However, Sipuleucel-T administration has thus far only been tested with concurrent or prior to enzalutamide therapy (NCT01981122), where both treatment schedules seem to result in similarly robust immune responses with no differences in median OS[124,125]. Until now, Sipuleucel-T is therefore considered as a therapeutic option prior to docetaxel and enzalutamide, as recommended by a European expert consensus panel, unless further studies demonstrate its effectiveness in the enzalutamide-resistant mCRPC setting[126].

Radium-223

In symptomatic mCRPC patients with skeletal metastases, Radium-223 dichloride (Radium-223) is an additional therapeutic option that improves overall survival[112]. Radium-223 is a bone-seeking calcium-mimetic that concentrates at areas of increased bone turnover, as found in osteoblastic bone metastases from prostate cancer, where it emits high-energy alpha-particle radiation that causes severe DNA damage in nearby cells[112,127-129] (**Fig. 5B**).

Median Overall Survival (95% CI)		Hazard Ratio (95% CI; *P*-value)	References	Sequence
Treatment	Control			
34.7 months (32.7-36.8)	30.3 months (28.7-33.3)	0.81 (0.70-0.93; *P* = 0.0033)	Ryan, et al. [45], Rathkopf, et al. [105], Ryan, et al. [106]	Progression after ADT without chemotherapy
15.8 months (14.8-17.0)	11.2 months (10.4-13.1)	0.74 (0.64-0.86; *P* < 0.0001)	De Bono, et al. [107], Fizazi, et al. [108]	Progression after ADT and docetaxel
15.1 months (14.1-16.3)	12.7 months (11.6-13.7)	0.70 (0.59-0.83; *P* < 0.0001)	de Bono, et al. [109], Bahl, et al. [110]	
25.8 months (22.8-27.7)	21.7 months (17.7-23.8)	0.78 (0.61-0.98; *P* = 0.03)	Kantoff, et al. [111]	Progression after ADT, unspecified docetaxel status
14.9 months (13.9-16.1)	11.3 months (10.1-12.8)	0.70 (0.58-0.83; *P* < 0.001)	Parker, et al. [112]	

Therapeutics in clinical development

The antiandrogens apalutamide (ARN-509)[130] and darolutamide (ODM-201)[131] are two novel therapeutics, which are currently under clinical investigation. Whereas apalutamide's structure is highly similar to enzalutamide's, darolutamide is structurally distinct. Nevertheless, both novel antiandrogens possess a higher affinity for the AR LBD and less passage through the blood-brain barrier compared to enzalutamide. This should reduce the risk of seizures – a common side-effect of non-steroidal antiandrogens, potentially due to an off-target binding to $GABA_A$ receptors in the brain[132], which in the initial phase I/II dose-escalation study occurred in about 2.1% of enzalutamide-treated patients (3 out of 140), all of whom, however, received doses that were more than twice as high as the later on approved dosage of 160 mg/day[43,133]. The results of a placebo-controlled phase III trial showed significantly improved metastasis-free survival and time to symptomatic progression upon apalutamide treatment in men with non-metastatic CRPC[134]. Similarly, a study investigating the efficacy of darolutamide in this setting is presently running (NCT02200614). Another drug that is currently being studied with regards to overcoming enzalutamide resistance is niclosamide. It is an FDA-approved anthelminthic drug, which has been identified as a potent AR-V7 inhibitor in PCa cells, resulting in PCa cell growth inhibition *in vitro* and tumor growth inhibition *in vivo*. Further, if administered in combination with enzalutamide, niclosamide could re-sensitize enzalutamide-resistant tumors to the antiandrogen[135]. Currently, the safety and pharmacokinetics of the combination therapy are being tested in phase I trials (NCT02532114, NCT03123978), in which the poor oral bioavailability of niclosamide has

recently been reported to limit its efficacy[136]. Therefore, the current oral formulation of niclosamide might not be effective enough as a mCRPC intervention, demonstrating the importance of further clinical testing along with the development of niclosamide analogues with improved pharmacokinetic and antitumor properties[136].

Taken together, there are – at least theoretically – several alternative treatment options for mCRPC patients whose disease progressed on or after enzalutamide treatment. However, while choosing an appropriate subsequent therapeutic option, possible cross-resistance needs to be considered – especially among the next-generation antiandrogens. Moreover, a potential attenuation in a drug's clinical efficiency may occur if used as a second- or third-line intervention, emphasizing the importance of optimal treatment scheduling.

Optimizing the sequence of therapies

The introduction of the aforementioned novel effective therapies has added an additional dimension to the complex therapeutic landscape of mCRPC. As all of them have proven survival advantages, diverse scenarios of therapeutic interventions could be generated, but it still remains elusive how best to sequence and/or combine these treatment options.

Clinical and translational research exploring enzalutamide scheduling

Since it is out of the scope of this review to discuss all ongoing clinical studies with enzalutamide (co)treatment, we have compiled a non-exhaustive list of clinical trials registered on clinicaltrials.gov (Supplementary Table S1). Herein, we will focus on the limited number of studies that compare the efficacy of the various treatment options with the aim to identify an optimal sequence of treatments. One such trial is the ongoing OSTRICh study, in which patients with poor prognostic features who progressed on docetaxel therapy are randomized between cabazitaxel and either enzalutamide or abiraterone (NCT03295565). Sequential treatment with different AR-targeting agents has shown limited efficacy as exemplified by modest PSA responses when sequentially treated with enzalutamide and abiraterone or vice versa[51,137-143]. Furthermore, it is suggested that docetaxel has a reduced activity after prior therapy with enzalutamide or abiraterone[144-146]. A possible combinatorial treatment regimen is currently being tested in trials that evaluate the efficacy of enzalutamide in combination with taxane-based chemotherapeutics for the treatment of mCRPC. Such chemohormonal therapies have proven benefit in the metastatic non-castrate PCa setting, prior to developing hormone insensitivity. Therein, the CHAARTED[147-149] and STAMPEDE[150] trials showed that upfront addition of docetaxel chemotherapy to ADT at diagnosis of treatment-naïve metastatic PCa improves overall survival as compared to standard of care ADT. Based on these

results, upfront docetaxel combined with ADT is considered to be a treatment option in men with *de novo* metastatic hormone-naïve PCa[151]. However, its benefit in the mCRPC setting remains elusive, as such chemohormonal combinations (such as enzalutamide + docetaxel (NCT01565928) or enzalutamide + cabazitaxel (NCT02522715)) have thus far only been tested in phase I/II trials with relatively small sample sizes and consequently require further study in a larger population[152,153].

Up to now, the consensus on therapy sequencing in the mCRPC setting is mostly based on small retrospective studies that are unable to give a clear answer. Recently, a post-registration study evaluated the efficacy and safety of enzalutamide treatment in patients with mCRPC who had previously progressed on abiraterone. Therein, enzalutamide therapy was beneficial in some patients, whereas the majority presented cross-resistance between the two hormonal agents[154]. Similar results were shown in a retrospective study, in which the response to enzalutamide was associated with a longer interval between end of abiraterone and start of enzalutamide treatment, suggesting that over time the chance for a subsequent enzalutamide response potentially increases[155]. On the basis of the observed cross-resistance, it is important to evaluate which of the endocrine treatment options is more effective as first-line therapy for patients with mCRPC. This issue is currently being addressed in the ENABLE study for prostate cancer, a phase III multicenter randomized controlled trial, in which the efficacies of enzalutamide and abiraterone will be compared head-to-head[156]. Additionally, a randomized controlled trial (NCT02125357) is currently being performed, which assesses PSA response rates in therapy-naïve mCRPC patients being sequentially treated with abiraterone and enzalutamide or vice versa[157]. Combining different AR-targeting drugs simultaneously might improve efficacy as compared to consecutive treatment. This is being investigated in patients treated with enzalutamide or abiraterone alone versus a combination therapy consisting of both antiandrogens (NCT01949337, NCT01995513). Furthermore, although in the hormone-naïve setting, the result update of the STAMPEDE trial is awaited with high expectations, as it includes an arm with such a combination therapy (NCT00268476, Arm J). Another approach to re-challenge enzalutamide-resistant mCRPC has been described by Schweizer, et al. [158] and is referred to as bipolar androgen therapy (BAT). BAT is exploiting the adaptive increase of AR levels in CRPC, allowing the tumor cells to cope with castrate levels of testosterone, by rapidly cycling between androgen stimulation and deprivation. A subsequent phase II study of BAT in mCRPC patients that progressed on enzalutamide showed successful re-sensitization to the drug, when the patients were re-challenged with the antiandrogen upon progression on testosterone therapy[159].

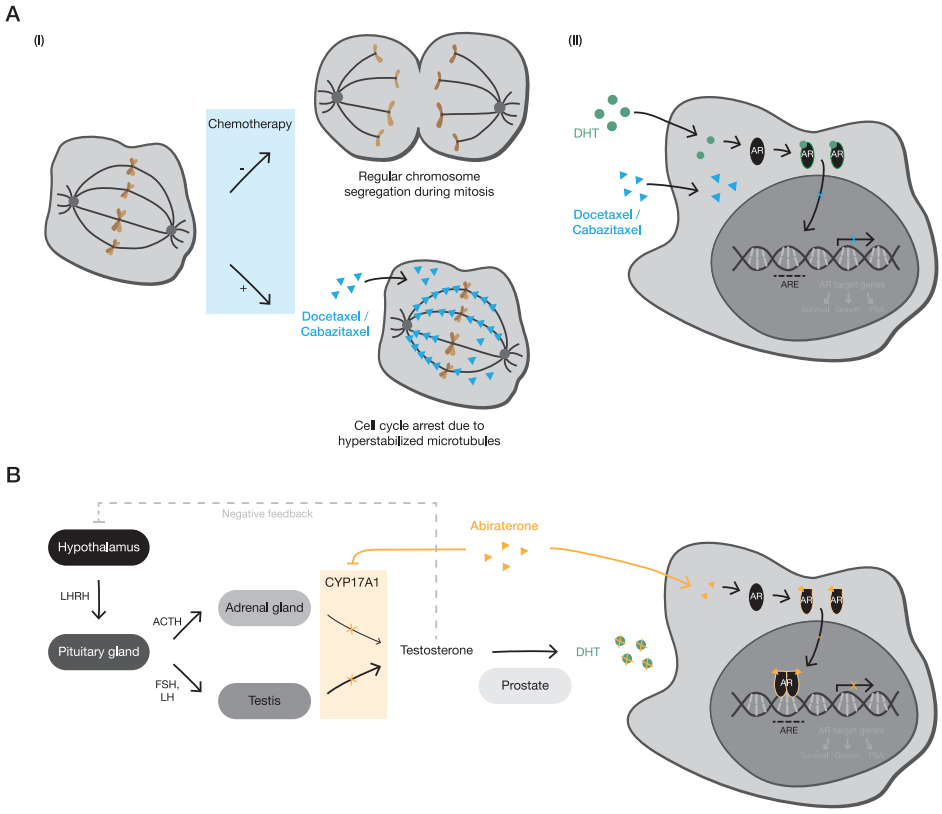

Figure 4: Mechanisms of action of taxane chemotherapeutics and the antiandrogen abiraterone acetate. (**A**) Taxane chemotherapeutics, such as docetaxel and cabazitaxel, act by hyperstabilizing microtubules, which – due to the microtubules' role in chromosome segregation during mitosis – causes a cell cycle arrest in metaphase followed by apoptosis. Moreover, taxanes directly affect AR signaling by inhibiting the microtubule-dependent AR nuclear translocation in response to androgen stimulation. DHT, dihydrotestosterone; AR, androgen receptor; ARE, AR-response element. (**B**) Abiraterone is a cytochrome P450 17A1 (CYP17A1) inhibitor that leads to androgen deprivation by inhibiting the intracellular biosynthesis of androgens in the testis and adrenal glands. Androgens are produced via the hypothalamic-pituitary-testis and to a small degree also via the hypothalamic-pituitary-adrenal axis. Within these axes, CYP17A1 is responsible for converting cholesterol to androgens, such as testosterone, which gets reduced to the potent AR agonist DHT in the prostate. In addition to androgen deprivation, abiraterone is capable of directly interacting with the AR and thereby blocks the signaling of this hormone-responsive transcription factor. LHRH, luteinizing hormone-releasing hormone; FSH, follicle-stimulating hormone; LH, luteinizing hormone; ACTH, adrenocorticotropic hormone; NRC, nuclear receptor coregulator.

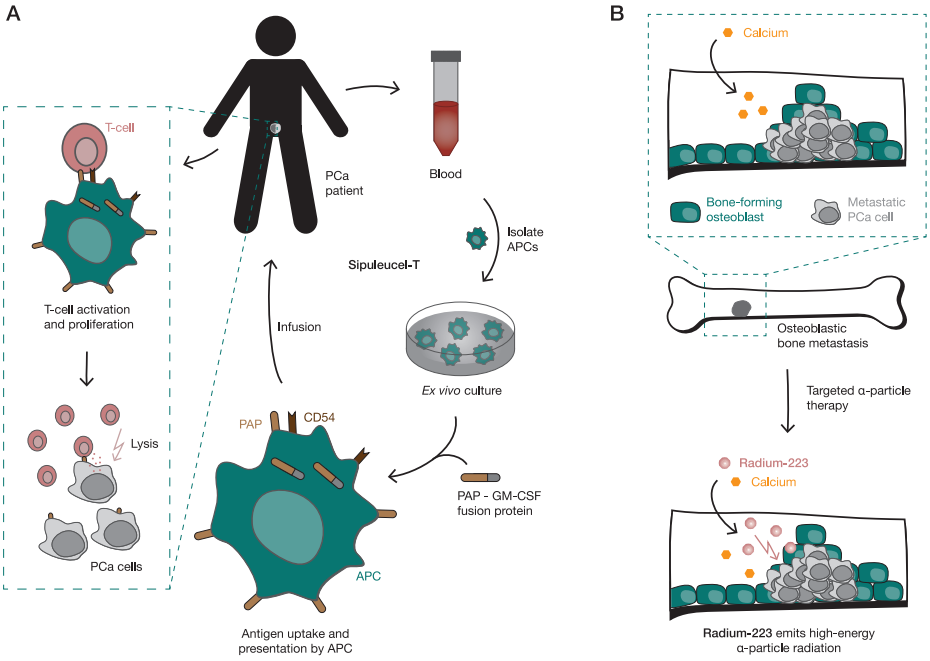

Figure 5: Mechanisms of action of Sipuleucel-T and Radium-223. (**A**) Sipuleucel-T is a cancer immunotherapy, which makes use of autologous antigen-presenting cells (APCs) to activate the patient's immune system against PCa cells. Dendritic cells, the most efficient APCs, are isolated from blood samples and cultured *ex vivo* together with a recombinant fusion protein, composed of prostatic acid phosphatase (PAP) – an enzyme overexpressed in PCa; and granulocyte-macrophage colony-stimulating factor (GM-CSF) – a cytokine that enhances immune responses. The APCs take up these antigens, present them on their surface, and upon activation express the surface marker Cluster of Differentiation 54 (CD54) – a glycoprotein that is involved in APC - T-cell interactions. The activated APCs are then reinfused into the patient to trigger a T-cell response against PAP-expressing PCa cells. (**B**) Targeted alpha-particle therapy with Radium-223 is a treatment option in symptomatic mCRPC patients with skeletal metastasis. Radium-223 is a radioactive calcium analog that – like calcium itself – gets incorporated by osteoblasts into the bone matrix. This especially occurs at sites of increased bone formation, as found in bone metastasis from PCa, where Radium-223 emits high-energy alpha-particle radiation that causes severe DNA damage in nearby cells.

Current consensus guidelines for enzalutamide treatment and therapy sequencing

The St. Gallen Advanced Prostate Cancer Consensus Conference (APCCC) assists clinicians in their therapeutic decision-making regarding the management of patients with advanced prostate cancer[151,160]. The recommendations most relevant to this review have been summarized in Supplementary Table S2. Accordingly, enzalutamide is considered as a first-line treatment in patients with asymptomatic mCRPC, regardless of whether they had received ADT alone or in combination with docetaxel in the castration-

sensitive setting. Similarly, enzalutamide is a first-line option for symptomatic men who received docetaxel in the castration-naïve setting; whereas either docetaxel, abiraterone or enzalutamide treatment are the therapies of choice for symptomatic patients who did not receive docetaxel in this setting. Furthermore, there was consensus that both, asymptomatic as well as symptomatic mCRPC patients, progressing on or after first-line docetaxel chemotherapy should receive either enzalutamide or abiraterone as a second-line agent.

Novel therapeutic targets

In addition to the clinically used enzalutamide alternatives described above, there are currently several treatment strategies in development. The studies with the most promising (pre-) clinical data and/or ongoing clinical trials are discussed hereafter.

In clinical development

Recently whole-exome and transcriptome analysis of advanced PCa revealed that 89% of 150 mCRPC patients had clinically targetable aberrations[161]. Next to well-known frequently occurring aberrations (*AR*, *ETS*, *TP53* and *PTEN*), new genomic alterations were found to be highly enriched in mCRPC patients, including *PIK3CA/B, R-spondin, BRAF/RAF1, APC, b-catenin* and *ZBTB16/PLZF*. Furthermore, genes involved in DNA damage repair (*BRCA2*, *BRCA1* and *ATM*) were altered more frequently than expected[161]. More recently, Pritchard, et al. [162] have found that 11.8% of patients with metastatic PCa have inherited germline mutations in DNA damage repair genes, which seem to be effectively treatable with the PARP-inhibitor Olaparib[163]. In consequence of the identification of these genomic alterations in mCRPC, there is a great interest in the design of clinical trials targeting these pathways in combination with enzalutamide treatment. Trials that are currently running include PI3K/AKT/mTOR pathway inhibition using LY3023414 (NCT02407054), TGF-β receptor I pathway inhibition using Galunisertib (NCT02452008), and IGF1 pathway inhibition using Xentuzumab (NCT02204072).

mCRPC is also characterized by changes in the epigenetic and chromatin status like altered histone acetylation or DNA methylation, based on which chromatin readers/modifiers are regarded as potential therapeutic targets[164-167]. Therefore, the BET family of proteins which recognize and bind acetylated histones and are implicated in transcriptional regulation processes are potential therapeutic targets[168]. In particular, BRD4, a conserved member of the BET family of chromatin readers, has a crucial role in global RNA-polymerase II (RNA-Pol II)-mediated transcription[169,170]. Inhibition of BRD4 recruitment to active chromatin results in displacement of RNA-Pol II from its target genes and eventually leads to growth inhibitory effects in CRPC xenograft models[170-173]. Besides, BRD4 can physically interact with the N-terminal domain of

the AR to mediate its transcriptional signaling[170,174,175]. Hence, clinical trials have been initiated that investigate safety, pharmacodynamics, pharmacokinetics and clinical responses to a BET inhibitor (GSK525762) as monotherapy (NCT01587703) or in combination with antiandrogens (NCT03150056) in men with chemo-naïve or chemo-treated CRPC.

Different types of immunotherapies, e.g., anti-PD-L1 antibodies, are being examined in nearly all types of cancer, showing most efficacy in tumors with a high mutational load and an immunologically "hot" tumor microenvironment[176-179]. However, PCa is generally characterized by a relatively "cold" microenvironment with little cytotoxic T-cell infiltration[180]. Moreover, the mutational frequency is comparatively low, possibly restricting successful immunotherapy-mediated interventions to prostate tumors with deficient DNA damage repair[181]. Recently, Zehir, et al. [182] reported a patient case with castration- and enzalutamide-resistant PCa, who responded exceptionally well to anti-PD-L1 immunotherapy. Prospective clinical sequencing of the patient's tumor and blood samples revealed a DNA mismatch-repair (MMR) deficiency signature in the cancerous tissue without a clear underlying somatic or germline MMR pathway lesion[182]. Hence, clinical trials are currently investigating the safety and efficacy of PD-L1 checkpoint inhibition as a monotherapy (using Avelumab) in patients with metastatic neuroendocrine-like PCa (NCT03179410), and as a combinatorial treatment (using Atezolizumab and enzalutamide) in patients with mCRPC (NCT03016312).

In the pre-clinical phase

Besides targeting AR itself, translational research has focused over the last couple of years on finding treatment options interfering with molecules that are associated with the AR signaling pathway and thus required for proper AR action. By now, hundreds of these AR regulators and interactors have been identified, all of which could be of interest for future drug development[183-185]. In the following, we briefly discuss therapeutic intervention strategies with promising pre-clinical results that target a subset of AR coregulators and thus serve as a proof-of-principle.

Recently, several inhibitors of the histone acetyltransferases E1A binding protein (P300) and cAMP response element binding protein (CREB)-binding protein (CBP) have been developed; such as GNE-049[186], A-485[187] and CCS1477[188]. CBP and P300 are two closely related and known transcriptional AR coactivators that have been suggested to play an important role in PCa progression[189,190]. In preclinical studies P300/CBP inhibitors block the AR transcriptional program and PCa cell proliferation in cell lines as well as castration-resistant xenograft models[186-188], supporting their potential clinical impact, which needs to be further validated in clinical trials. Very

recently, a phase I/II trial assessing the safety and biological activity of the P300/CBP inhibitor CCS1477 as monotherapy or in combination with abiraterone or enzalutamide in mCRPC patients has been initiated (NCT03568656). Other AR-coactivators that are currently being studied regarding their potential as therapeutic targets are the P160 steroid receptor coactivators SRC-1, SRC-2 and SRC-3[191]. SRC-1 and SRC-3 have been reported to be overexpressed in PCa cell lines and clinical specimens, where their expression levels have been associated with tumor grade and disease-specific survival[191,192]. Moreover, SRC-3 knockdown experiments in mice have shown decreased tumor growth, indicating its importance in prostate cancer proliferation and progression[193,194]. SRC-2 has been suggested as an PCa oncogene on the basis of integrated genomic profiling of 218 prostate tumors, illustrating *SRC-2* gene amplifications, mutations or overexpression to occur in 8% of primary and 37% of metastatic PCa lesions[195]. Rather recently, a novel potent small molecule inhibitor for SRCs (SI-2) has been developed, which is setting the stage for further (pre-)clinical validation[196]. Paradoxically, not only SRC inhibition, but also hyper-stimulation can be exploited to selectively induce cancer cell death and *in vivo* tumor growth inhibition. A high-throughput screen identified a small molecule (MCB-613), which over-activates SRC transcriptional programs, leading to excessive cellular stress in cancer cells that highly rely on proper SRC functioning[197].

While most of the above-mentioned novel therapeutic approaches represent systemic treatments, interventions that specifically interfere with acquired features in PCa and thus would limit off-target effects, are of prime interest. A fusion of the androgen-responsive transmembrane protease serine 2 (TMPRSS2) and the v-ets erythroblastosis virus E26 oncogene homolog (ERG) is found in approximately 50% of prostate cancer cases, making it the most common genetic aberration in PCa[198,199]. *TMPRSS2-ERG* gene fusions lead to overexpression of the usually lowly expressed ERG master transcription factor driven by the androgen-regulated promoter of *TMPRSS2*. This is considered an early event in PCa development and phenotypically results in increased PCa cell migration, invasion and incomplete differentiation compared to benign prostate epithelial cells due to an altered transcriptional profile[200-202]. Thus far, three preclinical approaches have been published using either a peptide-based vaccine to prime the patient's immune system to recognize the TMPRSS2-ERG fusion as an antigen[203]; liposomal nanovectors containing TMPRSS2-ERG-specific siRNAs[204]; or cell-permeable ERG inhibitory peptides that specifically block ERG-mediated transcription by interacting with its DNA-binding domain[205]. However, much more preclinical validations and targeting strategies have to be explored until this therapeutic approach could potentially move to the clinic.

Although AR action remains essential in mCRPC, this is not the only targetable molecule driving this complex disease. Indeed, increasing evidence suggests that a subset of antiandrogen-resistant tumors show neuroendocrine features which seem to be a consequence of treatment-induced adaptation of adenocarcinomas with genomic and epigenomic drivers associated with decreased AR activity and epithelial plasticity[206,207]. Efficacy of platinum-based chemotherapy has been suggested in small-cell neuroendocrine PCa before and a trial (NCT02208583) is currently investigating this, based on the molecular phenotype of mCRPC[208].

Conclusions and future perspectives

The introduction of enzalutamide as a second-line hormonal therapy for patients with mCRPC has led to significant improvements in the management of the disease. Due to tumor heterogeneity, the duration of benefit to enzalutamide interventions varies between patients. While some men do respond extremely well and continue treatment for several years, others progress rapidly as a result of treatment resistance. The increasing number of ongoing clinical trials reflects the successful preclinical advances in understanding enzalutamide resistance mechanisms and in discovering novel therapeutic targets to maximize clinical outcome. However, the disease continues to be terminal and current treatment options, including enzalutamide and its alternatives, have only a modest impact on survival, highlighting that many aspects of the disease remain poorly understood. Only by understanding which mechanisms underlie treatment resistance, robust molecular or clinical biomarkers can be developed to guide therapeutic decision-making and to identify patient-subpopulations that benefit thereof mostly. That way, well thought-out therapeutic strategies can be designed, comprising optimal patient-tailored therapy sequencing and combination.

Conflict of interest

H. van der Poel reports grants from Astellas during the conduct of the study. A.M. Bergman reports grants from Astellas Pharma during the conduct of the study, as well as personal fees from Astellas Pharma outside the submitted work. W. Zwart reports grants from Astellas Pharma during the conduct of the study, as well as personal fees from Astellas Pharma, and grants from AstraZeneca outside the submitted work. No disclosures were reported by the other authors.

Acknowledgments

This work was supported by grants from the Alpe d'HuZes/Dutch Cancer Society KWF (10084), Movember (NKI01), and the Dutch Organization for scientific research NWO (91716401). The authors would like to thank Thomas van den Broeck, Steven Joniau and Frank Claessens for their contributions and input on the initial draft of the manuscript.

Supplementary tables

Supplementary Table S1: Non-exhaustive list of clinical trials regarding enzalutamide (co)treatment and resistance, registered on clinicaltrials.gov.

Trial and/or Registration Number	Treatment Regimen	Status
STRIVE, NCT01664923	Enzalutamide vs. Bicalutamide	completed
NCT03418324	Enzalutamide + TRC105 vs. Abiraterone + TRC105	recruiting
NCT01547299	Enzalutamide vs. Enzalutamide + Leuprolide + Dutasteride	completed
ENACT, NCT02799745	Enzalutamide vs. Active Surveillance	recruiting
NCT02294461	Enzalutamide vs. Placebo	active
NCT02640534	Enzalutamide vs. Enzalutamide + Metformin	recruiting
PLATO, NCT01995513	Enzalutamide + Abiraterone + Prednisone vs. Placebo + Abiraterone + Prednisone	active
PREVAIL, NCT01212991	Enzalutamide vs. Placebo	active
AFFIRM, NCT00974311	Enzalutamide vs. Placebo	completed
ARCHES, NCT02677896	Enzalutamide + ADT vs. Placebo + ADT	active
PROfound, NCT02987543	Enzalutamide/Abiraterone (+Prednisone) vs. Olaparib	recruiting
STRIDE, NCT01981122	Enzalutamide + Sipuleucel-T (concurrent) vs. Enzalutamide + Sipuleucel-T (sequential)	active
NCT02407054	Enzalutamide + LY3023414 vs. Enzalutamide + Placebo	recruiting
NCT02607228	Enzalutamide + GS-5829 vs. GS-5829	active
PRESIDE, NCT02288247	Enzalutamide + Docetaxel + Prednisolone vs. Placebo + Docetaxel + Prednisolone	active
NCT02918968	Enzalutamide + ADT (1st), Flutamide (2nd) vs. Flutamide + ADT (1st), Enzalutamide (2nd)	active
NCT02685267	Enzalutamide + Docetaxel + Prednisone vs. Docetaxel + Prednisone	active
PROSPER, NCT02003924	Enzalutamide vs. Placebo	active
EMBARK, NCT02319837	Enzalutamide vs. Enzalutamide + Leuprolide vs. Placebo + Leuprolide	recruiting
ENZAMET, NCT02446405	Enzalutamide + ADT vs. conventional non-steroidal antiandrogen + ADT	active

Supplementary Table S1: Continued.

Trial and/or Registration Number	Treatment Regimen	Status
NCT02452008	Enzalutamide vs. Enzalutamide + LY2157299	recruiting
NCT02012296	Enzalutamide vs. Enzalutamide + Mifepristone	recruiting
NCT01875250	Enzalutamide vs. Enzalutamide + PSA-TRICOM	active
ENZARAD, NCT02446444	Enzalutamide + ADT + Radiotherapy vs. conventional non-steroidal antiandrogen + ADT + Radiotherapy	recruiting
TERRAIN, NCT01288911	Enzalutamide vs. Bicalutamide	completed
PRIMCAB, NCT02379390	Enzalutamide/Abiraterone (+Prednisone) vs. Cabazitaxel + Prednisone	active
CHEIRON, NCT02453009	Enzalutamide + Docetaxel + Prednisone vs. Docetaxel + Prednisone	unknown
NCT02254785	Enzalutamide/Abiraterone vs. Cabazitaxel	active
NCT01867333	Enzalutamide vs. Enzalutamide + PSA-TRICOM	active
CheckMate 9KD, NCT03338790	Enzalutamide + Nivolumab vs. Docetaxel + Prednisone + Nivolumab vs. Rucaparib + Nivolumab	recruiting
NCT02204072	Enzalutamide vs. Enzalutamide + BI 836845	active
PEACE III, NCT02194842	Enzalutamide vs. Enzalutamide + Radium-223	recruiting
NCT02555189	Enzalutamide vs. Enzalutamide + Ribociclib	recruiting
NCT02125357	Enzalutamide (1st), Abiraterone + Prednisone (2nd) vs. Abiraterone + Prednisone (1st), Enzalutamide (2nd)	active
NCT02346578	Enzalutamide vs. Flutamide	recruiting
NCT02058706	Enzalutamide + ADT vs. Bicalutamide + ADT	active
CARD, NCT02485691	Enzalutamide/Abiraterone + Prednisone vs. Cabazitaxel + Prednisone	recruiting
NCT02034552	Enzalutamide + Radium-223 vs. Abiraterone + Prednisone + Radium-223 vs. Radium-223	active
TRITON3, NCT02975934	Enzalutamide/Abiraterone (+Prednisone)/Docetaxel + Prednisone vs. Rucaparib	recruiting
NCT01949337	Enzalutamide vs. Enzalutamide + Abiraterone + Prednisone	active
Transformer, NCT02286921	Enzalutamide vs. Testosterone Cypionate/Enanthate	recruiting
NCT02278185	Enzalutamide vs. ADT	recruiting
NCT02268175	Enzalutamide + ADT vs. Enzalutamide + ADT + Abiraterone + Prednisone	active
IMbassador250, NCT03016312	Enzalutamide vs. Enzalutamide + Atezolizumab	recruiting

Supplementary Table S1: Continued.

Trial and/or Registration Number	Treatment Regimen	Status
PCS IX, NCT02685397	Enzalutamide + ADT vs. Enzalutamide + ADT + Radiotherapy	recruiting
OSTRICh, NCT03295565	Enzalutamide/Abiraterone + Prednisone vs. Cabazitaxel	recruiting
KEYNOTE-365, NCT02861573	Enzalutamide + Pembrolizumab vs. Docetaxel + Prednisone + Dexamethasone + Pembrolizumab vs. Olaparib + Pembrolizumab	recruiting
NCT03150056	Enzalutamide + GSK525762 vs. Abiraterone + Prednisone + GSK525762	recruiting
STAMPEDE (Arm J), NCT00268476	Enzalutamide + Abiraterone + Prednisolone + ADT vs. Abiraterone + ADT vs. Docetaxel + Prednisolone + ADT vs. more	active
NCT02203695	Enzalutamide + Radiotherapy vs. Placebo + Radiotherapy	recruiting
RE-AKT, NCT02525068	Enzalutamide + Placebo vs. Enzalutamide + AZD5363	recruiting
TALAPRO-2, NCT03395197	Enzalutamide/Abiraterone (+Prednisone) + Talazoparib vs. Enzalutamide/Abiraterone (+Prednisone) + Placebo	recruiting
NCT03568656	Enzalutamide + CCS1477 vs. Abiraterone + CCS1477 vs. CCS1477	recruiting

NOTE: The search terms used were: "enzalutamide", study type: "interventional study", and conditions: "prostate cancer" without time restrictions. Single-arm trials or trials without PSA progression, radiographic progression, or overall survival as outcomes; and suspended, terminated or withdrawn trials were excluded from the list.

Supplementary Table S2: Summary of the 2017 Advanced Prostate Cancer Consensus Conference (APCCC) recommendations relevant to this review.

Sequence:	What is your preferred mCRPC treatment option:	Therapy:	Panel agreement:
First-line	For asymptomatic men who did not received docetaxel in the castration-naïve setting?	• Enzalutamide or Abiraterone • Docetaxel • Sipuleucel-T	• 86% • 6% • 8%
	For symptomatic men who did not receive docetaxel in the castration-naïve setting?	• Enzalutamide or Abiraterone • Docetaxel • No preferred option	• 52% • 46% • 2%
	For asymptomatic men who did receive docetaxel in the castration-naïve setting?	• Enzalutamide or Abiraterone • Cabazitaxel • Docetaxel • Sipuleucel-T	• 90% • 2% • 2% • 6%
	For symptomatic men who did receive docetaxel in the castration-naïve setting?	• Enzalutamide or Abiraterone • Cabazitaxel • Docetaxel • Radium-223	• 73% • 19% • 6% • 2%
	For asymptomatic men who received chemohormonal therapy and progressed within ≤6 months after completion of docetaxel in the castration-naïve setting?	• Enzalutamide or Abiraterone • Cabazitaxel • Docetaxel • Platinum-based chemotherapy • No preferred option	• 77% • 17% • 2% • 2% • 2%
	For symptomatic men who received chemohormonal therapy and progressed within ≤6 months after completion of docetaxel in the castration-naïve setting?	• Enzalutamide or Abiraterone • Cabazitaxel • Platinum-based chemotherapy • Radium-223 • Sipuleucel-T • No preferred option	• 57% • 27% • 4% • 8% • 2% • 2%
	The first-line AR pathway inhibitor should be:	• Enzalutamide • Abiraterone • No preferred option	• 24% • 35% • 37%

Supplementary Table S2: Continued.

Sequence:	What is your preferred mCRPC treatment option:	Therapy:	Panel agreement:
Second-line	For men with asymptomatic mCRPC who had progressive disease as best response to first-line enzalutamide or abiraterone?	• Enzalutamide or Abiraterone‡ • Taxane • Radium-223 • Sipuleucel-T • No preferred option	• 14% • 70% • 4% • 6% • 6%
	For men with symptomatic mCRPC and acquired resistance (initial response followed by progression) after use of first-line enzalutamide or abiraterone?	• Taxane • Radium-223	• 96% • 4%
	For men with asymptomatic mCRPC who had progressive disease as best response to first-line enzalutamide or abiraterone?	• Enzalutamide or Abiraterone‡ • Taxane • Radium-223 • Sipuleucel-T • No preferred option	• 27% • 57% • 10% • 4% • 2%
	For men with symptomatic mCRPC who had progressive disease as best response to first-line enzalutamide or abiraterone?	• Taxane • Radium-223 • No preferred option	• 90% • 8% • 2%
	For asymptomatic men progressing on or after docetaxel for mCRPC (without prior enzalutamide or abiraterone)?	• Enzalutamide or Abiraterone‡ • Taxane • Radium-223	• 92% • 6% • 2%
	For symptomatic men progressing on or after docetaxel for mCRPC (without prior enzalutamide or abiraterone)?	• Enzalutamide or Abiraterone‡ • Taxane • Radium-223	• 76% • 18% • 6%
Third-line	For men who have received enzalutamide or abiraterone as first-line treatment, and docetaxel as second-line treatment?	• Enzalutamide or Abiraterone‡ • Cabazitaxel • Radium-223 • Platinum-based chemotherapy • No preferred choice	• 8% • 61% • 15% • 6% • 8%

NOTE: Data extracted from the St. Gallen Advanced Prostate Cancer Consensus Conference (APCCC) manuscript Gillessen, et al. [151]. ‡ Depending on which antiandrogen has already been used as first-line treatment.

References

1 Tran, C. *et al.* Development of a second-generation antiandrogen for treatment of advanced prostate cancer. *Science* **324**, 787-790 (2009). https://doi.org:10.1126/science.1168175

2 Scher, H. I. *et al.* Increased survival with enzalutamide in prostate cancer after chemotherapy. *N Engl J Med* **367**, 1187-1197 (2012). https://doi.org:10.1056/NEJMoa1207506

3 Attard, G. *et al.* Selective inhibition of CYP17 with abiraterone acetate is highly active in the treatment of castration-resistant prostate cancer. *J Clin Oncol* **27**, 3742-3748 (2009). https://doi.org:10.1200/JCO.2008.20.0642

4 Brinkmann, A. O. *et al.* Mechanisms of androgen receptor activation and function. *J Steroid Biochem Mol Biol* **69**, 307-313 (1999). https://doi.org:10.1016/s0960-0760(99)00049-7

5 Itkonen, H. & Mills, I. G. Chromatin binding by the androgen receptor in prostate cancer. *Mol Cell Endocrinol* **360**, 44-51 (2012). https://doi.org:10.1016/j.mce.2011.09.037

6 Mills, I. G. Maintaining and reprogramming genomic androgen receptor activity in prostate cancer. *Nat Rev Cancer* **14**, 187-198 (2014). https://doi.org:10.1038/nrc3678

7 Harris, W. P., Mostaghel, E. A., Nelson, P. S. & Montgomery, B. Androgen deprivation therapy: progress in understanding mechanisms of resistance and optimizing androgen depletion. *Nat Clin Pract Urol* **6**, 76-85 (2009). https://doi.org:10.1038/ncpuro1296

8 Karantanos, T., Corn, P. G. & Thompson, T. C. Prostate cancer progression after androgen deprivation therapy: mechanisms of castrate resistance and novel therapeutic approaches. *Oncogene* **32**, 5501-5511 (2013). https://doi.org:10.1038/onc.2013.206

9 Massard, C. & Fizazi, K. Targeting continued androgen receptor signaling in prostate cancer. *Clin Cancer Res* **17**, 3876-3883 (2011). https://doi.org:10.1158/1078-0432.CCR-10-2815

10 Helsen, C. *et al.* Androgen receptor antagonists for prostate cancer therapy. *Endocr Relat Cancer* **21**, T105-118 (2014). https://doi.org:10.1530/ERC-13-0545

11 Sanford, M. Enzalutamide: A Review of Its Use in Metastatic, Castration-Resistant Prostate Cancer. *Drugs* **73**, 1723-1732 (2013). https://doi.org:10.1007/s40265-013-0129-9

12 van Soest, R. J. *et al.* Cross-resistance between taxanes and new hormonal agents abiraterone and enzalutamide may affect drug sequence choices in metastatic castration-resistant prostate cancer. *Eur J Cancer* **49**, 3821-3830 (2013). https://doi.org:10.1016/j.ejca.2013.09.026

13 Antonarakis, E. S. Enzalutamide: The emperor of all anti-androgens. *Transl Androl Urol* **2**, 119-120 (2013). https://doi.org:10.3978/j.issn.2223-4683.2012.09.04

14 Boyd, L. K., Mao, X. & Lu, Y. J. The complexity of prostate cancer: genomic alterations and heterogeneity. *Nat Rev Urol* **9**, 652-664 (2012). https://doi.org:10.1038/nrurol.2012.185

15 Beer, T. M. *et al.* Enzalutamide in metastatic prostate cancer before chemotherapy. *N Engl J Med* **371**, 424-433 (2014). https://doi.org:10.1056/NEJMoa1405095

16 Merseburger, A. S., Haas, G. P. & von Klot, C. A. An update on enzalutamide in the treatment of prostate cancer. *Ther Adv Urol* **7**, 9-21 (2015). https://doi.org:10.1177/1756287214555336

17 Merseburger, A. S., Alcaraz, A. & von Klot, C. A. Androgen deprivation therapy as backbone therapy in the management of prostate cancer. *Onco Targets Ther* **9**, 7263-7274 (2016). https://doi.org:10.2147/OTT.S117176

18 Scher, H. I. & Sawyers, C. L. Biology of progressive, castration-resistant prostate cancer: directed therapies targeting the androgen-receptor signaling axis. *J Clin Oncol* **23**, 8253-8261 (2005). https://doi.org:10.1200/JCO.2005.03.4777

19 Prekovic, S. *et al.* Molecular underpinnings of enzalutamide resistance. *Endocr Relat Cancer* **25**, R545-R557 (2018). https://doi.org:10.1530/ERC-17-0136
20 Taylor, C. D., Elson, P. & Trump, D. L. Importance of continued testicular suppression in hormone-refractory prostate cancer. *J Clin Oncol* **11**, 2167-2172 (1993). https://doi.org:10.1200/JCO.1993.11.11.2167
21 Hussain, M., Wolf, M., Marshall, E., Crawford, E. D. & Eisenberger, M. Effects of continued androgen-deprivation therapy and other prognostic factors on response and survival in phase II chemotherapy trials for hormone-refractory prostate cancer: a Southwest Oncology Group report. *J Clin Oncol* **12**, 1868-1875 (1994). https://doi.org:10.1200/JCO.1994.12.9.1868
22 Tannock, I. F. *et al.* Docetaxel plus prednisone or mitoxantrone plus prednisone for advanced prostate cancer. *N Engl J Med* **351**, 1502-1512 (2004). https://doi.org:10.1056/NEJMoa040720
23 Tannock, I. F. *et al.* Chemotherapy with mitoxantrone plus prednisone or prednisone alone for symptomatic hormone-resistant prostate cancer: a Canadian randomized trial with palliative end points. *J Clin Oncol* **14**, 1756-1764 (1996). https://doi.org:10.1200/JCO.1996.14.6.1756
24 Beer, T. M., Pierce, W. C., Lowe, B. A. & Henner, W. D. Phase II study of weekly docetaxel in symptomatic androgen-independent prostate cancer. *Ann Oncol* **12**, 1273-1279 (2001). https://doi.org:10.1023/A:1012258723075
25 Berry, W., Dakhil, S., Gregurich, M. A. & Asmar, L. Phase II trial of single-agent weekly docetaxel in hormone-refractory, symptomatic, metastatic carcinoma of the prostate. *Semin Oncol* **28**, 8-15 (2001). https://doi.org:10.1016/S0093-7754(01)90149-6
26 Pommier, Y., Leo, E., Zhang, H. & Marchand, C. DNA topoisomerases and their poisoning by anticancer and antibacterial drugs. *Chem Biol* **17**, 421-433 (2010). https://doi.org:10.1016/j.chembiol.2010.04.012
27 Nitiss, J. L. Targeting DNA topoisomerase II in cancer chemotherapy. *Nat Rev Cancer* **9**, 338-350 (2009). https://doi.org:10.1038/nrc2607
28 Fitzpatrick, J. M. & de Wit, R. Taxane mechanisms of action: potential implications for treatment sequencing in metastatic castration-resistant prostate cancer. *Eur Urol* **65**, 1198-1204 (2014). https://doi.org:10.1016/j.eururo.2013.07.022
29 Kuroda, K. *et al.* Docetaxel down-regulates the expression of androgen receptor and prostate-specific antigen but not prostate-specific membrane antigen in prostate cancer cell lines: implications for PSA surrogacy. *Prostate* **69**, 1579-1585 (2009). https://doi.org:10.1002/pros.21004
30 Zhu, M. L. *et al.* Tubulin-targeting chemotherapy impairs androgen receptor activity in prostate cancer. *Cancer Res* **70**, 7992-8002 (2010). https://doi.org:10.1158/0008-5472.CAN-10-0585
31 Darshan, M. S. *et al.* Taxane-induced blockade to nuclear accumulation of the androgen receptor predicts clinical responses in metastatic prostate cancer. *Cancer Res* **71**, 6019-6029 (2011). https://doi.org:10.1158/0008-5472.CAN-11-1417
32 Berthold, D. R. *et al.* Docetaxel plus prednisone or mitoxantrone plus prednisone for advanced prostate cancer: updated survival in the TAX 327 study. *J Clin Oncol* **26**, 242-245 (2008). https://doi.org:10.1200/JCO.2007.12.4008
33 Beer, T. M., Garzotto, M., Henner, W. D., Eilers, K. M. & Wersinger, E. M. Multiple cycles of intermittent chemotherapy in metastatic androgen-independent prostate cancer. *Br J Cancer* **91**, 1425-1427 (2004). https://doi.org:10.1038/sj.bjc.6602198
34 Seruga, B., Ocana, A. & Tannock, I. F. Drug resistance in metastatic castration-resistant prostate cancer. *Nat Rev Clin Oncol* **8**, 12-23 (2011). https://doi.org:10.1038/nrclinonc.2010.136
35 Ranganathan, S., Benetatos, C. A., Colarusso, P. J., Dexter, D. W. & Hudes, G. R. Altered beta-tubulin isotype expression in paclitaxel-resistant human prostate carcinoma cells. *Br J Cancer* **77**, 562-566 (1998). https://doi.org:10.1038/bjc.1998.91

36 Yin, S., Bhattacharya, R. & Cabral, F. Human mutations that confer paclitaxel resistance. *Mol Cancer Ther* **9**, 327-335 (2010). https://doi.org:10.1158/1535-7163.MCT-09-0674

37 Zhu, Y. *et al.* Inhibition of ABCB1 expression overcomes acquired docetaxel resistance in prostate cancer. *Mol Cancer Ther* **12**, 1829-1836 (2013). https://doi.org:10.1158/1535-7163.MCT-13-0208

38 Marignol, L., Coffey, M., Lawler, M. & Hollywood, D. Hypoxia in prostate cancer: a powerful shield against tumour destruction? *Cancer Treat Rev* **34**, 313-327 (2008). https://doi.org:10.1016/j.ctrv.2008.01.006

39 Zhu, M. L. & Kyprianou, N. Androgen receptor and growth factor signaling cross-talk in prostate cancer cells. *Endocr Relat Cancer* **15**, 841-849 (2008). https://doi.org:10.1677/ERC-08-0084

40 Beer, T. M. *et al.* Enzalutamide in Men with Chemotherapy-naive Metastatic Castration-resistant Prostate Cancer: Extended Analysis of the Phase 3 PREVAIL Study. *Eur Urol* **71**, 151-154 (2017). https://doi.org:10.1016/j.eururo.2016.07.032

41 Chen, C. D. *et al.* Molecular determinants of resistance to antiandrogen therapy. *Nat Med* **10**, 33-39 (2004). https://doi.org:10.1038/nm972

42 Bambury, R. M. & Scher, H. I. Enzalutamide: Development from bench to bedside. *Urol Oncol* **33**, 280-288 (2015). https://doi.org:10.1016/j.urolonc.2014.12.017

43 Scher, H. I. *et al.* Antitumour activity of MDV3100 in castration-resistant prostate cancer: a phase 1-2 study. *Lancet* **375**, 1437-1446 (2010). https://doi.org:10.1016/S0140-6736(10)60172-9

44 Hussain, M. *et al.* Enzalutamide in Men with Nonmetastatic, Castration-Resistant Prostate Cancer. *N Engl J Med* **378**, 2465-2474 (2018). https://doi.org:10.1056/NEJMoa1800536

45 Ryan, C. J. *et al.* Abiraterone in metastatic prostate cancer without previous chemotherapy. *N Engl J Med* **368**, 138-148 (2013). https://doi.org:10.1056/NEJMoa1209096

46 Oesterling, J. E. Prostate specific antigen: a critical assessment of the most useful tumor marker for adenocarcinoma of the prostate. *J Urol* **145**, 907-923 (1991). https://doi.org:10.1016/S0022-5347(17)38491-4

47 Salman, J. W., Schoots, I. G., Carlsson, S. V., Jenster, G. & Roobol, M. J. in *Advances in Cancer Biomarkers: From biochemistry to clinic for a critical revision* (ed Roberto Scatena) 93-114 (Springer Netherlands, 2015).

48 Scher, H. I. *et al.* Design and end points of clinical trials for patients with progressive prostate cancer and castrate levels of testosterone: recommendations of the Prostate Cancer Clinical Trials Working Group. *J Clin Oncol* **26**, 1148-1159 (2008). https://doi.org:10.1200/JCO.2007.12.4487

49 Fuerea, A. *et al.* Early PSA response is an independent prognostic factor in patients with metastatic castration-resistant prostate cancer treated with next-generation androgen pathway inhibitors. *Eur J Cancer* **61**, 44-51 (2016). https://doi.org:10.1016/j.ejca.2016.03.070

50 Rescigno, P. *et al.* Prostate-specific Antigen Decline After 4 Weeks of Treatment with Abiraterone Acetate and Overall Survival in Patients with Metastatic Castration-resistant Prostate Cancer. *Eur Urol* **70**, 724-731 (2016). https://doi.org:10.1016/j.eururo.2016.02.055

51 Brasso, K. *et al.* Enzalutamide Antitumour Activity Against Metastatic Castration-resistant Prostate Cancer Previously Treated with Docetaxel and Abiraterone: A Multicentre Analysis. *Eur Urol* **68**, 317-324 (2015). https://doi.org:10.1016/j.eururo.2014.07.028

52 Prekovic, S. *et al.* Treatment-induced changes in the androgen receptor axis: Liquid biopsies as diagnostic/prognostic tools for prostate cancer. *Mol Cell Endocrinol* **462**, 56-63 (2018). https://doi.org:10.1016/j.mce.2017.08.020

53 Scher, H. I. *et al.* Circulating tumor cell biomarker panel as an individual-level surrogate for survival in metastatic castration-resistant prostate cancer. *J Clin Oncol* **33**, 1348-1355 (2015). https://doi.org:10.1200/JCO.2014.55.3487

54 Heller, G. *et al.* The Added Value of Circulating Tumor Cell Enumeration to Standard Markers in Assessing Prognosis in a Metastatic Castration-Resistant Prostate Cancer Population. *Clin Cancer Res* **23**, 1967-1973 (2017). https://doi.org:10.1158/1078-0432.CCR-16-1224

55 Lorente, D. *et al.* Decline in Circulating Tumor Cell Count and Treatment Outcome in Advanced Prostate Cancer. *Eur Urol* **70**, 985-992 (2016). https://doi.org:10.1016/j.eururo.2016.05.023

56 Attard, G. & Antonarakis, E. S. Prostate cancer: AR aberrations and resistance to abiraterone or enzalutamide. *Nat Rev Urol* **13**, 697-698 (2016). https://doi.org:10.1038/nrurol.2016.212

57 D'Amico, A. V. *et al.* Biochemical outcome after radical prostatectomy, external beam radiation therapy, or interstitial radiation therapy for clinically localized prostate cancer. *JAMA* **280**, 969-974 (1998). https://doi.org:10.1001/jama.280.11.969

58 Stelloo, S. *et al.* Androgen receptor profiling predicts prostate cancer outcome. *EMBO Mol Med* **7**, 1450-1464 (2015). https://doi.org:10.15252/emmm.201505424

59 Irshad, S. *et al.* A molecular signature predictive of indolent prostate cancer. *Sci Transl Med* **5**, 202ra122 (2013). https://doi.org:10.1126/scitranslmed.3006408

60 Knezevic, D. *et al.* Analytical validation of the Oncotype DX prostate cancer assay - a clinical RT-PCR assay optimized for prostate needle biopsies. *BMC Genomics* **14**, 690 (2013). https://doi.org:10.1186/1471-2164-14-690

61 Wyatt, A. W. *et al.* Genomic Alterations in Cell-Free DNA and Enzalutamide Resistance in Castration-Resistant Prostate Cancer. *JAMA Oncol* **2**, 1598-1606 (2016). https://doi.org:10.1001/jamaoncol.2016.0494

62 Conteduca, V. *et al.* Androgen receptor gene status in plasma DNA associates with worse outcome on enzalutamide or abiraterone for castration-resistant prostate cancer: a multi-institution correlative biomarker study. *Ann Oncol* **28**, 1508-1516 (2017). https://doi.org:10.1093/annonc/mdx155

63 Schwarzenbach, H. *et al.* Cell-free tumor DNA in blood plasma as a marker for circulating tumor cells in prostate cancer. *Clin Cancer Res* **15**, 1032-1038 (2009). https://doi.org:10.1158/1078-0432.CCR-08-1910

64 Diaz, L. A., Jr. & Bardelli, A. Liquid biopsies: genotyping circulating tumor DNA. *J Clin Oncol* **32**, 579-586 (2014). https://doi.org:10.1200/JCO.2012.45.2011

65 Salvi, S. *et al.* Circulating AR copy number and outcome to enzalutamide in docetaxel-treated metastatic castration-resistant prostate cancer. *Oncotarget* **7**, 37839-37845 (2016). https://doi.org:10.18632/oncotarget.9341

66 Antonarakis, E. S. *et al.* AR-V7 and resistance to enzalutamide and abiraterone in prostate cancer. *N Engl J Med* **371**, 1028-1038 (2014). https://doi.org:10.1056/NEJMoa1315815

67 Claessens, F. *et al.* Emerging mechanisms of enzalutamide resistance in prostate cancer. *Nat Rev Urol* **11**, 712-716 (2014). https://doi.org:10.1038/nrurol.2014.243

68 Kumar, A. *et al.* Substantial interindividual and limited intraindividual genomic diversity among tumors from men with metastatic prostate cancer. *Nat Med* **22**, 369-378 (2016). https://doi.org:10.1038/nm.4053

69 Coutinho, I., Day, T. K., Tilley, W. D. & Selth, L. A. Androgen receptor signaling in castration-resistant prostate cancer: a lesson in persistence. *Endocr Relat Cancer* **23**, T179-T197 (2016). https://doi.org:10.1530/ERC-16-0422

70 Pal, S. K. *et al.* Identification of mechanisms of resistance to treatment with abiraterone acetate or enzalutamide in patients with castration-resistant prostate cancer (CRPC). *Cancer* **124**, 1216-1224 (2018). https://doi.org:10.1002/cncr.31161

71 Rathkopf, D. E. *et al.* Androgen receptor mutations in patients with castration-resistant prostate cancer treated with apalutamide. *Ann Oncol* **28**, 2264-2271 (2017). https://doi.org:10.1093/annonc/mdx283

72 Taplin, M. E. *et al.* Selection for androgen receptor mutations in prostate cancers treated with androgen antagonist. *Cancer Res* **59**, 2511-2515 (1999).

73 Grossmann, M. E., Huang, H. & Tindall, D. J. Androgen receptor signaling in androgen-refractory prostate cancer. *J Natl Cancer Inst* **93**, 1687-1697 (2001). https://doi.org:10.1093/jnci/93.22.1687

74 Nadal, M. *et al.* Structure of the homodimeric androgen receptor ligand-binding domain. *Nat Commun* **8**, 14388 (2017). https://doi.org:10.1038/ncomms14388

75 Prekovic, S. *et al.* The Effect of F877L and T878A Mutations on Androgen Receptor Response to Enzalutamide. *Mol Cancer Ther* **15**, 1702-1712 (2016). https://doi.org:10.1158/1535-7163.MCT-15-0892

76 Lallous, N. *et al.* Functional analysis of androgen receptor mutations that confer anti-androgen resistance identified in circulating cell-free DNA from prostate cancer patients. *Genome Biol* **17**, 10 (2016). https://doi.org:10.1186/s13059-015-0864-1

77 Azad, A. A. *et al.* Androgen Receptor Gene Aberrations in Circulating Cell-Free DNA: Biomarkers of Therapeutic Resistance in Castration-Resistant Prostate Cancer. *Clin Cancer Res* **21**, 2315-2324 (2015). https://doi.org:10.1158/1078-0432.CCR-14-2666

78 Guo, Z. *et al.* A novel androgen receptor splice variant is up-regulated during prostate cancer progression and promotes androgen depletion-resistant growth. *Cancer Res* **69**, 2305-2313 (2009). https://doi.org:10.1158/0008-5472.CAN-08-3795

79 Hu, R. *et al.* Ligand-independent androgen receptor variants derived from splicing of cryptic exons signify hormone-refractory prostate cancer. *Cancer Res* **69**, 16-22 (2009). https://doi.org:10.1158/0008-5472.CAN-08-2764

80 Antonarakis, E. S., Armstrong, A. J., Dehm, S. M. & Luo, J. Androgen receptor variant-driven prostate cancer: clinical implications and therapeutic targeting. *Prostate Cancer Prostatic Dis* **19**, 231-241 (2016). https://doi.org:10.1038/pcan.2016.17

81 Scher, H. I. *et al.* Association of AR-V7 on Circulating Tumor Cells as a Treatment-Specific Biomarker With Outcomes and Survival in Castration-Resistant Prostate Cancer. *JAMA Oncol* **2**, 1441-1449 (2016). https://doi.org:10.1001/jamaoncol.2016.1828

82 Li, Y. *et al.* Androgen receptor splice variants mediate enzalutamide resistance in castration-resistant prostate cancer cell lines. *Cancer Res* **73**, 483-489 (2013). https://doi.org:10.1158/0008-5472.CAN-12-3630

83 Del Re, M. *et al.* The Detection of Androgen Receptor Splice Variant 7 in Plasma-derived Exosomal RNA Strongly Predicts Resistance to Hormonal Therapy in Metastatic Prostate Cancer Patients. *Eur Urol* **71**, 680-687 (2017). https://doi.org:10.1016/j.eururo.2016.08.012

84 Qu, F. *et al.* Association of AR-V7 and Prostate-Specific Antigen RNA Levels in Blood with Efficacy of Abiraterone Acetate and Enzalutamide Treatment in Men with Prostate Cancer. *Clin Cancer Res* **23**, 726-734 (2017). https://doi.org:10.1158/1078-0432.CCR-16-1070

85 Todenhofer, T. *et al.* AR-V7 Transcripts in Whole Blood RNA of Patients with Metastatic Castration Resistant Prostate Cancer Correlate with Response to Abiraterone Acetate. *J Urol* **197**, 135-142 (2017). https://doi.org:10.1016/j.juro.2016.06.094

86 Antonarakis, E. S. *et al.* Clinical Significance of Androgen Receptor Splice Variant-7 mRNA Detection in Circulating Tumor Cells of Men With Metastatic Castration-Resistant Prostate Cancer Treated With First- and Second-Line Abiraterone and Enzalutamide. *J Clin Oncol* **35**, 2149-2156 (2017). https://doi.org:10.1200/JCO.2016.70.1961

87 Li, J. *et al.* Aberrant corticosteroid metabolism in tumor cells enables GR takeover in enzalutamide resistant prostate cancer. *Elife* **6**, e20183 (2017). https://doi.org:10.7554/eLife.20183
88 Puhr, M. *et al.* The Glucocorticoid Receptor Is a Key Player for Prostate Cancer Cell Survival and a Target for Improved Antiandrogen Therapy. *Clin Cancer Res* **24**, 927-938 (2018). https://doi.org:10.1158/1078-0432.CCR-17-0989
89 Shah, N. *et al.* Regulation of the glucocorticoid receptor via a BET-dependent enhancer drives antiandrogen resistance in prostate cancer. *Elife* **6**, e27861 (2017). https://doi.org:10.7554/eLife.27861
90 Kach, J., Conzen, S. D. & Szmulewitz, R. Z. Targeting the glucocorticoid receptor in breast and prostate cancers. *Sci Transl Med* **7**, 305ps319 (2015). https://doi.org:10.1126/scitranslmed.aac7531
91 Arora, V. K. *et al.* Glucocorticoid receptor confers resistance to antiandrogens by bypassing androgen receptor blockade. *Cell* **155**, 1309-1322 (2013). https://doi.org:10.1016/j.cell.2013.11.012
92 Locke, J. A. *et al.* Androgen levels increase by intratumoral de novo steroidogenesis during progression of castration-resistant prostate cancer. *Cancer Res* **68**, 6407-6415 (2008). https://doi.org:10.1158/0008-5472.CAN-07-5997
93 Liu, C. *et al.* Inhibition of AKR1C3 Activation Overcomes Resistance to Abiraterone in Advanced Prostate Cancer. *Mol Cancer Ther* **16**, 35-44 (2017). https://doi.org:10.1158/1535-7163.MCT-16-0186
94 Liu, C. *et al.* Intracrine Androgens and AKR1C3 Activation Confer Resistance to Enzalutamide in Prostate Cancer. *Cancer Res* **75**, 1413-1422 (2015). https://doi.org:10.1158/0008-5472.CAN-14-3080
95 Hamid, A. R. *et al.* Aldo-keto reductase family 1 member C3 (AKR1C3) is a biomarker and therapeutic target for castration-resistant prostate cancer. *Mol Med* **18**, 1449-1455 (2013). https://doi.org:10.2119/molmed.2012.00296
96 Pfeiffer, M. J., Smit, F. P., Sedelaar, J. P. & Schalken, J. A. Steroidogenic enzymes and stem cell markers are upregulated during androgen deprivation in prostate cancer. *Mol Med* **17**, 657-664 (2011). https://doi.org:10.2119/molmed.2010.00143
97 Wako, K. *et al.* Expression of androgen receptor through androgen-converting enzymes is associated with biological aggressiveness in prostate cancer. *J Clin Pathol* **61**, 448-454 (2008). https://doi.org:10.1136/jcp.2007.050906
98 Pan, C.-x. *et al.* A phase Ib/II trial of indomethacin and enzalutamide to treat castration-resistant prostate cancer (CRPC). *Journal of Clinical Oncology* **36**, TPS394-TPS394 (2018). https://doi.org:10.1200/JCO.2018.36.6_suppl.TPS394
99 Cui, Y. *et al.* Upregulation of glucose metabolism by NF-kappaB2/p52 mediates enzalutamide resistance in castration-resistant prostate cancer cells. *Endocr Relat Cancer* **21**, 435-442 (2014). https://doi.org:10.1530/ERC-14-0107
100 Itkonen, H. M. *et al.* Inhibition of O-GlcNAc transferase activity reprograms prostate cancer cell metabolism. *Oncotarget* **7**, 12464-12476 (2016). https://doi.org:10.18632/oncotarget.7039
101 Nguyen, H. G. *et al.* Targeting autophagy overcomes Enzalutamide resistance in castration-resistant prostate cancer cells and improves therapeutic response in a xenograft model. *Oncogene* **33**, 4521-4530 (2014). https://doi.org:10.1038/onc.2014.25
102 Lee, E., Ha, S. & Logan, S. K. Divergent Androgen Receptor and Beta-Catenin Signaling in Prostate Cancer Cells. *PLoS One* **10**, e0141589 (2015). https://doi.org:10.1371/journal.pone.0141589
103 Liu, C. *et al.* Inhibition of constitutively active Stat3 reverses enzalutamide resistance in LNCaP derivative prostate cancer cells. *Prostate* **74**, 201-209 (2014). https://doi.org:10.1002/pros.22741
104 Sartor, O. & Gillessen, S. Treatment sequencing in metastatic castrate-resistant prostate cancer. *Asian J Androl* **16**, 426-431 (2014). https://doi.org:10.4103/1008-682X.126378

105 Rathkopf, D. E. *et al.* Updated interim efficacy analysis and long-term safety of abiraterone acetate in metastatic castration-resistant prostate cancer patients without prior chemotherapy (COU-AA-302). *Eur Urol* **66**, 815-825 (2014). https://doi.org:10.1016/j.eururo.2014.02.056

106 Ryan, C. J. *et al.* Abiraterone acetate plus prednisone versus placebo plus prednisone in chemotherapy-naive men with metastatic castration-resistant prostate cancer (COU-AA-302): final overall survival analysis of a randomised, double-blind, placebo-controlled phase 3 study. *Lancet Oncol* **16**, 152-160 (2015). https://doi.org:10.1016/S1470-2045(14)71205-7

107 De Bono, J. S. *et al.* Abiraterone and increased survival in metastatic prostate cancer. *New England Journal of Medicine* **364**, 1995-2005 (2011).

108 Fizazi, K. *et al.* Abiraterone acetate for treatment of metastatic castration-resistant prostate cancer: final overall survival analysis of the COU-AA-301 randomised, double-blind, placebo-controlled phase 3 study. *Lancet Oncol* **13**, 983-992 (2012). https://doi.org:10.1016/S1470-2045(12)70379-0

109 de Bono, J. S. *et al.* Prednisone plus cabazitaxel or mitoxantrone for metastatic castration-resistant prostate cancer progressing after docetaxel treatment: a randomised open-label trial. *Lancet* **376**, 1147-1154 (2010). https://doi.org:10.1016/S0140-6736(10)61389-X

110 Bahl, A. *et al.* Impact of cabazitaxel on 2-year survival and palliation of tumour-related pain in men with metastatic castration-resistant prostate cancer treated in the TROPIC trial. *Ann Oncol* **24**, 2402-2408 (2013). https://doi.org:10.1093/annonc/mdt194

111 Kantoff, P. W. *et al.* Sipuleucel-T immunotherapy for castration-resistant prostate cancer. *N Engl J Med* **363**, 411-422 (2010). https://doi.org:10.1056/NEJMoa1001294

112 Parker, C. *et al.* Alpha emitter radium-223 and survival in metastatic prostate cancer. *N Engl J Med* **369**, 213-223 (2013). https://doi.org:10.1056/NEJMoa1213755

113 Quinn, D. I., Sandler, H. M., Horvath, L. G., Goldkorn, A. & Eastham, J. A. The evolution of chemotherapy for the treatment of prostate cancer. *Ann Oncol* **28**, 2658-2669 (2017). https://doi.org:10.1093/annonc/mdx348

114 Paller, C. J. & Antonarakis, E. S. Cabazitaxel: a novel second-line treatment for metastatic castration-resistant prostate cancer. *Drug Des Devel Ther* **5**, 117-124 (2011). https://doi.org:10.2147/DDDT.S13029

115 Montgomery, R. B. *et al.* Maintenance of intratumoral androgens in metastatic prostate cancer: a mechanism for castration-resistant tumor growth. *Cancer Res* **68**, 4447-4454 (2008). https://doi.org:10.1158/0008-5472.CAN-08-0249

116 Richards, J. *et al.* Interactions of abiraterone, eplerenone, and prednisolone with wild-type and mutant androgen receptor: a rationale for increasing abiraterone exposure or combining with MDV3100. *Cancer Res* **72**, 2176-2182 (2012). https://doi.org:10.1158/0008-5472.CAN-11-3980

117 Soifer, H. S. *et al.* Direct regulation of androgen receptor activity by potent CYP17 inhibitors in prostate cancer cells. *J Biol Chem* **287**, 3777-3787 (2012). https://doi.org:10.1074/jbc.M111.261933

118 Li, Z. *et al.* Conversion of abiraterone to D4A drives anti-tumour activity in prostate cancer. *Nature* **523**, 347-351 (2015). https://doi.org:10.1038/nature14406

119 James, N. D. *et al.* Abiraterone for Prostate Cancer Not Previously Treated with Hormone Therapy. *N Engl J Med* **377**, 338-351 (2017). https://doi.org:10.1056/NEJMoa1702900

120 Fizazi, K. *et al.* Abiraterone plus Prednisone in Metastatic, Castration-Sensitive Prostate Cancer. *N Engl J Med* **377**, 352-360 (2017). https://doi.org:10.1056/NEJMoa1704174

121 Higano, C. S. *et al.* Sipuleucel-T. *Nat Rev Drug Discov* **9**, 513-514 (2010). https://doi.org:10.1038/nrd3220

122 Handy, C. E. & Antonarakis, E. S. Sipuleucel-T for the treatment of prostate cancer: novel insights and future directions. *Future Oncol* **14**, 907-917 (2018). https://doi.org:10.2217/fon-2017-0531

123 Di Lorenzo, G., Buonerba, C. & Kantoff, P. W. Immunotherapy for the treatment of prostate cancer. *Nat Rev Clin Oncol* **8**, 551-561 (2011). https://doi.org:10.1038/nrclinonc.2011.72

124 Antonarakis, E. S. *et al.* Antigen-Specific CD8 Lytic Phenotype Induced by Sipuleucel-T in Hormone-Sensitive or Castration-Resistant Prostate Cancer and Association With Overall Survival. *Clin Cancer Res* (2018). https://doi.org:10.1158/1078-0432.CCR-18-0638

125 Petrylak, D. P. *et al.* Overall survival and immune responses with sipuleucel-T and enzalutamide: STRIDE study. *Journal of Clinical Oncology* **36**, 246-246 (2018). https://doi.org:10.1200/JCO.2018.36.6_suppl.246

126 Fitzpatrick, J. M. *et al.* Optimal management of metastatic castration-resistant prostate cancer: highlights from a European Expert Consensus Panel. *Eur J Cancer* **50**, 1617-1627 (2014). https://doi.org:10.1016/j.ejca.2014.03.010

127 Henriksen, G., Breistol, K., Bruland, O. S., Fodstad, O. & Larsen, R. H. Significant antitumor effect from bone-seeking, alpha-particle-emitting (223)Ra demonstrated in an experimental skeletal metastases model. *Cancer Res* **62**, 3120-3125 (2002).

128 Bruland, O. S., Nilsson, S., Fisher, D. R. & Larsen, R. H. High-linear energy transfer irradiation targeted to skeletal metastases by the alpha-emitter 223Ra: adjuvant or alternative to conventional modalities? *Clin Cancer Res* **12**, 6250s-6257s (2006). https://doi.org:10.1158/1078-0432.CCR-06-0841

129 Deshayes, E. *et al.* Radium 223 dichloride for prostate cancer treatment. *Drug Des Devel Ther* **11**, 2643-2651 (2017). https://doi.org:10.2147/DDDT.S122417

130 Dellis, A. E. & Papatsoris, A. G. Apalutamide: the established and emerging roles in the treatment of advanced prostate cancer. *Expert Opin Investig Drugs* **27**, 553-559 (2018). https://doi.org:10.1080/13543784.2018.1484107

131 Shore, N. D. Darolutamide (ODM-201) for the treatment of prostate cancer. *Expert Opin Pharmacother* **18**, 945-952 (2017). https://doi.org:10.1080/14656566.2017.1329820

132 Imamura, Y. & Sadar, M. D. Androgen receptor targeted therapies in castration-resistant prostate cancer: Bench to clinic. *Int J Urol* **23**, 654-665 (2016). https://doi.org:10.1111/iju.13137

133 Higano, C. S. *et al.* Long-term Safety and Antitumor Activity in the Phase 1-2 Study of Enzalutamide in Pre- and Post-docetaxel Castration-Resistant Prostate Cancer. *Eur Urol* **68**, 795-801 (2015). https://doi.org:10.1016/j.eururo.2015.01.026

134 Smith, M. R. *et al.* Apalutamide Treatment and Metastasis-free Survival in Prostate Cancer. *N Engl J Med* **378**, 1408-1418 (2018). https://doi.org:10.1056/NEJMoa1715546

135 Liu, C. *et al.* Niclosamide inhibits androgen receptor variants expression and overcomes enzalutamide resistance in castration-resistant prostate cancer. *Clin Cancer Res* **20**, 3198-3210 (2014). https://doi.org:10.1158/1078-0432.CCR-13-3296

136 Schweizer, M. T. *et al.* A phase I study of niclosamide in combination with enzalutamide in men with castration-resistant prostate cancer. *PLoS One* **13**, e0198389 (2018). https://doi.org:10.1371/journal.pone.0198389

137 Bianchini, D. *et al.* Antitumour activity of enzalutamide (MDV3100) in patients with metastatic castration-resistant prostate cancer (CRPC) pre-treated with docetaxel and abiraterone. *Eur J Cancer* **50**, 78-84 (2014). https://doi.org:10.1016/j.ejca.2013.08.020

138 Cheng, H. H. *et al.* Activity of enzalutamide in men with metastatic castration-resistant prostate cancer is affected by prior treatment with abiraterone and/or docetaxel. *Prostate Cancer Prostatic Dis* **18**, 122-127 (2015). https://doi.org:10.1038/pcan.2014.53

139 Petrelli, F. *et al.* Enzalutamide after docetaxel and abiraterone acetate treatment in prostate cancer: a pooled analysis of 10 case series. *Clin Genitourin Cancer* **13**, 193-198 (2015). https://doi.org:10.1016/j.clgc.2014.10.006

140 Schrader, A. J. *et al.* Enzalutamide in castration-resistant prostate cancer patients progressing after docetaxel and abiraterone. *Eur Urol* **65**, 30-36 (2014). https://doi.org:10.1016/j.eururo.2013.06.042

141 Loriot, Y. *et al.* Antitumour activity of abiraterone acetate against metastatic castration-resistant prostate cancer progressing after docetaxel and enzalutamide (MDV3100). *Ann Oncol* **24**, 1807-1812 (2013). https://doi.org:10.1093/annonc/mdt136

142 Noonan, K. L. *et al.* Clinical activity of abiraterone acetate in patients with metastatic castration-resistant prostate cancer progressing after enzalutamide. *Ann Oncol* **24**, 1802-1807 (2013). https://doi.org:10.1093/annonc/mdt138

143 Badrising, S. K. *et al.* Enzalutamide as a Fourth- or Fifth-Line Treatment Option for Metastatic Castration-Resistant Prostate Cancer. *Oncology* **91**, 267-273 (2016). https://doi.org:10.1159/000448219

144 Aggarwal, R. *et al.* The effect of prior androgen synthesis inhibition on outcomes of subsequent therapy with docetaxel in patients with metastatic castrate-resistant prostate cancer: results from a retrospective analysis of a randomized phase 3 clinical trial (CALGB 90401) (Alliance). *Cancer* **119**, 3636-3643 (2013). https://doi.org:10.1002/cncr.28285

145 Mezynski, J. *et al.* Antitumour activity of docetaxel following treatment with the CYP17A1 inhibitor abiraterone: clinical evidence for cross-resistance? *Ann Oncol* **23**, 2943-2947 (2012). https://doi.org:10.1093/annonc/mds119

146 Suzman, D. L., Luber, B., Schweizer, M. T., Nadal, R. & Antonarakis, E. S. Clinical activity of enzalutamide versus docetaxel in men with castration-resistant prostate cancer progressing after abiraterone. *Prostate* **74**, 1278-1285 (2014). https://doi.org:10.1002/pros.22844

147 Kyriakopoulos, C. E. *et al.* Chemohormonal Therapy in Metastatic Hormone-Sensitive Prostate Cancer: Long-Term Survival Analysis of the Randomized Phase III E3805 CHAARTED Trial. *J Clin Oncol* **36**, 1080-1087 (2018). https://doi.org:10.1200/JCO.2017.75.3657

148 Sweeney, C. J. *et al.* Chemohormonal Therapy in Metastatic Hormone-Sensitive Prostate Cancer. *N Engl J Med* **373**, 737-746 (2015). https://doi.org:10.1056/NEJMoa1503747

149 Sweeney, C. *et al.* Long term efficacy and QOL data of chemohormonal therapy (C-HT) in low and high volume hormone naïve metastatic prostate cancer (PrCa): E3805 CHAARTED trial. *Annals of Oncology* **27**, 720PD (2016). https://doi.org:10.1093/annonc/mdw372.4

150 James, N. D. *et al.* Addition of docetaxel, zoledronic acid, or both to first-line long-term hormone therapy in prostate cancer (STAMPEDE): survival results from an adaptive, multiarm, multistage, platform randomised controlled trial. *Lancet* **387**, 1163-1177 (2016). https://doi.org:10.1016/S0140-6736(15)01037-5

151 Gillessen, S. *et al.* Management of Patients with Advanced Prostate Cancer: The Report of the Advanced Prostate Cancer Consensus Conference APCCC 2017. *Eur Urol* **73**, 178-211 (2018). https://doi.org:10.1016/j.eururo.2017.06.002

152 Sternberg, C. N. Improving Survival for Metastatic Castrate-resistant Prostate Cancer: Will Combination Therapy Help Us To Move Forward? *Eur Urol* **70**, 722-723 (2016). https://doi.org:10.1016/j.eururo.2016.05.030

153 Morris, M. J. *et al.* Phase Ib Study of Enzalutamide in Combination with Docetaxel in Men with Metastatic Castration-Resistant Prostate Cancer. *Clin Cancer Res* **22**, 3774-3781 (2016). https://doi.org:10.1158/1078-0432.CCR-15-2638

154 de Bono, J. S. *et al.* Antitumour Activity and Safety of Enzalutamide in Patients with Metastatic Castration-resistant Prostate Cancer Previously Treated with Abiraterone Acetate Plus Prednisone for >/=24 weeks in Europe. *Eur Urol* **74**, 37-45 (2018). https://doi.org:10.1016/j.eururo.2017.07.035

155 Badrising, S. K. *et al.* Prognostic parameters for response to enzalutamide after docetaxel and abiraterone treatment in metastatic castration-resistant prostate cancer patients; a possible time relation. *Prostate* **76**, 32-40 (2016). https://doi.org:10.1002/pros.23094

156 Izumi, K. *et al.* Enzalutamide versus abiraterone as a first-line endocrine therapy for castration-resistant prostate cancer (ENABLE study for PCa): a study protocol for a multicenter randomized phase III trial. *BMC Cancer* **17**, 677 (2017). https://doi.org:10.1186/s12885-017-3661-2

157 Chi, K. N. *et al.* A randomized phase II cross-over study of abiraterone + prednisone (ABI) vs enzalutamide (ENZ) for patients (pts) with metastatic, castration-resistant prostate cancer (mCRPC). *Journal of Clinical Oncology* **35**, 5002-5002 (2017). https://doi.org:10.1200/JCO.2017.35.15_suppl.5002

158 Schweizer, M. T. *et al.* Effect of bipolar androgen therapy for asymptomatic men with castration-resistant prostate cancer: results from a pilot clinical study. *Sci Transl Med* **7**, 269ra262 (2015). https://doi.org:10.1126/scitranslmed.3010563

159 Teply, B. A. *et al.* Bipolar androgen therapy in men with metastatic castration-resistant prostate cancer after progression on enzalutamide: an open-label, phase 2, multicohort study. *Lancet Oncol* **19**, 76-86 (2018). https://doi.org:10.1016/S1470-2045(17)30906-3

160 Gillessen, S., de Bono, J. S., Sartor, O. & Omlin, A. G. Reply to Finn E. von Eyben, Irene Virgolini and Giandomenico Roviello's Letter to the Editor re: Silke Gillessen, Gerhardt Attard, Tomasz M. Beer, et al. Management of Patients with Advanced Prostate Cancer: The Report of the Advanced Prostate Cancer Consensus Conference APCCC 2017. Eur Urol 2018;73:178-211. *Eur Urol* **73**, e32-e33 (2018). https://doi.org:10.1016/j.eururo.2017.08.014

161 Robinson, D. *et al.* Integrative clinical genomics of advanced prostate cancer. *Cell* **161**, 1215-1228 (2015). https://doi.org:10.1016/j.cell.2015.05.001

162 Pritchard, C. C. *et al.* Inherited DNA-Repair Gene Mutations in Men with Metastatic Prostate Cancer. *N Engl J Med* **375**, 443-453 (2016). https://doi.org:10.1056/NEJMoa1603144

163 Mateo, J. *et al.* DNA-Repair Defects and Olaparib in Metastatic Prostate Cancer. *N Engl J Med* **373**, 1697-1708 (2015). https://doi.org:10.1056/NEJMoa1506859

164 Bennett, R. L. & Licht, J. D. Targeting Epigenetics in Cancer. *Annu Rev Pharmacol Toxicol* **58**, 187-207 (2018). https://doi.org:10.1146/annurev-pharmtox-010716-105106

165 Li, L. C., Carroll, P. R. & Dahiya, R. Epigenetic changes in prostate cancer: implication for diagnosis and treatment. *J Natl Cancer Inst* **97**, 103-115 (2005). https://doi.org:10.1093/jnci/dji010

166 Metzger, E. *et al.* LSD1 demethylates repressive histone marks to promote androgen-receptor-dependent transcription. *Nature* **437**, 436-439 (2005). https://doi.org:10.1038/nature04020

167 Spans, L. *et al.* Genomic and epigenomic analysis of high-risk prostate cancer reveals changes in hydroxymethylation and TET1. *Oncotarget* **7**, 24326-24338 (2016). https://doi.org:10.18632/oncotarget.8220

168 Padmanabhan, B., Mathur, S., Manjula, R. & Tripathi, S. Bromodomain and extra-terminal (BET) family proteins: New therapeutic targets in major diseases. *J Biosci* **41**, 295-311 (2016). https://doi.org:10.1007/s12038-016-9600-6

169 Jang, M. K. *et al.* The bromodomain protein Brd4 is a positive regulatory component of P-TEFb and stimulates RNA polymerase II-dependent transcription. *Mol Cell* **19**, 523-534 (2005). https://doi.org:10.1016/j.molcel.2005.06.027

170 Asangani, I. A. *et al.* Therapeutic targeting of BET bromodomain proteins in castration-resistant prostate cancer. *Nature* **510**, 278-282 (2014). https://doi.org:10.1038/nature13229

171 Filippakopoulos, P. *et al.* Selective inhibition of BET bromodomains. *Nature* **468**, 1067-1073 (2010). https://doi.org:10.1038/nature09504

172 Asangani, I. A. *et al.* BET Bromodomain Inhibitors Enhance Efficacy and Disrupt Resistance to AR Antagonists in the Treatment of Prostate Cancer. *Mol Cancer Res* **14**, 324-331 (2016). https://doi.org:10.1158/1541-7786.MCR-15-0472

173 Welti, J. *et al.* Targeting Bromodomain and Extra-Terminal (BET) Family Proteins in Castration-Resistant Prostate Cancer (CRPC). *Clin Cancer Res* **24**, 3149-3162 (2018). https://doi.org:10.1158/1078-0432.CCR-17-3571

174 Yang, Z. *et al.* Recruitment of P-TEFb for stimulation of transcriptional elongation by the bromodomain protein Brd4. *Mol Cell* **19**, 535-545 (2005). https://doi.org:10.1016/j.molcel.2005.06.029

175 Urbanucci, A. *et al.* Androgen Receptor Deregulation Drives Bromodomain-Mediated Chromatin Alterations in Prostate Cancer. *Cell Rep* **19**, 2045-2059 (2017). https://doi.org:10.1016/j.celrep.2017.05.049

176 Hodi, F. S. *et al.* Improved survival with ipilimumab in patients with metastatic melanoma. *N Engl J Med* **363**, 711-723 (2010). https://doi.org:10.1056/NEJMoa1003466

177 Powles, T. *et al.* MPDL3280A (anti-PD-L1) treatment leads to clinical activity in metastatic bladder cancer. *Nature* **515**, 558-562 (2014). https://doi.org:10.1038/nature13904

178 Rizvi, N. A. *et al.* Cancer immunology. Mutational landscape determines sensitivity to PD-1 blockade in non-small cell lung cancer. *Science* **348**, 124-128 (2015). https://doi.org:10.1126/science.aaa1348

179 Spranger, S. Mechanisms of tumor escape in the context of the T-cell-inflamed and the non-T-cell-inflamed tumor microenvironment. *Int Immunol* **28**, 383-391 (2016). https://doi.org:10.1093/intimm/dxw014

180 Wargo, J. A., Reddy, S. M., Reuben, A. & Sharma, P. Monitoring immune responses in the tumor microenvironment. *Curr Opin Immunol* **41**, 23-31 (2016). https://doi.org:10.1016/j.coi.2016.05.006

181 Sartor, O. & de Bono, J. S. Metastatic Prostate Cancer. *N Engl J Med* **378**, 645-657 (2018). https://doi.org:10.1056/NEJMra1701695

182 Zehir, A. *et al.* Mutational landscape of metastatic cancer revealed from prospective clinical sequencing of 10,000 patients. *Nat Med* **23**, 703-713 (2017). https://doi.org:10.1038/nm.4333

183 Stelloo, S. *et al.* Endogenous androgen receptor proteomic profiling reveals genomic subcomplex involved in prostate tumorigenesis. *Oncogene* **37**, 313-322 (2018). https://doi.org:10.1038/onc.2017.330

184 Paltoglou, S. *et al.* Novel Androgen Receptor Coregulator GRHL2 Exerts Both Oncogenic and Antimetastatic Functions in Prostate Cancer. *Cancer Res* **77**, 3417-3430 (2017). https://doi.org:10.1158/0008-5472.CAN-16-1616

185 Heemers, H. V. & Tindall, D. J. Androgen receptor (AR) coregulators: a diversity of functions converging on and regulating the AR transcriptional complex. *Endocr Rev* **28**, 778-808 (2007). https://doi.org:10.1210/er.2007-0019

186 Jin, L. *et al.* Therapeutic Targeting of the CBP/p300 Bromodomain Blocks the Growth of Castration-Resistant Prostate Cancer. *Cancer Res* **77**, 5564-5575 (2017). https://doi.org:10.1158/0008-5472.CAN-17-0314

187 Lasko, L. M. *et al.* Discovery of a selective catalytic p300/CBP inhibitor that targets lineage-specific tumours. *Nature* **550**, 128-132 (2017). https://doi.org:10.1038/nature24028

188 Pegg, N. *et al.* Characterisation of CCS1477: A novel small molecule inhibitor of p300/CBP for the treatment of castration resistant prostate cancer. *Journal of Clinical Oncology* **35**, 11590-11590 (2017). https://doi.org:10.1200/JCO.2017.35.15_suppl.11590

189 Debes, J. D. *et al.* p300 in prostate cancer proliferation and progression. *Cancer Res* **63**, 7638-7640 (2003).
190 Heemers, H. V. *et al.* Androgen deprivation increases p300 expression in prostate cancer cells. *Cancer Res* **67**, 3422-3430 (2007). https://doi.org:10.1158/0008-5472.CAN-06-2836
191 Lonard, D. M. & O'Malley, B. W. Molecular Pathways: Targeting Steroid Receptor Coactivators in Cancer. *Clin Cancer Res* **22**, 5403-5407 (2016). https://doi.org:10.1158/1078-0432.CCR-15-1958
192 Gnanapragasam, V. J., Leung, H. Y., Pulimood, A. S., Neal, D. E. & Robson, C. N. Expression of RAC 3, a steroid hormone receptor co-activator in prostate cancer. *Br J Cancer* **85**, 1928-1936 (2001). https://doi.org:10.1054/bjoc.2001.2179
193 Zhou, H. J. *et al.* SRC-3 is required for prostate cancer cell proliferation and survival. *Cancer Res* **65**, 7976-7983 (2005). https://doi.org:10.1158/0008-5472.CAN-04-4076
194 Zhou, X. E. *et al.* Identification of SRC3/AIB1 as a preferred coactivator for hormone-activated androgen receptor. *J Biol Chem* **285**, 9161-9171 (2010). https://doi.org:10.1074/jbc.M109.085779
195 Taylor, B. S. *et al.* Integrative genomic profiling of human prostate cancer. *Cancer Cell* **18**, 11-22 (2010). https://doi.org:10.1016/j.ccr.2010.05.026
196 Song, X. *et al.* Development of potent small-molecule inhibitors to drug the undruggable steroid receptor coactivator-3. *Proc Natl Acad Sci U S A* **113**, 4970-4975 (2016). https://doi.org:10.1073/pnas.1604274113
197 Wang, L. *et al.* Characterization of a Steroid Receptor Coactivator Small Molecule Stimulator that Overstimulates Cancer Cells and Leads to Cell Stress and Death. *Cancer Cell* **28**, 240-252 (2015). https://doi.org:10.1016/j.ccell.2015.07.005
198 Tomlins, S. A. *et al.* Recurrent fusion of TMPRSS2 and ETS transcription factor genes in prostate cancer. *Science* **310**, 644-648 (2005). https://doi.org:10.1126/science.1117679
199 Cancer Genome Atlas Research, N. The Molecular Taxonomy of Primary Prostate Cancer. *Cell* **163**, 1011-1025 (2015). https://doi.org:10.1016/j.cell.2015.10.025
200 Kron, K. J. *et al.* TMPRSS2-ERG fusion co-opts master transcription factors and activates NOTCH signaling in primary prostate cancer. *Nat Genet* **49**, 1336-1345 (2017). https://doi.org:10.1038/ng.3930
201 Tomlins, S. A. *et al.* Role of the TMPRSS2-ERG gene fusion in prostate cancer. *Neoplasia* **10**, 177-188 (2008). https://doi.org:10.1593/neo.07822
202 Mounir, Z. *et al.* TMPRSS2:ERG blocks neuroendocrine and luminal cell differentiation to maintain prostate cancer proliferation. *Oncogene* **34**, 3815-3825 (2015). https://doi.org:10.1038/onc.2014.308
203 Kissick, H. T., Sanda, M. G., Dunn, L. K. & Arredouani, M. S. Development of a peptide-based vaccine targeting TMPRSS2:ERG fusion-positive prostate cancer. *Cancer Immunol Immunother* **62**, 1831-1840 (2013). https://doi.org:10.1007/s00262-013-1482-y
204 Shao, L. *et al.* Highly specific targeting of the TMPRSS2/ERG fusion gene using liposomal nanovectors. *Clin Cancer Res* **18**, 6648-6657 (2012). https://doi.org:10.1158/1078-0432.CCR-12-2715
205 Wang, X. *et al.* Development of Peptidomimetic Inhibitors of the ERG Gene Fusion Product in Prostate Cancer. *Cancer Cell* **31**, 844-847 (2017). https://doi.org:10.1016/j.ccell.2017.05.001
206 Epstein, J. I. *et al.* Proposed morphologic classification of prostate cancer with neuroendocrine differentiation. *Am J Surg Pathol* **38**, 756-767 (2014). https://doi.org:10.1097/PAS.0000000000000208
207 Beltran, H. *et al.* Divergent clonal evolution of castration-resistant neuroendocrine prostate cancer. *Nat Med* **22**, 298-305 (2016). https://doi.org:10.1038/nm.4045
208 Aparicio, A. M. *et al.* Platinum-based chemotherapy for variant castrate-resistant prostate cancer. *Clin Cancer Res* **19**, 3621-3630 (2013). https://doi.org:10.1158/1078-0432.CCR-12-3791

RESEARCH ARTICLE

Drug-induced epigenomic plasticity reprograms circadian rhythm regulation to drive prostate cancer toward androgen-independence

Simon Linder[‡], Marlous Hoogstraat[‡], Suzan Stelloo, Nils Eickhoff, Karianne Schuurman, Hilda de Barros, Maartje Alkemade, Elise M. Bekers, Tesa M. Severson, Joyce Sanders, Chia-Chi Flora Huang, Tunc Morova, Umut Berkay Altintas, Liesbeth Hoekman, Yongsoo Kim, Sylvan C. Baca, Martin Sjöström, Anniek Zaalberg, Dorine C. Hintzen, Jeroen de Jong, Roelof J.C. Kluin, Iris de Rink, Claudia Giambartolomei, Ji-Heui Seo, Bogdan Pasaniuc, Maarten Altelaar, René H. Medema, Felix Y. Feng, Amina Zoubeidi, Matthew L. Freedman, Lodewyk F.A. Wessels, Lisa M. Butler, Nathan A. Lack, Henk van der Poel[#], Andries M. Bergman[#], and Wilbert Zwart[#]

[‡] These authors contributed equally to this work as co-first authors.
[#] These authors contributed equally to this work as co-senior authors.

Adapted from *Cancer Discovery* 12 (9), 2074-2097 (2022).

Abstract

In prostate cancer, androgen receptor (AR)–targeting agents are very effective in various disease stages. However, therapy resistance inevitably occurs, and little is known about how tumor cells adapt to bypass AR suppression. Here, we performed integrative multi-omics analyses on tissues isolated before and after 3 months of AR-targeting enzalutamide monotherapy from patients with high-risk prostate cancer enrolled in a neoadjuvant clinical trial. Transcriptomic analyses demonstrated that AR inhibition drove tumors toward a neuroendocrine-like disease state. Additionally, epigenomic profiling revealed massive enzalutamide-induced reprogramming of pioneer factor FOXA1 from inactive chromatin sites toward active *cis*-regulatory elements that dictate prosurvival signals. Notably, treatment-induced FOXA1 sites were enriched for the circadian clock component ARNTL. Posttreatment ARNTL levels were associated with patients' clinical outcomes, and ARNTL knockout strongly decreased prostate cancer cell growth. Our data highlight a remarkable cistromic plasticity of FOXA1 following AR-targeted therapy and revealed an acquired dependency on the circadian regulator ARNTL, a novel candidate therapeutic target.

Significance

Understanding how prostate cancers adapt to AR-targeted interventions is critical for identifying novel drug targets to improve the clinical management of treatment-resistant disease. Our study revealed an enzalutamide-induced epigenomic plasticity toward prosurvival signaling and uncovered the circadian regulator ARNTL as an acquired vulnerability after AR inhibition, presenting a novel lead for therapeutic development.

Introduction

Androgen ablation is the mainstay treatment for patients with metastatic prostate cancer (PCa), ever since the direct critical link between androgens and prostate tumor progression was first described[1]. The androgen receptor (AR) is the key driver of PCa development and progression, and multiple therapeutic strategies have been developed over the years to effectively block the activity of this hormone-driven transcription factor. Upon androgen binding, AR associates with the chromatin at distal *cis*-regulatory enhancer elements, where it regulates the expression of genes through long-range chromatin interactions in three-dimensional genomic space[2,3]. AR does not operate in isolation, but rather recruits a large spectrum of coregulators and other transcription factors to promote expression of genes that drive cancer cell proliferation[4]. Critical AR interactors in the transcription complex are HOXB13 and FOXA1, which are both upregulated in primary PCa[4-6] and demarcate enhancers that drive not only primary tumorigenesis but also metastatic disease progression[7]. Mechanistically, FOXA1 acts as a pioneer factor, rendering the chromatin accessible for AR to bind[8-11]. *FOXA1* is frequently mutated in PCa[12-16] which was shown to alter its pioneering capacities, perturb luminal epithelial differentiation programs, and promote tumor growth, further highlighting the critical role of FOXA1 in human prostate tumors[17,18].

Most patients are diagnosed with organ-confined PCa, which can potentially be cured through locoregional therapies, such as surgery (radical prostatectomy), radiotherapy and/or brachytherapy[19]. However, approximately 30% of these patients experience a biochemical recurrence (BCR) – a rise in prostate-specific antigen (PSA) serum levels – indicating PCa relapse[20]. At this stage of the disease, suppression of androgen production is a commonly applied therapeutic intervention that can delay further cancer progression for years[21,22]. Nevertheless, the development of resistance to androgen deprivation is inevitable, resulting in castration-resistant prostate cancer (CRPC) for which there is no cure[23]. Most CRPC tumors acquired molecular features that enable active AR signaling despite low circulating androgen levels, a finding that led to the development of several highly effective AR-targeted therapies. Enzalutamide (ENZ) is one of the most frequently used AR-targeting agents, which functions through a combined mechanism of blocked AR nuclear import, diminished AR chromatin binding and decreased transcription complex formation, effectively impairing AR-driven PCa growth[24]. ENZ's potent anti-tumor activity has been demonstrated in multiple clinical trials, which led to its FDA approval in various PCa disease stages – from metastatic CRPC[25,26], to metastatic hormone-sensitive[27], and even non-metastatic CRPC[28] – illustrating how AR-targeted therapies are being progressively introduced earlier in clinical practice. A clinical benefit of ENZ monotherapy as a neoadjuvant treatment

prior to prostatectomy for patients with localized disease, has not been established. Although effective in the CRPC setting, resistance to AR pathway inhibition will ultimately develop, and the management of advanced PCa with this acquired resistance remains a major clinical challenge, especially since the underlying mechanisms are still not fully elucidated[29]. Therefore, furthering our understanding of how ENZ affects PCa biology may lead to the identification of acquired cellular vulnerabilities that could be therapeutically exploited.

To study global drug-induced transcriptional and epigenetic plasticity in human prostate tumors and identify cellular adaptation mechanisms to evade drug treatment, we designed a phase 2 clinical trial to perform multi-omics studies in pre- and post-treatment samples from high-risk localized PCa patients, treated with neoadjuvant ENZ monotherapy. We identified transcriptional reprogramming after treatment, with deactivation of AR signaling and an activation of cell plasticity with neuroendocrine (NE)-like features upon 3 months of AR suppression. Post treatment, these tumors harbored a distinct set of 1,430 *de novo* occupied FOXA1-positive *cis*-regulatory elements, positive for – yet independent of – AR activity, which are dictated by circadian clock core regulator ARNTL to drive tumor cell proliferation instead. Using ARNTL knockout experiments we could further enhance ENZ sensitivity in cell line and xenograft models, revealing an unexpected biological interplay between hormonal resistance and circadian rhythm regulation, and identifying a novel highly promising candidate drug target in the clinical management of primary high-risk PCa.

Results

Neoadjuvant ENZ therapy for patients with high-risk localized prostate cancer

To study how early ENZ intervention affects prostate tumor biology in a non-castrate environment, we performed integrative multi-omics analyses as part of a single-arm, open-label phase 2 clinical trial: the DARANA study (Dynamics of Androgen Receptor Genomics and Transcriptomics After Neoadjuvant Androgen Ablation; ClinicalTrials.gov number, NCT03297385). In this trial, 56 men with primary high-risk (Gleason score ≥ 7) PCa were enrolled (**Fig. 1A**). Patient demographics and disease characteristics are summarized in **Table 1**, and clinical outcomes of this study are discussed in the Supplementary Data (Supplementary Fig. S1A-F; Supplementary Table S1). Prior to ENZ therapy, magnetic resonance imaging (MRI)-guided core needle tumor biopsies were taken – hereafter referred to as the pre-treatment setting. Subsequently, patients received neoadjuvant ENZ treatment (160 mg/day) without additional androgen deprivation therapy for three months, followed by robotic-assisted laparoscopic prostatectomy. Based on baseline MRI information and palpation, additional tumor-targeted core needle biopsies were taken *ex vivo* – representing the post-treatment setting. This pre- and post-treatment sampling allowed us to study the epigenetic, genomic, transcriptomic and proteomic effects of neoadjuvant ENZ therapy in individual patients (**Fig. 1A**). We generated chromatin immunoprecipitation (ChIP-seq) profiles of the prostate cancer drivers AR and FOXA1, as well as the histone modification H3K27ac before and after ENZ treatment, and integrated these cistromic findings with pre- and post-treatment gene expression (RNA-seq), copy number (CNV-seq) and immunohistochemistry (IHC) data from the same tumors. Stringent quality control (QC) analyses were performed on all data streams (Supplementary Fig. S2), and the following number of samples passed all QC measures (**Fig. 1B**): AR ChIP-seq (pre: $n = 10$; post: $n = 12$), FOXA1 ChIP-seq (pre: $n = 17$; post: $n = 17$), H3K27ac ChIP-seq (pre: $n = 24$; post: $n = 23$), CNV-seq (pre: $n = 24$; post: $n = 24$), RNA-seq (pre: $n = 42$; post: $n = 52$) and IHC (post: $n = 51$).

Collectively, we performed integrative multi-omics analyses as part of a clinical trial that enabled us to examine ENZ-induced oncogenomic changes to identify early epigenetic steps in treatment response, but also therapy-induced resistance.

Table 1: Characteristics of the DARANA cohort.

DARANA cohort (*N* = 56)		
Age, years (95% CI)	67 (65-68)	
Baseline PSA level, ng/mL (95% CI)	12.8 (10.4-15.2)	
Baseline ISUP grade, *n* (%)		
ISUP GG1 (GS 3+3)	0 (0)	
ISUP GG2 (GS 3+4)	16 (28)	
ISUP GG3 (GS 4+3)	9 (16)	
ISUP GG4 (GS 4+4, 3+5, 5+3)	20 (36)	
ISUP GG5 (GS 4+5, 5+4, 5+5)	11 (20)	
T-stage (T), *n* (%)	Pre (cT)	Post (ypT)
T1	1 (2)	0 (0)
T2	25 (44)	20 (36)
T3	29 (52)	36 (64)
T4	1 (2)	0 (0)
Lymph node status (N), *n* (%)	Pre (cN)	Post (ypN)
N0	53 (95)	39 (70)
N1	3 (5)	17 (30)
Surgical margins, *n* (%)		
Negative	39 (70)	
Positive	17 (30)	
Biochemical recurrence (BCR), *n* (%)	23 (41)	
5-year BCR-free survival – % (95% CI)	38 (28-51)	
Radiological recurrence (RR), *n* (%)	18 (32)	
5-year RR-free survival – % (95% CI)	64 (50-82)	
ADT salvage therapy (ADT), *n* (%)	15 (27)	
5-year ADT-free survival – % (95% CI)	67 (53-85)	
Distant metastasis (DM), *n* (%)	16 (28)	
5-year DM-free survival – % (95% CI)	74 (61-91)	
Mean time to last follow-up – months (95% CI)	51 (47-55)	

NOTE: Table summarizing the patient baseline demographics, and pre- and post-treatment disease characteristics of the DARANA cohort. Shown are age (years), initial serum PSA levels (ng/mL) and International Society of Urological Pathology (ISUP) grade group (GG) at diagnosis [with associated Gleason scores (GS)]. In addition, T-stage (T) and Lymph node status (N) before (pre = at diagnosis) and after (post = at surgery) neoadjuvant ENZ therapy, as well as the surgical margin status of the prostatectomy specimens are shown. Pre-treatment measures are based on histological evaluation of biopsy material and radiographic evaluation (clinical grading; c), while post-treatment assessments are based on histological evaluations of prostatectomy specimens (pathological grading after neoadjuvant therapy; yp). Biochemical recurrence (BCR) was defined as a rise in PSA of ≥ 0.2 ng/mL at two consecutive time points, radiological recurrence (RR) was defined as detection of local

Table 1: Continued.

or distant metastases by PSMA PET scanning, ADT salvage therapy was defined as the onset of ADT, and distant metastases (DM) were defined as detection of distant metastases by PSMA PET scanning (M1a-c). 5-year recurrence-free survival (% of patients and 95% CI) and time to last follow-up (months) are indicated. For continuous variables (age, baseline PSA, and time to last follow-up) the mean and 95% confidence interval (CI) are shown. For categorical variables (baseline ISUP GG, T stage, N status, surgical margins, BCR, RR, ADT, and DM) the number of patients (*n*) and percentages (%) are indicated.

Characterization of tissue ChIP-seq data

To assess how neoadjuvant ENZ treatment affects the *cis*-regulatory landscape in primary PCa, we generated human tumor ChIP-seq profiles for the transcription factors AR and FOXA1, along with the active enhancer/promoter histone mark H3K27ac before and after neoadjuvant intervention. ChIP-seq quality metrics are summarized in the Supplementary Data (Supplementary Fig. S3A-E; Supplementary Table S2). Visual inspection at known AR target genes showed high-quality data for all ChIP-factors in both clinical settings (**Fig. 2A**). On a genome-wide scale, the H3K27ac ChIP-seq profiles were highly distinct from the transcription factors (TFs) and divided the samples into two main clusters irrespective of their treatment status (**Fig. 2B and 2C**). Notably, AR and FOXA1 ChIP-seq datasets were intermingled in the clustering analysis, suggesting largely comparable binding profiles which is in line with FOXA1's role as a canonical AR pioneer factor (Supplementary Fig. S4)[5,30]. As described previously[31], highest Pearson correlation was found between H3K27ac samples, indicating comparable histone acetylation profiles among primary PCa samples (**Fig. 2B**; Supplementary Fig. S4). Much greater heterogeneity in chromatin binding was observed for the TFs AR and FOXA1, which is further supported by the steep decrease in the number of overlapping AR and FOXA1 peaks with increasing number of samples compared to H3K27ac (**Fig. 2D**; Supplementary Fig. S4). Heterogeneity was comparable when separately analyzing pre- versus post-treatment specimens, and in the same order of magnitude as compared to previous reports describing TF cistromics and epigenomics in clinical samples[31,32] (Supplementary Fig. S5A and S5B) with comparable overlap of peaks for AR and FOXA1 (Supplementary Fig. S5C and S5D). In order to maintain the high-confidence peaks that have been reproducibly identified in multiple patients without losing too much binding site heterogeneity between samples, we decided to generate consensus peaksets. To this end, we only considered binding sites that were present in at least 3 out of 22 AR samples, 7 out of 34 FOXA1 samples and 13 out of 47 H3K27ac samples, which corresponds to ~25% of all binding sites identified for each factor (**Fig. 2D**). Genomic distribution analyses of these consensus sites revealed distinct enrichments for annotated genomic regions: While AR and FOXA1 were almost exclusively found at intronic and distal intergenic regions, H3K27ac peaks were also enriched at promoters (**Fig. 2E**), which is in line with previously published genomic distributions of AR[5,31], FOXA1[5,9], and H3K27ac[31,33]. In addition,

motif enrichment analyses at AR and FOXA1 consensus peaks identified, as expected, androgen and Forkhead response elements among the top-ranked motifs, respectively (**Fig. 2F**). Analyses on correlations between factors (**Fig. 2B-D**), genomic distributions (**Fig. 2E**) and motif enrichment (**Fig. 2F**) were repeated for the pre-treatment samples exclusively, supporting the same conclusions (Supplementary Fig. S6A-E).

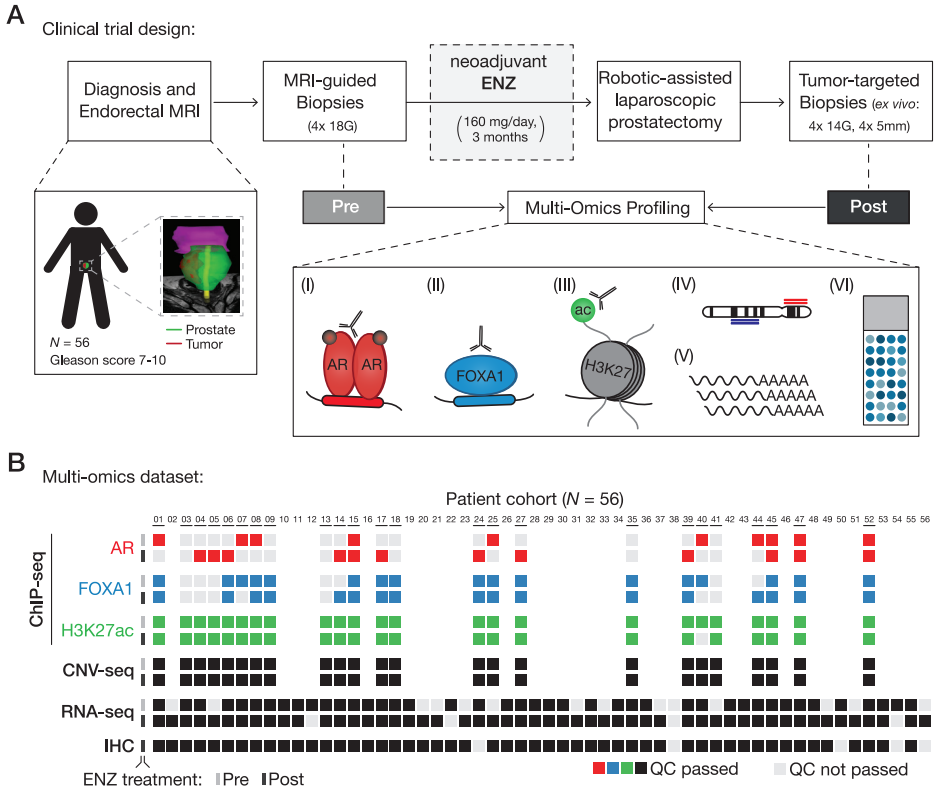

Figure 1: Clinical trial design and omics data sample collection. (**A**) Study design of the DARANA trial (NCT03297385). Multi-omics profiling, consisting of (I) Androgen Receptor (AR) ChIP-seq, (II) FOXA1 ChIP-seq, (III) H3K27ac ChIP-seq, (IV) DNA copy number sequencing (CNV-seq), (V) gene expression profiling (RNA-seq) and (VI) immunohistochemistry (IHC) analysis, was performed on MRI-guided biopsy samples prior to ENZ treatment (Pre) and tumor-target prostatectomy specimens after 3 months of neoadjuvant ENZ therapy (Post). (**B**) Overview of data availability and quality control analyses for each sample. Individual data streams are indicated separately with ChIP-seq for AR (red), FOXA1 (blue), H3K27ac (green), CNV-seq, RNA-seq and IHC (all black). The ENZ treatment status indicates the pre-treatment (top) and post-treatment samples (bottom) per omics dataset. Samples not passing QC (light gray) were successfully applied for focused raw data analyses. Blank spots for ChIP-seq or CNV-seq samples indicate that the fresh-frozen material didn't pass the tumor cell percentage cutoff of ≥ 50%.

Taken together, we generated multiple high-quality tissue ChIP-seq data streams that now allowed us to study ENZ-induced changes in primary PCa patients.

ENZ treatment enriches for newly acquired FOXA1-bound regulatory regions

To identify ENZ-induced TF reprogramming and epigenetic changes, we performed differential binding analyses comparing the pre- and post-treatment tissue ChIP-seq samples. Therefore, we first ran occupancy-based unsupervised principal component analyses (PCA) to detect whether ENZ treatment led to differences in TF chromatin binding. While the sample size of the AR ChIP-seq data stream was not sufficient to observe significant differences in peak occupancy pre- versus post-treatment (Supplementary Fig. S7A), the FOXA1 data did show such differences, with a clear separation of pre- and post-treatment FOXA1 samples in the second principal component (**Fig. 3A**). Subsequent supervised analysis (pre vs. post) revealed a total of 1,905 genomic regions [475 pretreatment-enriched (pre-enriched), 1,430 posttreatment-enriched (post-enriched); Supplementary Table S3] that showed significant differential FOXA1 binding between both clinical settings [false discovery rate (FDR) < 0.05; **Fig. 3B and 3C**; Supplementary Fig. S7B-D]. Further characterization of these differential FOXA1 regions showed that both sets of binding sites were still preferentially located in intronic and distal intergenic regions (with a slight enrichment for promoters at the post-enriched sites; Supplementary Fig. S7E). In addition, Forkhead domain family motifs were the top enriched motifs at both pre- and post-enriched sites, illustrating that treatment does not alter FOXA1 motif preference and still occupies canonical FOXA1 binding sites (Supplementary Fig. S7F). To examine whether structural variations are underlying these differential FOXA1 binding events, we performed CNV-seq on the same tumor specimens and then projected onto the differential FOXA1 cistromics the structural copy-number data. These analyses revealed a comparable level of CNV at pre- and post-treatment enriched FOXA1 sites before and after ENZ treatment, with an overall trend toward less CNV upon treatment (Supplementary Fig. S8A-C). However, in none of the matched sample pairs (pre- and post-CNV-seq, and FOXA1 ChIP-seq; n = 15) a strong correlation between copy number difference and ChIP-seq signal difference was observed (R = 0.11; Supplementary Fig. S8D). In total, at only 44 out of 1,905 differential FOXA1 binding sites (< 2.5%), we observed copy number differences between post- and pre-treatment samples that could potentially explain binding site occupancy in 3 or more patients, indicating that the vast majority of these differential binding events is based on treatment-induced transcription factor reprogramming, rather than structural variation (Supplementary Fig. S8E).

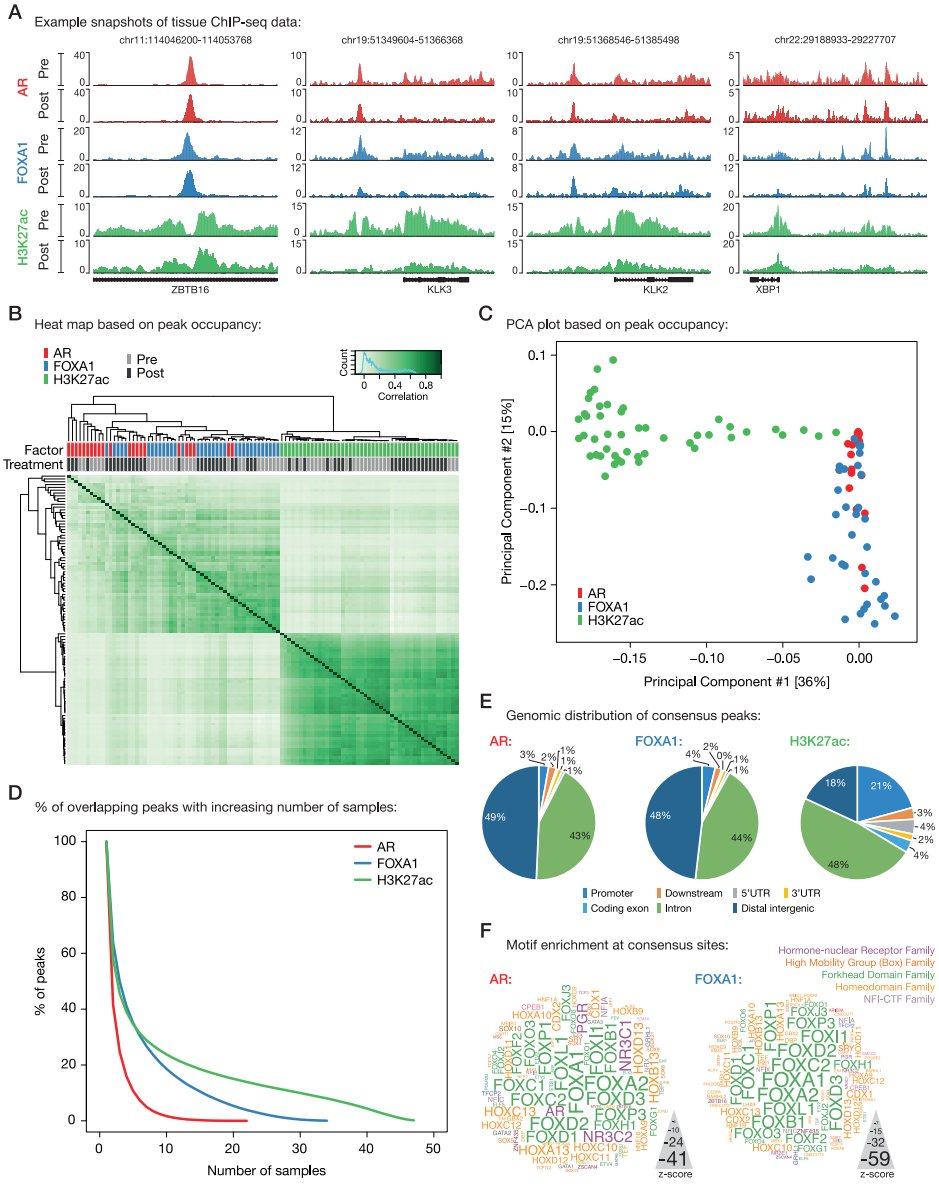
A
Example snapshots of tissue ChIP-seq data:
chr11:114046200-114053768
chr19:51349604-51366368
chr19:51368546-51385498
chr22:29188933-29227707
AR
FOXA1
H3K27ac
Pre
Post
ZBTB16
KLK3
KLK2
XBP1
B
Heat map based on peak occupancy:
AR
FOXA1
H3K27ac
Pre
Post
Count
Correlation
Factor
Treatment
C
PCA plot based on peak occupancy:
Principal Component #2 [15%]
Principal Component #1 [36%]
AR
FOXA1
H3K27ac
D
% of overlapping peaks with increasing number of samples:
% of peaks
Number of samples
AR
FOXA1
H3K27ac
E
Genomic distribution of consensus peaks:
AR:
FOXA1:
H3K27ac:
Promoter
Downstream
5'UTR
3'UTR
Coding exon
Intron
Distal intergenic
F
Motif enrichment at consensus sites:
AR:
FOXA1:
Hormone-nuclear Receptor Family
High Mobility Group (Box) Family
Forkhead Domain Family
Homeodomain Family
NFI-CTF Family
z-score

◂ **Figure 2:** Characterization of tissue ChIP-seq data streams. (**A**) Representative example snapshots of AR (red), FOXA1 (blue) and H3K27ac (green) ChIP-seq data for four genomic loci in one patient (DAR45). Pre- (light colors) and post-ENZ treatment (dark colors) is indicated. Y-axes indicate ChIP-seq signal in fragments per kilobase per million reads mapped (FPKM). (**B**) Correlation heatmap based on peak occupancy. Clustering of the samples is based on all called peaks and represents Pearson correlations between individual ChIP-seq samples. The column color bars indicate the ChIP-seq factor (AR, FOXA1, H3K27ac) and treatment status (Pre, Post). (**C**) Principal component analysis (PCA) plot based on peak occupancy. Each dot represents a ChIP-seq sample that is colored per factor. (**D**) Elbow plot depicting the peak overlap between ChIP-seq samples per factor. Shown is the percentage of overlapping peaks with increasing number of samples. Consensus peaksets were designed by using a cutoff of peaks present in at least 3 AR, 7 FOXA1, or 13 H3K27ac samples. (**E**) Pie charts showing the genomic distribution of AR (left), FOXA1 (middle) and H3K27ac (right) consensus peaks. (**F**) Word clouds show motif enrichment at AR (left) and FOXA1 (right) consensus sites. The font size represents the z-score and colors correspond to transcription factor families.

As FOXA1 dictates AR chromatin binding capacity[5], epigenetic plasticity of FOXA1 induced by treatment may be associated with alterations in the AR cistrome. To assess this, and to explore the epigenetic landscape surrounding the differentially bound FOXA1 regions, we compared the ChIP-seq signal of all three factors (AR, FOXA1, H3K27ac) at differential (pre- / post-enriched) and consensus (shared by ≥ 30 patients; n = 338) FOXA1 sites before and after ENZ therapy. While the FOXA1 ChIP-seq signal was highest at consensus binding sites, the pre- and post-treatment enriched regions followed the expected trend and showed significantly higher signal in the corresponding settings (**Fig. 3D**). Notably, we also observed less binding of FOXA1 to consensus sites when treated with ENZ, although the differences are much milder compared to the effects seen at pre-enriched FOXA1 sites (P_{adj} = 3.62 x 10^{-22} at consensus vs. 3.76 x 10^{-130} at pre-enriched sites, Mann-Whitney U test; **Fig. 3D**; Supplementary Fig. S9A). This could possibly be explained by decreased FOXA1 gene expression levels upon ENZ treatment (Supplementary Fig. S9B). The AR ChIP-seq signal followed the same patterns as observed for FOXA1, suggesting that relocated FOXA1 upon treatment functionally drives alterations in the AR cistrome (**Fig. 3D**). Unexpectedly, the pre-enriched FOXA1 sites were completely devoid of any H3K27ac signal in both pre- and post-treatment samples, while the post-enriched counterparts were positive for this active enhancer/promoter mark with a significant increase post-ENZ (P_{adj} = 5.59 x 10^{-4}, Mann-Whitney U test; **Fig. 3D**; Supplementary Fig. S9C and S9D), suggesting that pre-ENZ FOXA1 sites are inactive. To validate these observations in an independent cohort, we analyzed previously published AR (n = 87), H3K27ac (n = 92) and H3K27me3 (n = 76) ChIP-seq data from a cohort of 100 primary treatment-naïve PCa samples[31]. Supporting our previous analyses, the vast majority of post-enriched FOXA1 sites were H3K27ac-positive and their histone acetylation status positively correlated with AR

binding (R = 0.78) (**Fig. 3E**; Supplementary Fig. S9E). The pre-enriched FOXA1 sites, however, were again H3K27ac-negative, while the repressive histone modification H3K27me3 was present, which further points toward an inactive epigenetic state of these regulatory regions (**Fig. 3E**).

Recently, we reported that prostate cancers can reactivate developmental programs during metastatic progression[7]. These sentinel enhancers appeared to be pre-marked by FOXA1 from prostate gland development, and albeit inactive in normal prostate and primary tumor specimens, the sites get reactivated by AR during metastatic outgrowth. Given the inactivity of the pre-enriched FOXA1 sites, we hypothesized that FOXA1 might be decommissioned at such developmental enhancers prior to hormonal intervention. To test this, we overlapped the differential FOXA1 binding sites with the metastasis-specific AR binding sites (met-ARBS; n = 17,655), which revealed a strong enrichment for these developmental regulatory elements at pre-treatment FOXA1 sites ($P = 2.13 \times 10^{-16}$, Fisher exact test; Supplementary Fig. S9F). But are the inactive pre-enriched FOXA1 sites solely epigenetically suppressed, or are these regions intrinsically incapable of being active in this cellular context? To address this question and to further elucidate the role of AR at these differentially bound FOXA1 sites, we integrated our tissue ChIP-seq findings with previously identified tumor-specific AR binding sites[5] (n = 3,230) that were functionally characterized using Self-Transcribing Active Regulatory Regions sequencing (STARR-seq), a massive parallel reporter assay to systematically annotate intrinsic enhancer activity[34]. With this, three distinct classes of AR binding sites (ARBS) were identified (Supplementary Table S4): enhancers that were active regardless of AR stimulation (constitutively active; n = 465), ARBS with no significant enhancer activity (inactive; n = 2,479) and inducible AR enhancers that increase activity upon androgen treatment (inducible; n = 286). Interestingly, we found that post-treatment FOXA1 sites were enriched for constitutively active ARBS, which further supports the high enhancer activity and H3K27ac positivity observed at these sites, but also illustrates that this activity is constitutive and AR-independent (**Fig. 3F**). Consistent with our postulated inactivity of the pre-treatment enriched FOXA1 sites, these regions overlapped highly significantly with inactive ARBS ($P = 8.60 \times 10^{-9}$, Fisher exact test), which implies that these DNA elements are intrinsically inactive and incapable to act as functional enhancers, and possibly explains why these AR-bound sites did not show active regulatory marks (**Fig. 3E and 3F**). As no enrichment of our differential FOXA1 sites was observed with inducible ARBS (pre-enriched: 4/475; post-enriched: 2/1,430), these data further support a conclusion that AR itself is not a driver at FOXA1 sites that are differentially occupied after ENZ exposure in patients.

Overall, these results suggest that prior to hormonal intervention, FOXA1 is decommissioned at inactive developmental enhancer elements, which based on their primary DNA sequence are intrinsically incapable of being active – at least in the tested hormone-sensitive disease setting. However, upon ENZ treatment, FOXA1 gets reprogrammed to highly active *cis*-regulatory regions, which act in an AR-independent manner.

Transcriptional rewiring upon neoadjuvant ENZ

Having assessed the cistromic and epigenomic changes in response to neoadjuvant ENZ, we next determined how transcriptional programs were affected by this hormonal intervention. Principal component analysis (PCA) across both treatment states revealed that three months of ENZ therapy has a major effect on global gene expression profiles (**Fig. 4A**). Subsequently, we performed differential gene expression analysis, in which we compared pre- and post-treatment RNA-seq samples. Gene set enrichment analysis (GSEA) showed that AR signaling, along with mitosis and MYC signals, was strongly decreased upon treatment (**Fig. 4B and 4C**; Supplementary Fig. S10A). Since ENZ blocks the AR signaling axis, we analyzed the androgen-response pathway in more detail, which revealed a strong downregulation of AR target genes in almost every patient (**Fig. 4D**). In contrast to this, TNFa signaling, IFN-g response and epithelial-mesenchymal transition (EMT) signals were most upregulated (**Fig. 4B**; Supplementary Fig. S10B).

Previously, we identified three distinct subtypes of primary treatment-naïve PCa[31], which we named Cluster 1-3 (CI1-3). While CI1 and CI2 were mainly dominated by their ERG fusion status – with CI1 expressing high ERG levels (ERG fusion-positive) and CI2 expressing low ERG levels (ERG fusion-negative) – CI3 was enriched for neuroendocrine (NE)-like features, including low AR activity and a high NE gene expression score. To assess the impact of neoadjuvant ENZ therapy on these PCa subtypes, we performed unsupervised hierarchical clustering in the pre- and post-treatment setting using the originally identified top 100 most differentially expressed genes per cluster. Prior to hormonal intervention, we could robustly assign the samples into all three clusters (CI1: n = 23, CI2: n = 11, CI3: n = 8) with highly comparable distributions as we previously reported in another cohort of patients [31] (Supplementary Fig. S11A). Our pre- and post-treatment sampling now allowed us to investigate how individual tumors were affected by neoadjuvant therapy. This revealed that three months of ENZ therapy pushed almost all of the tumors toward our NE-like cluster 3 (**Fig. 4E**; Supplementary Fig. S11B). To assure that the observed effects are not solely driven by the treatment-induced reduction in AR activity (**Fig. 4C and 4D**), we used a well-established neuroendocrine PCa (NEPC) signature[35] to calculate gene expression fold changes pre- vs. post-ENZ, which confirmed an induction of NE-like signaling upon treatment (**Fig. 4F**). We further validated this transcriptional rewiring using gene sets that distinguish the three major lineages of prostate epithelial cells

(luminal, basal, neuroendocrine)[36,37], which jointly illustrated reduced AR-driven luminal cell transcriptional activity accompanied by an enrichment of NE-like features along with a basal-type transcriptional program after treatment (Supplementary Fig. S12A). Along these lines, classical NEPC markers[38] and transcriptional disease drivers[39-41] were selectively upregulated upon treatment (CHGA, PEG10) with acquisition of promoter-enriched H3K27ac (Supplementary Fig. S12B-D), while others were not affected on expression level (SYP, N-MYC) or not even expressed in primary tumors – irrespective of neoadjuvant treatment status (BRN2, encoded by the *POU3F2* gene). For classical NEPC IHC markers chromogranin A (CHGA) and synaptophysin (SYP), tissue microarrays (TMAs) were stained and analyzed, showing no change (SYP) or a modest non-significant increase (CHGA) upon neoadjuvant ENZ treatment (Supplementary Fig. S12E).

Recently, N-MYC ChIP-seq data was reported in models of NEPC[40], which however showed limited overlap with our post-treatment FOXA1 cistrome (Supplementary Fig. S12F). While a subset of NEPC markers was enriched on RNA-seq level, FOXA1 reprogramming did not seem to be a crucial driver in this phenomenon, based on limited overlap of our differential FOXA1 cistromes with a recently reported NEPC FOXA1 cistrome[42] (Supplementary Fig. S13A), nor was FOXA1 ChIP-seq in our study enriched for classical NEPC signature genes (Supplementary Fig. S13B). Jointly, these data suggest that altered FOXA1 cistromics after neoadjuvant ENZ treatment present a different biological state as compared to the fully developed NEPC-associated FOXA1 cistrome that presents in the advanced disease stage and may represent an early intermediate state.

Figure 3: Differential FOXA1 binding upon ENZ treatment. (**A**) Principal component analysis (PCA) plot based on peak occupancy of FOXA1 ChIP-seq data. Color indicates pre-treatment (light blue) and post-treatment (dark blue) FOXA1 samples. (**B**) Coverage heatmap depicting differential FOXA1 binding sites, selectively enriched in the pre-treatment (n = 475) or post-treatment (n = 1,430) setting. (**C**) Representative example snapshots of FOXA1 ChIP-seq signal at two pre-enriched (left) and two post-enriched (right) FOXA1 sites in one patient (DAR45). Pre- (light blue) and post-ENZ treatment (dark blue) is indicated. Y-axes indicate ChIP-seq signal in fragments per kilobase per million reads mapped (FPKM). (**D**) Boxplots indicating ChIP-seq signal (z-scaled readcounts) at pre-enriched (n = 475), post-enriched (n = 1,430) and consensus FOXA1 peaks (shared by ≥ 30 patients; n = 338) for FOXA1 (blue), AR (red), and H3K27ac (green) ChIP-seq datasets before (Pre; light colors) and after (Post; dark colors) ENZ treatment. **, $P < 0.01$; ***, $P < 0.001$; ****, $P < 0.0001$ (Mann-Whitney U test adjusted for multiple testing using FDR). (**E**) Coverage heatmap showing occupancy of differential (pre-/post-enriched) and consensus FOXA1 peaks in an external ChIP-seq dataset consisting of 100 untreated primary tumors[31]. Heatmap color indicates region read counts (z-score) at pre-enriched, post-enriched and consensus FOXA1 sites (rows) in the AR (red), H3K27ac (green) and H3K27me3 (gray) ChIP-seq data streams (columns). (**F**) Bar chart representing the overlap between differential FOXA1 sites (pre-enriched or post-enriched) and constitutively active (left) or inactive (right) AR binding sites (ARBS), based on STARR-seq. *, $P < 0.05$; ****, $P < 0.0001$ (Fisher exact test). ►

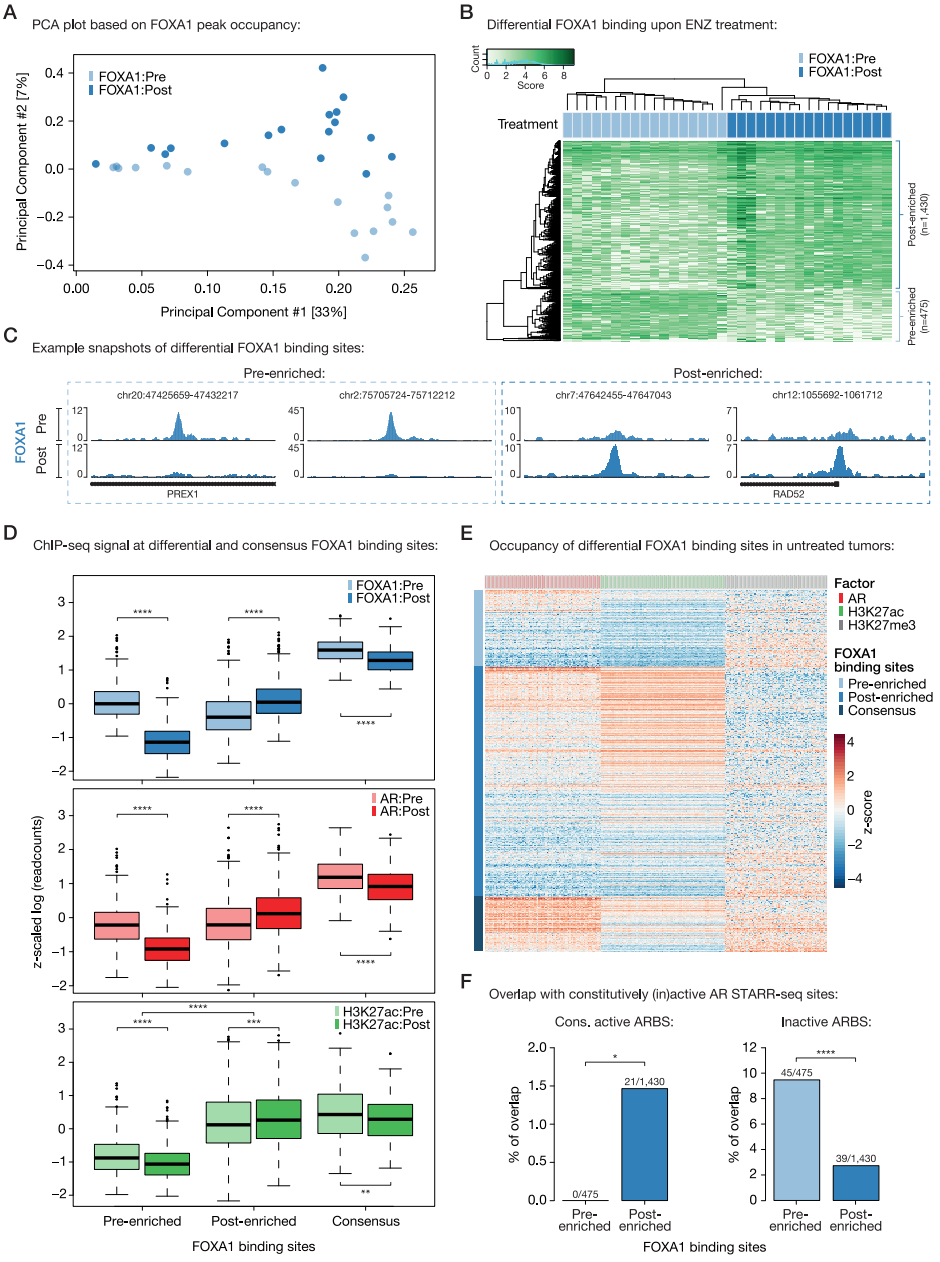

FOXA1 is frequently mutated in primary prostate cancer[14] and metastatic disease[17,18], where FOXA1 mutations were associated with loss of lineage-specific transcriptional programs and worse clinical outcome. Therefore, we determined the FOXA1 mutation status of our clinical samples using H3K27ac ChIP-seq and RNA-seq reads covering the

FOXA1 gene[43], and tested for possible enrichment for poor clinical outcome and NE-like gene expression features specifically in the FOXA1 mutant cases. While we observed a significant enrichment of FOXA1 mutant tumors among ENZ non-responders (BCR ≤ 6 months after surgery), no such enrichment was observed at the transcriptomic level, likely affected by the almost-complete transition of all our tumor samples toward the NE-like cluster 3 – irrespective of FOXA1 mutation status (Supplementary Fig. S13C-F).

Collectively, these results demonstrate that three months of neoadjuvant ENZ therapy not only uniformly diminish AR signaling, but also push practically all of our primary PCa samples to acquire some – but not all – features of NEPC, independently of their original subtype.

Figure 4: Neoadjuvant ENZ deactivates AR signaling and induces neuroendocrine (NE)-like gene expression signatures. (**A**) Principal component analysis (PCA) plot based on gene expression data. Color indicates pre-treatment (gray) and post-treatment (black) samples. Ellipses are based on the 80% confidence interval. (**B**) Gene set enrichment analyses (GSEA) for Hallmark gene sets. Shown are the top differentially enriched pathways upon ENZ treatment. Y-axis indicates the normalized enrichment score (NES). (**C**) Enrichment plot of the Hallmark Androgen Response pathway. Genes are ranked by differential expression upon ENZ treatment based on patient RNA-seq data (post vs. pre). Y-axis indicates enrichment score (ES). GSEA statistics (FDR, ES, NES, nominal *P*-value) are indicated. (**D**) Unsupervised hierarchical clustering of pre- and post-treatment RNA-seq samples based on the expression of AR-responsive genes. Color scale indicates gene expression (z-score). (**E**) River plot showing state transitions between Clusters 1 (dark blue), Cluster 2 (green) and Cluster 3 (light blue) for paired pre-treatment and post-treatment RNA-seq samples (n = 39). Number of samples assigned to each cluster before and after treatment as well as the hallmarks per cluster are indicated. (**F**) Waterfall plot depicting the Pearson correlation of neuroendocrine gene expression signature fold changes upon ENZ treatment per patient. Colors indicate the patients cluster affiliations after treatment. ►

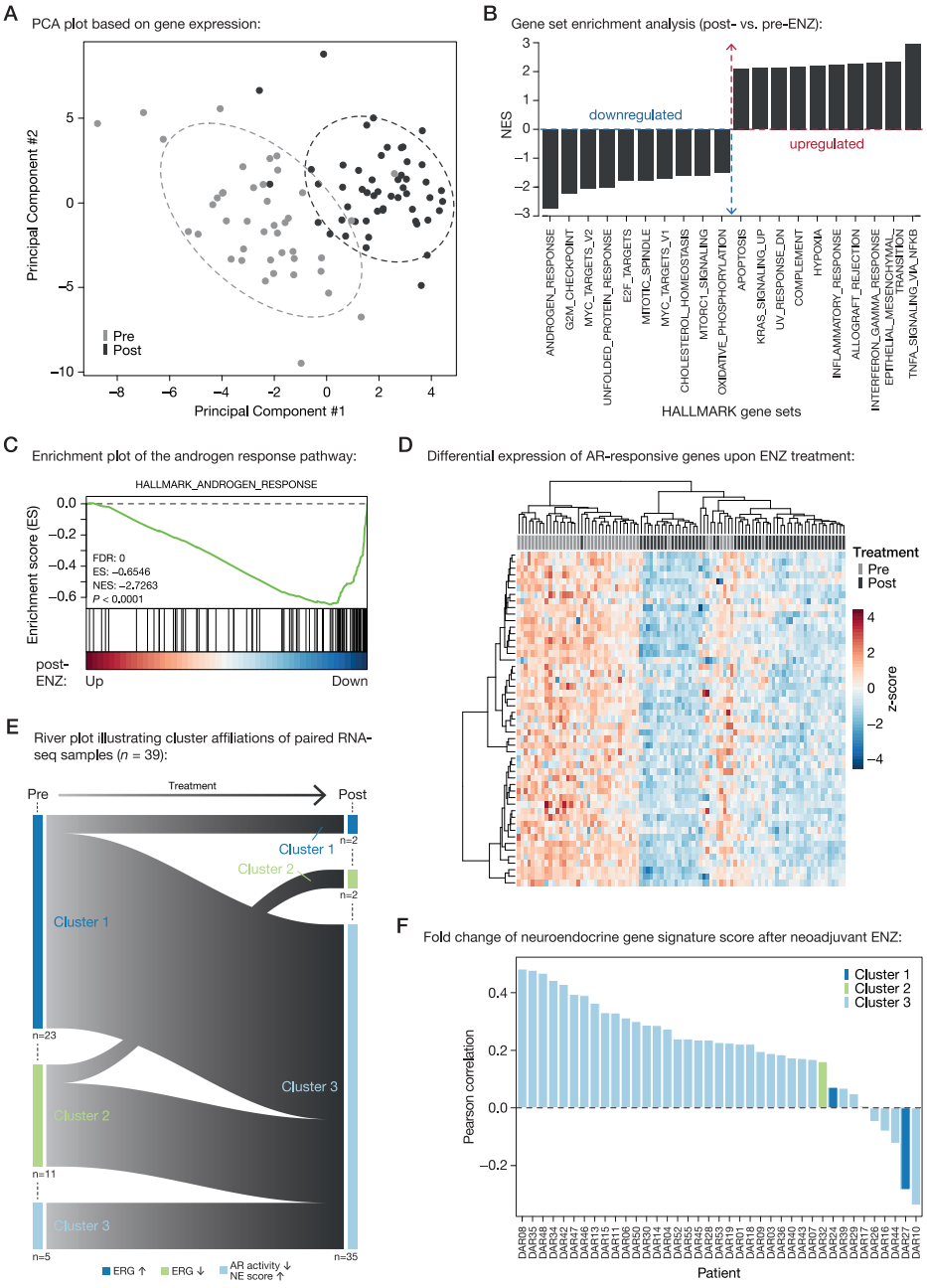
A
PCA plot based on gene expression:
Principal Component #2
Principal Component #1
Pre
Post
B
Gene set enrichment analysis (post- vs. pre-ENZ):
NES
downregulated
upregulated
ANDROGEN_RESPONSE
G2M_CHECKPOINT
MYC_TARGETS_V2
UNFOLDED_PROTEIN_RESPONSE
E2F_TARGETS
MITOTIC_SPINDLE
MYC_TARGETS_V1
CHOLESTEROL_HOMEOSTASIS
MTORC1_SIGNALING
OXIDATIVE_PHOSPHORYLATION
APOPTOSIS
KRAS_SIGNALING_UP
UV_RESPONSE_DN
COMPLEMENT
HYPOXIA
INFLAMMATORY_RESPONSE
ALLOGRAFT_REJECTION
INTERFERON_GAMMA_RESPONSE
EPITHELIAL_MESENCHYMAL_TRANSITION
TNFA_SIGNALING_VIA_NFKB
HALLMARK gene sets
C
Enrichment plot of the androgen response pathway:
HALLMARK_ANDROGEN_RESPONSE
Enrichment score (ES)
FDR: 0
ES: −0.6546
NES: −2.7263
P < 0.0001
post-ENZ:
Up
Down
D
Differential expression of AR-responsive genes upon ENZ treatment:
Treatment
Pre
Post
z-score
E
River plot illustrating cluster affiliations of paired RNA-seq samples (n = 39):
Pre
Treatment
Post
Cluster 1
Cluster 2
Cluster 3
n=23
n=11
n=5
n=2
n=2
n=35
ERG ↑
ERG ↓
AR activity ↓
NE score ↑
F
Fold change of neuroendocrine gene signature score after neoadjuvant ENZ:
Cluster 1
Cluster 2
Cluster 3
Pearson correlation
Patient

Post-treatment FOXA1 sites drive prosurvival gene programs, dictated by the circadian clock component ARNTL

Having examined the global cistromic and transcriptomic changes upon ENZ therapy, we next sought to characterize the biological consequences of the observed FOXA1 reprogramming using integrative analyses. We hypothesized that the newly acquired FOXA1 sites would be driving expression of genes associated with tumor cell survival programs. Using H3K27ac HiChIP data generated in LNCaP cells[44], pre- and post-treatment FOXA1 sites were coupled to their corresponding gene promoters (Supplementary Table S5). Subsequently, genome-wide CRISPR knockout screen data from Project Achilles (DepMap 20Q1 Public; VCaP) were used to identify those genes essential for prostate cancer cell proliferation[45,46]. While genes associated with pre-treatment FOXA1 sites were not enriched for essential genes (gene effect score < -1), genes under the control of post-treatment FOXA1 sites showed a significant enrichment ($P = 8.66 \times 10^{-8}$, Fisher exact test) for critical drivers of tumor cell proliferation (**Fig. 5A**), pointing toward a possible role of these sites in maintaining proliferative potential upon ENZ treatment. However, the factor regulating these genes to possibly drive proliferation remained elusive, especially since based on our STARR-seq and RNA-seq data, AR is likely not driving enhancer activity at post-treatment FOXA1 sites (**Fig. 3F**; **Fig. 4C and 4D**). Therefore, we sought to identify transcription factors involved in the activation of these regulatory regions that are selectively occupied by FOXA1 following treatment. To this end, we overlaid the genomic coordinates of the post-treatment enriched FOXA1 binding sites with those identified in publicly available ChIP-seq datasets ($n = 13{,}976$) as part of the Cistrome Data Browser transcription factor ChIP-seq sample collection[47,48]. Besides FOXA1 and AR, which were expected to bind at these regions (**Fig. 3D**), we also identified the glucocorticoid receptor (encoded by the *NR3C1* gene), which has previously been described to be upregulated upon antiandrogen treatment and able to drive the expression of a subset of AR-responsive genes, conferring resistance to AR blockade[49-51]. Unexpectedly, the second most enriched transcription factor after FOXA1 was circadian rhythm core component ARNTL (Aryl Hydrocarbon Receptor Nuclear Translocator Like; also known as BMAL1) which has not previously been implicated in PCa biology (**Fig. 5B**). Interestingly, ARNTL transcript levels were upregulated upon ENZ treatment ($P = 6.4 \times 10^{-3}$, Mann-Whitney *U* test; **Fig. 5C**), which was accompanied by increased H3K27ac ChIP-seq signals at the *ARNTL* locus (Supplementary Fig. S14A). Consistent with this, TMA IHC analysis also revealed elevated ARNTL protein levels after treatment when comparing the prostatectomy specimens post-ENZ with those of matched untreated control patients ($P = 6.89 \times 10^{-19}$, Fisher exact test; **Fig. 5D**). To assess whether ARNTL levels are also associated with patient outcome, we compared the average ARNTL gene expression of patients that did not experience a BCR (responders, $n = 29$) with those that experienced an early BCR within ≤ 6 months post-surgery

(non-responders, *n* = 8; Supplementary Table S1). While pre-treatment ARNTL levels were not significantly different between ENZ responders and non-responders, high ARNTL levels after treatment were associated with poor clinical outcome ($P = 4.79 \times 10^{-3}$, Mann-Whitney *U* test; **Fig. 5E**). In agreement with this observation, ARNTL levels were exclusively found upregulated in non-responders ($P = 3 \times 10^{-4}$, paired Mann-Whitney *U* test), while overall remaining unaffected upon neoadjuvant ENZ treatment in responders ($P = 0.33$; Supplementary Fig. S14B). Interestingly, while the CLOCK and NPAS2 proteins, which form a heterodimer with ARNTL to activate transcription of core clock genes, didn't show differential gene expression upon ENZ treatment (Supplementary Fig. S14C), all downstream ARNTL targets were upregulated upon treatment – except for CRY1, which has recently been shown to be AR- and thus ENZ-responsive[52]. In addition, the gene expression of these ARNTL dimerization partners was also not associated with clinical outcome (Supplementary Fig. S14D), hinting toward a treatment-induced role of ARNTL that is independent of its canonical function in the circadian machinery.

Notably, in two cohorts of metastatic castration-resistant PCa (mCRPC)[53,54], ARNTL expression was not associated with outcome (Supplementary Fig. S15A-D), suggesting a context-dependent prognostic potential of this gene – being associated with outcome in high-risk primary PCa upon treatment with ENZ.

Taken together, these data suggest that the circadian clock regulator ARNTL may be functionally involved in ENZ resistance in high-risk primary PCa by driving tumor cell proliferation processes.

Acquired ARNTL dependency in ENZ-resistant prostate cancer cells

To further investigate the relevance of ARNTL as a transcriptional driver at post-treatment FOXA1 sites, we performed *in vitro* validation experiments. To this end, we used hormone-sensitive LNCaP PCa cells, which we either cultured in full medium alone (Pre^{LNCaP}) or with ENZ for 48 hours ($Post^{LNCaP}$), mimicking our clinical trial setting (**Fig. 6A**). Based on the ENZ-induced acquisition of NE-like gene expression profiles in our patient cohort (**Fig. 4E and 4F**), we also included the ENZ-resistant LNCaP-42D model that possesses NE-features[41] ($Res^{LNCaP\text{-}42D}$; **Fig. 6A**), allowing us to further validate our patient-derived findings in cell lines recapitulating the transcriptional features of post-treatment clinical specimens.

We performed FOXA1 ChIP-seq experiments in all three cell line conditions (Supplementary Fig. S16A-D; Supplementary Table S6), which revealed highly similar FOXA1 chromatin binding dynamics as observed in our clinical samples: While the pre-enriched FOXA1 sites identified *in vivo* showed less binding upon treatment, we observed that merely 48 hours of ENZ exposure was sufficient to strongly induce binding at post-enriched sites, which was further increased in the long-term exposed, treatment-resistant LNCaP-42D cell line (Supplementary Fig. S16E and S16F). Similarly, genome-wide correlation analyses indicated that short-term ENZ treatment in cell lines induced FOXA1 reprogramming to regions that are FOXA1-bound in treatment-resistant but not in treatment-naïve cells (Supplementary Fig. S16G and S16H).

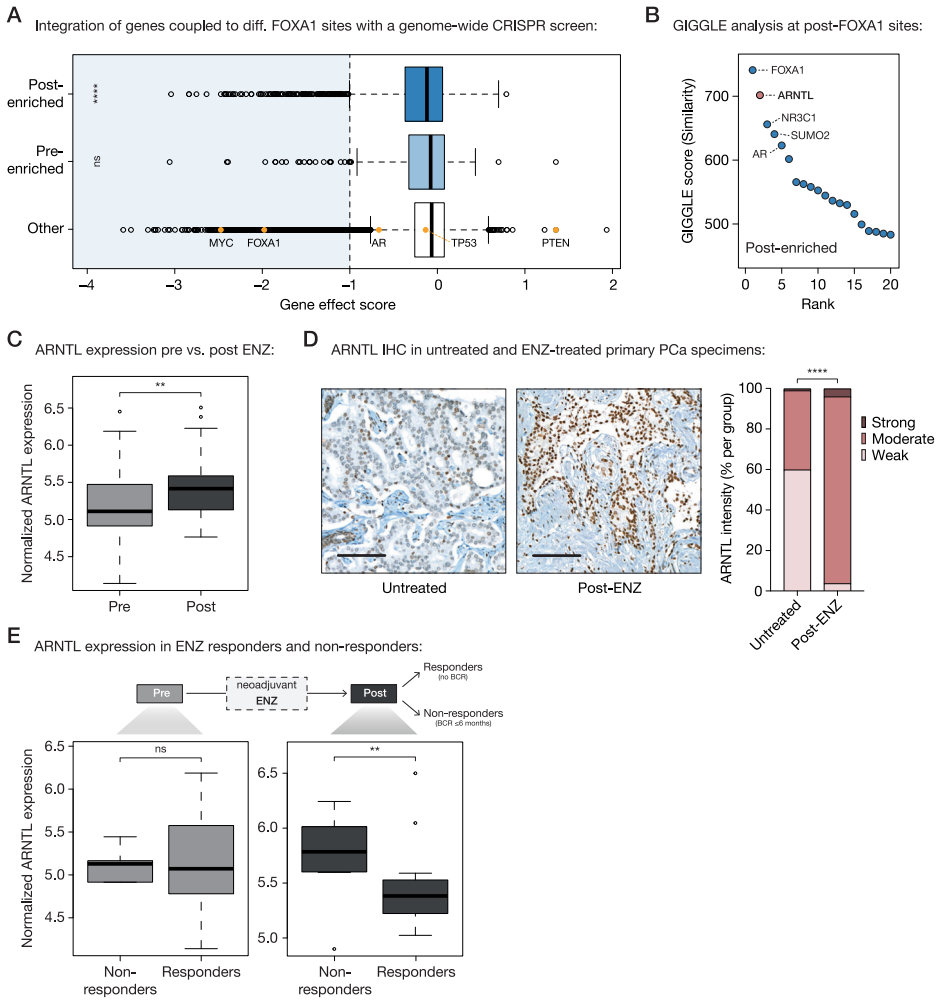

◂ **Figure 5:** Acquired FOXA1 sites drive key-survival genes that are under control of circadian rhythm regulator ARNTL. (**A**) Boxplot showing DepMap (20Q1) genome-wide loss-of-function CRISPR screen data for VCaP PCa cells, separately analyzing the gene effect score of genes associated with post-enriched FOXA1 sites (top), pre-enriched FOXA1 sites (middle) or all other tested genes (bottom). Differential FOXA1 binding sites were coupled to their respective target genes using H3K27ac HiChIP data. Indicated as controls are PCa-relevant driver genes: oncogenes *MYC*, *FOXA1*, *AR*, *TP53* and tumor suppressor *PTEN*. The recommended stringent gene effect score cutoff of -1 is shown (dotted vertical line) and all genes passing the essentiality threshold are highlighted in light blue. ns, $P > 0.05$; ****, $P < 0.0001$ (Fisher exact test). (**B**) Dot plot representing ranked GIGGLE similarity scores for transcriptional regulators identified at post-treatment FOXA1 sites. The top 20 identified factors are shown, and the 5 most enriched factors are labelled. (**C**) Boxplot showing normalized ARNTL gene expression before and after 3 months of neoadjuvant ENZ treatment. **, $P < 0.01$ (Mann-Whitney *U* test). (**D**) Representative ARNTL immunohistochemistry (IHC) stainings (left) and quantification of ARNTL staining intensity (right) in tissue microarrays consisting of prostatectomy specimens from untreated patients (not receiving neoadjuvant ENZ; $n = 110$) and DARANA patients post-ENZ ($n = 51$). Scale bars, 100 µm. ****, $P < 0.0001$ (Fisher exact test). (**E**) Boxplots depicting normalized ARNTL gene expression in ENZ non-responders (BCR ≤ 6 months; $n = 8$) and responders (no BCR; $n = 29$) in the pre- (left) and post- (right) treatment setting separately. ns, $P > 0.05$; **, $P < 0.01$ (Mann-Whitney *U* test).

Having shown that differential FOXA1 chromatin binding in tumors could be recapitulated *in vitro*, we next sought to further assess the role of ARNTL in these pre-clinical models. Therefore, we first measured the intrinsic enhancer activity of our patient-derived and cell line-validated differential FOXA1 binding sites by STARR-seq for 1,209/1,905 differential regions in LNCaP cells. Notably, we identified a subset of regions ($n = 968$) with sustained enhancer activity upon ENZ treatment (Supplementary Fig. S17A), confirming our initial STARR-seq analysis (**Fig. 3F**). While GIGGLE analyses on the inactive regions showed enrichment for FOXA1 and AR, active enhancers – irrespective of treatment – were specifically enriched for ARNTL (Supplementary Fig. S17B and S17C). These data are in full concordance with the tumor H3K27ac ChIP-seq (**Fig. 3D**) analyses, showing AR-independent activity at the post-treatment enriched FOXA1 sites, and uncovered once more ARNTL as a possible driver for transcriptional activity in case of AR suppression.

Next, we confirmed that treatment with ENZ increased ARNTL protein levels in PCa models (Supplementary Fig. S18A), recapitulating the clinical observations (**Fig. 5C and 5D**). Interestingly, this treatment-induced ARNTL upregulation appeared to be FOXA1-dependent, as FOXA1 knockdown abolished the ENZ-driven increase in ARNTL levels (Supplementary Fig. S18B). Since cistromic ARNTL profiling has to date not been reported in PCa models, we generated ARNTL ChIP-seq data (Supplementary Fig. S19A-C) to validate its binding at post-treatment FOXA1 sites.

Interestingly, while we already observed ARNTL binding to these regulatory regions in the pre-treatment setting, this was strongly enhanced upon ENZ exposure (**Fig. 6B**; Supplementary Fig. S19D-F).

Functional interactions between FOXA1 and ARNTL could be further validated using ARNTL RIME experiments in ENZ-treated LNCaP-42D and LNCaP cells, confirming interactions of ARNTL with AR and FOXA1, but also with other classical circadian rhythm components including CLOCK/NPAS2, CRYs (CRY1, CRY2), and PERs (PER1, PER2, PER3; **Fig. 6C**; Supplementary Fig. S20A). As FOXA1 acts as a pioneer factor, enabling chromatin binding for other TFs including AR[9], we hypothesized that FOXA1 serves a comparable role for ARNTL. To test this hypothesis, we performed ARNTL ChIP-seq upon FOXA1 knockdown (**Fig. 6D**; Supplementary Fig. S20B-E), showing a significant decrease of ARNTL chromatin interactions exclusively for those regions co-occupied by FOXA1 – highlighting FOXA1's critical role in determining ARNTL chromatin binding.

In agreement, at ARNTL consensus peaks, motifs were found to be enriched for CLOCK and MYC, but also FOXA1 and ARNTL itself (**Fig. 6E**). To identify functional differences in ARNTL cistromes induced upon treatment, we overlapped the ARNTL peaks identified in all tested cell line conditions, which revealed a massive cistromic reprogramming upon ENZ treatment (**Fig. 6F**; Supplementary Fig. S19E and S19F). Notably, ~70% of ENZ-gained ARNTL peaks (n = 1,752) in LNCaP cells were captured by the ARNTL cistrome in treatment-resistant cells. Interestingly, upon ENZ treatment ARNTL binding was found to be enriched at promoter regions of key NEPC drivers, including BRN2 (*POU3F2*), FOXA2, EZH2, ASCL1 and SOX2 (Supplementary Fig. S21A), positioning ARNTL as a possible driver of the NE-like transcriptional program we identified. In addition, pathway over-representation analyses of genes coupled to $Post^{LNCaP}$-$Res^{LNCaP\text{-}42D}$-shared ARNTL binding sites revealed a treatment-induced enrichment for gene sets implicated in cell cycle progression and cell division, further supporting a possible functional involvement of ARNTL in sustaining tumor cell proliferation when AR is blocked by ENZ (**Fig. 6F**). To challenge this hypothesis, we assessed whether ARNTL-knockdown affects the viability of hormone-sensitive and in particular of long-term ENZ-exposed cell lines. While ARNTL-targeting had minimal effect on LNCaP cell proliferation (with or without ENZ), ARNTL knockdown significantly suppressed cell growth of ENZ-resistant LNCaP-42D cells in the absence (P = 0.031, two-way ANOVA) and even more so in the presence of ENZ (P = 7 x 10^{-4}, two-way ANOVA), indicating that targeting ARNTL also partially restores ENZ-sensitivity in this treatment-resistant cell line model (**Fig. 6G**). While ARNTL was essential for sustaining cellular fitness upon ENZ treatment, exogenously introduced ARNTL did not suffice to further enhance cell proliferation when exposing LNCaP and LCNaP-42D cells to ENZ (Supplementary Fig. S21B), suggesting that ARNTL

is required but not sufficient to drive the observed phenotype. Importantly, we could successfully validate the functional role of ARNTL in additional cell line models of ENZ resistance (LNCaP-ResV, originally referred to as LNCaP-EnzR[55]; and LNCaP-ResA[56]) using ARNTL knockdown and CRISPR/Cas9-mediated ARNTL knockout (Supplementary Fig. S21C-E). In line with these *in vitro* validation experiments, ARNTL knockout also strongly inhibited the growth of LNCaP-derived ENZ-resistant xenografts (LNCaP-42D, LNCaP-ResA) in intact mice upon ENZ exposure (**Fig. 6H**; Supplementary Fig. S21F). Importantly, parental LNCaP cells were not affected in their proliferation potential by ARNTL knockout (Supplementary Fig. S21F), supporting the acquired dependency of ENZ-resistant cells on this circadian factor, instead of a general impact on cellular fitness. Jointly, these data further highlight the treatment-induced ARNTL dependency of high-risk PCa models, both *in vitro* and *in vivo*, and position ARNTL as a novel candidate therapeutic target.

Glucocorticoid Receptor (GR) was identified in the GIGGLE analysis as the third-most enriched factor at post-treatment FOXA1 sites, directly following ARNTL and FOXA1 itself (**Fig. 5B**). Given the known GR function in driving ENZ resistance in advanced CRPC[49,57,58], we next tested whether sustained tumor cell survival after short-term antiandrogen treatment was not only ARNTL, but also GR-dependent. Interestingly, GR (encoded by the *NR3C1* gene) expression was upregulated upon neoadjuvant ENZ treatment in primary PCa patients (Supplementary Fig. S22A), but neither expression levels before nor after therapy were associated with clinical outcome (Supplementary Fig. S22B). Using publicly available GR ChIP-seq data from LNCaP-derived GR-positive LREX' cells[49], we could identify GR occupancy at the majority of pre-treatment FOXA1 sites and at a subset of post-treatment sites (Supplementary Fig. S22C and S22D). However, GR knockdown did not affect cellular fitness after short-term ENZ treatment in the majority of cell line models we tested (Supplementary Fig. S22E), suggesting the observed ARNTL-driven early adaptation to ENZ exposure represents a different biological entity as compared to the known GR-driven treatment resistance described in CRPC.

Overall, these data confirm the ENZ-induced FOXA1 reprogramming as observed in PCa patients upon neoadjuvant antiandrogen therapy and revealed an acquired dependency on circadian rhythm regulator ARNTL to drive tumor cell growth – positioning ARNTL as a highly promising new drug target in combination with ENZ for the treatment of high-risk PCa.

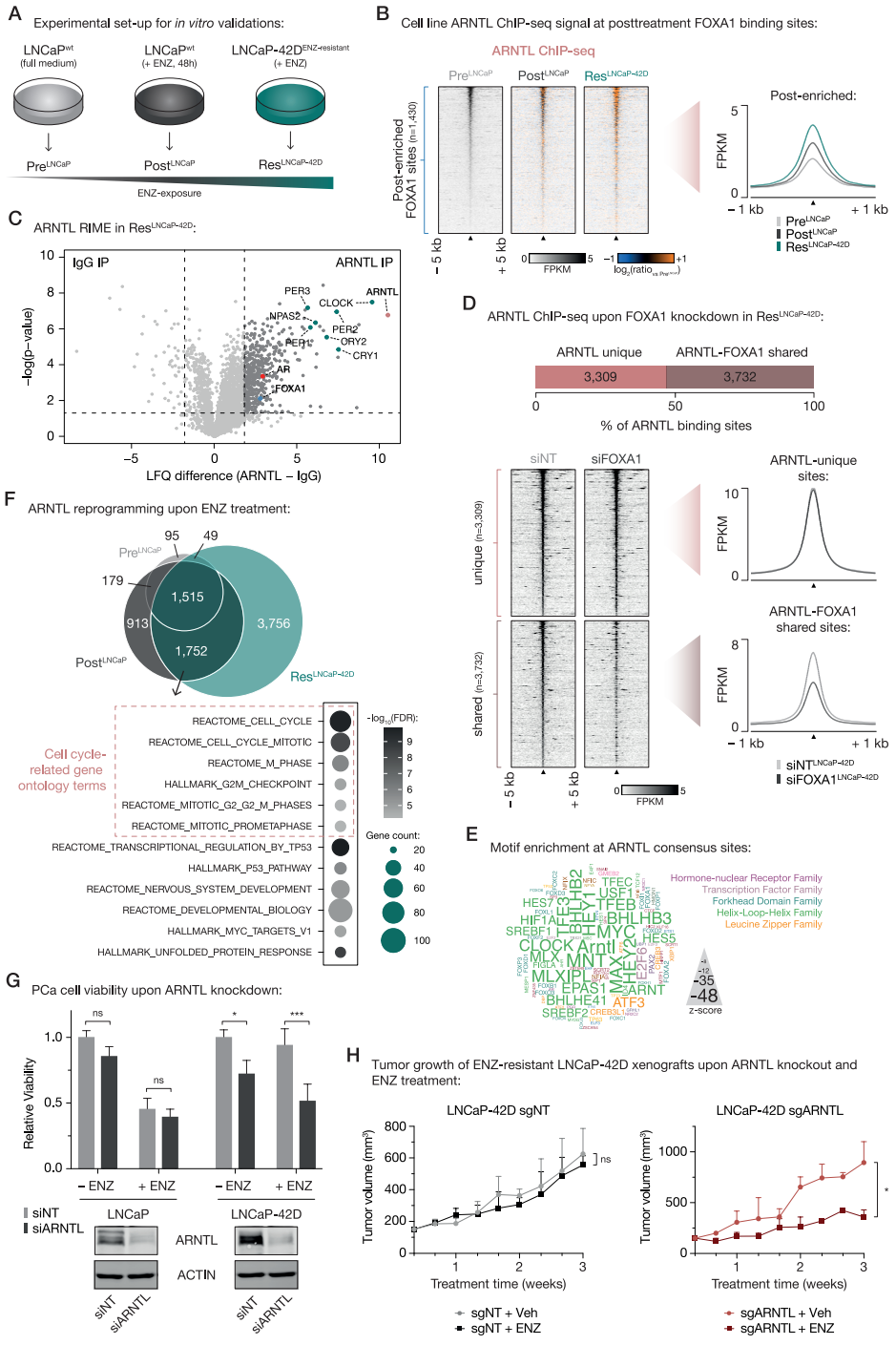
A
Experimental set-up for *in vitro* validations:
LNCaP^wt (full medium)
LNCaP^wt (+ ENZ, 48h)
LNCaP-42D^ENZ-resistant (+ ENZ)
Pre^LNCaP
Post^LNCaP
Res^LNCaP-42D
ENZ-exposure
B
Cell line ARNTL ChIP-seq signal at posttreatment FOXA1 binding sites:
ARNTL ChIP-seq
Post-enriched FOXA1 sites (n=1,430)
Post-enriched:
FPKM
log2(ratio vs Pre^LNCaP)
C
ARNTL RIME in Res^LNCaP-42D:
IgG IP
ARNTL IP
PER3
ARNTL
CLOCK
NPAS2
PER2
ORY2
PER1
CRY1
AR
FOXA1
–log(p–value)
LFQ difference (ARNTL – IgG)
D
ARNTL ChIP-seq upon FOXA1 knockdown in Res^LNCaP-42D:
ARNTL unique
ARNTL-FOXA1 shared
3,309
3,732
% of ARNTL binding sites
siNT
siFOXA1
unique (n=3,309)
shared (n=3,732)
ARNTL-unique sites:
ARNTL-FOXA1 shared sites:
siNT^LNCaP-42D
siFOXA1^LNCaP-42D
E
Motif enrichment at ARNTL consensus sites:
Hormone-nuclear Receptor Family
Transcription Factor Family
Forkhead Domain Family
Helix-Loop-Helix Family
Leucine Zipper Family
z-score
F
ARNTL reprogramming upon ENZ treatment:
95
49
179
1,515
913
3,756
1,752
Cell cycle-related gene ontology terms
REACTOME_CELL_CYCLE
REACTOME_CELL_CYCLE_MITOTIC
REACTOME_M_PHASE
HALLMARK_G2M_CHECKPOINT
REACTOME_MITOTIC_G2_G2_M_PHASES
REACTOME_MITOTIC_PROMETAPHASE
REACTOME_TRANSCRIPTIONAL_REGULATION_BY_TP53
HALLMARK_P53_PATHWAY
REACTOME_NERVOUS_SYSTEM_DEVELOPMENT
REACTOME_DEVELOPMENTAL_BIOLOGY
HALLMARK_MYC_TARGETS_V1
HALLMARK_UNFOLDED_PROTEIN_RESPONSE
-log10(FDR):
Gene count:
G
PCa cell viability upon ARNTL knockdown:
Relative Viability
– ENZ
+ ENZ
siNT
siARNTL
LNCaP
LNCaP-42D
ARNTL
ACTIN
H
Tumor growth of ENZ-resistant LNCaP-42D xenografts upon ARNTL knockout and ENZ treatment:
LNCaP-42D sgNT
LNCaP-42D sgARNTL
Tumor volume (mm³)
Treatment time (weeks)
sgNT + Veh
sgNT + ENZ
sgARNTL + Veh
sgARNTL + ENZ

◂ **Figure 6:** Treatment-induced dependency on ARNTL in ENZ-resistant PCa cells. (**A**) Experimental setup for *in vitro* validation experiments. (**B**) Tornado plots (left) and average density plot (right) visualizing ARNTL ChIP-seq signal [in fragments per kilobase per million reads mapped (FPKM)] at post-enriched FOXA1 binding sites in untreated (Pre^{LNCaP}), short-term ENZ-treated ($Post^{LNCaP}$), and ENZ-resistant NE-like LNCaP cells ($Res^{LNCaP\text{-}42D}$). Data are centered at post-treatment FOXA1 peaks depicting a 5-kb (heatmaps) or 1-kb (density plots) window around the peak center. Heatmap color depicts the ChIP-seq signal compared to the untreated condition (Pre^{LNCaP}), with blue indicating lower peak intensity and orange indicating higher peak intensity. (n = 2). (**C**) Volcano plot depicting ARNTL interactors in ENZ-treated LNCaP-42D ($Res^{LNCaP\text{-}42D}$) cells over IgG control. Significantly enriched interactors are highlighted and significance cutoffs are shown as dotted lines [label-free quantification (LFQ) difference ≥ 1.8; $P \leq 0.05$; n = 4]. (**D**) Stacked bar chart (top) indicating the fraction of ARNTL binding sites in ENZ-treated LNCaP-42D ($Res^{LNCaP\text{-}42D}$) cells that are ARNTL unique (n = 3,309) or shared with FOXA1 (n = 3,732). Tornado plots (lower left) and average density plot (lower right) visualize ARNTL ChIP-seq signal (in FPKM) at ARNTL unique or ARNTL-FOXA1 shared binding sites in LNCaP-42D cells upon transfection with non-targeting siRNA (siNT) or siFOXA1. Data are centered at ARNTL peaks depicting a 5-kb (heatmaps) or 1-kb (density plots) window around the peak center. (n = 2). (**E**) Word cloud shows motif enrichment at ARNTL consensus sites (n = 1,515) shown in (F). The font size represents the z-score and colors correspond to transcription factor families. Since the human ARNTL motif is not part of the tested database, the homologous mouse motif (Arntl) was included. (**F**) Venn diagram (top) indicating the overlap of ARNTL binding sites in all tested cell line conditions (Pre^{LNCaP}, $Post^{LNCaP}$, $Res^{LNCaP\text{-}42D}$). For each condition, only peaks present in both replicates were included. Gene ontology terms for ARNTL-bound gene sets uniquely shared between $Post^{LNCaP}$ and $Res^{LNCaP\text{-}42D}$ conditions are presented below. Overlapping ARNTL binding sites (n = 1,752) were coupled to their respective target genes using H3K27ac HiChIP data. Color indicates the gene set enrichment (FDR q-value) and size depicts the number of genes that overlap with the indicated gene sets. Cell cycle-related gene ontology terms are highlighted. (**G**) Bar chart (top) showing relative cell viability of LNCaP (left) and LNCaP-42D (right) cells upon transfection with non-targeting siRNA (siNT) or siARNTL, and exposure to ENZ. Treatment is indicated and data is shown relative to the untreated (– ENZ) siNT condition per cell line (n = 3). Western blots (bottom) indicate ARNTL protein levels in LNCaP (left) and LNCaP-42D (right) cells following siRNA-mediated silencing of ARNTL for 48 hours. Transfection with siNT and staining for ACTIN are included as controls for siRNA treatment and protein loading, respectively. Images are representative of three independent experiments. ns, $P > 0.05$; *, $P < 0.05$; ***, $P < 0.001$ (two-way ANOVA followed by Tukey multiple comparisons test). (**H**) Growth curves depict tumor volume (measured 3 times per week using calipers) of non-targeting control (sgNT) or ARNTL knockout (sgARNTL) LNCaP-42D xenografts upon daily treatment with vehicle-alone (sgNT +Veh: n = 4; sgARNTL +Veh: n = 3) or ENZ (sgNT +ENZ: n = 4; sgARNTL +ENZ: n = 2). ns, $P > 0.05$; *, $P < 0.05$ (t test).

Discussion

In medicine, the evolutionary selection pressure as imposed by drug treatment has been a well-known clinical challenge, ever since the first antibiotics were discovered in the early 20th century. Also in oncology, clear escape mechanisms for both targeted therapeutics and systemic treatments are known for many years, involving *ESR1* mutations in metastatic breast cancer[59], *EGFR* mutations in lung cancer[60], *KRAS* mutations in metastatic colorectal cancer[61], but also somatic amplification of the *AR* locus and/or an upstream *AR* enhancer in castration-resistant PCa[62,63]. Apart from genetic alterations, also epigenetic rewiring[7,50] or transdifferentiation are reported as mechanisms of resistance, including treatment-emergent neuroendocrine (NE) prostate cancers that occur as an adaptive response under the pressure of prolonged AR-targeted therapy[64,65].

Our unique clinical trial design with paired pre- and post-treatment biopsies of high-risk primary PCa treated with ENZ monotherapy, allowed us to unravel global ENZ-induced alterations in gene regulation. We report that large-scale treatment-induced dedifferentiation in PCa may be a gradual process, of which the early signs are identified on transcriptomic level within the first months of treatment onset. While complete adenocarcinoma-to-neuroendocrine transdifferentiation was not observed in any of our samples, cellular plasticity characterized by the acquisition of cistromic, transcriptomic and proteomic features of NE disease may not only be present in primary tumors prior to treatment[31], but also become enriched upon short-term exposure to endocrine treatment, and thus represent an early intermediate disease state.

In PCa development[5,32] and progression[7], AR has been reported to expose substantial plasticity in its enhancer repertoire, and we now illustrate this is also the case in primary disease upon short-term treatment. Besides AR, FOXA1 is considered a master transcription factor and critical prostate lineage specific regulator acting in PCa, that upon overexpression during tumorigenesis gives rise to a tumor-specific AR cistrome. Also in NEPC, FOXA1 cistromes are reprogrammed[42], which indicates a direct AR-independent role of FOXA1 in PCa progression. Our study confirms these observations and shows that, while co-occupied by AR, the pre- and post-ENZ enriched FOXA1 sites appeared indifferent to AR signaling.

The functional implications of the pre-treatment FOXA1 sites remain unclear, as those regions were inactive, both in primary tissues as well as in reporter assays. A subset of these *cis*-regulatory elements demarcates developmental epigenomic programs, that we previously reported as being occupied by FOXA1 from prostate development to tumorigenesis and metastatic progression[7], whereas others may be relevant for different physiological processes.

The treatment-induced cistromic repositioning of pioneer factor FOXA1 initiated a thus far unknown transcriptional rewiring, in which ARNTL, a classical circadian rhythm regulator and dimerization partner of CLOCK, compensates for AR inhibition and becomes essential to rescue cellular proliferation signals. Recently, it has been reported that CRY1 – a transcriptional coregulator of ARNTL – is AR-regulated in PCa, and modulates DNA repair processes in a circadian manner[52]. The current data illustrate that certain components of the circadian machinery may have a potential impact on drug response, as most clock components are not only temporally regulated at the transcriptional level, but are also dysregulated upon exposure to hormonal therapy. Our data now show that AR blockade forces tumor cells to adapt epigenetically, upon which these cells – over time – become dependent on ARNTL as a transcriptional regulator of proliferation processes. This acquired cellular vulnerability appears to be dependent on whether or not AR activity is inhibited and cells have had time to achieve full epigenetic reprogramming, explaining the limited effect of ARNTL knockdown in hormone-sensitive PCa cells, as compared to the long-term ENZ-exposed treatment-resistant models.

ARNTL expression did not correlate with outcome in mCRPC patients. Furthermore, post-treatment induced FOXA1 profiles showed limited overlap with NEPC-FOXA1 sites, and GR action – previously reported as a driver in CRPC – did not play a decisive role in our datasets to sustain cellular fitness following short-term enzalutamide exposure. Jointly, these data position the clinical state as induced by short-term neoadjuvant AR-targeted therapy in primary PCa as a separate biological entity, exposing already in this early clinical stage some – but not all – features of progressive therapy-resistant disease, that are invoked by drug-induced epigenetic plasticity.

With the identification of ARNTL as a rescue mechanism for tumor cells to evade AR blockade, the next question presents whether ARNTL could serve as a novel therapeutic target, which should be further pursued in future drug development and clinical research. Being critically relevant for circadian rhythm regulation, it would be imperative to balance ARNTL targeting in relation to any adverse side-effects. Additionally, we demonstrate that the surprisingly dynamic enhancer repertoire of FOXA1 is not only critical in prostate tumorigenesis[5] and neuroendocrine differentiation[42], but also appears crucial in evading AR therapy-induced growth inhibition, further supporting the rationale to intensify efforts in targeting this highly tissue-selective, yet critical transcriptional regulator, directly or indirectly[66].

Methods

Study design

Primary PCa tissues before and after enzalutamide (ENZ) treatment were acquired as part of the phase 2, prospective, single-arm DARANA study (ClinicalTrials.gov NCT03297385) at the Netherlands Cancer Institute Antoni van Leeuwenhoek hospital. The primary clinical outcome measure of the trial was the positive margins rate after neoadjuvant ENZ treatment. To allow sample size calculation, we performed a survey into the surgical margins of 1492 in-house prostatectomy specimens (Gleason ≥ 7), not treated with antihormonal therapy prior to surgery, which revealed 34% not-radical resections. Earlier randomized studies on neoadjuvant androgen ablation showed reductions in positive surgical margin rate of at least 50%[67-69]. To detect a reduction of positive surgical margins from 34% to 17% with a power of 80% and an alpha level set at 0.05, 55 patients needed to be included. Inclusion criteria were over 18 years of age, Gleason ≥ 7 PCa and planned for prostatectomy. Prior to treatment a multi-parametric MRI scan was made to identify tumors in the prostate (cT-stage) and pelvic lymph node metastasis (cN-stage). Patients were treated with ENZ, once daily 160 mg P.O. without androgen deprivation therapy, for three months prior to robotic-assisted laparoscopic prostatectomy (RALP) and a pelvic lymph node dissection. The resection specimen was assessed for tumor margins, prostate tumor stage (ypT-stage) and pelvic lymph node involvement (ypN-stage). Secondary endpoints included assessment of downstaging by comparison of pre-operative clinical cT and cN stage with post-treatment and post-operative ypT and ypN stage, and differences in pre- and post-treatment prostate cancer cleaved Caspase-3 and Ki-67 staining as markers of apoptosis and tumor cell proliferation, respectively. Moreover, various clinical time-to-event outcomes were included: time to biochemical recurrence, defined as time from trial inclusion to two consecutive rises of serum PSA with a minimal level of ≥ 0.2 ng/mL; ADT-free survival, defined as time from trial inclusion to the onset of ADT therapy; time to radiological recurrence, defined as time from trial inclusion until detection of local or distant metastases by PSMA PET scanning; and time to distant metastases, defined as time from trial inclusion until the detection of distant metastases by PSMA PET scanning. The trial was approved by the institutional review board of the Netherlands Cancer Institute, informed consent was signed by all participants enrolled in the study, and all research was carried out in accordance with relevant guidelines and regulations.

Pre- and post-treatment sampling

Prior to ENZ intervention, 4 x pre-operative MRI-guided 18-gauge core needle tumor biopsies were taken per patient. Directly after prostatectomy, 8 x additional tumor-targeted core needle biopsies (4 x 14-gauge, 4 x 5-mm) were taken from prostatectomy

specimens *ex vivo*, using previous MRI information and palpation. Biopsy and prostatectomy specimens were fresh frozen (FF) or formalin-fixed paraffin-embedded (FFPE) for ChIP-seq and CNV-seq, or RNA-seq and immunohistochemistry analyses, respectively. Prior to ChIP-seq experiments, FF material was cut in 30 µm sections, while FFPE material was cut in 10 µm sections prior to RNA extraction. Tissue sections were examined pathologically for tumor cell content and only samples with a tumor cell percentage of ≥ 50% were used for further downstream analyses.

ChIP-seq

Sample processing: Chromatin immunoprecipitations on PCa tissue specimens and cell line models were performed as previously described[70]. In brief, cryosectioned tissue samples were double-crosslinked in solution A (50 mM HEPES-KOH, 100 mM NaCl, 1 mM EDTA, 0.5 mM EGTA), first supplemented with 2 mM disuccinimidyl glutarate (DSG; CovaChem) for 25 min at room temperature. Then, 1% formaldehyde (Merck) was added for 20 min and subsequently quenched with a surplus of 2.5 M glycine. Cell lines were crosslinked using single-agent fixation. Therefore, 1% formaldehyde was added to the cell culture medium and incubated at room temperature for 10 min, followed by glycine-quenching as described above. Tissue and cell line samples were lysed as described[71] and sonicated for at least 10 cycles (30 sec on; 30 sec off) using a PicoBioruptor (Diagenode). For each ChIP, 5 µg of antibody were conjugated to 50 µL magnetic protein A or G beads (10008D or 10009D, Thermo Fisher Scientific). The following antibodies were used: AR (06-680, Merck Millipore), FOXA1 (ab5089, Abcam), H3K27ac (39133, Active Motif), and ARNTL (ab93806, Abcam).

ChIP-seq: Immunoprecipitated DNA was processed for library preparation using a KAPA library preparation kit (KK8234, Roche) and generated libraries were sequenced on the Illumina HiSeq2500 platform using the single end protocol with a read length of 65-bp, and aligned to the human reference genome hg19 using Burrows-Wheeler Aligner (v0.5.10)[72]. Reads were filtered based on mapping quality (MAPQ ≥ 20) and duplicate reads were removed.

Analysis of ChIP-seq: Peak calling over input controls (per tissue sample or cell line) was performed using MACS2 (v2.1.1) and Dfilter (v1.6) for tissues, and MACS2 (v2.1.2) for cell lines[73,74]. For tissue samples, only the peaks shared by both peak callers were used for downstream analyses. DeepTools[75] (v2.5.3) was used to calculated read counts in peaks (FRiP). Read counts and the number of aligned reads, as well as normalized strand coefficient (NSC) and relative strand correlation (RSC), which were calculated using phantompeaktools[76] (v1.10.1), are shown in Supplementary Table S2 for tissue ChIP-seq data and Supplementary Table S6 for cell line ChIP-seq data. Tissue ChIP-seq samples

that passed the following quality control measures were included in the final analyses; tumor cell percentage ≥ 50%, ChIP-qPCR enrichment, and more than 100 peaks called (Supplementary Fig. S2). For visualization of cell line ChIP-seq data, an average enrichment signal was generated by merging mapped reads of replicate samples using SAMtools[77] (v1.10-3). Genome browser snapshots, tornado and average density plots were generated using EaSeq[78] (v1.101). For snapshot overviews across multiple samples, bigWig files were generated from aligned bam files with the bamCoverage function from deepTools (v2.0), and snapshots were produced using pyGenomeTracks[79] (v3.6) with the added NCBI RefSeq genome track[80,81]. Genomic distribution and motif enrichment analyses were performed using the CEAS and the SeqPos motif tools on Galaxy Cistrome[82], respectively. CistromeDB Toolkit was used to probe which TFs and chromatin regulators have a significant binding overlap with the differential FOXA1 peak sets[48]. For this, genomic coordinates of high-confidence binding sites (FC ≥ 1.2) were converted between assemblies (from hg19 to hg38), using the UCSC genome browser liftOver tool[83]. The DiffBind[84] R package (v2.10) was used to generate correlation heatmaps and PCA plots based on occupancy, to perform differential binding analyses using a false discovery rate (FDR) < 0.05, and to generate consensus peaklists. ChIP-seq signal of various datasets (FOXA1, AR and H3K27ac from this study; AR, H3K27ac and H3K27me3 from a previously reported study[31]) at differential and consensus FOXA1 sites was investigated by counting mapped reads in FOXA1 peak regions using bedtools[85] multicov (v2.27.1). Readcounts were subsequently z-transformed and visualized using the aheatmap function from the R package NMF[86] (v0.21.0) with a color scheme from RColorBrewer (v1.1-2; https://CRAN.R-project.org/package=RColorBrewer). To determine significance in binding site occupancy differences between pre- and post-treatment FOXA1 sites, median z-transformed readcounts were calculated per sample and compared using a Mann-Whitney *U* test. These median readcounts per sample were also used to assess the correlation between ChIP-seq signals of AR, FOXA1 and H3K27ac at pre-enriched, post-enriched and consensus FOXA1 binding sites. Bedtools[85] intersect (v2.27.1) was used to determine overlap of differential FOXA1 binding sites and inactive, constitutively active and inducible AR-binding sites. To assign FOXA1 and ARNTL binding regions to potential target genes, we overlapped differential FOXA1 binding sites with H3K27ac HiChIP data[44] using bedtools intersect. To assess whether or not genes coupled to FOXA1 binding sites were considered to be essential for the VCAP prostate cancer cell line, we used the DepMap (Broad 2020) 20Q1 Public gene effect dataset[45] with a stringent gene effect score cutoff ≤ -1. Gene set overlaps between genes linked to ChIP-seq binding sites and the Molecular Signatures Database (v7.4) were computed using Gene Set Enrichment Analysis[87] (GSEA) with an FDR q-value cutoff ≤ 0.05.

RNA-seq

RNA isolation: Prior to RNA isolation, FFPE material was pathologically assessed. The expert pathologist scored tumor cell percentage and indicated most tumor-dense regions for isolation on a hematoxylin and eosin (H&E) slide. RNA and DNA from FFPE material were simultaneously isolated from 3-10 sections (depending on tumor size) of 10 µm using the AllPrep DNA/RNA FFPE isolation kit (80234, Qiagen) and the QIAcube according to the manufacturer's instructions. cDNA was synthesized from 250 ng RNA using SuperScript III Reverse Transcriptase (Invitrogen) with random hexamer primers.

RNA-seq: Strand-specific libraries were generated with the TruSeq RNA Exome kit (Illumina) and sequenced on the Illumina HiSeq2500 platform using the single end protocol with a read length of 65-bp. equencing data were aligned to the human reference genome hg38 using HISAT2[88] (v2.1.0) and the number of reads per gene was measured with HTSeq count[89] (v0.5.3). For QC purposes, total readcounts per sample were determined and hierarchical clustering based on the Euclidean distance was applied. Samples with a readcount ≥ 2 standard deviations below the mean of all sample readcounts were removed, as well as samples that clustered in a separate branch.

Analysis of RNA-seq: Global gene expression differences between pre- and post-treatment samples passing QC were determined using DESeq2[90] (v1.22.2). Significance of expression level differences between pre- and post-treatment samples was determined using a paired *t* test. Gene set enrichment was performed using pre-ranked GSEA[87] based on the Wald statistic provided by DESeq2. For visualization purposes, the data were z-transformed per gene. Heatmaps of gene expression values were created using the aheatmap function from the R package NMF[86] (v0.21.0) with a color scheme from RColorBrewer (v1.1-2; https://CRAN.R-project.org/package=RColorBrewer). To assign samples to previously described PCa subtypes Stelloo, et al. [31], the z-transformed expression levels of the top ~100 most differentially expressed genes (*n* = 285) in each of the three clusters were investigated. Using these values, samples were clustered based on their Pearson correlation. The resulting tree was divided into 3 clusters, corresponding to the previously published PCa subtypes. Potential transitioning of samples from one cluster to another after treatment was visualized using a riverplot (v0.6; https://CRAN.R-project.org/package=riverplot). To calculate fold changes of neuroendocrine scores upon treatment, expression of 70 neuroendocrine signature genes were obtained from castration-resistant neuroendocrine and prostate adenocarcinoma samples as published previously[35]. The expression of 5 of the 70 neuroendocrine signature genes were not included in the analysis (KIAA0408, SOGA3, LRRC16B,

ST8SIA3, SVOP) because the genes are not expressed in these samples. Expression fold changes between paired pre- and post-treatment samples were calculated (*n* = 39) and concordance in gene expression differences (fold change sign) were measured using Pearson correlation.

CNV-seq

CNV-seq: Low-coverage whole-genome sequencing of ChIP-seq input samples was performed on a HiSeq2500 system (single end, 65-bp), and samples were aligned to hg19 with Burrows-Wheeler Aligner[72] (BWA) backtrack algorithm (v0.5.10). Per sample, the mappability of all reads with a phred quality score of 37 and higher per 20-kb on the genome was rated against a similarly obtained mappability for all known and tiled 65-bp subsections of hg19. Sample counts were corrected per bin for local guanine–cytosine (GC) content effects using a nonlinear Loess fit of mappabilities over 0.8 on autosomes. Reference values were scaled according to the slope of a linear fit, forced to intercept at the origin, of reference mappabilities after GC correction. Ratios of corrected sample counts and reference values left out bins with mappability below 0.2 or overlapping ENCODE blacklisted regions[91].

Analysis of CNV-seq: Copy number log ratios were smoothed and segmented using the R package DNACopy (v1.50.1; https://bioconductor.org/packages/release/bioc/html/DNAcopy.html) with the parameters set to alpha=0.00000000001, undo.SD=2, and undo.splits="sdundo". Bedtools[85] intersect (v2.27.1) was used to determine overlap between copy number segments and differential FOXA1 binding sites. These data were subsequently visualized using the aheatmap function from the R package NMF[86] (v0.21.0) with a color scheme from RColorBrewer (v1.1-2; https://CRAN.R-project.org/package=RColorBrewer). To correlate FOXA1 ChIP-seq signal with copy number status at differential FOXA1 sites, we employed the z-transformed FOXA1 ChIP-seq readcounts as described in the ChIP-seq section. The difference in transformed ChIP-seq readcounts and the difference in normalized segmented copy number data between matched post-treatment and pre-treatment samples was calculated for every patient. Subsequently, the Pearson correlation between these two sets of differences was calculated.

Immunohistochemistry

For immunohistochemistry (IHC) analysis, we matched our ENZ-treated patient cohort (*n* = 51) in a 1:2 ratio to untreated control patients (not receiving ENZ prior to prostatectomy; *n* = 110) based on clinicopathological parameters (initial PSA, Gleason score, TNM stage, age) using the R package MatchIt[92] (v.4.1.0). Tissue microarrays (TMAs) were prepared containing 3 cores per FFPE tumor sample. Tumor-dense areas in FFPE megablocks were marked by an expert pathologist on a H&E slide. Cores were drilled

in a receptor block using the TMA grandmaster (3D Histech/Sysmex). Next, cores were taken from the donor block and placed in the receptor block using the manual tissue arrayer (4508-DM, Beecher instruments). The filled receptor block was placed in a 70°C stove for 9 minutes and cooled overnight at RT. IHC was applied to TMA slides using a BenchMark Ultra autostainer (Ventana Medical Systems). In brief, paraffin sections were cut at 3 μm, heated at 75°C for 28 minutes and deparaffinized in the instrument with EZ prep solution (Ventana Medical Systems). Heat-induced antigen retrieval was carried out using Cell Conditioning 1 (CC1, Ventana Medical Systems) for 24 minutes (cleaved-Caspase-3), 32 minutes (Chromogranin, Synaptophysin) or 64 minutes (ARNTL, Ki-67) at 95°C. The following antibodies and staining conditions were used: anti-ARNTL (ab230822, Abcam; 1:1000 dilution; 60 min at room temperature), anti-Ki-67 (M7240, Agilent; 1;100 dilution; 60 min at 37°C), anti-cleaved-Caspase-3 (9661, Cell Signaling; 1:100 dilution; 32 min at room temperature), anti-Chromogranin (760-2519, Ventana Medical Systems; undiluted; 32 min at 37°C), and anti-Synaptophysin (SYNAP-299-L-CE, Leica; 1:100; 32 min at 37°C). For Synaptophysin signal amplification was applied using the OptiView Amplification Kit (Ventana Medical Systems; 4 min). Bound antibody was detected using the OptiView DAB Detection Kit (Ventana Medical Systems). Slides were counterstained with hematoxylin and bluing reagent (Ventana Medical Systems). Percentage of positive tumor cells or IHC staining intensity (weak, moderate, strong) in tumor cells were scored by an expert pathologist and used for statistical analysis.

FOXA1 mutation status

FOXA1 mutation status was assessed from H3K27ac ChIP-seq and RNA-seq reads covering the gene. We focused our search to genomic coordinates with mutations previously reported in cBioPortal (https://www.cbioportal.org). cBioPortal was queried for all somatic mutations in FOXA1 (n = 567 mutations) across all PCa samples (n = 6,875 patients). Non-reference alleles were called from bam files with H3K27ac ChIP-seq or RNA-seq reads using the mpileup and call commands from bcftools (v1.9). The --prior variable for call was set to 0.05 to enhance sensitivity in the setting of low read coverage. The genomic coordinates of variants were listed in bed files and tested for overlap with FOXA1 mutations from cbioPortal.

Survival analysis in mCRPC cohorts

RNA-seq data from mCRPC was processed as previously described[53,54,93] and converted to transcripts per million (TPM) or fragments per kilobase per million reads mapped (FPKM). Patients were grouped by ARNTL expression levels as low (< median) or high (≥ median). Survival analysis was performed using the Kaplan-Meier method with endpoint overall survival from diagnosis of mCRPC and the Wald test was used to test for statistical significance.

Cell lines and cell culture

LNCaP human PCa cell line and HEK293T cells were purchased from the American Type Culture Collection (ATCC). Enzalutamide-resistant LNCaP-42D[41] and LNCaP-ResA[56] cells were described previously. LNCaP clones were maintained in RPMI-1640 medium (Gibco, Thermo Fisher Scientific) supplemented with 10% FBS (Sigma-Aldrich), with ENZ-resistant cell lines further supplemented with 10 μM ENZ (MedChemExpress). HEK293T cells were cultured in DMEM (Gibco, Thermo Fisher Scientific) supplemented with 10% FBS. Cell lines were subjected to regular mycoplasma testing and all cell lines underwent authentication by short tandem repeat profiling (Eurofins Genomics). For hormone stimulation with synthetic androgen, cells were treated with 10 nM R1881 (PerkinElmer) for 48 hours. For *in vitro* AR blockade, cells were treated with 10 μM ENZ and harvested at the indicated time points.

STARR-seq

Generation of FOXA1-focused STARR-seq library: Pooled human male genomic DNA (Promega) was randomly sheared, end-repaired, and ligated with Illumina compatible xGen CS stubby adaptors (IDT) containing 3-bp unique molecular identifiers (UMI). The adaptor-ligated gDNA fragments (500-800 bp) were hybridized to a custom biotinylated oligonucleotide probe (Agilent) and captured by Dynabeads M-270 Streptavidin beads (NEB). The library was designed to capture regions from clinical ChIP-seq. Any overlapping reads were collapsed using BedTools' `merge` (v2.30.0) command to eliminate possible over-representation. Target regions were PCR-amplified with STARR_in-fusion_F (TAGAGCATGCACCGGACACTCTTTCCCTAC ACGACGCTCTTCCGATCT) and STARR_in-fusion_R (GGCCGAATTCGTCGAGTGAC TGGAGTTCAGACGTGTGCTCTTCCGATCT) primers and cloned into AgeI-HF (NEB) and SalI-HF (NEB) digested hSTARR-ORI plasmid (#99296, Addgene) by Gibson Assembly. STARR-seq capture library was transformed into MegaX DH10B T1R electrocompetent cells (Invitrogen). Plasmid DNA was extracted using the Qiagen Plasmid Maxi Kit.

STARR-seq: LNCaP cells (> 1.6 x 10^8 cells/replicate; 3 biological replicates for each cell line) were electroporated with the STARR-seq capture library (1 x 10^6 cells: 2 μg DNA; ~320 μg plasmid DNA/replicate) using the Neon Transfection System (Invitrogen). Electroporated LNCaP cells were immediately recovered in RPMI-1640 medium supplemented with 10% FBS and the culture medium was refreshed 24hours after electroporation. LNCaP cells (~0.5 x 10^8 cells) were treated with dimethylsulfoxide (DMSO) or 10 μM ENZ for 48 hours and then either EtOH or 10 nM DHT for 4 hours. All electroporated LNCaP cells were harvested 72 h post electroporation. Cell samples

were lysed with the Precellys CKMix Tissue Homegenizing Kit and Precellys 24 Tissue/Cell Ruptor (Berin Technologies). Total RNA was extracted using Qiagen Rneasy Maxi Kit (Qiagen) and poly-A mRNA was isolated using the Oligo $(dT)_{25}$ Dynabeads (Thermo Fisher). FOXA1-focused STARR-seq cDNA was synthesized with the gene-specific primer (CTCATCAATGTATCTTATCATGTCTG) and amplified by junction PCR (15 cycles) with the RNA_jPCR_f (TCGTGAGGCACTGGGCAG*G*T*G*T*C) and jPCR-r (CTTATCATGTCTGCTCGA*A*G*C) primers. FOXA1-focused STARR-seq capture library plasmid DNA was extracted from 0.1 x 10^8 transfected but untreated cells using the QIAprep Spin Miniprep Kit (Qiagen). The extracted plasmid DNA and the input plasmid DNA were PCR amplified with the DNA-specific junction PCR primer (DNA_jPCR_f, CCTTTCTCTCCACAGGT*G*T*C) and jPCR-r primer. After purification with Ampure XP beads, Illumina compatible libraries were generated by PCR amplification with NEBNext universal and single indexing primers (NEB), and were sequenced on Illumina NovaSeq6000 (150-bp; paired-end).

Analysis of STARR-seq: STARR-seq sequencing data was analyzed using a custom Snakemake pipeline (https://github.com/birkiy/starr-pipe). Briefly, paired-end STARR-seq samples were aligned to hg19 genome using BWA (v0.7.17). Raw alignment files were converted into BEDPE format using BedTools (v2.30.0) `bamtobed -bedpe` command. The start of the first paired read and the end of its mate defined the fragments from the BEDPE file. Any fragments overlapping with hg19 blacklisted regions (https://github.com/Boyle-Lab/Blacklist) or MAPQ scores < 30 were filtered from downstream analysis. Fragments containing unique genomic positions were counted using `uniq -c` UNIX command. A count table of the unique fragment collection count was generated using a custom Julia script (v1.5.2) *fragments.jl* which uses library input samples to first generate the reference fragment population and then quantifies the frequencies of each fragment. STARR-seq aligned files were downsampled using SAMtools (v1.10) to make files with equivalent readcounts across conditions. Next, count tables were generated from the downsampled files for all tested FOXA1 regions (n = 1,209) using the deepTools (v2.0) multiBamSummary function. The most correlated replicates were chosen for further analysis using the cor function in R (v3.4.4). Regions with zero counts across samples were removed leaving 968 regions. These count tables were used as input for a differential expression analysis using DESeq2 (v1.22.2) in R. Regions with non-significant changes (FDR ≤ 0.05, logFC ≥ |2|) in readcounts upon ENZ treatment were identified and k-means clustering from the plotHeatmap function of deepTools was performed. To determine possible functional associations within these clusters the sets of regions were queried using the CistromeDB Toolkit to identify factors with significant overlap.

RIME

Sample processing: Following treatment of LNCaP and LNCaP-42D cells with ENZ (10 μM) for 48 hours, cells were fixed, lysed and sonicated as previously described[94]. The nuclear lysates were incubated with 50 μL magnetic protein A beads (10008D, Thermo Fisher Scientific) conjugated to 7.5 μg ARNTL antibody (ab93806, Abcam) or rabbit IgG control (12-370, Merck Millipore).

LC-MS/MS: Peptide mixtures were prepared and measured as previously described[4], with the following exceptions. Peptide mixtures (10% of total digest) were loaded directly onto the analytical column (ReproSil-Pur 120 C18-AQ, 2.4 μm, 75 μm x 500 mm, packed in-house) and analyzed by nanoLC-MS/MS on an Orbitrap Fusion Tribrid mass spectrometer equipped with a Proxeon nLC1200 system (Thermo Scientific). Solvent A was 0.1% formic acid/water and solvent B was 0.1% formic acid/80% acetonitrile. Peptides were eluted from the analytical column at a constant flow of 250 nL/min in a 120 min gradient, containing a 105 min step-wise increase from 7% to 34% solvent B, followed by a 15 min wash at 80% solvent B.

Analysis of RIME data: Raw data were analyzed by MaxQuant (v2.0.1.0)[95] using standard settings for label-free quantitation (LFQ). MS/MS data were searched against the Swissprot human database (20,397 entries, release 2021_01) complemented with a list of common contaminants and concatenated with the reversed version of all sequences. The maximum allowed mass tolerance was 4.5 ppm in the main search and 0.5 Da for fragment ion masses. False discovery rates for peptide and protein identification were set to 1%. Trypsin/P was chosen as cleavage specificity allowing two missed cleavages. Carbamidomethylation was set as a fixed modification, while oxidation and deamidation were used as variable modifications. LFQ intensities were $\log_2$-transformed in Perseus (v1.6.15.0)[96], after which proteins were filtered for at least 3 out of 4 valid values in at least one sample group. Missing values were replaced by imputation based on a normal distribution (width: 0.3 and downshift: 1.8). Differentially enriched proteins were determined using a Student *t* test (threshold: $P \leq 0.05$ and $[x\text{-}y] \geq 1.8 \mid [x\text{-}y] \leq -1.8$).

Transient cell line transfections

Transient transfections of cell lines were performed according to the manufacturer's instructions using Lipofectamine 2000 (Invitrogen) or Lipofectamine RNAiMAX (Invitrogen) for overexpression or siRNA knockdown experiments, respectively. ARNTL containing expression plasmid was obtained from the CCSB-Broad Lentiviral Expression Library. siRNA oligos targeting ARNTL (M-010261-00-0005), FOXA1 (M-010319-01-0020), NR3C1 (M-003424-03-0005) and the non-targeting control (D-

001206-14, D-001210-05-20) were purchased from Dharmacon. For ARNTL ChIP-seq upon FOXA1 knockdown, LNCaP and LNCaP-42D cells were reverse transfected with 50 nM siFOXA1 using Lipofectamine RNAiMAX. ENZ (10 μM) was added after 24 hours, and cells were fixed and harvested for ChIP-seq analysis 72 hours post-transfection.

CRISPR/Cas9-mediated knockout cell lines

Guide RNAs targeting human ARNTL (CTGGACATTGCGTTGCATGT) and a non-targeting control guide (AACTACAAGTAAAAGTATCG) were individually cloned into the lentiCRISPR v2 plasmid[97]. CRISPR vectors were co-expressed with 3rd generation viral vectors in HEK293T cells using polyethyleneimine (PEI; Polysciences). After lentivirus production, the medium was harvested and transferred to the designated cell lines. Two days post infection, cells were put on puromycin (Sigma-Aldrich) selection for 3 weeks and knockout efficiency was tested using western blot analysis.

Western blotting

Total proteins were extracted from cells using Laemmli lysis buffer, supplemented with a complete protease inhibitor cocktail (Roche). Per sample, 40 μg of protein was resolved by SDS-PAGE (10%) and transferred on nitrocellulose membranes (Santa Cruz Biotechnology). The following antibodies were used for Western blot stainings: ARNTL (ab93806, Abcam), PSA (5365, Cell Signaling Technology), FOXA1 (ab5089, Abcam), GR (12041, Cell Signaling Technology) and ACTIN (MAB1501R, Merck Millipore). Blots were incubated overnight at 4°C with designated primary antibodies at 1:1000 (ARNTL, PSA) or 1:5000 (ACTIN) dilution and visualized using the Odyssey system (Li-Cor Biosciences).

RNA isolation and mRNA expression

Total RNA from cell lines was isolated using TRIzol Reagent (Thermo Fisher Scientific), and cDNA was synthesized from 2 μg RNA using the SuperScript™ III Reverse Transcriptase system (Thermo Fisher Scientific) with random hexamer primers according to the manufacturer's instructions. Quantitative PCR (qPCR) was performed using the SensiMix™ SYBR Kit (Bioline) according to the instructions provided by the manufacturer on a QuantStudio™ 6 Flex System (Thermo Fisher Scientific). Primer sequences for mRNA expression analyses are FOXA1 (*forward*: CGACTGGAACAGCTACTACG; *reverse*: TGGTGTTCATGGTCATGTAGGT) and ARNTL (*forward*: CTGGAGCACGACGTTCTTTCTT; *reverse*: GGATTGTGCAGAAGCTTTTTCG). mRNA levels are shown relative to the expression of housekeeping gene *TBP* (*forward*: GTTCTGGGAAAATGGTGTGC; *reverse*: GCTGGAAAACCCAACTTCTG).

Cell viability and proliferation assays

For cell viability assays, LNCaP, LNCaP-42D or LNCaP-ResA cells were seeded at 2 x 10^3 cells per well in 96-well plates (Greiner) ± 10 μM ENZ, and reverse transfected with 50-100 nM siRNA (Dharmacon) using Lipofectamine RNAiMAX (Invitrogen). Cell viability was assessed 7 days post-transfection using the CellTiter-Glo Luminescent Cell Viability Assay kit (Promega), as per the manufacturer's instructions. Bar charts were plotted using GraphPad Prism 9 software. Proliferation curves for stable ARNTL knockout clones were generated using a Lionheart FX automated microscope (BioTek). Cells (LNCaP, LNCaP-42D, LNCaP-ResA) were seeded at 2 x 10^3 cells per well in 96-well plates ± 10 μM ENZ. SiR-DNA (Spirochrome) live cell nuclear stain was added 2 hours before imaging. Cell growth was recorded with a time resolution of 4 hours for a total time span of 144 hours. The microscope was maintained at 37°C, 5% CO2 and live-cell imaging was performed using a 4X lens and a Sony CCD, 1,25-megapixel camera with two times binning (BioTek). Gen5 software (BioTek) was used to quantify cell numbers and growth curves were plotted using GraphPad Prism 9 software.

Xenograft studies

For *in vivo* tumor growth studies, 7.5 x 10^6 sgNT or sgARNTL (LNCaP, LNCaP-42D, LNCaP-ResA) cells in PBS with 50% BME (3536-005-02, Bio-Techne) were injected subcutaneously into one of the flanks of ~seven-week-old male NOD-SCID (NSG) mice. Once tumor size reached 150 mm^3, mice were randomized and treated with either 10 mg/kg ENZ (MedChemExpress), or vehicle control (1% carboxymethylcellulose sodium salt, 0.1% Tween-80, 5% DMSO; Sigma-Aldrich) through oral gavage on a daily basis. Tumor volume was monitored by caliper measurements 3 times a week. Mice were kept under standard temperature and humidity conditions in individually ventilated cages, with food and water provided *ad libitum*. All animal experiments were approved by the Animal Welfare Committee of the Netherlands Cancer Institute and performed in accordance with institutional, national and European guidelines for animal research.

Statistical analysis

For differential binding and differential gene expression analyses (pre- vs. post-ENZ), an FDR cutoff < 0.05 (P < 0.01) and P_{adj} < 0.01 was used, respectively. A Mann-Whitney U test was used to determine differences in region readcounts (adjusted for multiple testing using FDR) and differences in gene expression levels before and after ENZ treatment. For peak set and gene set overlaps as well as to determine differences in IHC staining intensities, Fisher exact tests were applied. Differences in cell viability or cell/tumor growth were tested using a two-way or one-way ANOVA followed by Tukey multiple comparisons test, respectively (GraphPad Prism 9). Corresponding bar chart or

growth curves show the mean with error bars representing the SD. All boxplots indicate the median (center line), upper- (75) and lower- (25) quartile range (box limits) and 1.5 x interquartile range (whiskers). Significance is indicated as follows: ns, $P > 0.05$; *, $P < 0.05$; **, $P < 0.01$; ***, $P < 0.001$; ****, $P < 0.0001$. Further details of statistical tests are provided in the figure legends.

Data availability

All tissue ChIP-seq and RNA-seq raw data generated in this study have been deposited in the European Genome-Phenome Archive (EGA) under the accession numbers EGAS00001006017 and EGAS00001006016, respectively. The cell line ChIP-seq, as well as all processed tissue ChIP-seq and RNA-seq data have been deposited in the Gene Expression Omnibus (GEO) database, under accession number GSE197781. The mass spectrometry proteomics (RIME) data have been deposited to the ProteomeXchange Consortium via the PRIDE partner repository with the dataset identifier PXD032041. Public ChIP-seq datasets used in this study are available from GEO or the EGA under the following accession code: GSE120738 (AR, H3K27ac ChIP-seq), GSE51497 (GR ChIP-seq), GSE117306 (N-MYC ChIP-seq) and EGAS00001003928 (FOXA1 ChIP-seq).

Conflict of interest

S.C. Baca reports other support from Precede Biosciences outside the submitted work. F.Y. Feng reports personal fees from Janssen Oncology, Bayer, Exact Sciences, Blue Earth Diagnostics, Myovant Sciences, Roivant Sciences, Astellas Pharma, Foundation Medicine, Varian, Bristol Meyers Squibb, Bluestar Genomics, Novartis, and Tempus and other support from PFS Genomics, SerImmune, and Artera AI outside the submitted work. M.L. Freedman reports other support from Precede Bio outside the submitted work. L.F.A. Wessels reports grants from Genmab outside the submitted work. N.A. Lack reports grants, personal fees, and other support from Nido Biosciences and grants from AstraZeneca outside the submitted work. H. van der Poel reports grants from Astellas during the conduct of the study. A.M. Bergman reports grants from Movember, the Dutch Cancer Society, and Astellas Pharma during the conduct of the study, as well as personal fees from Astellas Pharma outside the submitted work. W. Zwart reports grants from Astellas Pharma during the conduct of the study, as well as grants and personal fees from Astellas Pharma, and grants from AstraZeneca outside the submitted work. No disclosures were reported by the other authors.

Author contributions

S. Linder: Conceptualization, data curation, formal analysis, validation, investigation, visualization, methodology, writing–original draft, writing–review and editing. M. Hoogstraat: Conceptualization, data curation, software, formal analysis, investigation, visualization, methodology, writing–original draft, writing–review and editing. S. Stelloo: Conceptualization, funding acquisition, investigation, methodology, writing–review and editing. N. Eickhoff: Resources, formal analysis, validation, investigation, methodology, writing–review and editing. K. Schuurman: Formal analysis, investigation, methodology, writing–review and editing. H. de Barros: Resources, data curation, formal analysis, investigation, writing–review and editing. M. Alkemade: Data curation, investigation, methodology, writing–review and editing. E.M. Bekers: Formal analysis, investigation, methodology, writing–review and editing. T.M. Severson: Data curation, software, formal analysis, investigation, visualization, methodology, writing–review and editing. J. Sanders: Formal analysis, investigation, methodology, writing–review and editing. C.-C.F. Huang: Investigation, methodology, writing–review and editing. T. Morova: Software, formal analysis, methodology, writing–review and editing. U.B. Altintas: Software, formal analysis, methodology, writing–review and editing. L. Hoekman: Data curation, formal analysis, investigation, methodology, writing–review and editing. Y. Kim: Resources, software, formal analysis, investigation, visualization, methodology, writing–review and

editing. S.C. Baca: Resources, data curation, software, formal analysis, investigation, methodology, writing–review and editing. M. Sjostrom: Resources, data curation, software, formal analysis, investigation, visualization, methodology, writing–review and editing. A. Zaalberg: Investigation, methodology, writing–review and editing. D.C. Hintzen: Data curation, software, investigation, methodology, writing–review and editing. J. de Jong: Formal analysis, investigation, methodology, writing– review and editing. R.J.C. Kluin: Software, investigation, methodology, writing–review and editing. I. de Rink: Data curation, software, formal analysis, methodology, writing–review and editing. C. Giambartolomei: Resources. J.-H. Seo: Resources. B. Pasaniuc: Resources. M. Altelaar: Software, supervision, methodology, writing– review and editing. R.H. Medema: Software, supervision, methodology, writing–review and editing. F.Y. Feng: Resources, supervision, methodology, writing–review and editing. A. Zoubeidi: Resources, writing–review and editing. M.L. Freedman: Resources, formal analysis, investigation, writing–review and editing. L.F.A. Wessels: Supervision, writing–review and editing. L.M. Butler: Writing– review and editing. N.A. Lack: Resources, supervision, investigation, methodology, writing–review and editing. H. van der Poel: Conceptualization, resources, data curation, formal analysis, supevision, funding acquisition, methodology, project administration, writing–review and editing. A.M. Bergman: Conceptualization, resources, supervision, funding acquisition, investigation, writing– original draft, project administration, writing–review and editing. W. Zwart: Conceptualization, resources, supervision, funding acquisition, investigation, methodology, writing–original draft, project administration, writing–review and editing.

Acknowledgments

This work was supported by Movember (NKI01 to A.M. Bergman and W. Zwart), KWF Dutch Cancer Society (10084 ALPE to A.M. Bergman and W. Zwart), KWF Dutch Cancer Society/Alpe d'HuZes Bas Mulder Award (NKI 2014-6711 to W. Zwart), the Netherlands Organization for Scientific Research (NWO-VIDI-016.156.401 to W. Zwart), Department of Defense (W81XWH-19-1-0565 to W. Zwart), and Astellas Pharma (to W. Zwart, A.M. Bergman, and H. van der Poel). The authors thank the NKI-AVL Core Facility Molecular Pathology and Biobanking, the NKI Proteomics/Mass Spectrometry facility (supported by the Dutch NWO X-omics Initiative), and the NKI Preclinical Intervention Unit (MCCA) for experimental assistance; the NKI Genomics Core facility for next-generation sequencing and bioinformatics support; and the NKI Research High Performance Computing facility for computational infrastructure. We also thank all Zwart/Bergman lab members for fruitful discussions and technical advice. Finally, we thank all patients and clinical staff who were involved in the DARANA trial.

Supplementary Data

Primary clinical outcomes

We conducted a single-arm, open-label phase II clinical trial: the DARANA study (Dynamics of Androgen Receptor Genomics and Transcriptomics After Neoadjuvant Androgen Ablation; NCT03297385). In this study, 56 men with primary high-risk (Gleason score ≥ 7) PCa were enrolled. Mean age at inclusion was 67 years, baseline serum PSA 12.8 ng/mL and the majority of patients had ISUP GG2 (28%) or ISUP GG4 (36%) PCa (**Fig. 1A**; **Table 1**; Supplementary Table S1). 55 patients completed therapy without dose adjustments, while one patient (DAR37) discontinued ENZ three weeks prematurely. All patients underwent a robotic-assisted laparoscopic prostatectomy (RALP). Primary outcome of the trial was the rate of positive margins after neoadjuvant ENZ treatment. 30% of prostatectomy specimens had positive surgical margins, which was comparable to 1492 non-treated historical controls with Gleason ≥ 7 (34%; see methods). Consequently, this trial did not provide evidence that neoadjuvant ENZ treatment reduces the surgical margin rate. This finding is analogous to a previous neoadjuvant study on ENZ alone versus ENZ in combination with the 5a-reductase inhibitor dutasteride and androgen deprivation therapy (ADT) in high-risk patients for 6 months, describing 26.1% positive margins in the triple-therapy arm[98]. However, a significantly increased staining of post-treatment prostate samples for cleaved Caspase-3 compared to untreated control samples suggested an upregulation of apoptosis signals in prostate cancer cells, and a significantly decreased staining for Ki-67 in post-therapy samples, indicated a decrease in prostate cancer cell proliferation upon treatment (Supplementary Fig. S1A and S1B). Despite these biomarker responses, after a mean follow-up of 51 months, no significant improvement of time-to-biochemical recurrence, time-to-ADT, time-to-radiological recurrence and time-to-distant metastasis were found when comparing these ENZ-treated patients to matched untreated control patients (Supplementary Fig. S1C-F). There is no previous data available on time-to-BCR following neoadjuvant ENZ treatment, compared with a not-treated comparator or a historical cohort, but a pooled analysis of three trials of neoadjuvant ENZ and/or abiraterone-treated patients[99] reported a 3-year BCR-free survival of 59,1%, which is in line with our findings. No differences in pre- and post-treatment T stages were observed. In contrast, several studies have reported pathological responses after 6 months of neoadjuvant ENZ and ADT with or without abiraterone treatment[98,100,101], which may be related to the additional treatment with ADT and/or the longer treatment duration. A higher incidence of ypN1 lymph nodes than cN1 lymph nodes in the current trial was possibly due to differences in accuracy of radiographic pre-treatment assessments versus post-treatment histological assessments. In conclusion, neoadjuvant ENZ monotherapy for 3 months resulted in increased expression of apoptosis and decreased expression of cell proliferation markers, but not in tumor-downstaging or changes in time-to-recurrence endpoints.

Supplementary tables

Due to print size limitations, all supplementary data tables are available online via the DOI: https://doi.org/10.1158/2159-8290.CD-21-0576 or via the PMID: 35754340.

Supplementary Table S1: Clinical outcome.
Supplementary Table S2: ChIP-seq quality control metrics.
Supplementary Table S3: Differential FOXA1 binding sites.
Supplementary Table S4: Intrinsic enhancer activity of tumor-specific ARBS.
Supplementary Table S5: List of genes coupled to differential FOXA1 sites based on H3K27ac HiChIP enhancer-promoter coupling.
Supplementary Table S6: Cell line ChIP-seq quality control metrics.

Supplementary Figures

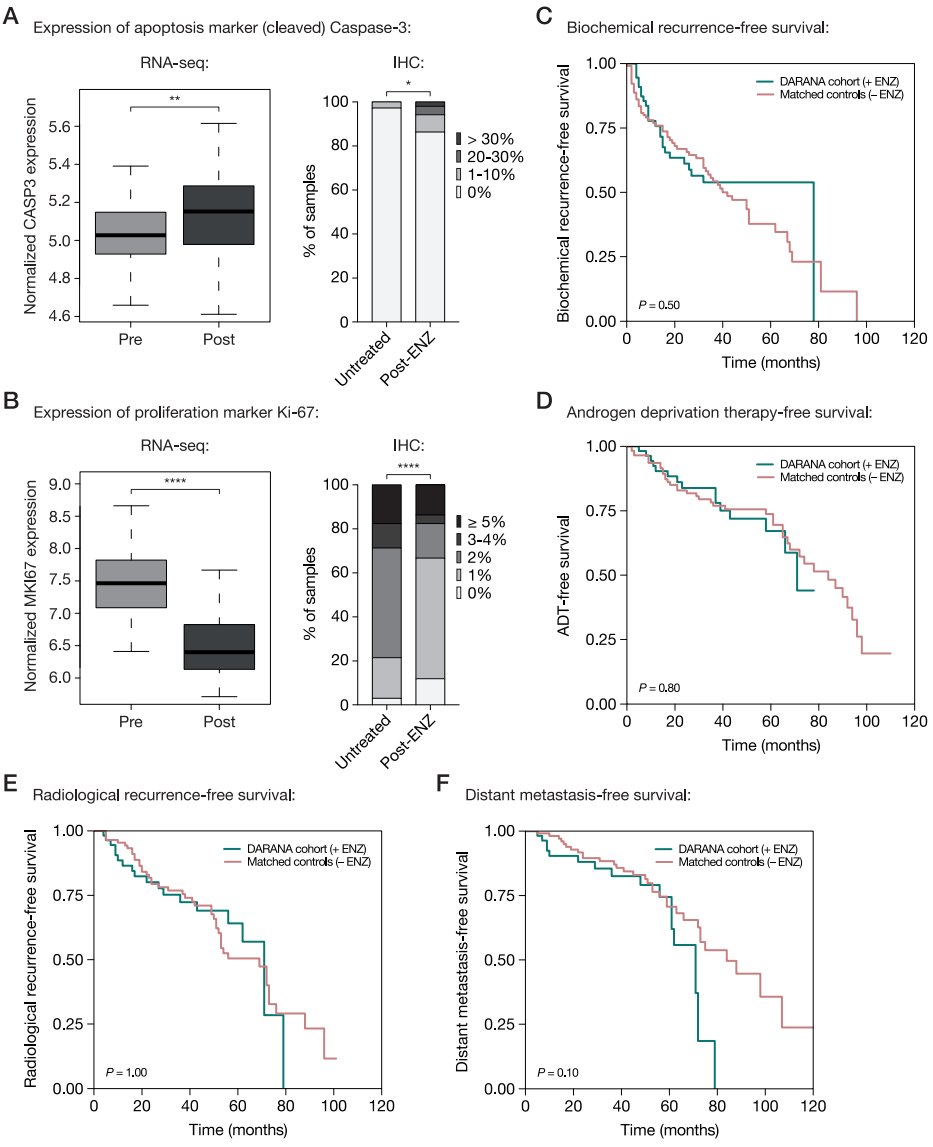

◂ **Supplementary Figure S1:** Pathological and clinical outcome measures. (**A**) Expression of apoptosis marker (cleaved) Caspase-3. Boxplot (left) showing normalized CASP3 gene expression before and after 3 months of neoadjuvant ENZ treatment, and stacked bar graphs (right) indicating quantification of cleaved Caspase-3-positive tumor cells in tissue microarrays consisting of prostatectomy specimens from untreated patients (not receiving neoadjuvant ENZ; *n* = 109) and DARANA patients post-ENZ (*n* = 51). **, $P < 0.01$ (Mann-Whitney *U* test; RNA-seq); *, $P < 0.05$ (Fisher exact test; IHC). (**B**) Expression of proliferation marker Ki-67. Boxplot (left) showing normalized MKI67 gene expression before and after 3 months of neoadjuvant ENZ treatment, and stacked bar graphs (right) indicating quantification of Ki-67-positive tumor cells in tissue microarrays consisting of prostatectomy specimens from untreated patients and DARANA patients post-ENZ. ****, $P < 0.0001$ (Mann-Whitney *U* test; RNA-seq); ****, $P < 0.0001$ (Fisher exact test; IHC). (**C-F**) Kaplan-Meier curves showing the biochemical recurrence-free survival (C), androgen deprivation therapy-free survival (D), radiological recurrence-free survival (E), and distant metastasis-free survival (F) of the DARANA cohort treated with neoadjuvant ENZ prior to prostatectomy (*n* = 55) and a matched untreated control cohort (*n* = 115).

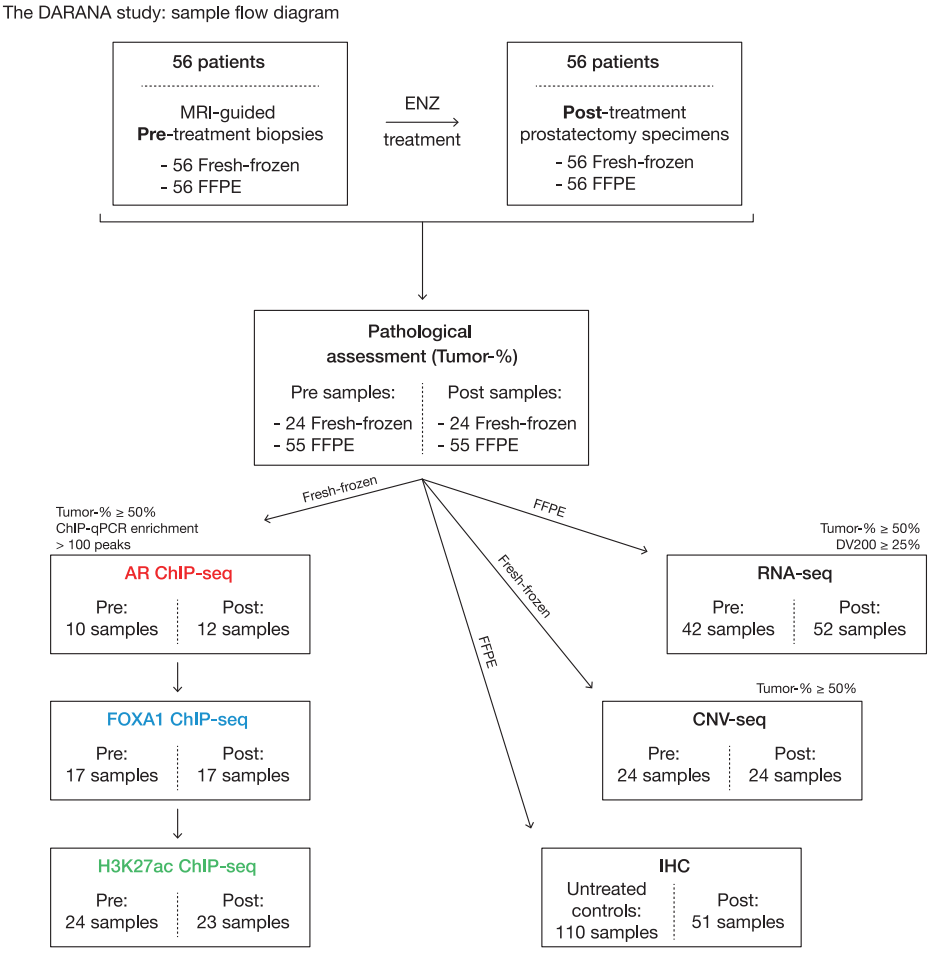

Supplementary Figure S2: The DARANA study. Sample flow diagram indicating the quality control measures applied to each sample, and the number of samples passing the respective cut-offs per omics data stream.

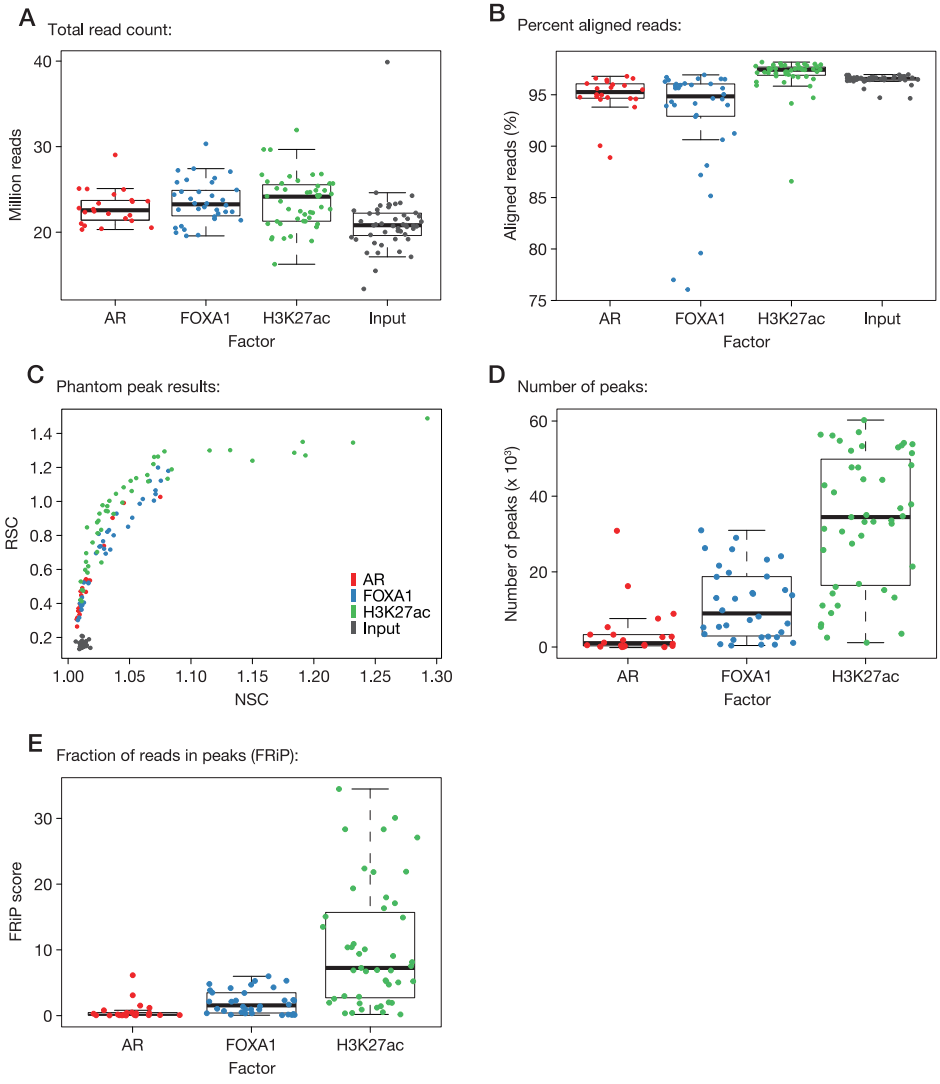

Supplementary Figure S3: Tissue ChIP-seq quality metrics. (**A**) Boxplots showing the median total number of reads for AR (red), FOXA1 (blue) and H3K27ac (green) ChIP-seq, as well as ChIP-seq input (gray) samples. (**B**) Boxplots indicating the percentage of aligned reads per ChIP factor. (**C**) Scatter plot of phantom peak results, showing the normalized strand cross-correlation coefficient (NSC) and relative strand cross-correlation coefficient (RSC) scores for each ChIP-seq and input sample. (**D**) Boxplot showing the number of peaks per ChIP-seq sample. Peak calling was performed over matched input control samples. (**E**) Boxplots indicating the fraction of reads in peaks (FRiP) score per sample.

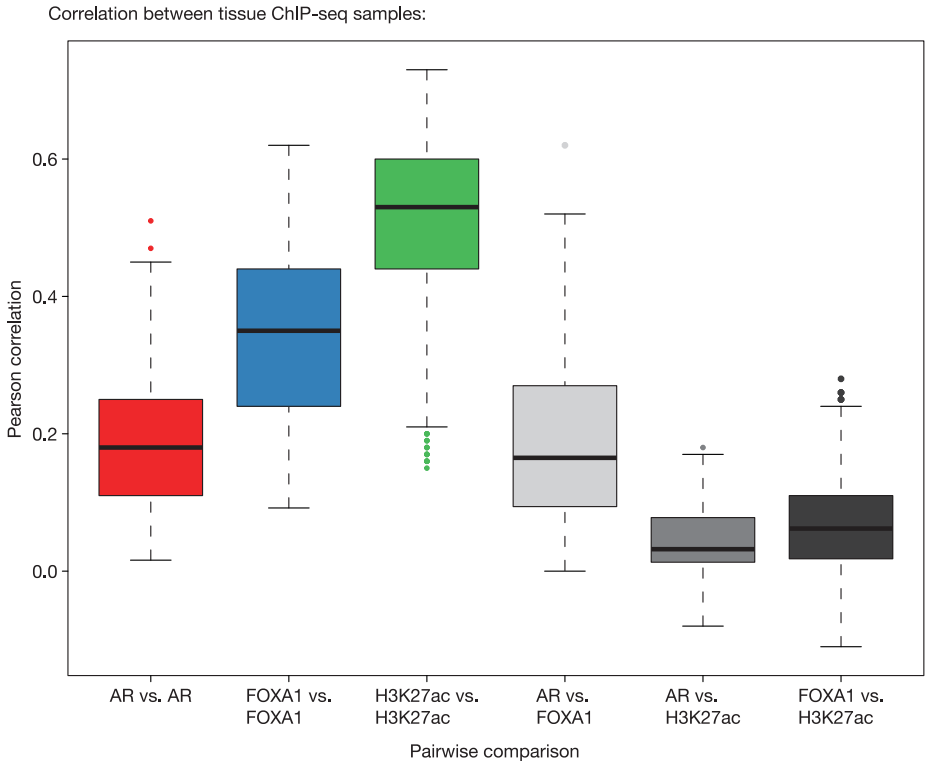

Supplementary Figure S4: Correlation between tissue ChIP-seq samples. Boxplots indicating the Pearson correlation of ChIP-seq samples based on peak occupancy. Both, pairwise comparisons within the same ChIP-seq dataset (AR vs. AR, FOXA1 vs. FOXA1, H3K27ac vs. H3K27ac), and between different datasets (AR vs. FOXA1, AR vs. H3K27ac, FOXA1 vs. H3K27ac) are shown. The corresponding correlation matrix is shown in **Figure 2B**.

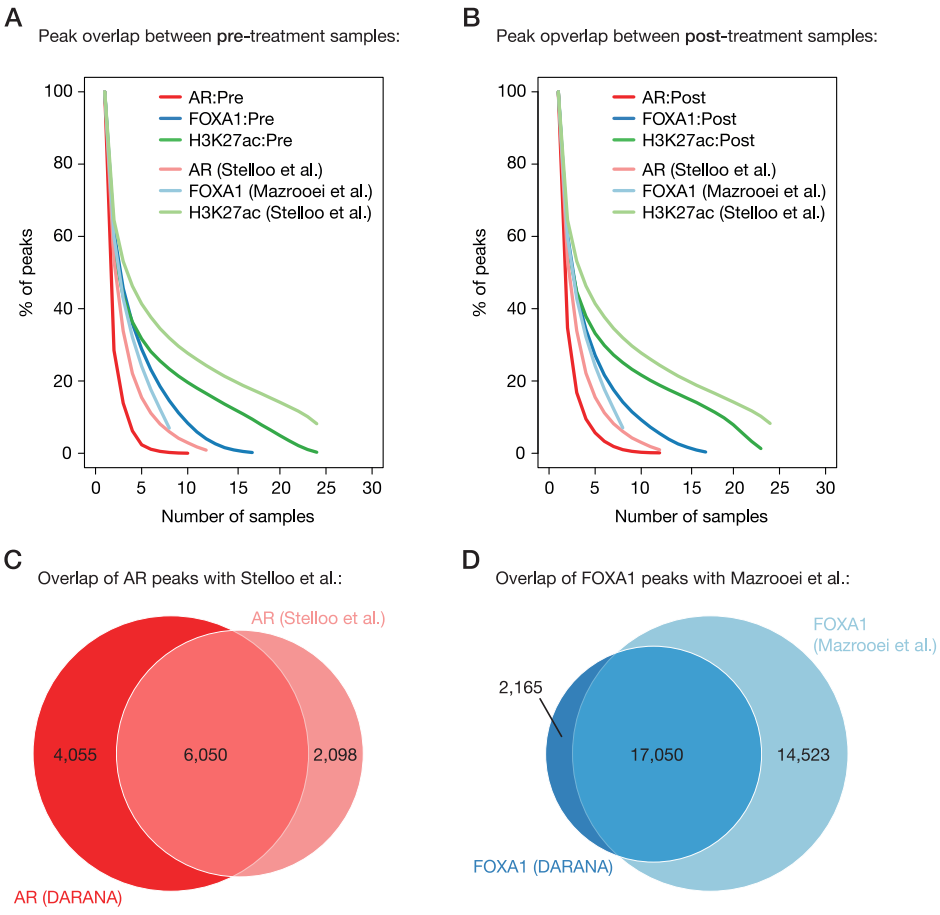

Supplementary Figure S5: Overlap with published tissue ChIP-seq datasets. (**A-B**) Elbow plot depicting the peak overlap between pre-treatment (A) and post-treatment (B) ChIP-seq samples with publicly available datasets per factor. Sample sizes were matched per ChIP factor and the percentage of overlapping peaks with increasing number of samples is shown. (**C**) Venn diagram indicating the overlap of AR consensus sites (present in at least 3 out of 22 AR samples) with AR consensus sites identified in Stelloo et al. (present in at least 25 out of 88 AR samples[31]). (**D**) Venn diagram indicating the overlap of FOXA1 consensus sites (present in at least 7 out of 34 FOXA1 samples) with FOXA1 consensus sites identified in Mazrooei et al. (present in at least 3 out of 8 FOXA1 samples[32]).

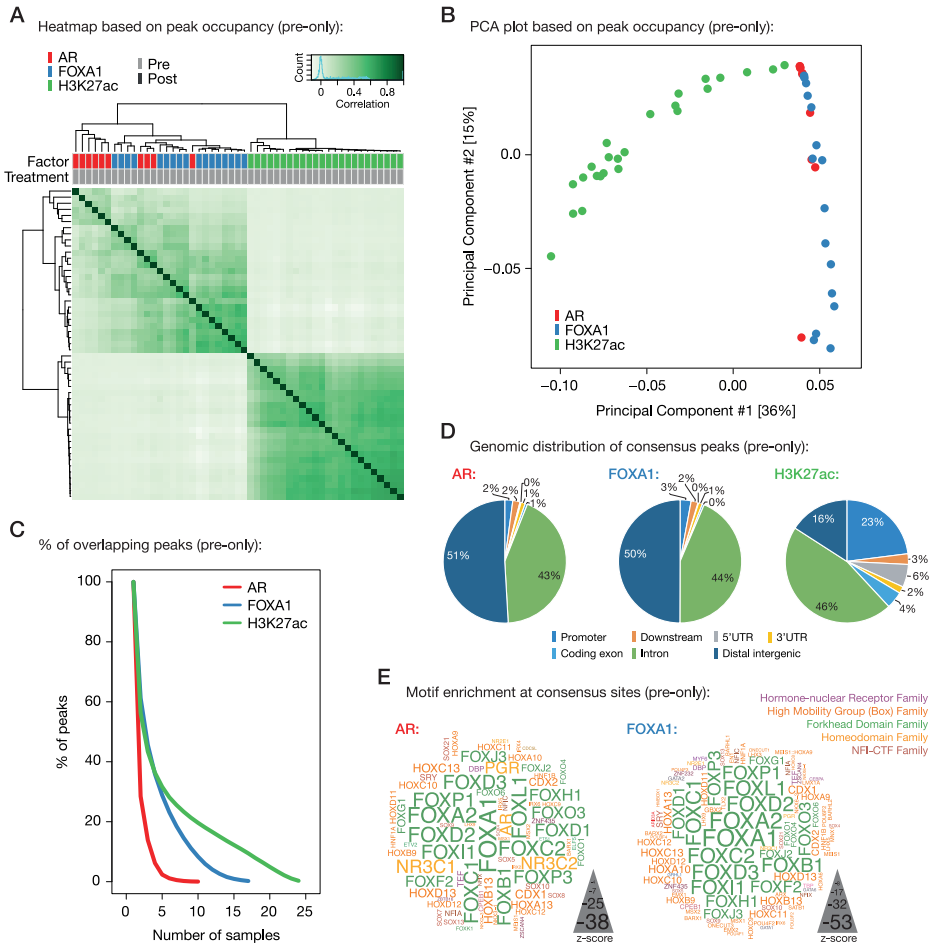

Supplementary Figure S6: Characterization of pre-treatment ChIP-seq samples. (**A**) Correlation heatmap based on peak occupancy of pre-treatment samples. Clustering of the samples is based on all called peaks and represents Pearson correlations between individual ChIP-seq samples. The column color bars indicate the ChIP-seq factor (AR, FOXA1, H3K27ac) and treatment status (Pre-only). (**B**) Principal component analysis (PCA) plot based on peak occupancy. Each dot represents a pre-treatment ChIP-seq sample that is colored per factor. (**C**) Elbow plot depicting the peak overlap between pre-treatment ChIP-seq samples per factor. Shown is the percentage of overlapping peaks with increasing number of samples. Consensus peaksets were designed by using a cutoff of peaks present in at least 3 AR, 7 FOXA1, or 13 H3K27ac pre-treatment samples. (**D**) Pie charts showing the genomic distribution of AR (left), FOXA1 (middle) and H3K27ac (right) consensus peaks identified in pre-treatment ChIP-seq samples. (**E**) Word clouds show motif enrichment at AR (left) and FOXA1 (right) consensus sites identified in pre-treatment ChIP-seq samples. The font size represents the z-score and colors correspond to transcription factor families.

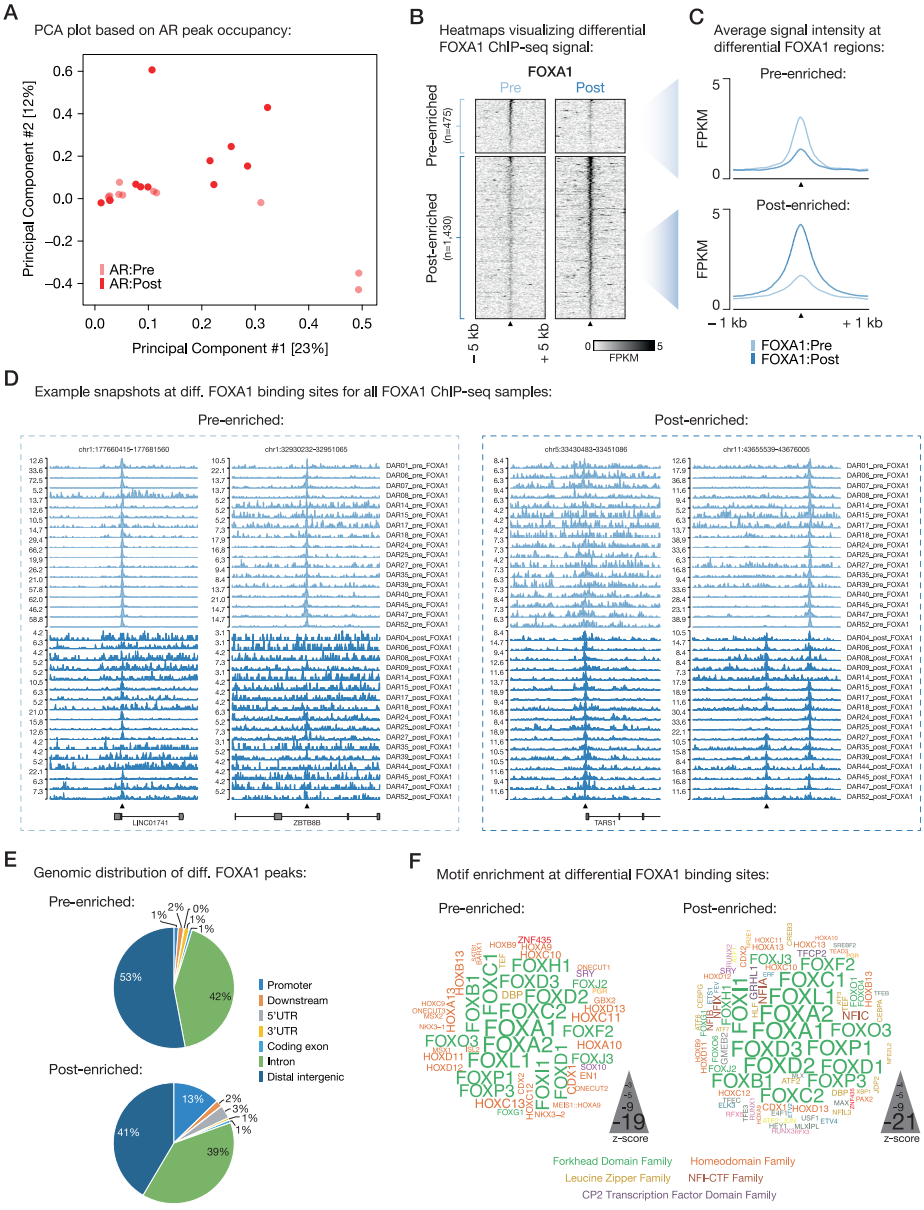
A
PCA plot based on AR peak occupancy:
Principal Component #2 [12%]
Principal Component #1 [23%]
AR:Pre
AR:Post
B
Heatmaps visualizing differential FOXA1 ChIP-seq signal:
FOXA1
Pre
Post
Pre-enriched (n=475)
Post-enriched (n=1,430)
– 5 kb
+ 5 kb
FPKM
C
Average signal intensity at differential FOXA1 regions:
Pre-enriched:
Post-enriched:
FPKM
– 1 kb
+ 1 kb
FOXA1:Pre
FOXA1:Post
D
Example snapshots at diff. FOXA1 binding sites for all FOXA1 ChIP-seq samples:
Pre-enriched:
Post-enriched:
LINC01741
ZBTB8B
TARS1
E
Genomic distribution of diff. FOXA1 peaks:
Pre-enriched:
Post-enriched:
Promoter
Downstream
5'UTR
3'UTR
Coding exon
Intron
Distal intergenic
F
Motif enrichment at differential FOXA1 binding sites:
Pre-enriched:
Post-enriched:
z-score
Forkhead Domain Family
Homeodomain Family
Leucine Zipper Family
NFI-CTF Family
CP2 Transcription Factor Domain Family

◂ **Supplementary Figure S7:** Differential FOXA1 chromatin binding upon ENZ treatment. (**A**) Principal component analysis (PCA) plot based on peak occupancy of AR ChIP-seq data. Color indicates the treatment status of pre- (light red) and post- (dark red) ENZ AR samples. (**B**) Representative tornado plots visualizing FOXA1 ChIP-seq signal [in fragments per kilobase per million reads mapped (FPKM)] at pre-enriched and post-enriched FOXA1 binding sites before (pre) and after (post) ENZ treatment in one patient (DAR39). Data are centered at FOXA1 peaks depicting a 5-kb window around the peak center. (**C**) Quantification of the average signal intensity at pre-enriched (top) and post-enriched (bottom) FOXA1 binding sites before (light blue) and after (dark blue) ENZ treatment shown in (B). Data are centered at FOXA1 peaks depicting a 2.5-kb window around the peak center. (**D**) Snapshot overviews across all FOXA1 ChIP-seq samples for two pre-enriched (left) and two post-enriched (right) FOXA1 binding sites. Y-axes indicate ChIP-seq readcounts. Note differences in Y-axis between sample groups. (**E**) Pie charts showing the genomic distribution of pre-enriched (top) and post-enriched (bottom) FOXA1 binding sites. (**F**) Word clouds show motif enrichment at pre-enriched (left) and post-enriched (right) FOXA1 sites. The font size represents the z-score and colors correspond to transcription factor families.

Supplementary Figure S8: Copy number variation at differential FOXA1 sites. (**A**) Boxplot showing the median copy number ratio at pre-enriched (left) and post-enriched (right) FOXA1 binding sites over all pre-treatment and post-treatment samples. (**B-C**) Heatmap depicting segmented CNV data at pre-enriched (B) and post-enriched (C) FOXA1 binding sites in pre- and post-treatment samples (columns). Differential FOXA1 sites are ordered per chromosome (rows) and heatmap color indicates copy number gains and losses (z-score). (**D**) Scatter plot showing the correlation between FOXA1 ChIP-seq data and CNV-seq data for paired pre-treatment and post-treatment samples (n = 15). Plotted is the normalized ChIP readcount difference (post- vs. pre-ENZ) against the CNV ratio difference (post- vs. pre-ENZ) at all differential FOXA1 binding sites (n = 1,905) per patient. CNV cut-offs of ± 0.1 (dotted vertical lines) and mean Pearson correlation (R = 0.11; range: -0.02 – 0.26) are indicated. Differential FOXA1 binding sites (dots) are colored based on their enrichment (pre-enriched vs. post-enriched) and recurrent CNV events found in ≥ 3 patients are highlighted. (**E**) Stacked bar plot indicating the fraction of differential FOXA1 sites that show recurrent CNVs shown in (D) with CNV ratio > 0.1 for post-enriched and < 0.1 for pre-enriched FOXA1 sites in 3 or more patients (pre: n = 24/475, post: n = 20/1,430). ns, P > 0.05 (Fisher exact test). ▸

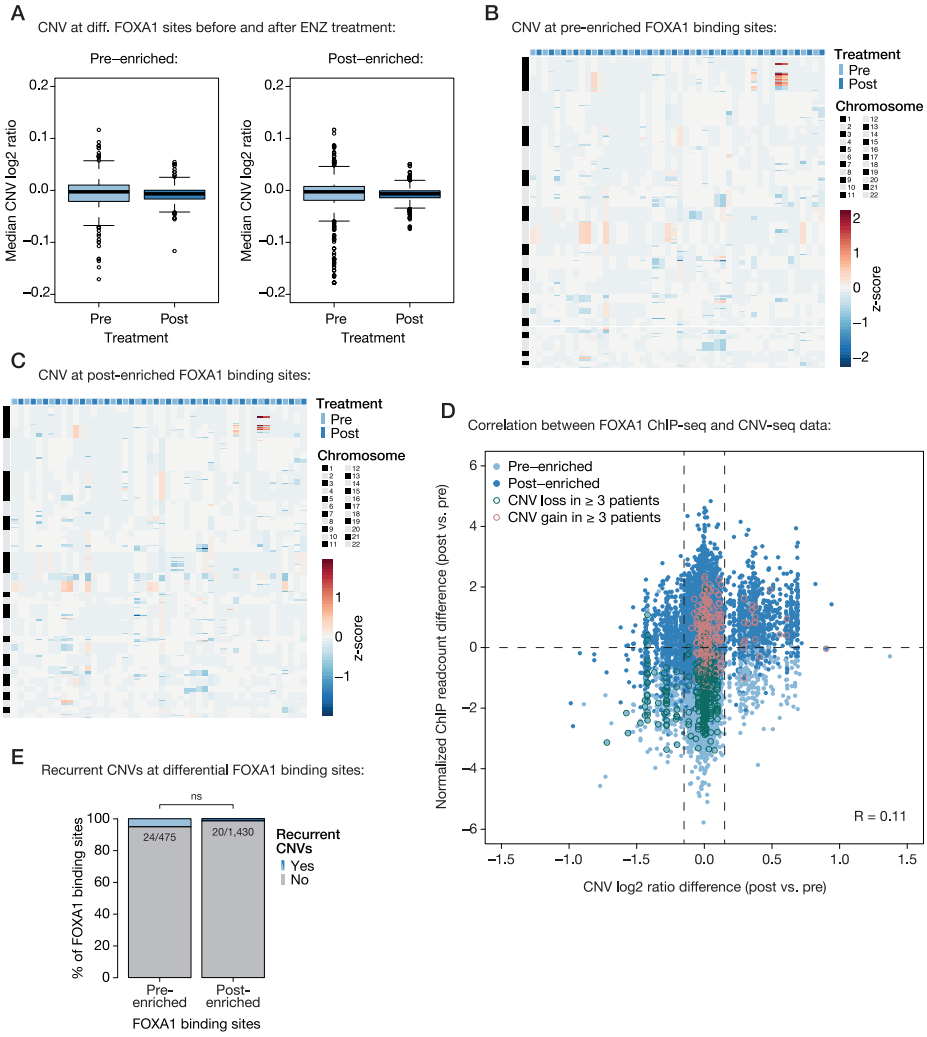
A
CNV at diff. FOXA1 sites before and after ENZ treatment:
Pre–enriched:
Post–enriched:
Median CNV log2 ratio
0.2
0.1
0.0
−0.1
−0.2
Pre
Post
Treatment
B
CNV at pre-enriched FOXA1 binding sites:
Treatment
Pre
Post
Chromosome
z-score
2
1
0
−1
−2
C
CNV at post-enriched FOXA1 binding sites:
D
Correlation between FOXA1 ChIP-seq and CNV-seq data:
Pre–enriched
Post–enriched
CNV loss in ≥ 3 patients
CNV gain in ≥ 3 patients
Normalized ChIP readcount difference (post vs. pre)
CNV log2 ratio difference (post vs. pre)
R = 0.11
E
Recurrent CNVs at differential FOXA1 binding sites:
ns
% of FOXA1 binding sites
24/475
20/1,430
Recurrent CNVs
Yes
No
Pre-enriched
Post-enriched
FOXA1 binding sites

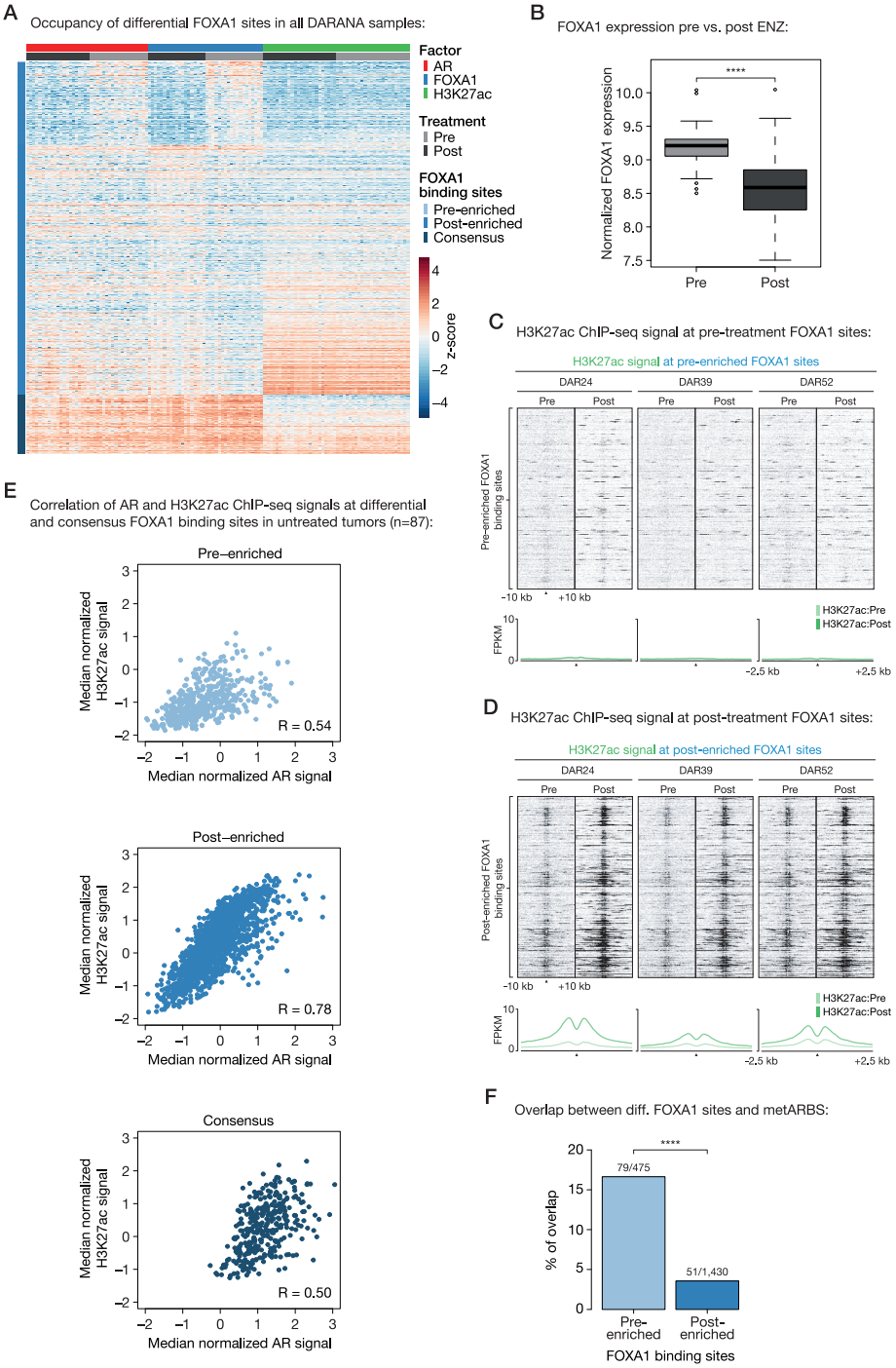
A
Occupancy of differential FOXA1 sites in all DARANA samples:
Factor
AR
FOXA1
H3K27ac
Treatment
Pre
Post
FOXA1 binding sites
Pre-enriched
Post-enriched
Consensus
z-score
B
FOXA1 expression pre vs. post ENZ:
Normalized FOXA1 expression
****
Pre
Post
C
H3K27ac ChIP-seq signal at pre-treatment FOXA1 sites:
H3K27ac signal at pre-enriched FOXA1 sites
DAR24
DAR39
DAR52
Pre-enriched FOXA1 binding sites
-10 kb
+10 kb
FPKM
H3K27ac:Pre
H3K27ac:Post
-2.5 kb
+2.5 kb
D
H3K27ac ChIP-seq signal at post-treatment FOXA1 sites:
H3K27ac signal at post-enriched FOXA1 sites
Post-enriched FOXA1 binding sites
E
Correlation of AR and H3K27ac ChIP-seq signals at differential and consensus FOXA1 binding sites in untreated tumors (n=87):
Pre–enriched
R = 0.54
Post–enriched
R = 0.78
Consensus
R = 0.50
Median normalized H3K27ac signal
Median normalized AR signal
F
Overlap between diff. FOXA1 sites and metARBS:
% of overlap
79/475
51/1,430
Pre-enriched
Post-enriched
FOXA1 binding sites

◂ **Supplementary Figure S9:** Characterization of differential FOXA1 sites. (**A**) Coverage heatmap showing occupancy of differential (pre-/post-enriched) and consensus FOXA1 peaks in all generated pre- and post-treatment ChIP-seq samples. Heatmap color indicates region read counts (z-score) at pre-enriched, post-enriched and consensus FOXA1 sites (rows) in the pre- and post-treatment AR (red), FOXA1 (blue) and H3K27ac (green) ChIP-seq data streams (columns). (**B**) Boxplot showing normalized FOXA1 gene expression before and after 3 months of neoadjuvant ENZ treatment. ****, $P < 0.0001$ (Mann-Whitney U test). (**C-D**) Representative tornado plots (top) and average density plots (bottom) visualizing H3K27ac ChIP-seq signal [in fragments per kilobase per million reads mapped (FPKM)] at pre-enriched (C) and post-enriched (D) FOXA1 binding sites in 3 patients (DAR24, DAR39, DAR52) before and after ENZ treatment. Data are centered at FOXA1 peaks depicting a 10-kb (heatmaps) or 2.5-kb (density plots) window around the peak center. (**E**) Scatter plots showing the correlation between AR and H3K27ac ChIP-seq signals at pre-enriched (top), post-enriched (middle) and consensus (bottom) FOXA1 sites in treatment-naïve primary prostate tumors ($n = 87$). Pearson correlations for pre-enriched ($R = 0.54$), post-enriched ($R = 0.78$) and consensus ($R = 0.50$) FOXA1 sites are indicated. (**F**) Bar chart indicating the overlap between pre-enriched (left) and post-enriched (right) FOXA1 binding sites, and previously identified metastasis-specific AR binding sites[7] (metARBS). ****, $P < 0.0001$ (Fisher exact test).

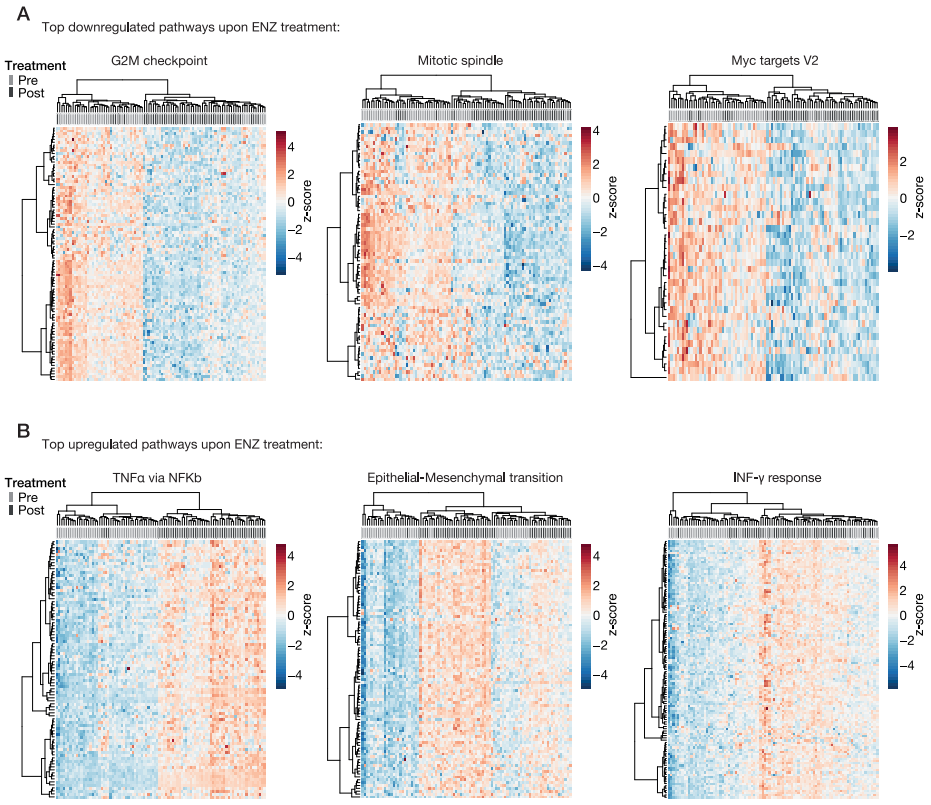

Supplementary Figure S10: Top differentially expressed pathways upon neoadjuvant ENZ treatment. Heatmaps depicting differential gene expression of top downregulated (**A**) and top upregulated (**B**) pathways upon ENZ treatment. Unsupervised hierarchical clustering of pre- and post-treatment RNA-seq samples is based on the expression of genes that define the respective hallmark gene sets. Color scale indicates gene expression (z-score).

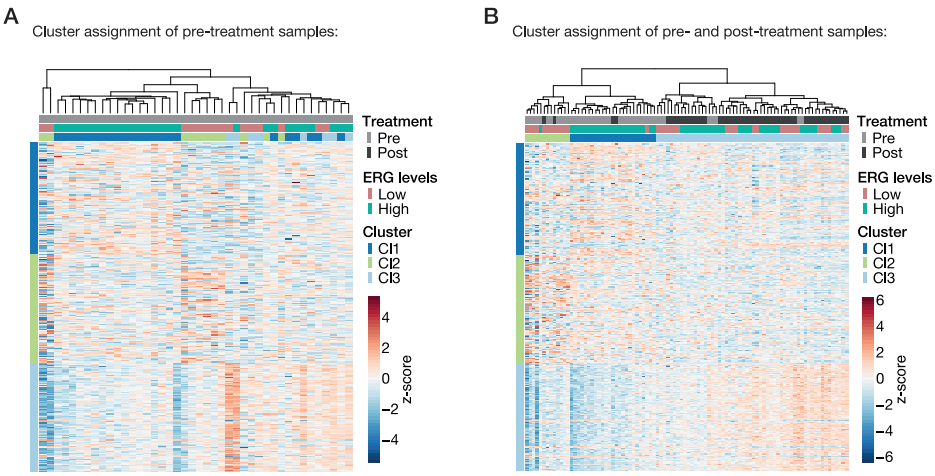

Supplementary Figure S11: The effect of neoadjuvant ENZ on molecular PCa subtyping. Unsupervised hierarchical clustering of pre-treatment (**A**) or pre- and post-treatment (**B**) RNA-seq samples using 285 genes differentially expressed across 3 previously reported PCa subtypes[31]. For each sample, the assigned cluster affiliation as well as the ERG gene expression levels are indicated below the branching. The genes (rows) are ordered per cluster and the color scale of the heatmap indicates gene expression (z-score).

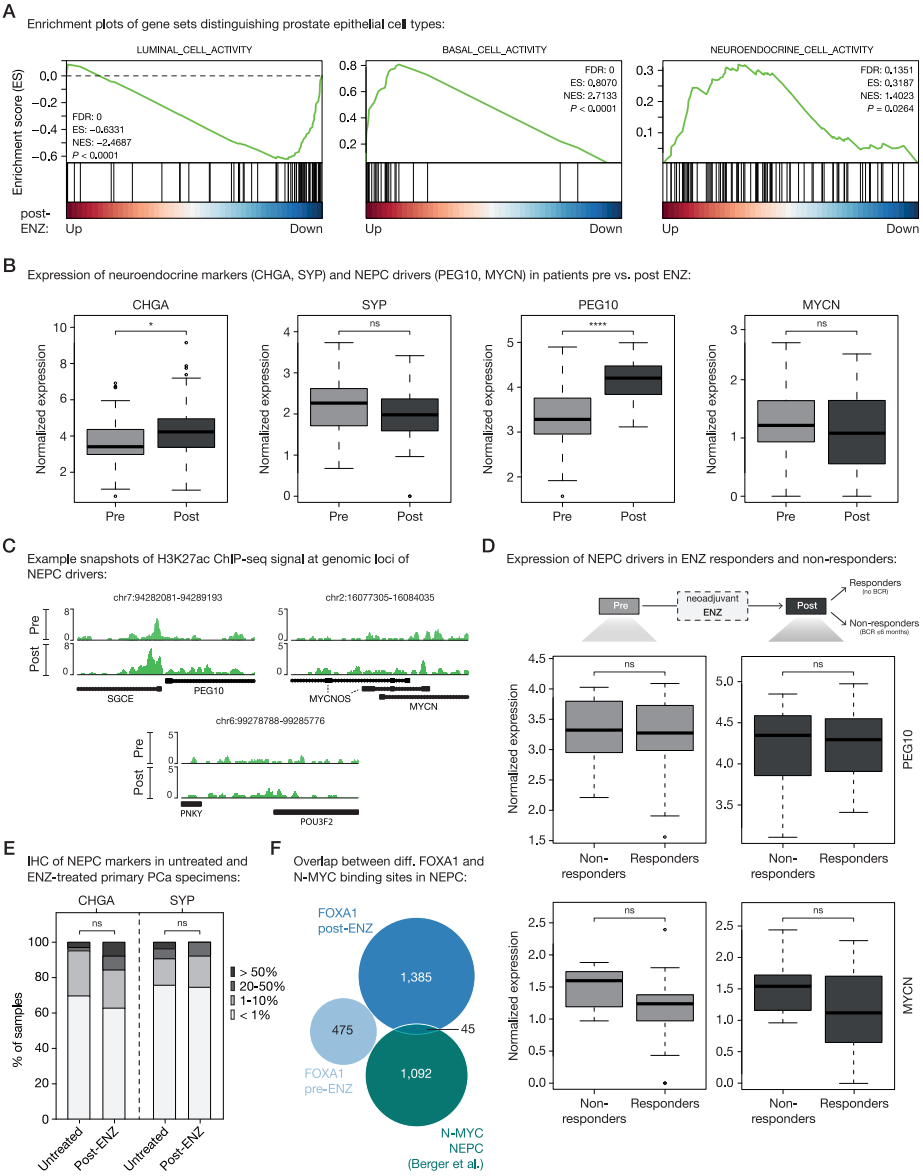
A
Enrichment plots of gene sets distinguishing prostate epithelial cell types:
LUMINAL_CELL_ACTIVITY
BASAL_CELL_ACTIVITY
NEUROENDOCRINE_CELL_ACTIVITY
Enrichment score (ES)
FDR: 0
ES: −0.6331
NES: −2.4687
P < 0.0001
FDR: 0
ES: 0.8070
NES: 2.7133
P < 0.0001
FDR: 0.1351
ES: 0.3187
NES: 1.4023
P = 0.0264
post-ENZ:
Up
Down
B
Expression of neuroendocrine markers (CHGA, SYP) and NEPC drivers (PEG10, MYCN) in patients pre vs. post ENZ:
CHGA
SYP
PEG10
MYCN
Normalized expression
Pre
Post
ns
C
Example snapshots of H3K27ac ChIP-seq signal at genomic loci of NEPC drivers:
chr7:94282081-94289193
chr2:16077305-16084035
chr6:99278788-99285776
SGCE
PEG10
MYCNOS
MYCN
PNKY
POU3F2
D
Expression of NEPC drivers in ENZ responders and non-responders:
Pre
neoadjuvant ENZ
Post
Responders
Non-responders
Normalized expression
PEG10
MYCN
Non-responders
Responders
E
IHC of NEPC markers in untreated and ENZ-treated primary PCa specimens:
CHGA
SYP
% of samples
> 50%
20-50%
1-10%
< 1%
Untreated
Post-ENZ
F
Overlap between diff. FOXA1 and N-MYC binding sites in NEPC:
FOXA1 post-ENZ
FOXA1 pre-ENZ
N-MYC NEPC (Berger et al.)
1,385
475
45
1,092

◂ **Supplementary Figure S12:** Induction of neuroendocrine-like signaling post-ENZ. (**A**) Enrichment plots of genes distinguishing prostate epithelial cell types (luminal, basal, neuroendocrine). Genes are ranked by differential expression upon ENZ treatment based on patient RNA-seq data (post- vs. pre-ENZ). Y-axis indicates enrichment score (ES). GSEA statistics (FDR, ES, NES, nominal *P*-value) are indicated. (**B**) Boxplots showing normalized gene expression of neuroendocrine markers (CHGA, SYP) and NEPC disease drivers (PEG10, MYCN) before and after 3 months of neoadjuvant ENZ treatment. ns, $P > 0.05$; *, $P < 0.05$; ***, $P < 0.001$ (Mann-Whitney *U* test). (**C**) Representative example snapshots of H3K27ac ChIP-seq signal at the *PEG10*, *MYCN* and *POU3F2* (BRN2) gene loci before (top) and after (bottom) ENZ treatment. Shown are matched pre- and post-treatment ChIP-seq data of one patient (DAR52). (**D**) Boxplots depicting normalized gene expression of NEPC drivers (PEG10, MYCN) in ENZ non-responders (BCR ≤ 6 months; $n = 8$) and responders (no BCR; $n = 29$) in the pre- (left) and post-treatment (right) setting separately. ns, $P > 0.05$ (Mann-Whitney *U* test). (**E**) Quantification of NEPC marker (CHGA, SYP)-positive tumor cells in tissue microarrays consisting of prostatectomy specimens from untreated patients (not receiving neoadjuvant ENZ; $n = 110$) and DARANA patients post-ENZ ($n = 51$). ns, $P > 0.05$ (Fisher exact test). (**F**) Venn diagram indicating the overlap of differential FOXA1 binding sites (pre-ENZ or post-ENZ) with the N-MYC cistrome identified in an NEPC patient-derived organoid[40].

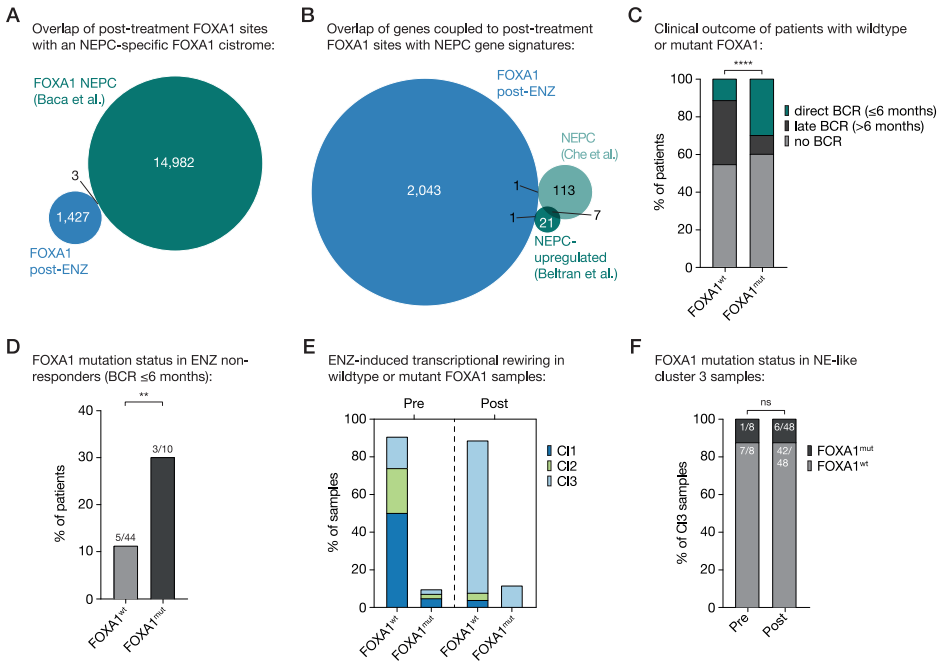

Supplementary Figure S13: Cistromic overlap with NEPC-FOXA1 and impact of FOXA1 mutations on clinical outcome and gene expression programs. (**A**) Venn diagram showing the overlap of post-enriched FOXA1 binding sites with the FOXA1 cistrome identified in treatment-emergent NEPC[42]. (**B**) Venn diagram depicting the overlap of genes coupled to post-enriched FOXA1 binding sites with NEPC gene signatures[35,36]. Post-ENZ FOXA1 binding sites were coupled to their respective target genes using H3K27ac HiChIP data. (**C**) Stacked bar chart indicating the clinical outcomes of patients with wildtype ($FOXA1^{wt}$; $n = 44$) or mutant ($FOXA1^{mut}$; $n = 10$) FOXA1. ****, $P < 0.0001$ (Fisher exact test). (**D**) Bar graph showing the FOXA1 mutation status in ENZ non-responders (BCR ≤ 6 months). **, $P < 0.01$ (Fisher exact test). (**E**) Stacked bar charts depicting the molecular subtype affiliation (CI1, CI2, CI3) of samples with wildtype or mutant FOXA1 for pre-treatment and post-treatment samples separately. (**F**) Bar graph indicating the FOXA1 mutation status in NE-like cluster 3 (CI3) samples before and after neoadjuvant ENZ treatment. ns, $P > 0.05$ (Fisher exact test).

Supplementary Figure S14: Cistromic and transcriptomic profiling of core components of the circadian clock. (**A**) Representative example snapshots of H3K27ac ChIP-seq signal at the *ARNTL* gene locus before (top) and after (bottom) ENZ treatment. Shown are matched pre- and post-treatment ChIP-seq data of three patients (DAR04, DAR05, DAR06). (**B**) ARNTL expression changes in paired RNA-seq samples (pre- vs. post-ENZ) distinguishing ENZ responders (no BCR; $n = 22$; left) and non-responders (BCR ≤ 6 months and BCR > 6 months; $n = 17$; right). ns, $P > 0.05$; ***, $P < 0.001$ (paired Mann-Whitney *U* test). (**C**) Boxplots showing normalized gene expression of canonical circadian clock components before and after 3 months of neoadjuvant ENZ treatment. ns, $P > 0.05$; *, $P < 0.05$; ****, $P < 0.0001$ (Mann-Whitney *U* test). (**D**) Boxplots depicting normalized gene expression of ARNTL dimerization partners CLOCK (top) and NPAS2 (bottom) in ENZ non-responders (BCR ≤ 6 months; $n = 8$) and responders (no BCR; $n = 29$) in the pre- (left) and post-treatment (right) setting separately. ns, $P > 0.05$ (Mann-Whitney *U* test). ►

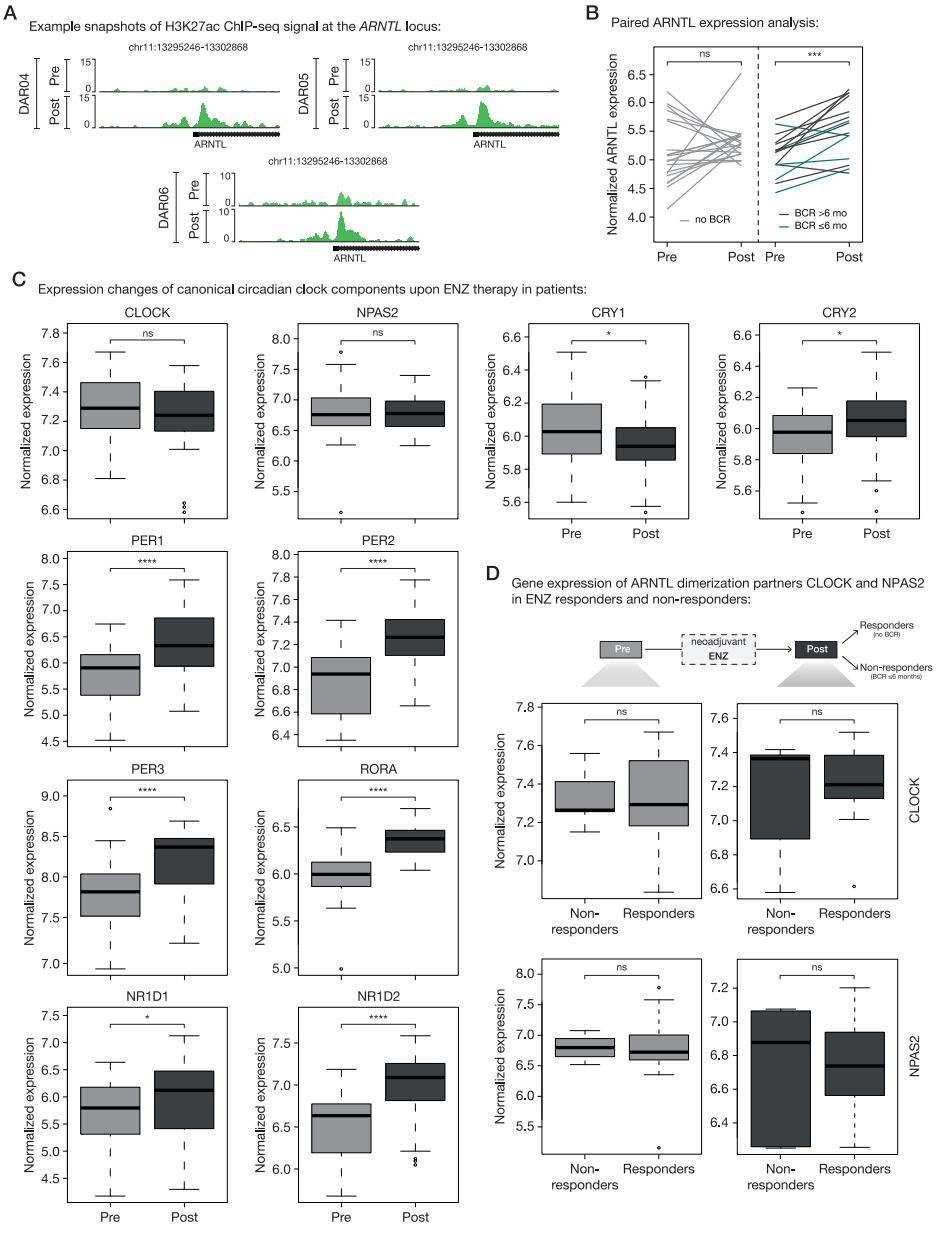
A
Example snapshots of H3K27ac ChIP-seq signal at the ARNTL locus:
chr11:13295246-13302868
DAR04
DAR05
DAR06
Pre
Post
ARNTL
B
Paired ARNTL expression analysis:
Normalized ARNTL expression
ns
***
no BCR
BCR >6 mo
BCR ≤6 mo
Pre
Post
C
Expression changes of canonical circadian clock components upon ENZ therapy in patients:
CLOCK
NPAS2
CRY1
CRY2
PER1
PER2
PER3
RORA
NR1D1
NR1D2
Normalized expression
D
Gene expression of ARNTL dimerization partners CLOCK and NPAS2
in ENZ responders and non-responders:
Pre
neoadjuvant
ENZ
Post
Responders
(no BCR)
Non-responders
(BCR ≤6 months)
Non-
responders
Responders
CLOCK
NPAS2

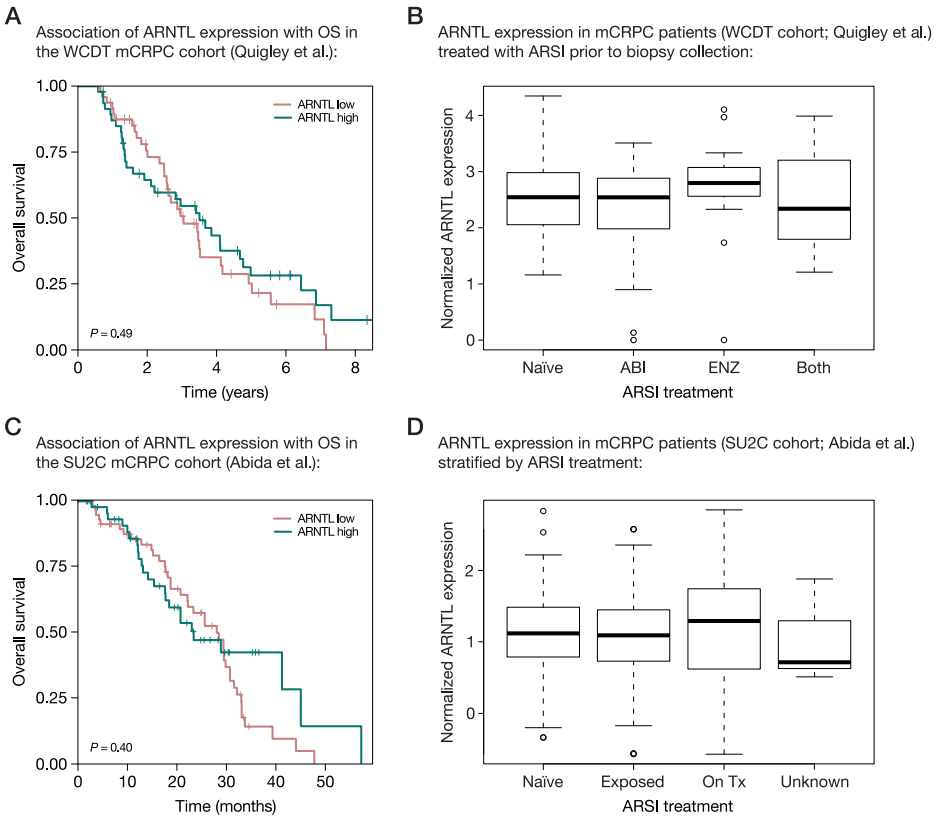

Supplementary Figure S15: Prognostic potential of ARNTL in mCRPC cohorts. (**A**) Kaplan-Meier curve showing the association of ARNTL expression levels (high: ≥ median; low < median) with overall survival (OS) in the WCDT mCRPC cohort[53]. (**B**) Boxplots indicating normalized ARNTL gene expression levels in mCRPC patients (WCDT cohort) stratified on exposure to AR signaling inhibitors (ARSI). (**C**) Kaplan-Meier curve depicting the association of ARNTL expression levels (high: ≥ median; low < median) with overall survival (OS) in the SU2C mCRPC cohort[54]. (**D**) Boxplots showing normalized ARNTL gene expression levels in mCRPC patients (SU2C cohort) stratified on exposure to AR signaling inhibitors (ARSI).

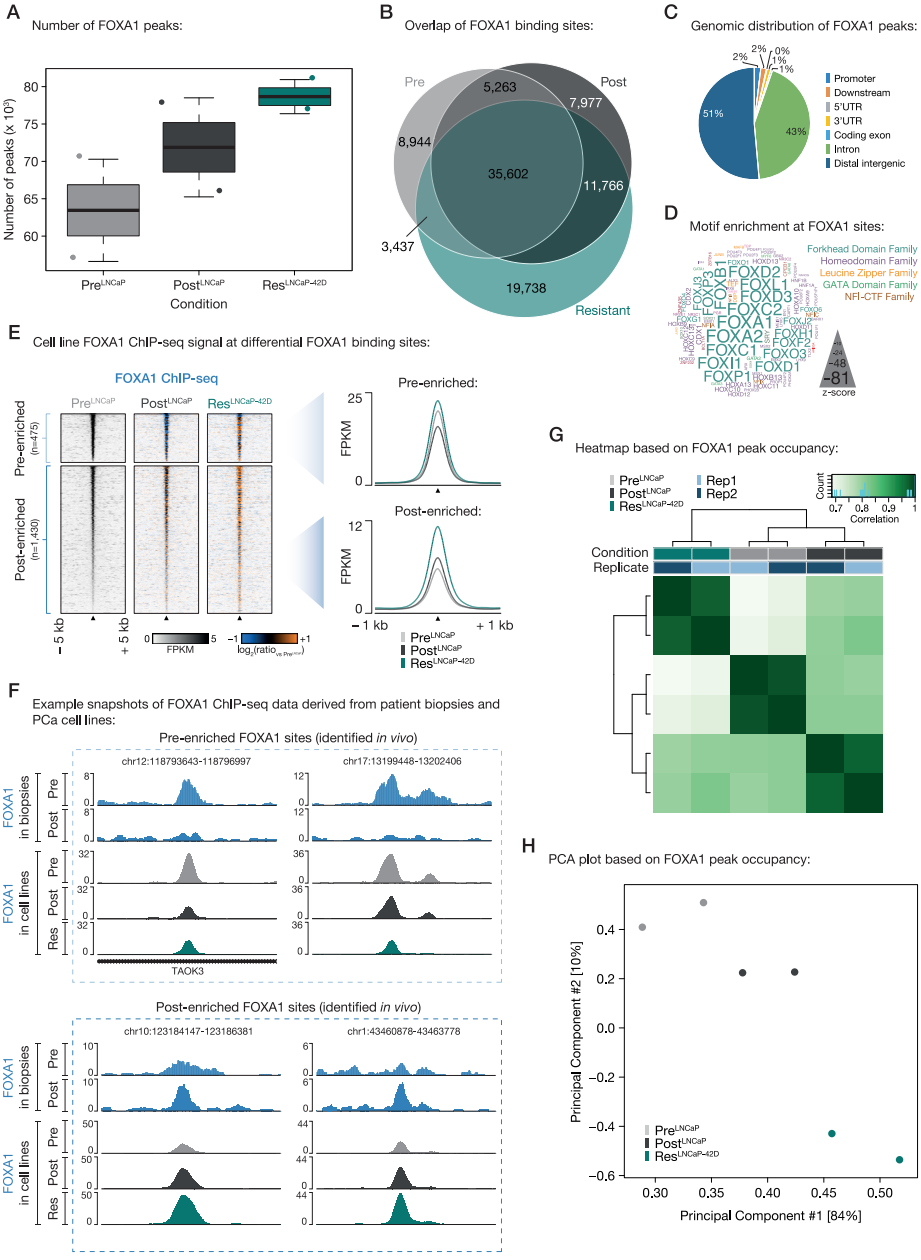
A
Number of FOXA1 peaks:
Number of peaks (x 10³)
Condition
B
Overlap of FOXA1 binding sites:
Pre
Post
Resistant
5,263
7,977
8,944
35,602
11,766
3,437
19,738
C
Genomic distribution of FOXA1 peaks:
Promoter
Downstream
5'UTR
3'UTR
Coding exon
Intron
Distal intergenic
51%
43%
D
Motif enrichment at FOXA1 sites:
Forkhead Domain Family
Homeodomain Family
Leucine Zipper Family
GATA Domain Family
NFI-CTF Family
z-score
E
Cell line FOXA1 ChIP-seq signal at differential FOXA1 binding sites:
FOXA1 ChIP-seq
Pre-enriched
Post-enriched
Pre-enriched:
Post-enriched:
FPKM
F
Example snapshots of FOXA1 ChIP-seq data derived from patient biopsies and PCa cell lines:
Pre-enriched FOXA1 sites (identified in vivo)
Post-enriched FOXA1 sites (identified in vivo)
FOXA1 in biopsies
FOXA1 in cell lines
TAOK3
G
Heatmap based on FOXA1 peak occupancy:
Count
Correlation
Condition
Replicate
H
PCA plot based on FOXA1 peak occupancy:
Principal Component #2 [10%]
Principal Component #1 [84%]

◄ **Supplementary Figure S16:** Treatment-induced FOXA1 reprogramming in PCa cell lines. (**A**) Boxplot showing the number of FOXA1 peaks per ChIP-seq condition (Pre^{LNCaP}, $Post^{LNCaP}$, $Res^{LNCaP\text{-}42D}$). Peak calling was performed over matched cell line input control samples. (**B**) Venn diagram indicating the overlap of FOXA1 binding sites in all tested cell line conditions (Pre^{LNCaP}, $Post^{LNCaP}$, $Res^{LNCaP\text{-}42D}$). For each condition, only peaks present in both replicates were included. The FOXA1 consensus cistrome across conditions (*n* = 35,602 sites) was used for genomic distribution (C) and motif enrichment (D) analyses. (**C**) Pie chart showing the genomic distribution of consensus FOXA1 binding sites. (**D**) Word cloud shows motif enrichment at consensus FOXA1 sites. The font size represents the *z*-score and colors correspond to transcription factor families. (**E**) Tornado plots (left) and average density plots (right) visualizing FOXA1 ChIP-seq signal [in fragments per kilobase per million reads mapped (FPKM)] at pre-enriched (top) and post-enriched (bottom) FOXA1 binding sites in untreated (Pre^{LNCaP}), short-term ENZ-treated ($Post^{LNCaP}$), and ENZ-resistant NE-like LNCaP cells ($Res^{LNCaP\text{-}42D}$). Data are centered at differential FOXA1 peaks depicting a 5-kb (heatmaps) or 1-kb (density plots) window around the peak center. Heatmap color depicts the ChIP-seq signal compared to the untreated condition (Pre^{LNCaP}), with blue indicating lower peak intensity and orange indicating higher peak intensity. (*n* = 2). (**F**) Representative example snapshots of FOXA1 ChIP-seq signal at two pre-enriched (left) and two post-enriched (right) FOXA1 binding sites. Per genomic location, the pre- and post-treatment FOXA1 ChIP-seq signal from one patient (DAR45; top), as well as the signal in all tested cell line models (bottom) is shown (*n* = 2). Y-axis indicates ChIP-seq signal in FPKM. (**G**) Correlation heatmap based on FOXA1 peak occupancy. Clustering of the samples is based on all called peaks and represents Pearson correlations between individual ChIP-seq samples. The column color bars indicate the ChIP-seq condition (Pre^{LNCaP}, $Post^{LNCaP}$, $Res^{LNCaP\text{-}42D}$) and replicate information (Rep1, Rep2). (**H**) Principal component analysis (PCA) plot based on FOXA1 peak occupancy. Each dot represents a ChIP-seq sample that is colored per condition (*n* = 2).

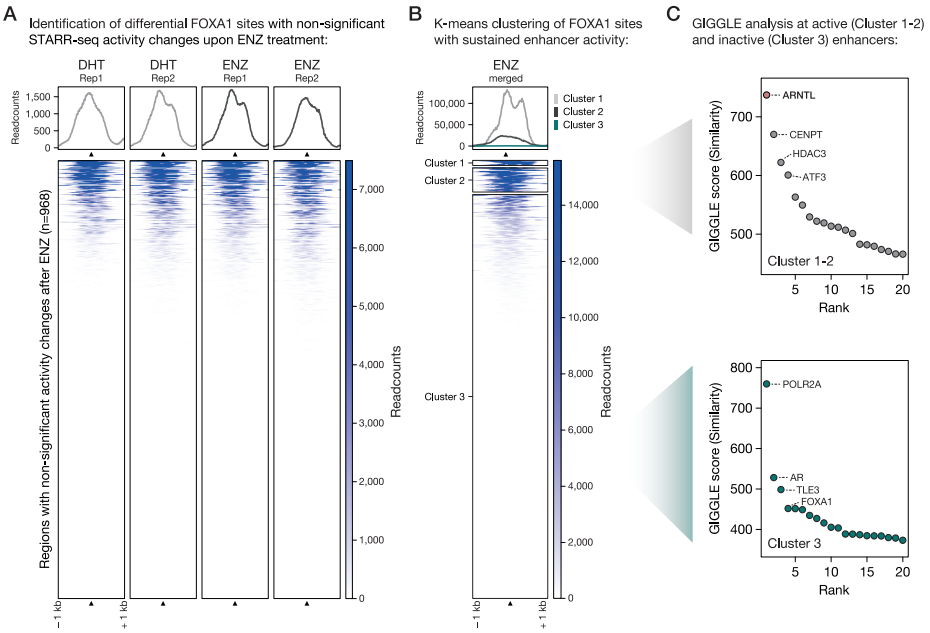

Supplementary Figure S17: Functional mapping of enhancer activity at differential FOXA1 sites. (**A**) Tornado plots (bottom) and average density plots (top) visualizing STARR-seq signal at differential FOXA1 binding sites in LNCaP cells treated with DHT or ENZ (n = 2). Shown are regions with non-significant enhancer activity changes upon ENZ treatment (n = 968). Data are centered at differential FOXA1 peaks depicting a 1-kb window around the peak center. Color depicts the STARR-seq signal (readcounts). (**B**) Same as in (A), but applying k-means clustering (n = 3) to the regions with sustained activity upon ENZ, dividing this set of binding sites into active (Cluster 1-2) and inactive (Cluster 3) enhancers. (**C**) Dot plots representing ranked GIGGLE similarity scores for transcriptional regulators identified at active (top) or inactive (bottom) FOXA1 sites. The top 20 identified factors are shown, and the 4 most enriched factors are labeled.

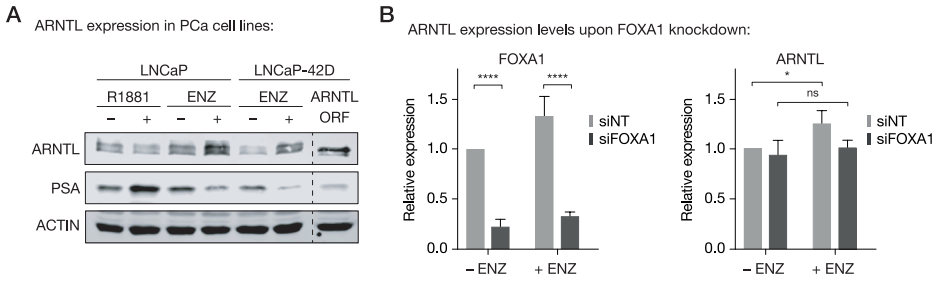

Supplementary Figure S18: FOXA1-dependent treatment-induced upregulation of ARNTL. (**A**) Western blot showing ARNTL protein levels in LNCaP and LNCaP-42D cells following treatment with synthetic androgen (R1881) and/or ENZ for 48 hours. ARNTL overexpression (in LNCaP-42D cells) as well as stainings for PSA and ACTIN are included as controls for antibody staining, hormonal treatment and protein loading, respectively. Images are representative of three independent experiments. (**B**) Bar graphs depicting relative FOXA1 (left) and ARNTL (right) mRNA levels in LNCaP-42D cells transfected with non-targeting siRNA (siNT) or siFOXA1 with and without ENZ treatment for 48 hours. Data is shown relative to the untreated (– ENZ) siNT condition (n = 3). ns, $P > 0.05$; *, $P < 0.05$; ****, $P < 0.0001$ (two-way ANOVA followed by Tukey multiple comparisons test).

Supplementary Figure S19: Characterizing the ARNTL cistrome in hormone-naïve and ENZ-resistant PCa cell lines. (**A**) Boxplot showing the number of ARNTL peaks per ChIP-seq condition (Pre^{LNCaP}, $Post^{LNCaP}$, $Res^{LNCaP\text{-}42D}$). Peak calling was performed over matched cell line input control samples. (**B**) Representative example snapshots of ARNTL ChIP-seq signal at canonical circadian rhythm genes. The average of two biological replicates is represented. Y-axis indicates ChIP-seq signal in FPKM. (**C**) Pie chart showing the genomic distribution of ARNTL consensus sites (shared across all conditions; n = 1,515 sites). The corresponding Venn diagram is shown in **Figure 6E**. (**D**) Representative example snapshots of ARNTL ChIP-seq signal at two post-enriched FOXA1 binding sites. Per genomic location, the pre- and post-treatment FOXA1 ChIP-seq signal from one patient (DAR45), as well as the ARNTL signal in all tested cell line models (bottom) is shown (n = 2). Y-axis indicates ChIP-seq signal in fragments per kilobase per million reads mapped (FPKM). (**E**) Correlation heatmap based on ARNTL peak occupancy. Clustering of the samples is based on all called peaks and represents Pearson correlations between individual ChIP-seq samples. The column color bars indicate the ChIP-seq condition (Pre^{LNCaP}, $Post^{LNCaP}$, $Res^{LNCaP\text{-}42D}$) and replicate information (Rep1, Rep2). (**F**) Principal component analysis (PCA) plot based on ARNTL peak occupancy. Each dot represents a ChIP-seq sample that is colored per condition (2 replicates each). ►

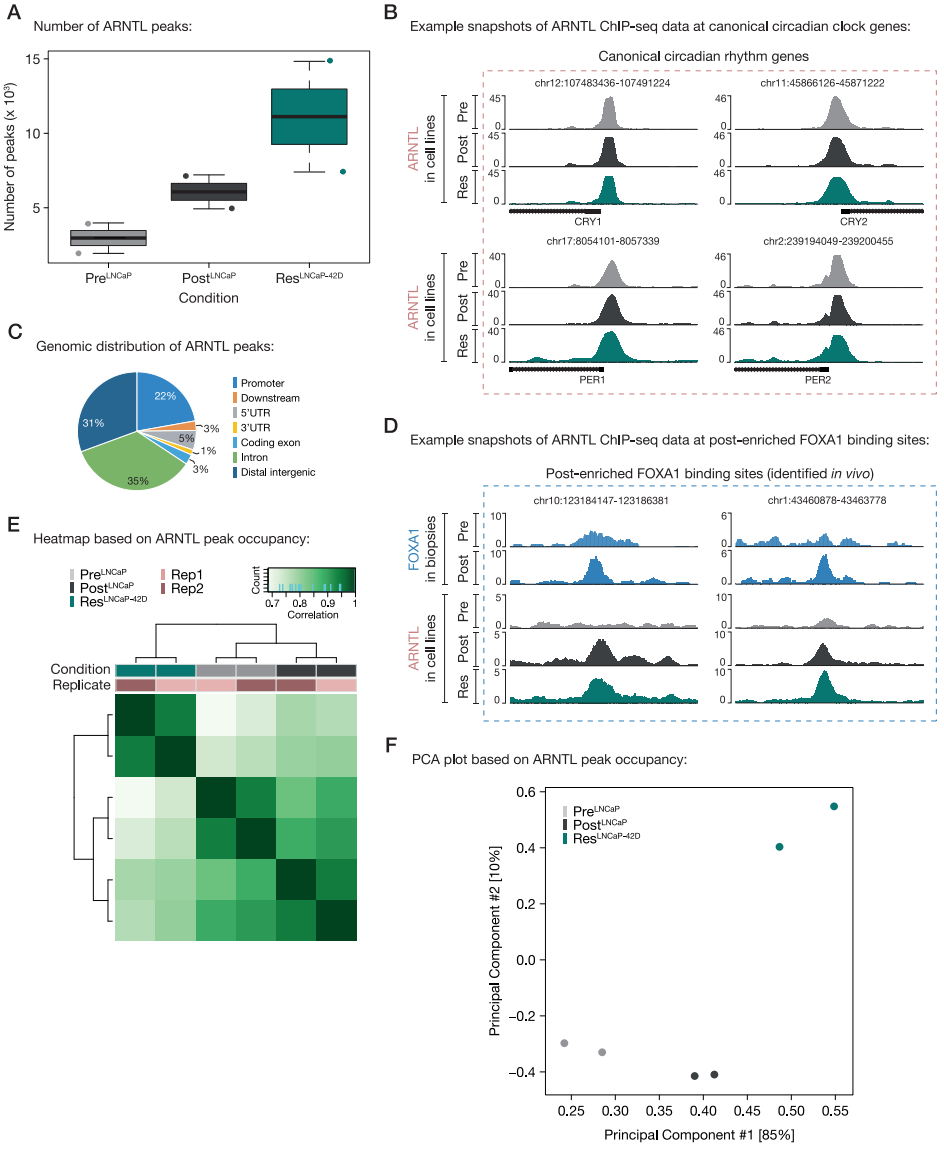
A
Number of ARNTL peaks:
Number of peaks (x 10³)
15
10
5
PreLNCaP
PostLNCaP
ResLNCaP-42D
Condition
B
Example snapshots of ARNTL ChIP-seq data at canonical circadian clock genes:
Canonical circadian rhythm genes
chr12:107483436-107491224
chr11:45866126-45871222
chr17:8054101-8057339
chr2:239194049-239200455
ARNTL in cell lines
Pre
Post
Res
CRY1
CRY2
PER1
PER2
C
Genomic distribution of ARNTL peaks:
22%
3%
5%
1%
3%
35%
31%
Promoter
Downstream
5'UTR
3'UTR
Coding exon
Intron
Distal intergenic
D
Example snapshots of ARNTL ChIP-seq data at post-enriched FOXA1 binding sites:
Post-enriched FOXA1 binding sites (identified in vivo)
chr10:123184147-123186381
chr1:43460878-43463778
FOXA1 in biopsies
ARNTL in cell lines
E
Heatmap based on ARNTL peak occupancy:
PreLNCaP
PostLNCaP
ResLNCaP-42D
Rep1
Rep2
Count
0.7
0.8
0.9
1
Correlation
Condition
Replicate
F
PCA plot based on ARNTL peak occupancy:
PreLNCaP
PostLNCaP
ResLNCaP-42D
Principal Component #2 [10%]
0.6
0.4
0.2
0.0
−0.2
−0.4
0.25
0.30
0.35
0.40
0.45
0.50
0.55
Principal Component #1 [85%]

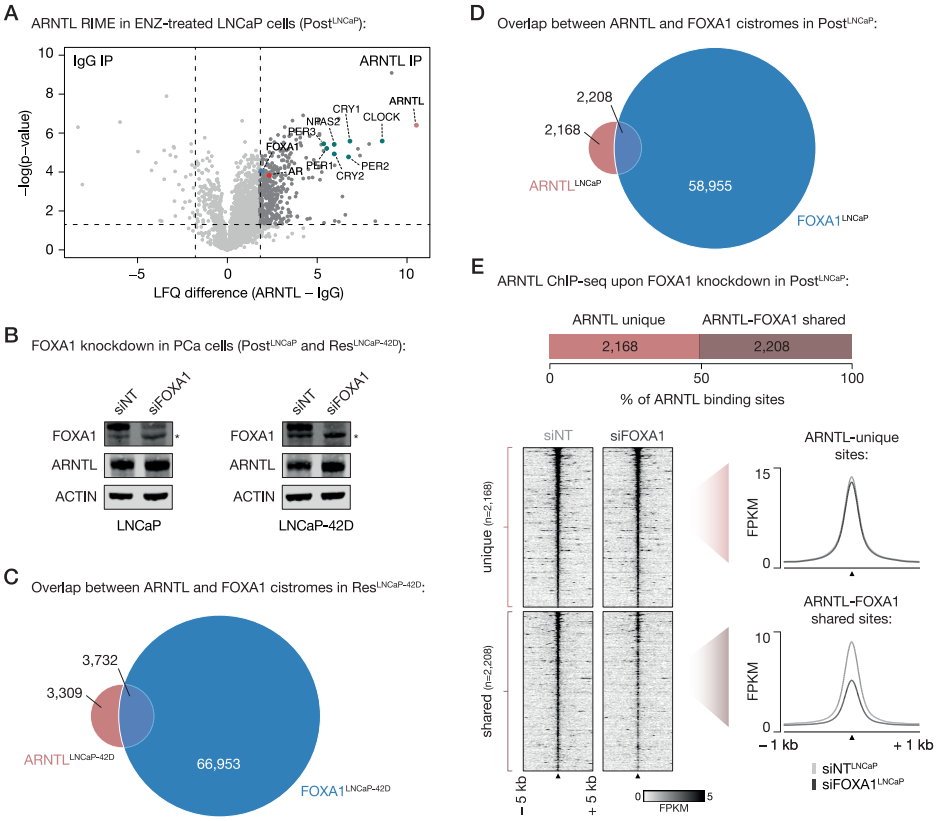

Supplementary Figure S20: Functional interaction between FOXA1 and ARNTL in PCa cell lines. (**A**) Volcano plot depicting ARNTL interactors in ENZ-treated LNCaP (Post^{LNCaP}) cells over IgG isotype control. Significantly enriched interactors are highlighted, and significance cutoffs are shown as dotted lines [label-free quantification (LFQ) difference ≥ 1.8; $P \leq 0.05$; $n = 4$]. (**B**) Western blots indicate FOXA1 and ARNTL protein levels in LNCaP (left) and LNCaP-42D (right) cell lysates used for ChIP-seq analysis upon siRNA-mediated silencing of FOXA1 and ENZ treatment. Transfection with siNT and staining for ACTIN are included as controls for siRNA treatment and protein loading, respectively. Images are representative of two independent experiments. *, indicates an unspecific band. (**C-D**) Venn diagrams showing the overlap between ARNTL and FOXA1 cistromes in ENZ-treated LNCaP-42D (C) and LNCaP cells (D). (**E**) Stacked bar chart (top) indicating the fraction of ARNTL binding sites in ENZ-treated LNCaP cells (Post^{LNCaP}) that are ARNTL unique (n = 2,168) or shared with FOXA1 (n = 2,208). Tornado plots (lower left) and average density plot (lower right) visualize ARNTL ChIP-seq signal [in fragments per kilobase per million reads mapped (FPKM)] at ARNTL unique or ARNTL-FOXA1 shared binding sites in LNCaP cells upon transfection with non-targeting siRNA (siNT) or siFOXA1. Data are centered at ARNTL peaks depicting a 5-kb (heatmaps) or 1-kb (density plots) window around the peak center. (n = 2)

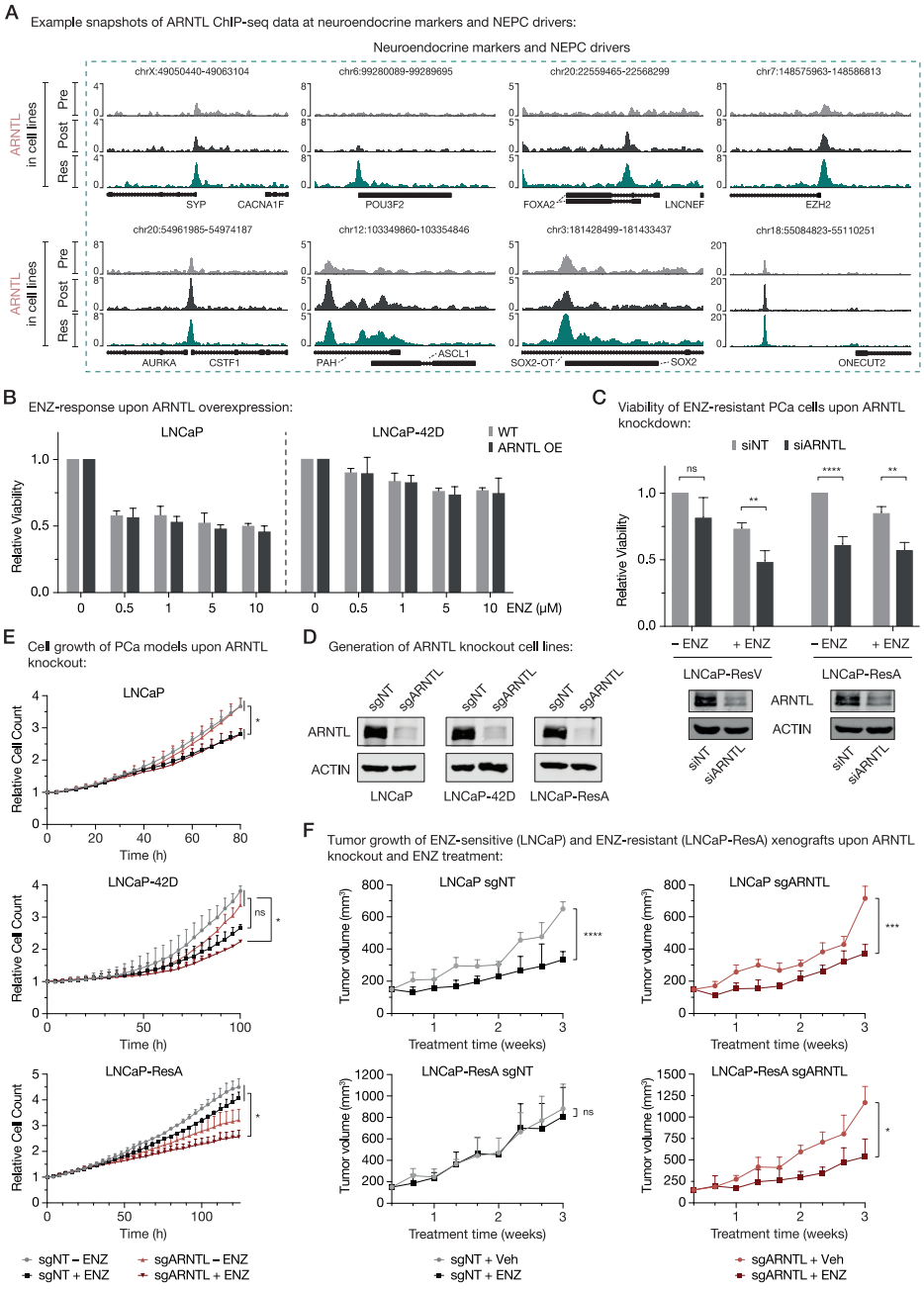
A
Example snapshots of ARNTL ChIP-seq data at neuroendocrine markers and NEPC drivers:
Neuroendocrine markers and NEPC drivers
ARNTL in cell lines
Pre
Post
Res
chrX:49050440-49063104
chr6:99280089-99289695
chr20:22559465-22568299
chr7:148575963-148586813
SYP
CACNA1F
POU3F2
FOXA2
LNCNEF
EZH2
chr20:54961985-54974187
chr12:103349860-103354846
chr3:181428499-181433437
chr18:55084823-55110251
AURKA
CSTF1
PAH
ASCL1
SOX2-OT
SOX2
ONECUT2
B
ENZ-response upon ARNTL overexpression:
LNCaP
LNCaP-42D
WT
ARNTL OE
Relative Viability
ENZ (μM)
C
Viability of ENZ-resistant PCa cells upon ARNTL knockdown:
siNT
siARNTL
Relative Viability
– ENZ
+ ENZ
LNCaP-ResV
LNCaP-ResA
ARNTL
ACTIN
D
Generation of ARNTL knockout cell lines:
sgNT
sgARNTL
ARNTL
ACTIN
LNCaP
LNCaP-42D
LNCaP-ResA
E
Cell growth of PCa models upon ARNTL knockout:
LNCaP
LNCaP-42D
LNCaP-ResA
Relative Cell Count
Time (h)
sgNT – ENZ
sgNT + ENZ
sgARNTL – ENZ
sgARNTL + ENZ
F
Tumor growth of ENZ-sensitive (LNCaP) and ENZ-resistant (LNCaP-ResA) xenografts upon ARNTL knockout and ENZ treatment:
LNCaP sgNT
LNCaP sgARNTL
LNCaP-ResA sgNT
LNCaP-ResA sgARNTL
Tumor volume (mm³)
Treatment time (weeks)
sgNT + Veh
sgNT + ENZ
sgARNTL + Veh
sgARNTL + ENZ

◄ **Supplementary Figure S21:** ENZ-induced ARNTL reprogramming and acquired dependency in treatment-resistant models. (**A**) Representative example snapshots of ARNTL ChIP-seq signal at promoter regions of NEPC markers and disease drivers. The average of two biological replicates is represented. Y-axis indicates ChIP-seq signal in fragments per kilobase per million reads mapped (FPKM). (**B**) Bar graphs show response of wildtype (WT) and ARNTL-overexpressing (ARNTL OE) LNCaP (left) and LNCaP-42D (right) cells to increasing concentrations of ENZ. (**C**) Bar chart (top) showing relative cell viability of LNCaP-ResV (left) and LNCaP-ResA (right) cells upon transfection with non-targeting siRNA (siNT) or siARNTL, and exposure to ENZ. Treatment is indicated and data is shown relative to the untreated (– ENZ) siNT condition per cell line (n = 3). Western blots (bottom) indicate ARNTL protein levels in LNCaP-ResV (left) and LNCaP-ResA (right) cells following siRNA-mediated silencing of ARNTL for 48 hours. Transfection with siNT and staining for ACTIN are included as controls for siRNA treatment and protein loading, respectively. Images are representative of three independent experiments. ns, $P > 0.05$; **, $P < 0.01$; ****, $P < 0.0001$ (two-way ANOVA followed by Tukey multiple comparisons test). (**D**) Western blots indicate ARNTL protein levels in LNCaP (left), LNCaP-42D (middle) and LNCaP-ResA (right) cells upon CRISPR/Cas9-mediated ARNTL knockout (sgARNTL) or in non-targeting control cells (sgNT). Staining for ACTIN is included as a loading control and images are representative of three independent experiments. (**E**) Growth curves depict proliferation of ARNTL knockout cells (sgARNTL) or non-targeting control cells (sgNT) upon treatment with ENZ (n = 2). ns, $P > 0.05$; *, $P < 0.05$ (one-way ANOVA followed by Tukey multiple comparisons test). (**F**) Growth curves depict tumor volume (measured 3 times per week using calipers) of non-targeting control (sgNT) or ARNTL knockout (sgARNTL) LNCaP (top) and LNCaP-ResA (bottom) xenografts upon treatment with vehicle-alone (LNCaP: sgNT +Veh: n = 4, sgARNTL +Veh: n = 4; LNCaP-ResA: sgNT +Veh: n = 4, sgARNTL +Veh: n = 2) or ENZ (LNCaP: sgNT +ENZ: n = 4, sgARNTL +ENZ: n = 3; LNCaP-ResA: sgNT +ENZ: n =3, sgARNTL +ENZ: n = 2). ns, $P > 0.05$; *, $P < 0.05$; ***, $P < 0.001$; ****, $P < 0.0001$ (t test).

Supplementary Figure S22: GR involvement at post-treatment FOXA1 sites. (**A**) Boxplots showing normalized NR3C1 (GR) gene expression before and after 3 months of neoadjuvant ENZ treatment. ****, $P < 0.0001$ (Mann-Whitney U test). (**B**) Boxplots depicting normalized NR3C1 gene expression in ENZ non-responders (BCR ≤ 6 months; n = 8) and responders (no BCR; n = 29) in the pre- (left) and post-treatment (right) setting separately. ns, $P > 0.05$ (Mann-Whitney U test). (**C**) Tornado plots (left) and average density plots (right) visualizing GR ChIP-seq signal [in fragments per kilobase per million reads mapped (FPKM)] in LREX' PCa cells at pre-enriched and post-enriched FOXA1 binding sites identified in patients upon neoadjuvant ENZ treatment. Data are centered at differential FOXA1 peaks depicting a 10-kb (heatmaps) or 1-kb (density plots) window around the peak center. (n = 3). (**D**) Venn diagram indicating the overlap of differential FOXA1 binding sites (pre-ENZ, post-ENZ) with the GR cistrome identified in LREX' PCa cells[49]. (**E**) Bar chart (top) showing relative cell viability of LNCaP, LNCaP-42D, LNCaP-ResV and LNCaP-ResA cells upon transfection with non-targeting siRNA (siNT) or siGR, and exposure to ENZ. Treatment is indicated and data is shown relative to the untreated (– ENZ) siNT condition per cell line (n = 3). Western blots (bottom) indicate GR protein levels in all models following siRNA-mediated silencing of GR for 48 hours. Transfection with siNT and staining for ACTIN are included as controls for siRNA treatment and protein loading, respectively. Images are representative of three independent experiments. ns, $P > 0.05$; *, $P < 0.05$; **, $P < 0.01$ (two-way ANOVA followed by Tukey multiple comparisons test). ►

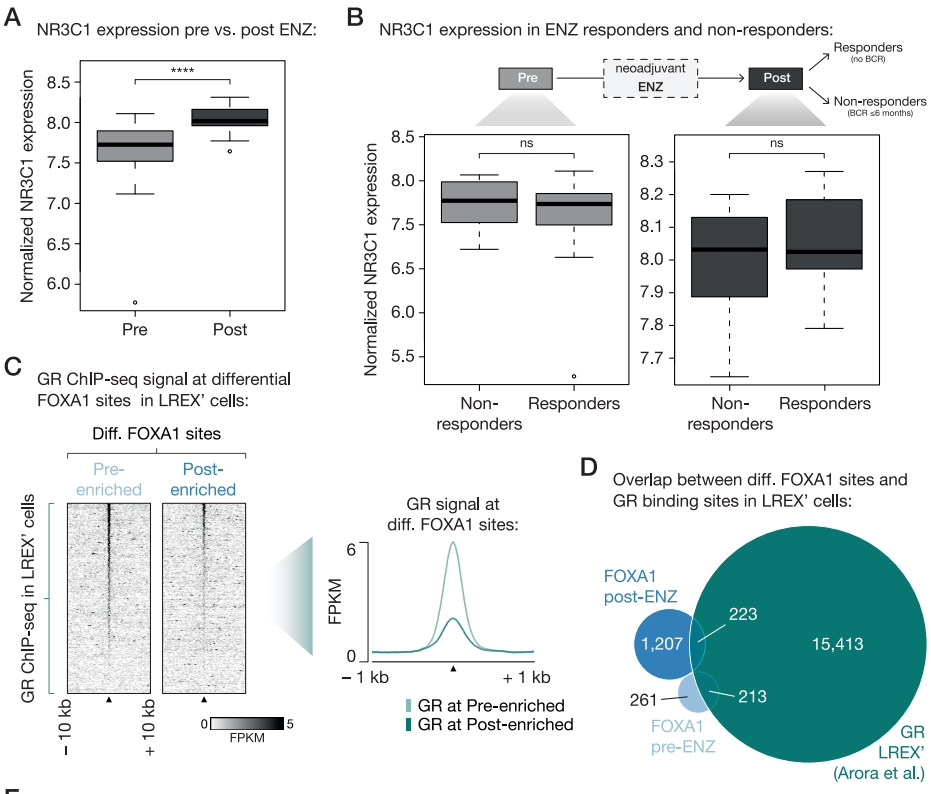
A
NR3C1 expression pre vs. post ENZ:
Normalized NR3C1 expression
****
Pre
Post
B
NR3C1 expression in ENZ responders and non-responders:
Pre
neoadjuvant ENZ
Post
Responders (no BCR)
Non-responders (BCR ≤6 months)
Normalized NR3C1 expression
ns
ns
Non-responders
Responders
Non-responders
Responders
C
GR ChIP-seq signal at differential FOXA1 sites in LREX' cells:
Diff. FOXA1 sites
Pre-enriched
Post-enriched
GR ChIP-seq in LREX' cells
– 10 kb
+ 10 kb
0
5
FPKM
GR signal at diff. FOXA1 sites:
FPKM
6
0
– 1 kb
+ 1 kb
GR at Pre-enriched
GR at Post-enriched
D
Overlap between diff. FOXA1 sites and GR binding sites in LREX' cells:
FOXA1 post-ENZ
1,207
223
15,413
261
213
FOXA1 pre-ENZ
GR LREX' (Arora et al.)
E
PCa cell viability upon siRNA-mediated GR knockdown:
Relative Viability
1.0
0.5
0.0
ns
**
*
siNT
siGR
– ENZ
+ ENZ
LNCaP
LNCaP-42D
LNCaP-ResV
LNCaP-ResA
GR
ACTIN
siNT
siGR

References

1 Huggins, C. & Hodges, C. V. Studies on prostatic cancer. I. The effect of castration, of estrogen and androgen injection on serum phosphatases in metastatic carcinoma of the prostate. *CA Cancer J Clin* **22**, 232-240 (1972). https://doi.org:10.3322/canjclin.22.4.232

2 Zhang, Z. *et al.* An AR-ERG transcriptional signature defined by long-range chromatin interactomes in prostate cancer cells. *Genome Res* **29**, 223-235 (2019). https://doi.org:10.1101/gr.230243.117

3 Stelloo, S., Bergman, A. M. & Zwart, W. Androgen receptor enhancer usage and the chromatin regulatory landscape in human prostate cancers. *Endocr Relat Cancer* **26**, R267-R285 (2019). https://doi.org:10.1530/ERC-19-0032

4 Stelloo, S. *et al.* Endogenous androgen receptor proteomic profiling reveals genomic subcomplex involved in prostate tumorigenesis. *Oncogene* **37**, 313-322 (2018). https://doi.org:10.1038/onc.2017.330

5 Pomerantz, M. M. *et al.* The androgen receptor cistrome is extensively reprogrammed in human prostate tumorigenesis. *Nat Genet* **47**, 1346-1351 (2015). https://doi.org:10.1038/ng.3419

6 Gerhardt, J. *et al.* FOXA1 promotes tumor progression in prostate cancer and represents a novel hallmark of castration-resistant prostate cancer. *Am J Pathol* **180**, 848-861 (2012). https://doi.org:10.1016/j.ajpath.2011.10.021

7 Pomerantz, M. M. *et al.* Prostate cancer reactivates developmental epigenomic programs during metastatic progression. *Nat Genet* **52**, 790-799 (2020). https://doi.org:10.1038/s41588-020-0664-8

8 Cirillo, L. A. *et al.* Opening of compacted chromatin by early developmental transcription factors HNF3 (FoxA) and GATA-4. *Mol Cell* **9**, 279-289 (2002). https://doi.org:10.1016/s1097-2765(02)00459-8

9 Lupien, M. *et al.* FoxA1 translates epigenetic signatures into enhancer-driven lineage-specific transcription. *Cell* **132**, 958-970 (2008). https://doi.org:10.1016/j.cell.2008.01.018

10 Sahu, B. *et al.* Dual role of FoxA1 in androgen receptor binding to chromatin, androgen signalling and prostate cancer. *EMBO J* **30**, 3962-3976 (2011). https://doi.org:10.1038/emboj.2011.328

11 Teng, M., Zhou, S., Cai, C., Lupien, M. & He, H. H. Pioneer of prostate cancer: past, present and the future of FOXA1. *Protein Cell* **12**, 29-38 (2021). https://doi.org:10.1007/s13238-020-00786-8

12 Grasso, C. S. *et al.* The mutational landscape of lethal castration-resistant prostate cancer. *Nature* **487**, 239-243 (2012). https://doi.org:10.1038/nature11125

13 Barbieri, C. E. *et al.* Exome sequencing identifies recurrent SPOP, FOXA1 and MED12 mutations in prostate cancer. *Nat Genet* **44**, 685-689 (2012). https://doi.org:10.1038/ng.2279

14 Cancer Genome Atlas Research, N. The Molecular Taxonomy of Primary Prostate Cancer. *Cell* **163**, 1011-1025 (2015). https://doi.org:10.1016/j.cell.2015.10.025

15 Robinson, D. *et al.* Integrative Clinical Genomics of Advanced Prostate Cancer. *Cell* **162**, 454 (2015). https://doi.org:10.1016/j.cell.2015.06.053

16 Wedge, D. C. *et al.* Sequencing of prostate cancers identifies new cancer genes, routes of progression and drug targets. *Nat Genet* **50**, 682-692 (2018). https://doi.org:10.1038/s41588-018-0086-z

17 Adams, E. J. *et al.* FOXA1 mutations alter pioneering activity, differentiation and prostate cancer phenotypes. *Nature* **571**, 408-412 (2019). https://doi.org:10.1038/s41586-019-1318-9

18 Parolia, A. *et al.* Distinct structural classes of activating FOXA1 alterations in advanced prostate cancer. *Nature* **571**, 413-418 (2019). https://doi.org:10.1038/s41586-019-1347-4

19 Mottet, N. *et al.* EAU-EANM-ESTRO-ESUR-SIOG Guidelines on Prostate Cancer-2020 Update. Part 1: Screening, Diagnosis, and Local Treatment with Curative Intent. *Eur Urol* **79**, 243-262 (2021). https://doi.org:10.1016/j.eururo.2020.09.042

20 Roehl, K. A., Han, M., Ramos, C. G., Antenor, J. A. & Catalona, W. J. Cancer progression and survival rates following anatomical radical retropubic prostatectomy in 3,478 consecutive patients: long-term results. *J Urol* **172**, 910-914 (2004). https://doi.org:10.1097/01.ju.0000134888.22332.bb

21 Harris, W. P., Mostaghel, E. A., Nelson, P. S. & Montgomery, B. Androgen deprivation therapy: progress in understanding mechanisms of resistance and optimizing androgen depletion. *Nat Clin Pract Urol* **6**, 76-85 (2009). https://doi.org:10.1038/ncpuro1296

22 Cornford, P. *et al.* EAU-EANM-ESTRO-ESUR-SIOG Guidelines on Prostate Cancer. Part II-2020 Update: Treatment of Relapsing and Metastatic Prostate Cancer. *Eur Urol* **79**, 263-282 (2021). https://doi.org:10.1016/j.eururo.2020.09.046

23 Zong, Y. & Goldstein, A. S. Adaptation or selection--mechanisms of castration-resistant prostate cancer. *Nat Rev Urol* **10**, 90-98 (2013). https://doi.org:10.1038/nrurol.2012.237

24 Linder, S., van der Poel, H. G., Bergman, A. M., Zwart, W. & Prekovic, S. Enzalutamide therapy for advanced prostate cancer: efficacy, resistance and beyond. *Endocr Relat Cancer* **26**, R31-R52 (2018). https://doi.org:10.1530/ERC-18-0289

25 Scher, H. I. *et al.* Increased survival with enzalutamide in prostate cancer after chemotherapy. *N Engl J Med* **367**, 1187-1197 (2012). https://doi.org:10.1056/NEJMoa1207506

26 Beer, T. M. *et al.* Enzalutamide in metastatic prostate cancer before chemotherapy. *N Engl J Med* **371**, 424-433 (2014). https://doi.org:10.1056/NEJMoa1405095

27 Armstrong, A. J. *et al.* ARCHES: A Randomized, Phase III Study of Androgen Deprivation Therapy With Enzalutamide or Placebo in Men With Metastatic Hormone-Sensitive Prostate Cancer. *J Clin Oncol* **37**, 2974-2986 (2019). https://doi.org:10.1200/JCO.19.00799

28 Hussain, M. *et al.* Enzalutamide in Men with Nonmetastatic, Castration-Resistant Prostate Cancer. *N Engl J Med* **378**, 2465-2474 (2018). https://doi.org:10.1056/NEJMoa1800536

29 Prekovic, S. *et al.* Molecular underpinnings of enzalutamide resistance. *Endocr Relat Cancer* **25**, R545-R557 (2018). https://doi.org:10.1530/ERC-17-0136

30 Gao, N. *et al.* The role of hepatocyte nuclear factor-3 alpha (Forkhead Box A1) and androgen receptor in transcriptional regulation of prostatic genes. *Mol Endocrinol* **17**, 1484-1507 (2003). https://doi.org:10.1210/me.2003-0020

31 Stelloo, S. *et al.* Integrative epigenetic taxonomy of primary prostate cancer. *Nat Commun* **9**, 4900 (2018). https://doi.org:10.1038/s41467-018-07270-2

32 Mazrooei, P. *et al.* Cistrome Partitioning Reveals Convergence of Somatic Mutations and Risk Variants on Master Transcription Regulators in Primary Prostate Tumors. *Cancer Cell* **36**, 674-689 e676 (2019). https://doi.org:10.1016/j.ccell.2019.10.005

33 Kron, K. J. *et al.* TMPRSS2-ERG fusion co-opts master transcription factors and activates NOTCH signaling in primary prostate cancer. *Nat Genet* **49**, 1336-1345 (2017). https://doi.org:10.1038/ng.3930

34 Huang, C. F. *et al.* Functional mapping of androgen receptor enhancer activity. *Genome Biol* **22**, 149 (2021). https://doi.org:10.1186/s13059-021-02339-6

35 Beltran, H. *et al.* Divergent clonal evolution of castration-resistant neuroendocrine prostate cancer. *Nat Med* **22**, 298-305 (2016). https://doi.org:10.1038/nm.4045

36 Che, M. *et al.* Opposing transcriptional programs of KLF5 and AR emerge during therapy for advanced prostate cancer. *Nat Commun* **12**, 6377 (2021). https://doi.org:10.1038/s41467-021-26612-1

37 Henry, G. H. *et al.* A Cellular Anatomy of the Normal Adult Human Prostate and Prostatic Urethra. *Cell Rep* **25**, 3530-3542 e3535 (2018). https://doi.org:10.1016/j.celrep.2018.11.086

38 Epstein, J. I. *et al.* Proposed morphologic classification of prostate cancer with neuroendocrine differentiation. *Am J Surg Pathol* **38**, 756-767 (2014). https://doi.org:10.1097/PAS.0000000000000208

39 Kim, S. *et al.* PEG10 is associated with treatment-induced neuroendocrine prostate cancer. *J Mol Endocrinol* **63**, 39-49 (2019). https://doi.org:10.1530/JME-18-0226

40 Berger, A. *et al.* N-Myc-mediated epigenetic reprogramming drives lineage plasticity in advanced prostate cancer. *J Clin Invest* **129**, 3924-3940 (2019). https://doi.org:10.1172/JCI127961

41 Bishop, J. L. *et al.* The Master Neural Transcription Factor BRN2 Is an Androgen Receptor-Suppressed Driver of Neuroendocrine Differentiation in Prostate Cancer. *Cancer Discov* **7**, 54-71 (2017). https://doi.org:10.1158/2159-8290.CD-15-1263

42 Baca, S. C. *et al.* Reprogramming of the FOXA1 cistrome in treatment-emergent neuroendocrine prostate cancer. *Nat Commun* **12**, 1979 (2021). https://doi.org:10.1038/s41467-021-22139-7

43 Baca, S. C. *et al.* Genetic determinants of chromatin reveal prostate cancer risk mediated by context-dependent gene regulation. *bioRxiv*, 2021.2005.2010.443466 (2021). https://doi.org:10.1101/2021.05.10.443466

44 Giambartolomei, C. *et al.* H3K27ac HiChIP in prostate cell lines identifies risk genes for prostate cancer susceptibility. *Am J Hum Genet* **108**, 2284-2300 (2021). https://doi.org:10.1016/j.ajhg.2021.11.007

45 Meyers, R. M. *et al.* Computational correction of copy number effect improves specificity of CRISPR-Cas9 essentiality screens in cancer cells. *Nat Genet* **49**, 1779-1784 (2017). https://doi.org:10.1038/ng.3984

46 Dempster, J. M. *et al.* Extracting Biological Insights from the Project Achilles Genome-Scale CRISPR Screens in Cancer Cell Lines. *bioRxiv*, 720243 (2019). https://doi.org:10.1101/720243

47 Layer, R. M. *et al.* GIGGLE: a search engine for large-scale integrated genome analysis. *Nat Methods* **15**, 123-126 (2018). https://doi.org:10.1038/nmeth.4556

48 Zheng, R. *et al.* Cistrome Data Browser: expanded datasets and new tools for gene regulatory analysis. *Nucleic Acids Res* **47**, D729-D735 (2019). https://doi.org:10.1093/nar/gky1094

49 Arora, V. K. *et al.* Glucocorticoid receptor confers resistance to antiandrogens by bypassing androgen receptor blockade. *Cell* **155**, 1309-1322 (2013). https://doi.org:10.1016/j.cell.2013.11.012

50 Shah, N. *et al.* Regulation of the glucocorticoid receptor via a BET-dependent enhancer drives antiandrogen resistance in prostate cancer. *Elife* **6** (2017). https://doi.org:10.7554/eLife.27861

51 Palit, S. A. *et al.* TLE3 loss confers AR inhibitor resistance by facilitating GR-mediated human prostate cancer cell growth. *Elife* **8** (2019). https://doi.org:10.7554/eLife.47430

52 Shafi, A. A. *et al.* The circadian cryptochrome, CRY1, is a pro-tumorigenic factor that rhythmically modulates DNA repair. *Nat Commun* **12**, 401 (2021). https://doi.org:10.1038/s41467-020-20513-5

53 Quigley, D. A. *et al.* Genomic Hallmarks and Structural Variation in Metastatic Prostate Cancer. *Cell* **175**, 889 (2018). https://doi.org:10.1016/j.cell.2018.10.019

54 Abida, W. *et al.* Genomic correlates of clinical outcome in advanced prostate cancer. *Proc Natl Acad Sci U S A* **116**, 11428-11436 (2019). https://doi.org:10.1073/pnas.1902651116

55 Kregel, S. *et al.* Acquired resistance to the second-generation androgen receptor antagonist enzalutamide in castration-resistant prostate cancer. *Oncotarget* **7**, 26259-26274 (2016). https://doi.org:10.18632/oncotarget.8456

56 Handle, F. *et al.* Drivers of AR indifferent anti-androgen resistance in prostate cancer cells. *Sci Rep* **9**, 13786 (2019). https://doi.org:10.1038/s41598-019-50220-1

57 Isikbay, M. *et al.* Glucocorticoid receptor activity contributes to resistance to androgen-targeted therapy in prostate cancer. *Horm Cancer* **5**, 72-89 (2014). https://doi.org:10.1007/s12672-014-0173-2

58 Zhang, Z. *et al.* Loss of CHD1 Promotes Heterogeneous Mechanisms of Resistance to AR-Targeted Therapy via Chromatin Dysregulation. *Cancer Cell* **37**, 584-598 e511 (2020). https://doi.org:10.1016/j.ccell.2020.03.001

59 Robinson, D. R. *et al.* Activating ESR1 mutations in hormone-resistant metastatic breast cancer. *Nat Genet* **45**, 1446-1451 (2013). https://doi.org:10.1038/ng.2823

60 Chabon, J. J. *et al.* Circulating tumour DNA profiling reveals heterogeneity of EGFR inhibitor resistance mechanisms in lung cancer patients. *Nat Commun* **7**, 11815 (2016). https://doi.org:10.1038/ncomms11815

61 Lievre, A. *et al.* KRAS mutation status is predictive of response to cetuximab therapy in colorectal cancer. *Cancer Res* **66**, 3992-3995 (2006). https://doi.org:10.1158/0008-5472.CAN-06-0191

62 Takeda, D. Y. *et al.* A Somatically Acquired Enhancer of the Androgen Receptor Is a Noncoding Driver in Advanced Prostate Cancer. *Cell* **174**, 422-432 e413 (2018). https://doi.org:10.1016/j.cell.2018.05.037

63 Viswanathan, S. R. *et al.* Structural Alterations Driving Castration-Resistant Prostate Cancer Revealed by Linked-Read Genome Sequencing. *Cell* **174**, 433-447 e419 (2018). https://doi.org:10.1016/j.cell.2018.05.036

64 Beltran, H. *et al.* Molecular characterization of neuroendocrine prostate cancer and identification of new drug targets. *Cancer Discov* **1**, 487-495 (2011). https://doi.org:10.1158/2159-8290.CD-11-0130

65 Davies, A. H., Beltran, H. & Zoubeidi, A. Cellular plasticity and the neuroendocrine phenotype in prostate cancer. *Nat Rev Urol* **15**, 271-286 (2018). https://doi.org:10.1038/nrurol.2018.22

66 Gao, S. *et al.* Chromatin binding of FOXA1 is promoted by LSD1-mediated demethylation in prostate cancer. *Nat Genet* **52**, 1011-1017 (2020). https://doi.org:10.1038/s41588-020-0681-7

67 Gleave, M. E. *et al.* Randomized comparative study of 3 versus 8-month neoadjuvant hormonal therapy before radical prostatectomy: biochemical and pathological effects. *J Urol* **166**, 500-506; discussion 506-507 (2001).

68 Klotz, L. H. *et al.* Long-term followup of a randomized trial of 0 versus 3 months of neoadjuvant androgen ablation before radical prostatectomy. *J Urol* **170**, 791-794 (2003). https://doi.org:10.1097/01.ju.0000081404.98273.fd

69 Soloway, M. S. *et al.* Neoadjuvant androgen ablation before radical prostatectomy in cT2bNxMo prostate cancer: 5-year results. *J Urol* **167**, 112-116 (2002).

70 Singh, A. A. *et al.* Optimized ChIP-seq method facilitates transcription factor profiling in human tumors. *Life Sci Alliance* **2**, e201800115 (2019). https://doi.org:10.26508/lsa.201800115

71 Schmidt, D. *et al.* ChIP-seq: using high-throughput sequencing to discover protein-DNA interactions. *Methods* **48**, 240-248 (2009). https://doi.org:10.1016/j.ymeth.2009.03.001

72 Li, H. & Durbin, R. Fast and accurate short read alignment with Burrows-Wheeler transform. *Bioinformatics* **25**, 1754-1760 (2009). https://doi.org:10.1093/bioinformatics/btp324

73 Kumar, V. *et al.* Uniform, optimal signal processing of mapped deep-sequencing data. *Nat Biotechnol* **31**, 615-622 (2013). https://doi.org:10.1038/nbt.2596

74 Zhang, Y. *et al.* Model-based analysis of ChIP-Seq (MACS). *Genome Biol* **9**, R137 (2008). https://doi.org:10.1186/gb-2008-9-9-r137

75 Ramirez, F. *et al.* deepTools2: a next generation web server for deep-sequencing data analysis. *Nucleic Acids Res* **44**, W160-165 (2016). https://doi.org:10.1093/nar/gkw257

76 Kharchenko, P. V., Tolstorukov, M. Y. & Park, P. J. Design and analysis of ChIP-seq experiments for DNA-binding proteins. *Nat Biotechnol* **26**, 1351-1359 (2008). https://doi.org:10.1038/nbt.1508

77 Li, H. *et al.* The Sequence Alignment/Map format and SAMtools. *Bioinformatics* **25**, 2078-2079 (2009). https://doi.org:10.1093/bioinformatics/btp352
78 Lerdrup, M., Johansen, J. V., Agrawal-Singh, S. & Hansen, K. An interactive environment for agile analysis and visualization of ChIP-sequencing data. *Nat Struct Mol Biol* **23**, 349-357 (2016). https://doi.org:10.1038/nsmb.3180
79 Lopez-Delisle, L. *et al.* pyGenomeTracks: reproducible plots for multivariate genomic datasets. *Bioinformatics* **37**, 422-423 (2021). https://doi.org:10.1093/bioinformatics/btaa692
80 Karolchik, D. *et al.* The UCSC Table Browser data retrieval tool. *Nucleic Acids Res* **32**, D493-496 (2004). https://doi.org:10.1093/nar/gkh103
81 Pruitt, K. D. *et al.* RefSeq: an update on mammalian reference sequences. *Nucleic Acids Res* **42**, D756-763 (2014). https://doi.org:10.1093/nar/gkt1114
82 Liu, T. *et al.* Cistrome: an integrative platform for transcriptional regulation studies. *Genome Biol* **12**, R83 (2011). https://doi.org:10.1186/gb-2011-12-8-r83
83 Kuhn, R. M., Haussler, D. & Kent, W. J. The UCSC genome browser and associated tools. *Brief Bioinform* **14**, 144-161 (2013). https://doi.org:10.1093/bib/bbs038
84 Ross-Innes, C. S. *et al.* Differential oestrogen receptor binding is associated with clinical outcome in breast cancer. *Nature* **481**, 389-393 (2012). https://doi.org:10.1038/nature10730
85 Quinlan, A. R. BEDTools: The Swiss-Army Tool for Genome Feature Analysis. *Curr Protoc Bioinformatics* **47**, 11 12 11-34 (2014). https://doi.org:10.1002/0471250953.bi1112s47
86 Gaujoux, R. & Seoighe, C. A flexible R package for nonnegative matrix factorization. *BMC Bioinformatics* **11**, 367 (2010). https://doi.org:10.1186/1471-2105-11-367
87 Subramanian, A. *et al.* Gene set enrichment analysis: a knowledge-based approach for interpreting genome-wide expression profiles. *Proc Natl Acad Sci U S A* **102**, 15545-15550 (2005). https://doi.org:10.1073/pnas.0506580102
88 Kim, D., Paggi, J. M., Park, C., Bennett, C. & Salzberg, S. L. Graph-based genome alignment and genotyping with HISAT2 and HISAT-genotype. *Nat Biotechnol* **37**, 907-915 (2019). https://doi.org:10.1038/s41587-019-0201-4
89 Anders, S., Pyl, P. T. & Huber, W. HTSeq--a Python framework to work with high-throughput sequencing data. *Bioinformatics* **31**, 166-169 (2015). https://doi.org:10.1093/bioinformatics/btu638
90 Love, M. I., Huber, W. & Anders, S. Moderated estimation of fold change and dispersion for RNA-seq data with DESeq2. *Genome Biol* **15**, 550 (2014). https://doi.org:10.1186/s13059-014-0550-8
91 Consortium, E. P. An integrated encyclopedia of DNA elements in the human genome. *Nature* **489**, 57-74 (2012). https://doi.org:10.1038/nature11247
92 Ho, D., Imai, K., King, G. & Stuart, E. A. MatchIt: Nonparametric Preprocessing for Parametric Causal Inference. *Journal of Statistical Software* **42**, 1 - 28 (2011). https://doi.org:10.18637/jss.v042.i08
93 Chen, W. S. *et al.* Genomic Drivers of Poor Prognosis and Enzalutamide Resistance in Metastatic Castration-resistant Prostate Cancer. *Eur Urol* **76**, 562-571 (2019). https://doi.org:10.1016/j.eururo.2019.03.020
94 Mohammed, H. *et al.* Rapid immunoprecipitation mass spectrometry of endogenous proteins (RIME) for analysis of chromatin complexes. *Nat Protoc* **11**, 316-326 (2016). https://doi.org:10.1038/nprot.2016.020
95 Cox, J. *et al.* Accurate proteome-wide label-free quantification by delayed normalization and maximal peptide ratio extraction, termed MaxLFQ. *Mol Cell Proteomics* **13**, 2513-2526 (2014). https://doi.org:10.1074/mcp.M113.031591
96 Tyanova, S. *et al.* The Perseus computational platform for comprehensive analysis of (prote)omics data. *Nat Methods* **13**, 731-740 (2016). https://doi.org:10.1038/nmeth.3901

97 Sanjana, N. E., Shalem, O. & Zhang, F. Improved vectors and genome-wide libraries for CRISPR screening. *Nat Methods* **11**, 783-784 (2014). https://doi.org:10.1038/nmeth.3047

98 Montgomery, B. *et al.* Neoadjuvant Enzalutamide Prior to Prostatectomy. *Clin Cancer Res* **23**, 2169-2176 (2017). https://doi.org:10.1158/1078-0432.CCR-16-1357

99 McKay, R. R. *et al.* Outcomes of Post-Neoadjuvant Intense Hormone Therapy and Surgery for High Risk Localized Prostate Cancer: Results of a Pooled Analysis of Contemporary Clinical Trials. *J Urol* **205**, 1689-1697 (2021). https://doi.org:10.1097/JU.0000000000001632

100 McKay, R. R. *et al.* Evaluation of Intense Androgen Deprivation Before Prostatectomy: A Randomized Phase II Trial of Enzalutamide and Leuprolide With or Without Abiraterone. *J Clin Oncol* **37**, 923-931 (2019). https://doi.org:10.1200/JCO.18.01777

101 Karzai, F. *et al.* Sequential Prostate Magnetic Resonance Imaging in Newly Diagnosed High-risk Prostate Cancer Treated with Neoadjuvant Enzalutamide is Predictive of Therapeutic Response. *Clin Cancer Res* **27**, 429-437 (2021). https://doi.org:10.1158/1078-0432.CCR-20-2344

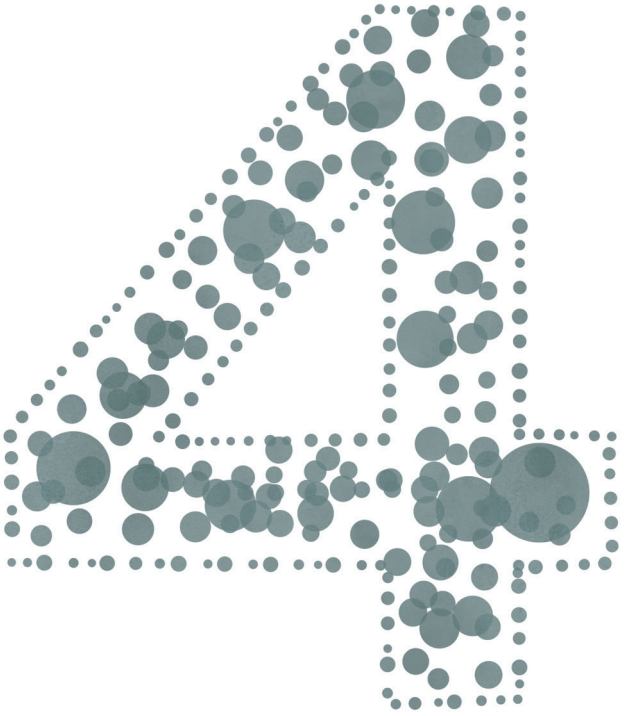

RESEARCH ARTICLE

Grade group 1 prostate cancers exhibit tumor-defining androgen receptor-driven programs

Simon Linder, Tesa M. Severson, J.C. Koen van der Mijn, Ekaterina Nevedomskaya, Joseph C. Siefert, Suzan Stelloo, Mark M. Pomerantz, Matthew L. Freedman, Henk van der Poel, Carmen Jerónimo, Rui Henrique, Andries M. Bergman[#], and Wilbert Zwart[#]

[#] These authors contributed equally to this work as co-senior authors.

Submitted (2023).

Abstract

Grade group 1 (GG1) primary prostate cancers with a pathologic Gleason score of 6 are considered indolent, generally not associated with fatal outcome and therefore treatment is not indicated for most cases. These low-grade cancers have an overall negligible risk of locoregional progression and metastasizing to distant organs, which is why there is an ongoing debate about whether these lesions should be reclassified as "non-cancerous". However, the underlying molecular activity of key disease drivers, such as the Androgen Receptor (AR), have thus far not been thoroughly characterized in low-grade tumors. Therefore, we set out to delineate the AR chromatin binding landscape in low-grade GG1 prostate cancers to gain insights into whether these AR-driven programs are actually tumor-specific or rather normal prostate epithelium-like. These analyses showed that GG1 tumors do not harbor a distinct AR cistrome and, similar to higher-grade cancers, AR preferentially binds to tumor-defining cis-regulatory elements. Furthermore, the enhancer activity of these regions and the expression of their respective target genes were not significantly different in GG1 tumors, which – from an epigenetic perspective – supports the cancer designation currently given to these low-grade tumors and clearly distinguishes them from non-cancerous benign tissue.

Patient summary

We carried out an in-depth characterization of the molecular activity of prostate cancer disease driver Androgen Receptor in low-grade tumors, which positioned these lesions as bona fide cancer and clearly separates them from benign prostate epithelium despite their clinical inoffensiveness.

Main

Adenocarcinoma of the prostate (PCa) is the second most common cancer in men, with almost 1.5 million newly diagnosed patients each year[1]. Most patients present with organ-confined disease, which can potentially be cured with loco-regional therapies, such as surgery (radical prostatectomy) or radiotherapy. However, approximately 30% of these patients will experience a rise in serum prostate-specific antigen (PSA) levels, which is referred to as a biochemical recurrence (BCR) and indicates a tumor relapse. At time of PCa diagnosis, tumor biopsies are histologically graded using the Gleason grading system[2], which helps predict the prognosis of these patients. The Gleason score (GS) describes the two most common cell morphologies based on their differentiation status and ranges from GS6 (lowest grade = International Society for Urological Pathology grade group 1, ISUP GG1) to GS9/GS10 (highest grades = ISUP GG5). However, there is an ongoing debate regarding whether low-grade GG1 lesions should be considered cancerous or rather benign neoplasms, given their overall low risk to metastasize[3]. It remains unclear how best to classify GG1 lesions from a biological perspective – do they resemble non-cancerous prostate tissue or rather share characteristics of higher-grade PCa. Here, we set out to characterize the chromatin binding landscape of the Androgen Receptor – the main driver of PCa development and progression[4] – in GG1 tumors specifically, to better understand if AR-driven programs in these low-grade lesions are more normal-like or exhibit tumor-specificity.

To address this, we analyzed AR chromatin immunoprecipitation sequencing (ChIP-seq) data[5] obtained from primary PCa specimens from radical prostatectomy resections of 82 patients covering the whole ISUP grade group spectrum (GG1: n = 17, GG2: n = 31; GG3: n = 11, GG4: n = 7, GG5: n = 16), reflecting the expected increased BCR rates with increasing GS (**Fig. 1A**; Supplementary Data) and exhibiting the expected molecular features, such as fusions of the *ERG* oncogene in half (51%) of the cohort (Supplementary Fig. S1A and S1B) and lower expression of tumor suppressor *PTEN* in patients with higher grade disease (Supplementary Fig. S1C-S1E). We further integrated the AR cistromics (**Fig. 1A**) with ChIP-seq data on the active enhancer and promoter histone mark H3K27ac (Supplementary Table S1) as well as gene expression data (RNA-seq) obtained from the same clinical specimens (Supplementary Table S2). To assess whether GG1 tumors harbor a distinct AR cistrome, we performed an unsupervised differential binding analysis on all AR ChIP-seq samples, which revealed no obvious clustering by grade group (**Fig. 1B and 1C**) and largely overlapping chromatin binding intervals (**Fig. 1D**; Supplementary Fig. S2A and S2B) and motif enrichment (**Fig.1E**), suggesting that, based on AR-chromatin interactions, GG1 tumors do not represent a different biological entity as compared to higher grade lesions. Supervised analyses

directly comparing GG1 and GG5 lesions revealed a subset of GG1-enriched binding sites (Supplementary Fig. S2C; Supplementary Table S3) that showed, however, no overlap with AR sites specific to normal prostate epithelium (Supplementary Fig. S2D). These data indicate that GG1-specific AR-regulated enhancers are distinctly different from *cis*-regulatory elements found in healthy tissue.

Figure 1: AR chromatin binding landscape in GG1 tumors is enriched for tumor-defining regulatory elements. (**A**) Study design and cohort overview. Multi-omics profiling consisting of (I) Androgen Receptor (AR) ChIP-seq, (II) H3K27ac ChIP-seq, and (III) gene expression profiling (RNA-seq) has been performed on prostate cancer tissue specimens from 82 patients[5]. The proportion of patients with a biochemical recurrence (BCR) is shown, stratified according to their respective ISUP grade group (GG1, GG2, GG3, GG4, GG5). (**B**) Correlation heatmap based on peak occupancy. Clustering of the samples (n = 82) is based on all called peaks and represents Pearson correlations between individual ChIP-seq samples. The column color bars indicate the grade group (GG1, GG2, GG3, GG4, GG5) and BCR status (Controls, Cases, NA). (**C**) Principal component analysis (PCA) plot based on peak occupancy. Each dot represents a ChIP-seq sample that is colored per grade group. (**D**) Venn diagram indicating the overlap of AR binding sites between GG1 and GG5 ChIP-seq samples, highlighting grade group-specific and common binding sites. For each group, the union of identified peaks was included. (**E**) Dot plot representing motif enrichment (z-score) at GG1-specific, GG1/GG5-common and GG5-specific AR binding sites depicted in (D). Dots are colored based on motif and sized based on significance (P-value). (**F**) Profile plots (top) and tornado plots (bottom) visualizing AR ChIP-seq signal at N- ARBS (n = 2,690), T-ARBS (n = 9,181) and Met-ARBS (n = 17,626) in GG1 tumors sorted by BCR status (left, controls: no BCR within 10 years after diagnosis; right, cases: BCR within 5 years after diagnosis), and a healthy prostate epithelium sample and a GG5 (P268T) prostate cancer as controls. Data are centered at ARBS depicting a 1-kb window around the peak center. Y-axes of profile plots and color scale indicate ChIP-seq signal in reads per genomic content (RPGC). (**G**) Boxplot indicating AR ChIP-seq counts in GG1 tumors at N-ARBS, T-ARBS and Met-ARBS. ****, $P < 0.0001$ (two sample t test). (**H**) Scatterplot showing correlation of AR ChIP-seq counts at T-ARBS between low-grade GG1 and high-grade GG5 tumors. Linear trend with confidence interval and Pearson correlation coefficient ($R = 0.89$, $P < 0.0001$) are shown. (**I**) Profile plots indicating AR ChIP-seq signal (RPGC) in GG1 tumors of cases (BCR within 5 years after diagnosis) and controls (no BCR within 10 years after diagnosis) at N-ARBS (left), T-ARBS (middle) and Met-ARBS (right) separately. ►

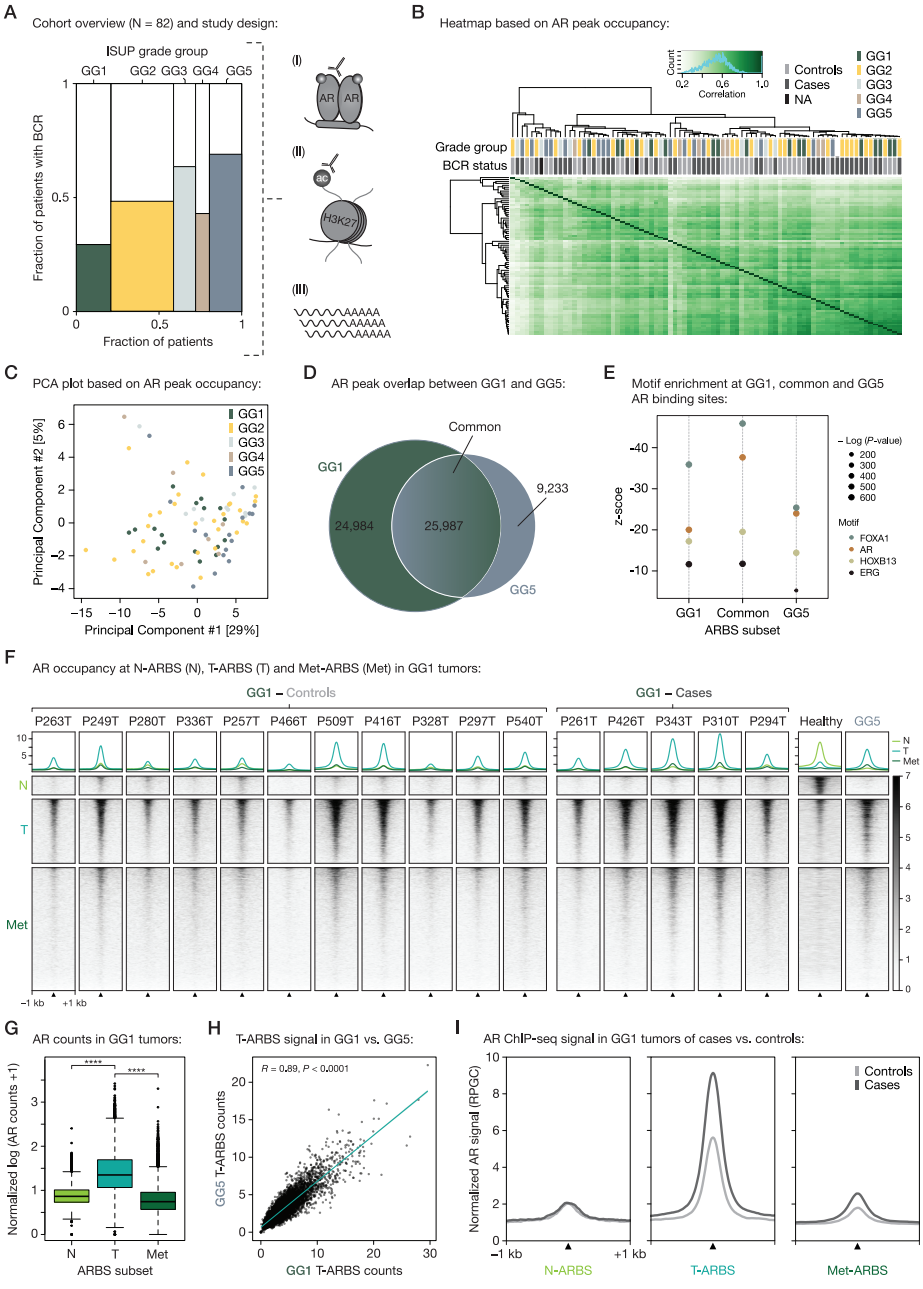
A
Cohort overview (N = 82) and study design:
ISUP grade group
GG1 GG2 GG3 GG4 GG5
Fraction of patients with BCR
Fraction of patients
(I)
(II)
(III)
AR
H3K27ac
B
Heatmap based on AR peak occupancy:
Count
Correlation
Controls
Cases
NA
GG1
GG2
GG3
GG4
GG5
Grade group
BCR status
C
PCA plot based on AR peak occupancy:
Principal Component #2 [5%]
Principal Component #1 [29%]
D
AR peak overlap between GG1 and GG5:
Common
GG1
24,984
25,987
9,233
GG5
E
Motif enrichment at GG1, common and GG5 AR binding sites:
z-score
Log (P-value)
Motif
FOXA1
AR
HOXB13
ERG
GG1
Common
GG5
ARBS subset
F
AR occupancy at N-ARBS (N), T-ARBS (T) and Met-ARBS (Met) in GG1 tumors:
GG1 – Controls
GG1 – Cases
P263T P249T P280T P336T P257T P466T P509T P416T P328T P297T P540T
P261T P426T P343T P310T P294T
Healthy
GG5
N
T
Met
−1 kb
+1 kb
G
AR counts in GG1 tumors:
Normalized log (AR counts +1)
ARBS subset
H
T-ARBS signal in GG1 vs. GG5:
R = 0.89, P < 0.0001
GG5 T-ARBS counts
GG1 T-ARBS counts
I
AR ChIP-seq signal in GG1 tumors of cases vs. controls:
Normalized AR signal (RPGC)
Controls
Cases
N-ARBS
T-ARBS
Met-ARBS

Given the importance of AR in driving context-dependent epigenomic and transcriptional programs that characterize normal prostate epithelium, primary tumors and metastatic lesions, we next investigated whether genome-wide AR binding in GG1 specimens is enriched for AR binding site (ARBS) profiles that hallmark a tumor (T) versus normal (N) state[6] (Supplementary Table S4). While healthy prostate tissue was strongly enriched for N-ARBS signal, GG1 lesions showed strongest AR binding at T-ARBS (**Fig. 1F and 1G**), phenocopying profiles observed in high-grade GG5 samples (**Fig. 1H**). These data further demonstrate that low-grade GG1 lesions harbor tumor- rather than healthy prostate epithelium-defining genomic AR programs. Since our cohort included patients with GG1 tumors that either did or did not develop a BCR within 5 years after diagnosis (cases and controls, respectively; **Fig. 1A**), we next hypothesized that these cases with future relapse, may be enriched for tumor-specific T-ARBS and particularly for more late-stage metastases-specific ARBS (Met-ARBS) signal[7]. To test this hypothesis, we also assessed the AR chromatin occupancy at Met-ARBS (**Fig. 1F**), and although the overall signal was rather low as expected for primary disease (**Fig. 1G**), we did observe a significant increase at these more aggressive metastatic binding sites in GG1 cases versus controls, which was accompanied by an increase in T-ARBS and no difference in N-ARBS signal (**Fig. 1I**). Notably, while the enrichment for T-ARBS and Met-ARBS signal was detected in both, GG1 cases and controls, the signal strength at these tumor-specific ARBS was significantly elevated in patients with future relapse and could help identify and stratify these cases (**Fig. 1F, 1G and 1I**; Supplementary Fig. S3A-C; Supplementary Fig. S4A).

Taken together, our analyses reveal that low-grade GG1 lesions do not harbor a distinct healthy prostate epithelium-like AR chromatin binding landscape that could explain their favorable prognosis but are rather enriched for tumor-defining AR-driven programs – similar to higher grade tumors.

Next, we investigated whether AR binding to T-ARBS was accompanied by changes in activity of these *cis*-regulatory elements as well as the target genes that are under their control. Therefore, we first examined the H3K27ac signal at T-ARBS, which revealed a highly comparable signal strength between low-grade GG1 and high-grade GG5 lesions (**Fig. 2A and 2B**). Similar to the increase in AR signals in GG1 cases versus controls, we also observed elevated H3K27ac at T-ARBS (**Fig. 2C**) in cases versus controls, while H3K27ac at N-ARBS and Met-ARBS was decreased and unchanged, respectively (Supplementary Fig. S4B).

Having shown prevalence of tumor-defining genomic features in low-grade lesions, we next sought to characterize whether the expression of the distal target genes associated could stratify GG1 tumors from higher grade lesions. Therefore, we made use of a T-ARBS gene set we previously identified, which was generated by integrating

differential gene expression with AR chromatin profiles that were gained during tumorigenesis [referred to as Gained in Tumor (GiT) genes[8]]. However, the expression of these tumor-specific AR-driven genes (*n* = 102; Supplementary Table S5) did not separate GG1 samples from higher grade lesions (**Fig. 2D**), but rather clustered them independent of their grade group (**Fig. 2E**) and revealed lower expression in controls and higher expression in cases (Supplementary Fig. S5A-C). Similarly, when performing differential gene expression analysis between GG5 and GG1 tumors (Supplementary Table S6), we observed enrichment of expected gene sets for high-grade (e.g., epithelial-mesenchymal transition and cell cycle-related gene ontology terms) or low-grade lesions (e.g., metabolic pathways and canonical – not tumor-specific – androgen response), clearly highlighting the aggressiveness of poorly differentiated high-risk disease (Supplementary Fig. S5D-F). However, projecting the expression of tumor-determining AR-regulated genes on top revealed that most of these T-ARBS genes (89/102) were not differentially expressed between these grade groups (**Fig. 2F**), further illustrating that also low-grade lesions express tumor-specific gene sets. Overall, these analyses demonstrate that not only the tumor-specific cistromic but also the transcriptomic activity of AR in low-grade lesions is not enriched for normal prostate epithelium-specific signaling, but rather shows high concordance with high-grade prostate cancer.

Although higher-grade tumors exhibit molecular characteristics not observed in low-grade lesions, ultimately resulting in their more aggressive phenotype and poorer clinical outcome, GG1 tumors are clearly distinguishable from healthy prostate epithelium. Previous studies have shown that GG1 tumors share morphological features with higher grade Gleason patterns, and also genomic alterations, such as *PTEN* deletions and *MYC* amplifications that are typically enriched in aggressive PCa, can be detected in these low-grade samples[9,10]. We now provide evidence that the epigenetic features of prostate cancer driver AR that hallmark primary adenocarcinomas as opposed to normal prostate epithelium, along with the genes it controls, are not distinct in GG1 tumors but, in contrast, are highly comparable between low- and high-grade disease, positioning grade group 1 (Gleason score 6) lesions as *bona fide* cancers from an epigenetic perspective.

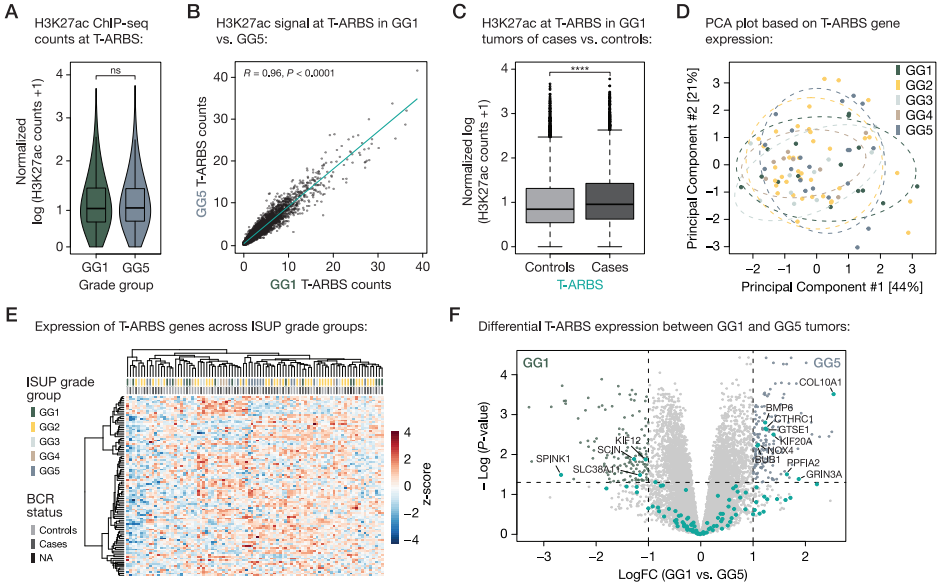

Figure 2: Enhancer activity and gene expression of tumor-specific AR targets are highly comparable between low- and high-grade prostate cancers. (**A**) Violin plot indicating H3K27ac ChIP-seq signal at T-ARBS of GG1 and GG5 tumors. ns, $P > 0.05$ (two sample t test). (**B**) Scatterplot showing correlation of H3K27ac ChIP-seq counts at T-ARBS between low-grade GG1 and high-grade GG5 tumors. Linear trend with confidence interval and Pearson correlation coefficient ($R = 0.96$, $P < 0.0001$) are shown. (**C**) Boxplot indicating H3K27ac ChIP-seq counts at T-ARBS in GG1 tumors of cases (BCR within 5 years after diagnosis) and controls (no BCR within 10 years after diagnosis). ****, $P < 0.0001$ (paired t test). (**D**) Principal component analysis (PCA) plot based on expression of a T-ARBS gene set[8]. Each dot represents an RNA-seq sample ($n = 91$) that is colored per ISUP grade group. Ellipses are based on the 80% confidence interval. (**E**) Unsupervised hierarchical clustering of RNA-seq samples based on the expression of T-ARBS genes. The color scale indicates gene expression (z-score), and the column color bars indicate the grade group (GG1, GG2, GG3, GG4, GG5) and BCR status (Controls, Cases, NA) per sample. (**F**) Volcano plot depicting differential gene expression between low-grade GG1 (left) and high-grade GG5 tumors (right). Significantly differentially expressed genes and T-ARBS genes are highlighted. Significance cutoffs are shown as dotted lines [log Fold Change (FC) between GG1 and GG5 ≥ 1; $P \leq 0.05$], and T-ARBS genes passing this threshold are labeled.

Conflict of interest

M.L. Freedman reports other support from Precede Bio outside the submitted work. H. van der Poel reports grants from Astellas outside the submitted work. A.M. Bergman reports grants and personal fees from Astellas Pharma outside the submitted work. W. Zwart reports grants and personal fees from Astellas Pharma, and grants from AstraZeneca outside the submitted work. No disclosures were reported by the other authors.

Author contributions

S. Linder: Conceptualization, Methodology, Software, Validation, Formal analysis, Investigation, Writing - Original Draft, Writing - Review & Editing, Visualization, Project administration. T.M. Severson: Methodology, Software, Validation, Formal analysis, Investigation, Resources, Data Curation, Visualization, Writing - Review & Editing. J.C.K. van der Mijn: Conceptualization, Writing - Review & Editing. E. Nevedomskaya: Methodology, Software, Formal analysis, Investigation, Resources, Data Curation, Writing - Review & Editing. J.C. Siefert: Methodology, Software, Resources, Writing - Review & Editing. S. Stelloo: Resources, Writing - Review & Editing. M.M. Pomerantz: Writing - Review & Editing, Funding acquisition. M.L. Freedman: Writing - Review & Editing, Funding acquisition. H. van der Poel: Conceptualization, Writing - Review & Editing. C. Jerónimo: Methodology, Formal analysis, Investigation, Resources, Data Curation, Writing - Review & Editing, Supervision. R. Henrique: Methodology, Formal analysis, Investigation, Resources, Data Curation, Writing - Review & Editing, Supervision. A.M. Bergman: Conceptualization, Writing - Original Draft, Writing - Review & Editing, Visualization, Supervision, Project administration, Funding acquisition. W. Zwart: Conceptualization, Writing - Original Draft, Writing - Review & Editing, Visualization, Supervision, Project administration, Funding acquisition.

Acknowledgments

This work was supported by Movember (NKI01 to A.M. Bergman and W. Zwart), KWF Dutch Cancer Society (10084 ALPE to A.M. Bergman and W. Zwart), KWF Dutch Cancer Society/ Alpe d'HuZes Bas Mulder Award (NKI 2014-6711 to W. Zwart), Netherlands Organization for Scientific Research (NWO-VIDI-016.156.401 to W. Zwart), and Department of Defense (W81XWH-19-1-0565 to M.M. Pomerantz, M.L. Freedman and W. Zwart). The authors would like to thank the NKI Genomics Core Facility (GCF) for bioinformatics support,

and the NKI Research High Performance Computing facility (RHPC) for computational infrastructure. We also thank all Zwart/Bergman lab members for fruitful discussions and technical advice. Finally, we would like to thank Peter S. Nelson (Divisions of Human Biology and Clinical Research, Fred Hutchinson Cancer Research Center, Seattle, WA, USA) for bringing this open debate to our attention and for his valuable input on the manuscript.

Supplementary data

Cohort and tissue samples

The presented prostate cancer patient cohort included cases that underwent radical prostatectomy between 2001 and 2008. Of note, during this period no active surveillance protocol existed at IPO Porto, which is why also low-risk GG1 (GS6) patients were submitted to prostatectomy. For all patients, prostate cancer tissue was systematic collected and sampled using a strategy which enables a very precise localization of tumor foci in frozen tissue. In brief, each prostate specimen was sectioned immediately after surgery, by an experienced uropathologist, using a long sharp blade resulting in the apex region with about 1 cm depth and transversal parallel slices of the remainder prostate gland with approximately 6-7 mm in thickness. Then, each slice was cut into quadrants and each quadrant was halved, providing a section which was immediately placed in a cassette and immersed in neutral buffered formalin for formalin fixation, processing, paraffin embedding and histopathological examination, and a "twin" fragment which was snap frozen. The reference in each of these tissue sections allowed for easy referral. Then, histopathological examination of FFPE sections enabled adequate grading and staging, as well as identification of the index tumor. Subsequently, a 5-µm thick section was cut in the corresponding "twin" frozen fragment in a cryostat and stained with HE for localization of the representative area of the tumor. Then, the frozen tissue block was trimmed to maximize the yield of target cells (> 70% of tumor cells), and an average of 50 x 12-µm thick sections were cut, interspersed at every fifth section with a 5-µm thick section for HE staining to control for percentage of target cells. The collected tissue was subsequently processed for nucleic acid extraction, minimizing cell death and autolysis, and providing optimal histopathological assessment as well as high-quality DNA and RNA samples for ChIP-seq and RNA-seq analyses, respectively. Furthermore, Gleason score 7 (GG2 + GG3) tumors were thoroughly revised to look for the presence of cribriform morphology, which was apparent in 12 out of 31 GG2 (39%) and 7 out of 11 GG3 (64%) tumors (see Supplementary Table S7). Biochemical recurrence (BCR) was defined as two consecutive rises in serum PSA of ≥ 0.2 ng/mL during follow-up.

ChIP-seq

For analysis of AR and H3K27ac ChIP-seq data, all 88 samples for which both cistromic data-streams are available and which passed the original quality controls metrics[5] were re-aligned to the human reference genome hg38 using Burrows-Wheeler Aligner (v0.5.10)[11]. Reads were filtered based on mapping quality (MAPQ ≥ 20) and duplicate reads were removed. Peak calling over mixed input controls were performed using MACS2 (v2.1.2)[12]. AR tissue ChIP-seq samples with more than 100 peaks called (n = 82),

and matched H3K27ac samples, were included in the final analyses. The DiffBind R package (v3.6.1) was used to generate correlation heatmaps and PCA plots based on chromatin occupancy, to generate union peaklists[13], and to generate Venn diagrams to illustrate peaklist overlaps. Genome browser snapshots were generated using EaSeq (v1.101)[14]. Motif enrichment analyses were performed using the SeqPos motif tool on Galaxy Cistrome[15]. ARBS[6,7] were converted between assemblies (from hg19 to hg38), using the UCSC genome browser liftOver tool[16]. AR and H3K27ac ChIP-seq counts at N-ARBS, T-ARBS and Met-ARBS were quantified using deepTools[17] multiBigwigSummary (v3.5.1). The DiffBind R package (v3.6.1) was used to generate correlation heatmaps and PCA plots based on AR peak occupancy, to perform differential binding analysis between GG1 and GG5 samples using an FDR < 0.05, and to generate union peak lists[13]. Signal differences between GG1 samples at different ARBS subsets, or across samples stratified by grade group, were visualized using the 'boxplot' or 'vioplot' function in R, respectively. Statistical differences were determined using a Mann-Whitney *U* test (not paired) or Wilcoxon signed-rank test (paired). For tornado or profile plots, the AR or H3K27ac signal at different genomic regions (ARBS subsets) were calculated using deepTools computeMatrix and plotted using the deepTools plotHeatmap or plotProfile functions. For profile plots, GG1 samples of cases or controls were first merged and down-sampled before the signal scores were calculated. The healthy prostate epithelium control sample (Patient1_healthy_ARChIP; wz2116) is available via the European Genome-phenome Archive (EGA) under the accession number EGAS00001003928[18]. Scatterplot showing correlation of AR or H3K27ac signal at T-ARBS in low-grade GG1 and high-grade GG5 samples were plotted using 'ggplot2' (v3.3.6; https://CRAN.R-project.org/package=ggplot2). Samples were colored by ISUP grade group using the 'Chevalier1' color palette of the 'wesanderson' R package (v0.3.6; https://cran.r-project.org/web/packages/wesanderson/), supplemented with the R color 'lightslategrey' for GG5 tumors.

RNA-seq

Heatmaps of gene expression data[5] were created using the aheatmap function from the R package NMF (v0.22.0)[19] with a color scheme from RColorBrewer (v1.1-2; https://CRAN.R-project.org/package=RColorBrewer). All genes identified in the original T-ARBS gene set[8] and expressed in this gene expression data set (n = 102) were used for downstream analyses. T-ARBS gene expression differences between GG1 cases and controls, or across grade groups, were visualized using the 'boxplot' function in R and significance of expression level differences were determined using a Wilcoxon signed-rank test (paired). Differentially expressed genes between low-grad GG1 and high-grade GG5 tumors were identified using an EdgeR[20] (v3.18.1)-Limma[21] (3.34) workflow and visualized in a volcano plot in R with the following significance cut-offs: log Fold Change

(FC) between GG1 and GG5 ≥ 1, and $P \leq 0.05$. Gene set enrichment was performed using pre-ranked GSEA[22] based on the expression fold change (GG5 vs. GG1) calculated with EdgeR-Limma. For visualization, GSEA plots were re-plotted using the 'ReplotGSEA' R function (https://github.com/PeeperLab/Rtoolbox/blob/master/R/ReplotGSEA.R).

Supplementary tables

Due to print size limitations, all supplementary data tables are available upon request from Andries M. Bergman (a.bergman@nki.nl) or Wilbert Zwart (w.zwart@nki.nl).

Supplementary Table S1: ChIP-seq samples (hg38).
Supplementary Table S2: RNA-seq samples.
Supplementary Table S3: Differential AR binding sites between GG1 and GG5 tumors.
Supplementary Table S4: ARBS subsets (lifted over to hg38).
Supplementary Table S5: Expression of T-ARBS genes.
Supplementary Table S6: Differentially expressed genes (GG5 vs. GG1).
Supplementary Table S7: Cribriform growth patterns in GG2 and GG3 ChIP-seq samples.

Supplementary figures

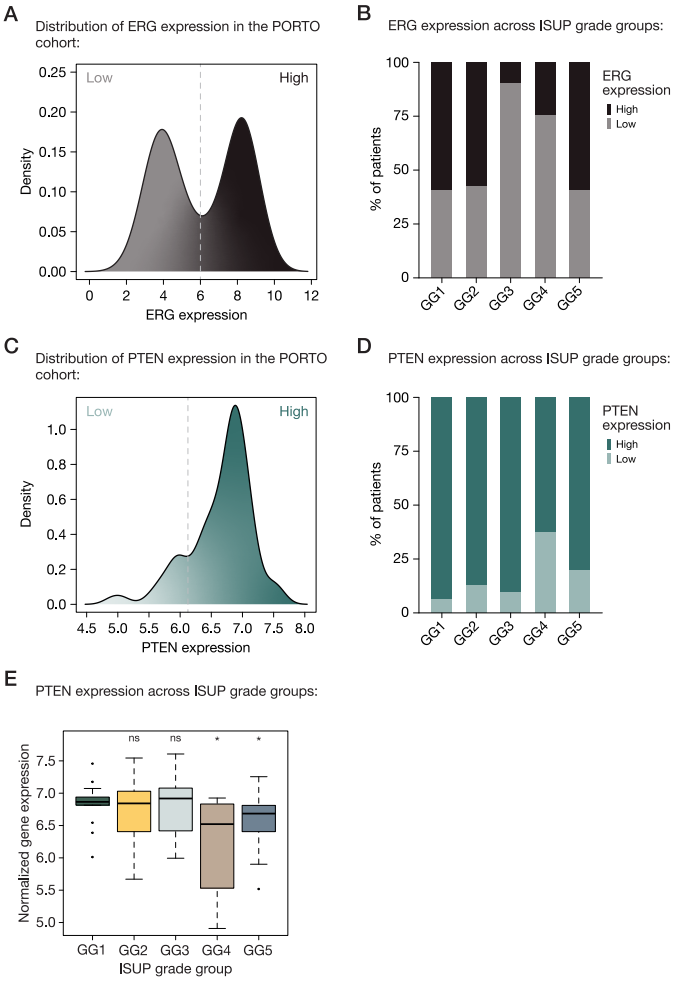

Supplementary Figure S1: Expression of oncogene *ERG* and tumor suppressor *PTEN* in the PORTO cohort. (**A**) Density map illustrating the distribution of ERG expression across all patients, demonstrating the expected two populations: low ERG-expressing (49%) tumors and high ERG-expressing tumors (51%), which indicates ERG fusion events, such as TMPRSS2-ERG[5,23]. Z-score cut-off (low: ≤ 6; high: > 6) is indicated. (**B**) Stacked bar graph showing the distribution of low- and high-ERG expressing tumors across ISUP grade groups. (**C**) Density map illustrating the distribution of PTEN expression across all patients, demonstrating primarily high-expressing tumors (83%) and fewer low-expressing tumors (17%). Z-score cut-off (low: ≤ 6.125; high: > 6.125) is indicated. (**D**) Stacked bar graph showing the distribution of low- and high-PTEN expressing tumors across ISUP grade groups. (**E**) Boxplot indicating PTEN expression across ISUP grades, which shows significantly lower PTEN levels in higher grade tumors (GG4/GG5) as compared to GG1. *, $P < 0.05$ (Mann–Whitney *U* test).

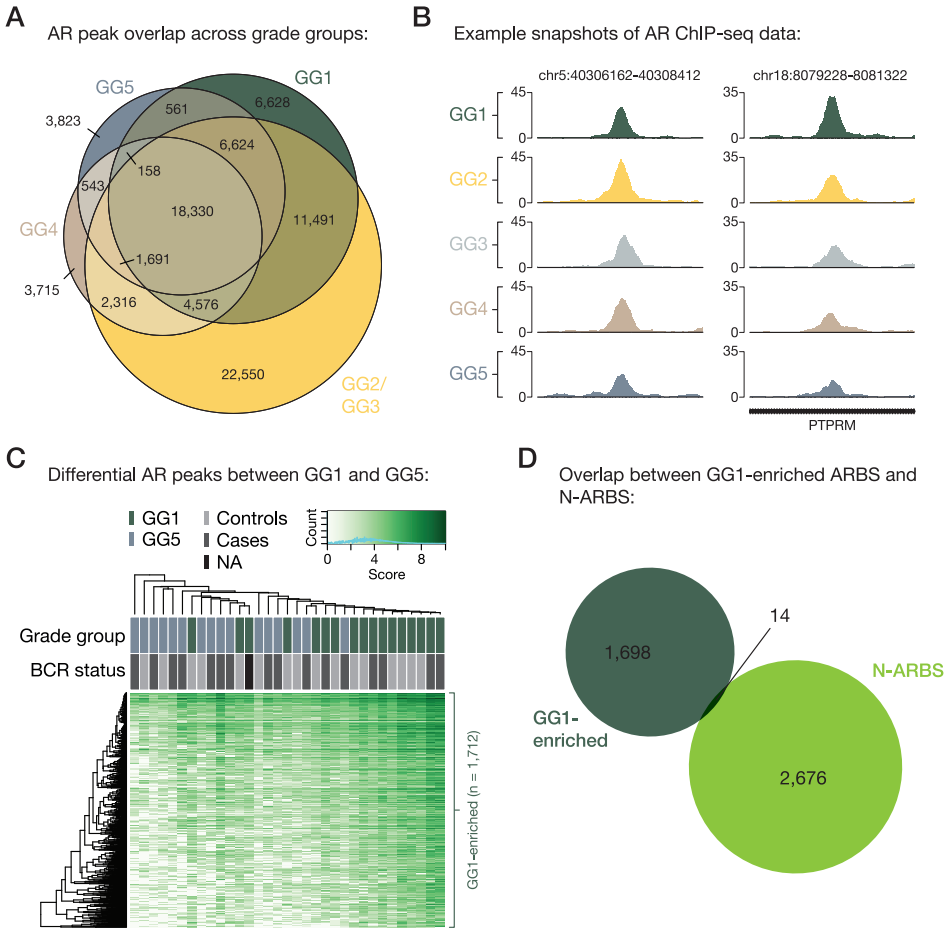

Supplementary Figure S2: AR cistromics across grade groups. (**A**) Venn diagram indicating the overlap of AR binding sites between GG1, GG2/GG3, GG4 and GG5 ChIP-seq samples. For each grade group, the union of identified peaks was included. (**B**) Representative example snapshots of AR ChIP-seq signal at two genomic locations shared across all grade groups [*n* = 18,330; depicted in (A)]. Y-axis indicates ChIP-seq signal in fragments per kilobase per million reads mapped (FPKM). (**C**) Coverage heat map depicting differential AR binding sites significantly enriched in GG1 lesions as compared to GG5 tumors (*n* = 1,712). The color scale indicates the score, and the column color bars indicate the grade group (GG1, GG5) and BCR status (Controls, Cases, NA) per sample. (**D**) Overlap of GG1-enriched AR binding sites (C) with regulatory elements specifically occupied by AR in normal prostate epithelium (N-ARBS), indicating that AR chromatin interactions lost in high-grade disease (GG5) are not normal-like.

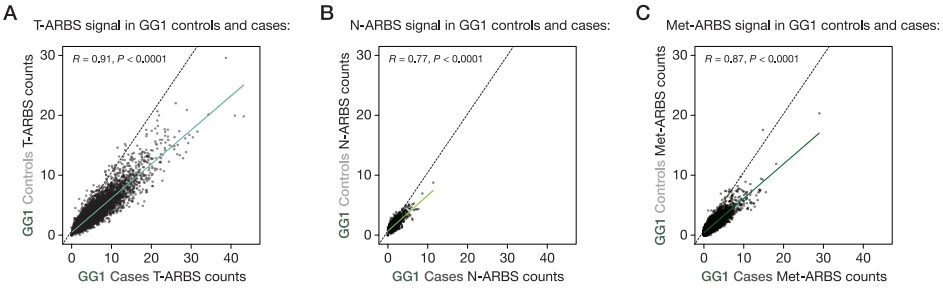

Supplementary Figure S3: Enrichment for tumor-specific AR binding in low-grade GG1 tumors. Scatterplots showing correlation of AR ChIP-seq counts at T-ARBS (**A**), N-ARBS (**B**) and Met-ARBS (**C**) between tumors of GG1 controls and GG1 cases, indicating enrichment for T-ARBS and Met-ARBS signals in both, GG1 controls and cases, which is, however, stronger in cases with future relapse (skewing of the trendline away from the dashed diagonal toward the cases). Linear trends with confidence intervals and Pearson correlation coefficients are indicated.

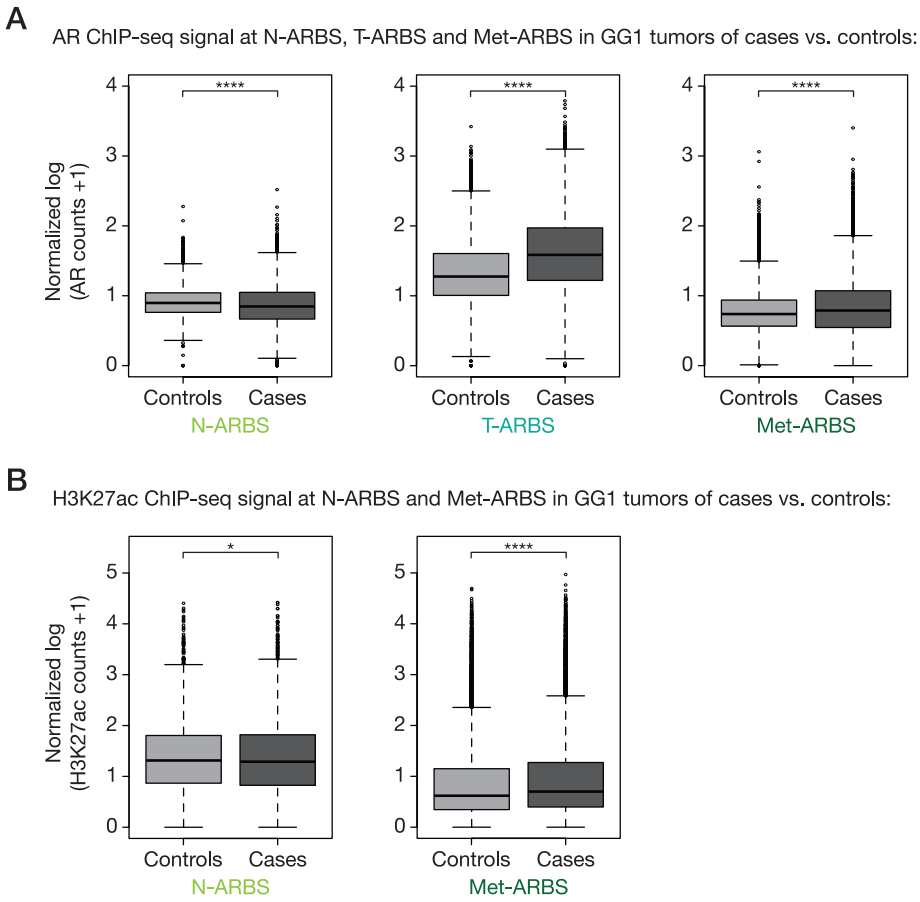

Supplementary Figure S4: AR-induced enhancer activity in low-grade GG1 tumors. (**A**) Boxplots indicating AR ChIP-seq counts [in reads per genomic content (RPGC)] at N-ARBS (left), T-ARBS (middle) and Met-ARBS (right) in GG1 tumors of cases (BCR within 5 years after diagnosis) and controls (no BCR within 10 years after diagnosis). ****, $P < 0.0001$ (paired *t* test). (**B**) Boxplots indicating H3K27ac ChIP-seq signal (RPGC) at N-ARBS (left) and Met-ARBS (right) in GG1 tumors of cases and controls. *, $P < 0.05$; ****, $P < 0.0001$ (paired *t* test).

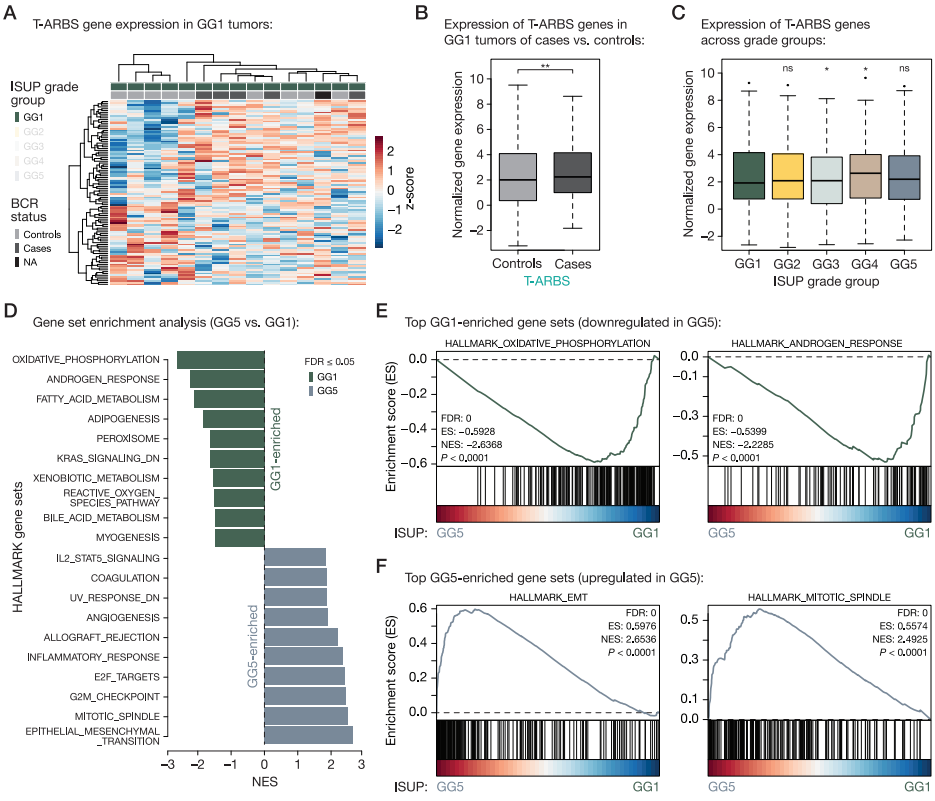

Supplementary Figure S5: Expression of tumor-specific AR target genes in low- and high-grade prostate cancers. (**A**) Unsupervised hierarchical clustering of low-grade (GG1) RNA-seq samples based on the expression of T-ARBS genes. The color scale indicates gene expression (z-score), and the column color bars indicate the ISUP grade group (GG1) and BCR status (Controls, Cases, NA) per sample. (**B**) Boxplot indicating normalized expression of T-ARBS genes in GG1 tumors of cases (BCR within 5 years after diagnosis) and controls (no BCR within 10 years after diagnosis). **, $P < 0.01$ (Wilcoxon signed-rank test). (**C**) Boxplot indicating normalized T-ARBS gene expression across grade groups. ns, $P > 0.05$; *, $P < 0.05$ (Wilcoxon signed-rank test). (**D**) Bar graph depicting gene set enrichment analysis (GSEA) results for Hallmark gene sets. Shown are the top 10 differentially enriched pathways (FDR ≤ 0.05) in GG1 (top) and GG5 (bottom). *X*-axis indicates the normalized enrichment score (NES). (**E**) Enrichment plots of the top 2 GG1-enriched Hallmark pathways: oxidative phosphorylation (left) and androgen response (right). Genes are ranked by differential expression between ISUP grades GG5 and GG1 based on patient RNA-seq data (GG5 vs. GG1). *Y*-axis indicates enrichment score (ES). GSEA statistics (FDR, ES, NES, nominal *P*-value) are shown. (**F**) Same as (E) but depicting the top 2 GG5-enriched Hallmark pathways: epithelial-mesenchymal transition (EMT; left) and mitotic spindle (right).

References

1 Sung, H. *et al.* Global Cancer Statistics 2020: GLOBOCAN Estimates of Incidence and Mortality Worldwide for 36 Cancers in 185 Countries. *CA Cancer J Clin* **71**, 209-249 (2021). https://doi.org:10.3322/caac.21660

2 Gleason, D. F. & Mellinger, G. T. Prediction of prognosis for prostatic adenocarcinoma by combined histological grading and clinical staging. *J Urol* **111**, 58-64 (1974). https://doi.org:10.1016/s0022-5347(17)59889-4

3 Ross, H. M. *et al.* Do adenocarcinomas of the prostate with Gleason score (GS) </=6 have the potential to metastasize to lymph nodes? *Am J Surg Pathol* **36**, 1346-1352 (2012). https://doi.org:10.1097/PAS.0b013e3182556dcd

4 Stelloo, S., Bergman, A. M. & Zwart, W. Androgen receptor enhancer usage and the chromatin regulatory landscape in human prostate cancers. *Endocr Relat Cancer* **26**, R267-R285 (2019). https://doi.org:10.1530/ERC-19-0032

5 Stelloo, S. *et al.* Integrative epigenetic taxonomy of primary prostate cancer. *Nat Commun* **9**, 4900 (2018). https://doi.org:10.1038/s41467-018-07270-2

6 Pomerantz, M. M. *et al.* The androgen receptor cistrome is extensively reprogrammed in human prostate tumorigenesis. *Nat Genet* **47**, 1346-1351 (2015). https://doi.org:10.1038/ng.3419

7 Pomerantz, M. M. *et al.* Prostate cancer reactivates developmental epigenomic programs during metastatic progression. *Nat Genet* **52**, 790-799 (2020). https://doi.org:10.1038/s41588-020-0664-8

8 Severson, T. *et al.* Androgen receptor reprogramming demarcates prognostic, context-dependent gene sets in primary and metastatic prostate cancer. *Clin Epigenetics* **14**, 60 (2022). https://doi.org:10.1186/s13148-022-01278-8

9 Carter, H. B. *et al.* Gleason score 6 adenocarcinoma: should it be labeled as cancer? *J Clin Oncol* **30**, 4294-4296 (2012). https://doi.org:10.1200/JCO.2012.44.0586

10 Gandellini, P. *et al.* Core Biopsies from Prostate Cancer Patients in Active Surveillance Protocols Harbor PTEN and MYC Alterations. *Eur Urol Oncol* **2**, 277-285 (2019). https://doi.org:10.1016/j.euo.2018.08.010

11 Li, H. & Durbin, R. Fast and accurate short read alignment with Burrows-Wheeler transform. *Bioinformatics* **25**, 1754-1760 (2009). https://doi.org:10.1093/bioinformatics/btp324

12 Zhang, Y. *et al.* Model-based analysis of ChIP-Seq (MACS). *Genome Biol* **9**, R137 (2008). https://doi.org:10.1186/gb-2008-9-9-r137

13 Ross-Innes, C. S. *et al.* Differential oestrogen receptor binding is associated with clinical outcome in breast cancer. *Nature* **481**, 389-393 (2012). https://doi.org:10.1038/nature10730

14 Lerdrup, M., Johansen, J. V., Agrawal-Singh, S. & Hansen, K. An interactive environment for agile analysis and visualization of ChIP-sequencing data. *Nat Struct Mol Biol* **23**, 349-357 (2016). https://doi.org:10.1038/nsmb.3180

15 Liu, T. *et al.* Cistrome: an integrative platform for transcriptional regulation studies. *Genome Biol* **12**, R83 (2011). https://doi.org:10.1186/gb-2011-12-8-r83

16 Kuhn, R. M., Haussler, D. & Kent, W. J. The UCSC genome browser and associated tools. *Brief Bioinform* **14**, 144-161 (2013). https://doi.org:10.1093/bib/bbs038

17 Ramirez, F. *et al.* deepTools2: a next generation web server for deep-sequencing data analysis. *Nucleic Acids Res* **44**, W160-165 (2016). https://doi.org:10.1093/nar/gkw257

18 Mazrooei, P. *et al.* Cistrome Partitioning Reveals Convergence of Somatic Mutations and Risk Variants on Master Transcription Regulators in Primary Prostate Tumors. *Cancer Cell* **36**, 674-689 e676 (2019). https://doi.org:10.1016/j.ccell.2019.10.005

19 Gaujoux, R. & Seoighe, C. A flexible R package for nonnegative matrix factorization. *BMC Bioinformatics* **11**, 367 (2010). https://doi.org:10.1186/1471-2105-11-367

20 Robinson, M. D., McCarthy, D. J. & Smyth, G. K. edgeR: a Bioconductor package for differential expression analysis of digital gene expression data. *Bioinformatics* **26**, 139-140 (2010). https://doi.org:10.1093/bioinformatics/btp616

21 Ritchie, M. E. *et al.* limma powers differential expression analyses for RNA-sequencing and microarray studies. *Nucleic Acids Res* **43**, e47 (2015). https://doi.org:10.1093/nar/gkv007

22 Subramanian, A. *et al.* Gene set enrichment analysis: a knowledge-based approach for interpreting genome-wide expression profiles. *Proc Natl Acad Sci U S A* **102**, 15545-15550 (2005). https://doi.org:10.1073/pnas.0506580102

23 Kron, K. J. *et al.* TMPRSS2-ERG fusion co-opts master transcription factors and activates NOTCH signaling in primary prostate cancer. *Nat Genet* **49**, 1336-1345 (2017). https://doi.org:10.1038/ng.3930

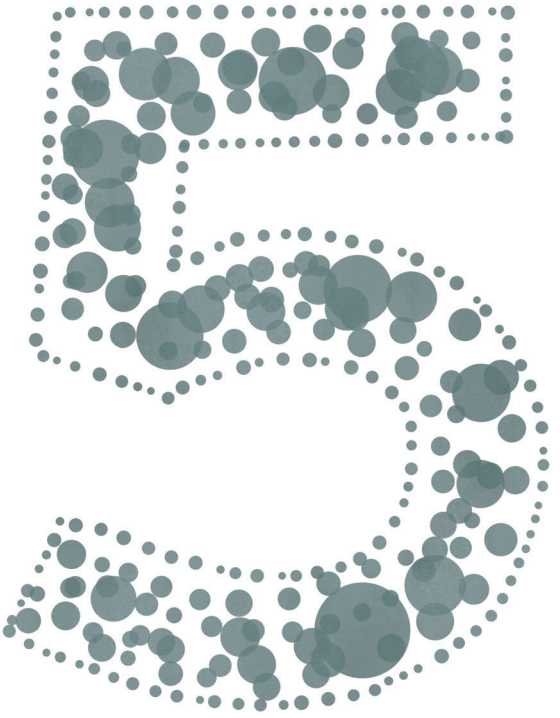

RESEARCH ARTICLE

Androgen modulation of XBP1 is functionally driving part of the AR transcriptional program

Suzan Stelloo[‡], Simon Linder[‡], Ekaterina Nevedomskaya, Eider Valle-Encinas, Iris de Rink, Lodewyk F.A. Wessels, Henk van der Poel, Andries M. Bergman[#], and Wilbert Zwart[#]

[‡] These authors contributed equally to this work as co-first authors.
[#] These authors contributed equally to this work as co-senior authors.

Adapted from *Endocrine-Related Cancer* 27 (2), 67-79 (2020).

Abstract

Prostate cancer development and progression is largely dependent on androgen receptor (AR) signaling. AR is a hormone-dependent transcription factor, which binds to thousands of sites throughout the human genome to regulate expression of directly responsive genes, including prosurvival genes that enable tumor cells to cope with increased cellular stress. ERN1 and XBP1 – two key players of the unfolded protein response (UPR) – are among such stress-associated genes. Here, we show that XBP1 levels in primary prostate cancer are associated with biochemical recurrence in five independent cohorts. Patients who received AR-targeted therapies had significantly lower XBP1 expression, whereas expression of the active form of XBP1 (XBP1s) was elevated. *In vitro* results show that AR-induced ERN1 expression led to increased XBP1s mRNA and protein levels. Furthermore, ChIP-seq analysis revealed that XBP1s binds enhancers upon stress stimuli regulating genes involved in UPR processes, eIF2 signaling and protein ubiquitination. We further demonstrate genomic overlap of AR and XBP1s binding sites, suggesting genomic conversion of the two signaling cascades. Transcriptomic effects of XBP1 were further studied by knockdown experiments, which lead to decreased expression of androgen-responsive genes and UPR genes. These results suggest a two-step mechanism of gene regulation, which involves androgen-induced expression of ERN1, thereby enhancing XBP1 splicing and transcriptional activity. This signaling cascade may prepare the cells for the increased protein folding, mRNA decay and translation that accompanies AR-regulated tumor cell proliferation.

Introduction

In eukaryotic cells, homeostasis between protein production and degradation is a tightly regulated process. This regulation is perturbed when unfolded or misfolded proteins build up in the endoplasmic reticulum (ER), which induces the unfolded protein response (UPR). Upon UPR activation, a distinct transcriptional program is induced that increases the production of chaperones and foldases to restore homeostasis. The UPR plays a key role in a large spectrum of diseases, including neurodegenerative disorders and this signaling cascade is also critically involved in many tumor types, including prostate cancer.

Prostate cancer development and progression is largely dictated by androgen receptor (AR) action; a hormone-dependent transcription factor that binds the genome at thousands of sites, regulating gene programs involved in tumor cell proliferation. There is growing evidence of a link between the UPR and AR function, in which AR directly regulates the expression of ER stress-associated genes, including endoplasmic reticulum to nucleus signaling 1 (*ERN1*) and X-box binding protein (*XBP1*)[1,2]. XBP1 is a basic leucine zipper (bZIP) transcription factor, triggered by the onset of ER stress and other physiological processes such as lipid and cholesterol metabolism, energy control, inflammation and cell differentiation[3]. Beyond AR signaling in prostate cancer, XBP1 gene expression is upregulated by other factors of the endocrine system, including parathyroid hormone stimulation in osteoblasts[4], growth hormone in adipocytes[5] and estradiol stimulation in breast cancer cells[6]. In addition to transcriptional control of XBP1, its function is also post-transcriptionally regulated through inositol-requiring enzyme (IRE1), which is encoded by the *ERN1* gene (hereafter both the gene and protein are referred to as ERN1, for simplicity). When ERN1 senses stress, its RNase function is activated, allowing excision of 26 nucleotides of the XBP1 mRNA which leads to a frameshift[3,7-9]. Consequently, XBP1 exists in two isoforms; XBP1 unspliced (XBP1u) and XBP1 spliced (XBP1s). Both isoforms contain a DNA binding domain, but only XBP1s has a transactivation domain enabling transcriptional induction of UPR genes including *DNAJB9* and *SEC11C*[8,10,11]. Even though the genome-wide chromatin binding features of XBP1 remain elusive in the context of prostate cancer, ChIP-on-ChIP and ChIP-seq analyses of XBP1 have been performed in other systems including skeletal muscle cells, breast cancer cells and liver tissue[12-14]. In these cells, XBP1 mainly binds promoters that contain ER stress response elements (ERSE: CCACG) or unfolded protein response elements (UPRE: ACGT)[12-14]. Besides regulating genes to maintain ER function, XBP1 also drives cell-type specific gene expression profiles, such as the *MIST* gene in the myoblast cell line C2C12 to drive myogenic differentiation[14]. Whether XBP1 induces a prostate-specific transcriptional program remains unknown.

In prostate cancer, XBP1 expression levels vary at different stages of the disease. XBP1 expression is higher in primary prostate cancer compared to benign tissue, while its expression is lower in metastases relative to primary lesions[15-17]. Furthermore, XBP1 knockdown reduced growth of prostate cancer cell lines, irrespective of AR expression[1,18,19].

We previously identified a prognostic 9-gene classifier for prostate cancer outcome, which included *XBP1*[15]. In this study, we further evaluated the prognostic value and biological function of XBP1 in prostate cancer. Low expression of XBP1 was consistently associated with biochemical progression in five independent cohorts. Using mRNA samples from a cohort of prostate cancer patients receiving neoadjuvant enzalutamide treatment, we could show that AR-targeted therapy reduced total XBP1 expression, while XBP1s levels were increased. Furthermore, *in vitro* assays showed that expression of both ERN1 and XBP1 and consequently XBP1 splicing is increased upon AR activation. ChIP-seq analysis revealed that spliced XBP1 binds the chromatin largely at promoters in the absence of hormonal cues, while AR activation induces XBP1s binding at enhancers that are co-occupied by AR to regulate genes involved in UPR processes and AR action. These findings illustrate a two-step mechanism of gene regulation, in which AR signaling through XBP1s primes the proliferating prostate tumor cell for increased protein folding, mRNA decay and protein translation.

Results

XBP1 expression is correlated with disease progression and response to hormone therapy

We previously identified a prognostic 9-gene signature, which among other genes included the transcription factor XBP1[15]. To further study the biological role of XBP1 in prostate cancer, we firstly evaluated the expression of XBP1 for prognostic relevance as a single gene by performing a meta-analysis of five publicly available datasets (743 cases and 170 events, in total). The patients were divided into low and high XBP1 expression groups on the basis of the median XBP1 expression within each cohort. We then tested the association of XBP1 expression with biochemical progression after radical prostatectomy. The combined hazard ratio (HR) for the five cohorts in univariate analysis is 0.52 (95% confidence interval: 0.38-0.72), indicating that low expression of XBP1 is associated with higher chance of biochemical recurrence in patients diagnosed with primary prostate cancer (**Fig. 1A**; **Table 1**). The relationship between XBP1 expression and clinicopathological parameters for each cohort is summarized in Supplementary Table S1. Low XBP1 expression is associated with higher Gleason score, tumor stage and presence of lymph node metastasis in the TCGA cohort, while none of the clinical parameters reached significance in the other smaller cohorts.

As microarray probes do not distinguish between XBP1u and XBP1s, we further explored the RNA-sequencing data from the TCGA cohort. XBP1s expression was quantified by measuring the number of reads spanning the 26 bp-long spliced region. Patients with low-XBP1s-expressing tumors have similar biochemical progression-free survival compared to patients with high-XBP1s-expressing tumors (P = 0.476, logrank test; Supplementary Fig. S1A). Also, none of the clinical parameters were associated with XBP1s transcript levels (Supplementary Table S2).

Table 1: Results of Cox regression model.

Dataset	Accession number	Patients (*N*)	Events (*n*)	Coefficient	HR	SE	z	95% CI	*P*-value
Taylor	GSE21034	131	27	-0.79	0.45	0.40	-1.97	0.21-1.00	0.05
TCGA[20]	–	424	83	-0.53	0.59	0.23	-2.34	0.38-0.92	0.02
Gulzar	GSE40272	82	19	-1.46	0.23	0.56	-2.59	0.08-0.70	0.00
Glinsky[21]	–	80	38	-0.59	0.55	0.33	-1.79	0.29-1.06	0.07
Boormans	GSE41408	48	28	-0.34	0.71	0.38	-0.89	0.34-1.51	0.37

NOTE: Coefficient, Cox regression coefficient; HR, hazard ratio [exp(coef)]; SE, standard error; z, Wald statistic value; 95% CI, 95% confidence interval.

As the 9-gene signature is based on differential AR chromatin binding between primary prostate tumors and tumors with an acquired resistance to hormone therapy, we examined the expression of the nine genes in tumors from seven patients with locally-advanced/metastatic prostate cancer before androgen deprivation therapy (ADT) and ~22 weeks after therapy initiation[22]. The clustering of the pre- and post-therapy samples by gene expression is displayed in a PCA biplot, showing that DNER and XBP1 expression are the two major contributors to the variance between pre- and post-therapy samples (**Fig. 1B**). Expression of XBP1 is downregulated following ADT (Supplementary Fig. S1B), which is in concordance with a recently reported neoadjuvant ADT study[23]. To study XBP1s in a neoadjuvant setting, we analyzed the expression of XBP1 by qPCR in 29 paired pre-treatment core needle biopsy samples and post-treatment surgical resection samples from patients who received 3 months neoadjuvant enzalutamide (DARANA, NCT03297385). In this series, we confirmed the marked downregulation of XBP1 in post-treatment samples compared to matched pre-treatment biopsies (**Fig. 1C**). Interestingly, XBP1s mRNA levels were significantly increased upon 3 months of enzalutamide treatment (**Fig. 1C**). A similar trend was observed in ADT-treated patients as well (Supplementary Fig. S1B), but did not reach statistical significance possibly due to the small sample size (n = 7).

Cumulatively, we found that XBP1 is decreased after hormonal therapy and low levels are associated with biochemical progression, while no prognostic value of XBP1s was observed.

XBP1 splicing is mediated by androgen receptor signaling

Analyzing XBP1 transcript levels in clinical samples illustrated that XBP1 was altered upon androgen-targeted therapy. We therefore wondered whether XBP1 is a direct androgen-responsive gene. To assess this, hormone-deprived LNCaP cells were exposed to synthetic androgen R1881 for 8, 16 or 24 hours, after which RNA was isolated (**Fig. 2A**). Total XBP1 mRNA levels were slightly increased in a time-dependent manner, whereas the XBP1 spliced mRNA was significantly increased (**Fig. 2A**). As splicing of XBP1 is known to be mediated by the endoribonuclease ERN1[7,8], we also examined ERN1 expression. Upon exposure to R1881, transcript levels of ERN1 were elevated over time (**Fig. 2A**), concordant with a previous study[1]. Expression and splicing of XBP1 was further confirmed in RNA-seq samples from LNCaP cells stimulated for 24 hours with R1881 or 3 hours with the ER stress inducer thapsigargin (Tg). The read count in exons and the splice junction reads were determined and plotted in **Figure 2B**. Expression of XBP1 was increased upon R1881 or Tg exposure, and splicing was clearly stronger induced (**Fig. 2B**). In addition, R1881-induced expression and splicing of XBP1 was validated in VCaP cells (Supplementary Fig. S2A).

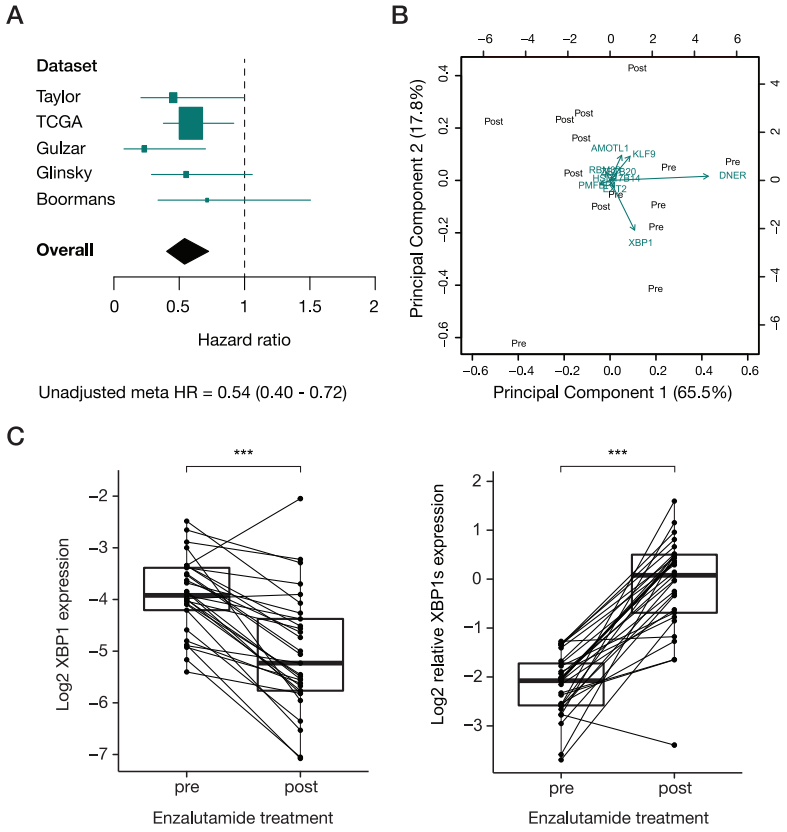

Figure 1: XBP1 expression is correlated with disease progression and response to hormone therapy. (**A**) Prognostic value of XBP1 expression represented by forest plot. The squares represent the hazard ratios of the individual studies and the horizontal lines the 95% confidence interval. The size of the squares is proportional to the number of patients in each study. The black diamond represents the overall hazard ratio. (**B**) Biplot of principal component analysis of the expression of the 9 genes (*AMOTL1*, *DNER*, *EXT2*, *HSD17B14*, *KLF9*, *PMFBP1*, *RBM33*, *XBP1* and *ZBTB20*) in tumors from patients before (pre) and after (post) androgen deprivation therapy (GSE48403). The arrows depict the contribution of each gene to the variance of the data. (**C**) Relative XBP1 and XBP1s expression in paired samples from pre- and post-enzalutamide treated patients (n = 29, DARANA[24]). ***, $P < 0.001$ (paired t test).

To assess the role of AR in the transcription regulation of both ERN1 and XBP1 as well as the subsequent splicing of XBP1, we knocked down AR expression. Quantification analyses showed that AR expression levels were reduced by ~30-40% (**Fig. 2C**). Knockdown of AR abrogates androgen-induced ERN1 and XBP1s expression. In contrast, the levels of total XBP1 mRNA were only slightly affected upon AR knockdown followed by short-term R1881 stimulation. Consistent with the mRNA data, Western blot analysis showed that AR knockdown prevented R1881-mediated increase of ERN1

and XBP1s protein levels (**Fig. 2D**; Supplementary Fig. S2C), while XBP1u protein levels remain relatively unaffected (Supplementary Fig. S2C). In addition, we observed AR-binding events in the first intron of *ERN1* and in the region upstream of the *XBP1* gene (Supplementary Fig. 2SB).

In conclusion, these results indicate that AR drives the expression of *XBP1* and *ERN1* and consequent splicing of XBP1.

R1881- and Tg-induced XBP1s chromatin binding at genes involved in the unfolded protein response

To identify the biological role of XBP1s in prostate cancer cells, we performed ChIP-seq for XBP1s in hormone-deprived LNCaP cells treated with either vehicle or R1881 for 24 hours. XBP1s ChIP-seq was also carried out under ER stress conditions (3 hours of Tg stimulation), boosting XBP1s protein levels (Supplementary Fig. S3A). Two independent XBP1s ChIP-seq replicates were generated, which were highly correlated (Supplementary Fig. S3B and S3C). To rule out aspecific ChIP-seq signal coming from the XBP1s antibody, ERN1 knockout LNCaP cells were used as a negative control, as these cells do express XBP1 but are unable to splice the protein (Supplementary Fig. S4A and S4B). No XBP1s ChIP-seq signal was observed in ERN1 knockout LNCaP cells (Supplementary Fig. S4C and S4D), confirming the specificity of the used XBP1s antibody in the ChIP experiments.

As exemplified at five genomic loci, XBP1s chromatin binding was induced upon R1881 and Tg exposure (**Fig. 3A**). Overexpression of XBP1s resulted in induced expression of these XBP1s-bound genes (Supplementary Fig. S5A). Besides induced peak intensity also the number of XBP1s peaks increased from 702 in vehicle-treated cells to 3,228 and 15,030 peaks in R1881 and Tg conditions, respectively (**Fig. 3B**). The induced binding of XBP1s upon R1881 and Tg stimulation is likely to reflect the abundance of XBP1s protein (Supplementary Fig. S3A; Supplementary Fig. S4B).

Next, we divided the XBP1s binding sites in those present in all conditions (shared) and those that are either R1881-induced or Tg-gained. The shared sites displayed the strongest XBP1s binding as compared to R1881- and Tg-induced peaks (**Fig. 3C and 3D**; Supplementary Fig. S5B). In addition, the shared XBP1s peaks show enrichment at promoters, marked with strong H3K4me3 and H3K27ac signal, and absence of AR binding (**Fig. 3C, 3E and 3F**). Conversely, R1881-induced sites are enriched at intronic and distal intergenic regions, with strong signal of AR binding (**Fig. 3C, 3E and 3F**). In line with these results, nuclear hormone receptor family motifs are enriched in this cluster (**Fig. 3G**). As expected for XBP1s ChIP-seq, we found significant enrichment

of the XBP1 motif consisting of an ACGT sequence in all clusters (**Fig. 3G**). Using the ReMap annotation tool containing a collection of various published ChIP-seq data sets[25], we found a number of transcription factors whose binding sites overlapped with XBP1s, including other bZIP transcription factors (e.g., FOS, JUN, CREB3), AR and FOXA1 (Supplementary Fig. S6A and S6B).

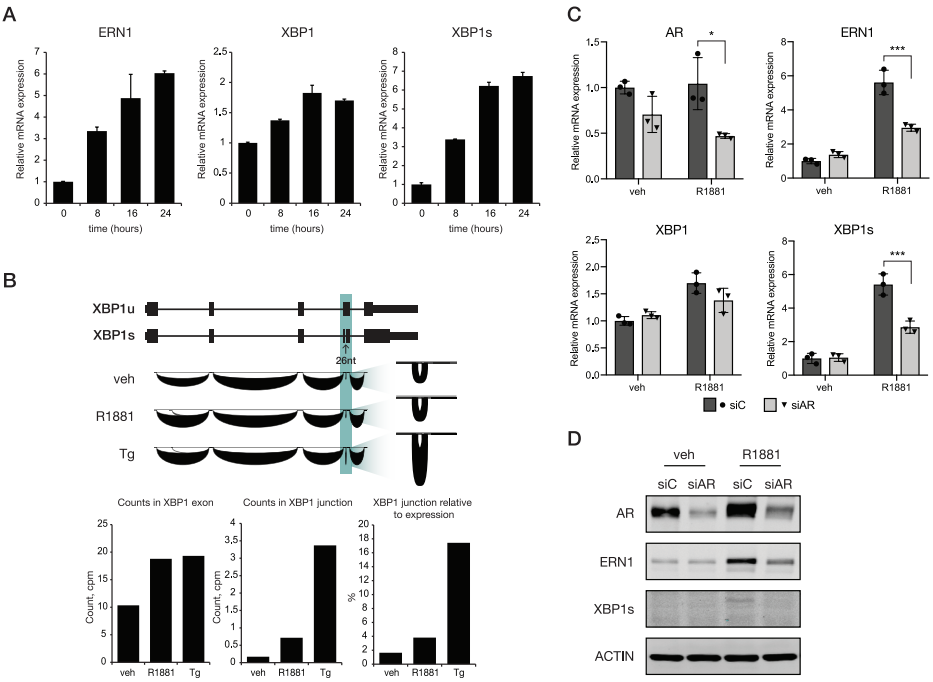

Figure 2: AR signaling triggers splicing of XBP1. (**A**) Relative mRNA expression levels of ERN1, XBP1 and XBP1s at 0, 8, 16 and 24 hours after R1881 stimulation. Shown is a representative experiment of two independent biological replicates. Error bars indicate standard deviation. (**B**) Splice junction tracks. Top: Exon-intron structure of XBP1u and XBP1s is shown. The arcs indicate splice junction reads and the height of the arc is proportional to the read counts in that area. The splicing region of the 26-nucleotide (nt; shaded area) is enlarged. Bottom: Quantification of XBP1 splicing in RNA-seq data from LNCaP cells treated with vehicle (veh), R1881 (24 hours) or Thapsigargin (Tg; 3 hours). Y-axis indicates counts per million (cpm), and the average of two biological replicates is shown. (**C**) Relative mRNA expression levels of AR, ERN1, XBP1 and XBP1s in LNCaP cells transfected with siControl (siC) or siAR and treated for 24 hours with either vehicle or R1881. Shown are individual datapoints and mean of three independent biological replicates. Error bars indicate standard deviation. *, $P < 0.05$; ***, $P < 0.001$ (2way ANOVA followed by Tukey multiple comparisons test). (**D**) Western blot showing AR, ERN1 and XBP1s expression in LNCaP cells transfected with siControl (siC) or siAR. Cells were vehicle- or R1881-treated for 24 hours. ACTIN was used as a loading control. A representative of three biological replicates is shown.

To identify XBP1s target genes, we scanned for genes with proximal XBP1s binding in a window of 20-kb upstream or within their gene body. Using ingenuity pathway analysis, we found that XBP1s target genes were enriched for genes involved in the unfolded protein response, eIF2 signaling and protein ubiquitination with no apparent differences between the subclusters (**Fig. 3H**).

Taken together, these analyses revealed that XBP1s binds the chromatin largely at promoters in hormone-deprived conditions, while AR stimulation induces XBP1s binding at enhancers that are co-occupied by AR.

Figure 3: XBP1s chromatin binding in LNCaP cells. (**A**) Snapshots of XBP1s chromatin binding at five example loci for vehicle (red), R1881 (24 hours; green) and Tg (3 hours; blue) conditions. Genomic coordinates are indicated. (**B**) Venn diagram showing overlapping XBP1s binding sites for indicated treatments. (**C**) Heatmap visualizing ChIP-seq signal [fragments per kilobase pair per million reads (FPKM)] in vehicle, R1881 and Tg conditions for XBP1s as well as AR, H3K4me3 and H3K27ac ChIP-seq signal from publicly available datasets. Data are centered at XBP1s peaks, depicting a 5-kb window around the peak. Subclassification of the binding events represent XBP1s sites shared among all conditions (shared, 590 binding sites), R1881-induced (298 + 2,313 binding sites) and Tg-gained (12,064 binding sites). (**D**) Average XBP1s signal (in FPKM) at either shared, R1881-induced or Tg-gained regions. Data are centered at XBP1s peaks, depicting a 2.5-kb window around the peak center. Vehicle-stimulated samples are shown in red, R1881-stimulated samples in green and Tg-stimulated samples in blue. (**E**) Average signal (in FPKM) for AR, H3K4me3 and H3K27ac at the three XBP1s binding site clusters defined in (C); shared, R1881-induced and Tg-gained. (**F**) Genomic distribution of XBP1s binding at shared, R1881-induced and Tg-gained regions across genomic features. (**G**) Enrichment of motifs at shared, R1881-induced and Tg-gained XBP1s binding sites. The font size represents the z-score and colors correspond to transcription factor families. (**H**) Top canonical pathways and top upstream regulators based on ingenuity pathway analysis of genes with proximal XBP1s binding. ►

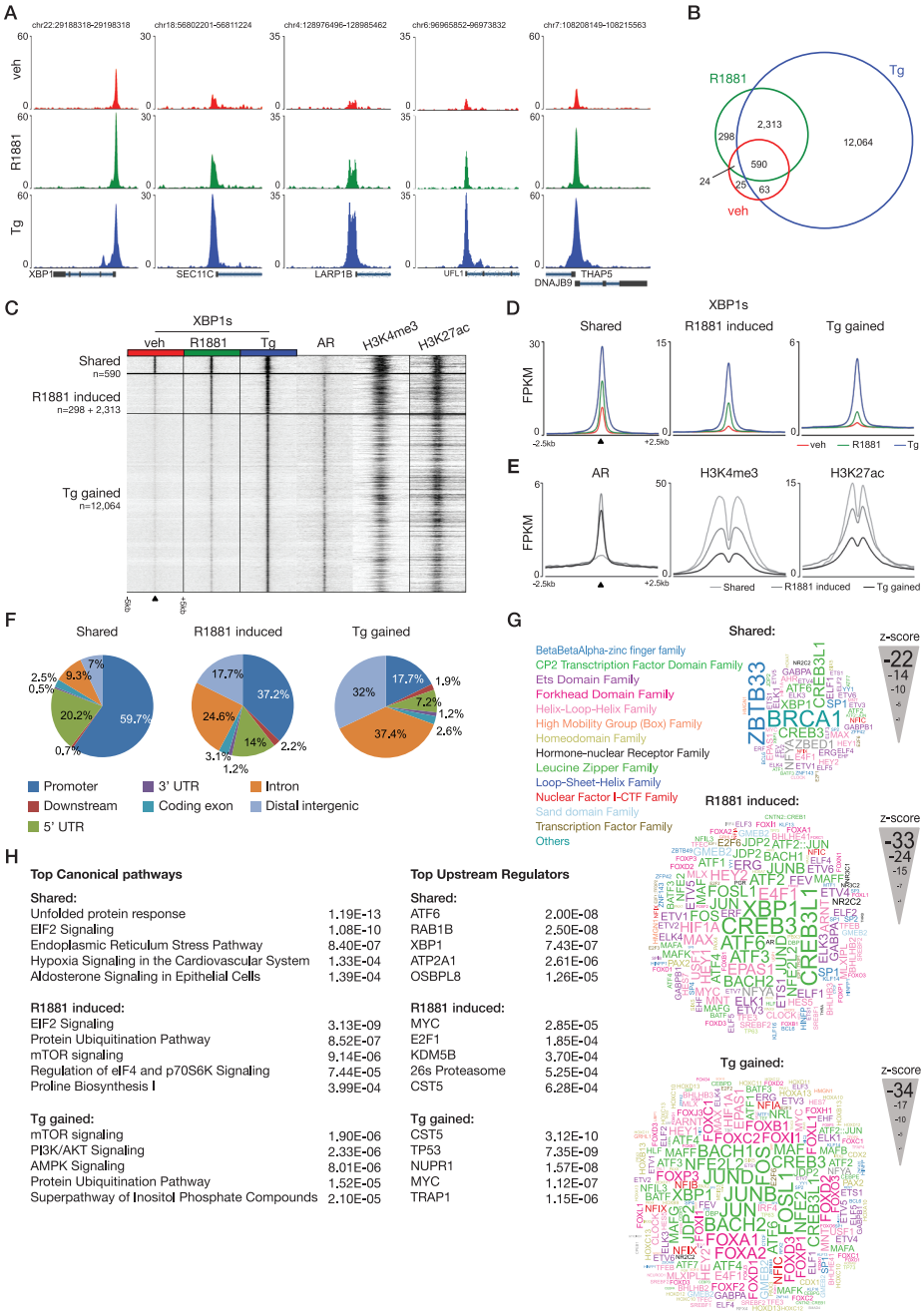

H

Top Canonical pathways

Shared:	
Unfolded protein response	1.19E-13
EIF2 Signaling	1.08E-10
Endoplasmic Reticulum Stress Pathway	8.40E-07
Hypoxia Signaling in the Cardiovascular System	1.33E-04
Aldosterone Signaling in Epithelial Cells	1.39E-04
R1881 induced:	
EIF2 Signaling	3.13E-09
Protein Ubiquitination Pathway	8.52E-07
mTOR signaling	9.14E-06
Regulation of eIF4 and p70S6K Signaling	7.44E-05
Proline Biosynthesis I	3.99E-04
Tg gained:	
mTOR signaling	1.90E-06
PI3K/AKT Signaling	2.33E-06
AMPK Signaling	8.01E-06
Protein Ubiquitination Pathway	1.52E-05
Superpathway of Inositol Phosphate Compounds	2.10E-05

Top Upstream Regulators

Shared:	
ATF6	2.00E-08
RAB1B	2.50E-08
XBP1	7.43E-07
ATP2A1	2.61E-06
OSBPL8	1.26E-05
R1881 induced:	
MYC	2.85E-05
E2F1	1.85E-04
KDM5B	3.70E-04
26s Proteasome	5.25E-04
CST5	6.28E-04
Tg gained:	
CST5	3.12E-10
TP53	7.35E-09
NUPR1	1.57E-08
MYC	1.12E-07
TRAP1	1.15E-06

Downregulation of androgen response genes and UPR genes upon knockdown of XBP1

By exploring gene expression of vehicle- and R1881- treated LNCaP cells, we identified 934 differentially expressed genes upon 24 hours R1881 stimulation ($P < 0.05$ and absolute $\log_2$ fold change > 2.0), including the *ERN1* gene among others. Gene set enrichment analysis demonstrated positive enrichment for genes involved in the unfolded protein response (UPR) as well as (as expected) AR target genes (**Fig. 4A**; Supplementary Fig. S8A). While XBP1s overexpression leads to upregulation of XBP1s target genes, no such effect can be observed when overexpressing the unspliced protein (Supplementary Fig. S5A; Supplementary Fig. S7A and S7B). AR target genes, however, remain unaffected when overexpressing either of the XBP1 variants (Supplementary Fig. S7A and S7B). Conversely, knockdown of XBP1 resulted in significant downregulation of AR target genes and unfolded protein response genes (**Fig. 4B**; Supplementary Fig. S8B and S8C). These results were successfully validated in an independent RNA-seq dataset[19] of LNCaP cells with siRNA-mediated XBP1 silencing (Supplementary Fig. S9A), as well as in LNCaP cells after treatment with an RNase-specific ERN1 inhibitor (**Fig. 4C**). In addition, upstream regulator analysis of the differentially expressed genes upon XBP1 knockdown revealed AR, dihydrotestosterone, ERN1 and XBP1 to be involved in transcriptional regulation of these genes (Supplementary Fig. S9B).

In conclusion, AR induces the expression of many genes including ERN1 and XBP1, enhancing XBP1s activity (**Fig. 5**). Subsequently, these events drive expression of a subset of canonical AR-responsive genes along with activation of the unfolded protein response in prostate cancer cells (**Fig. 5**).

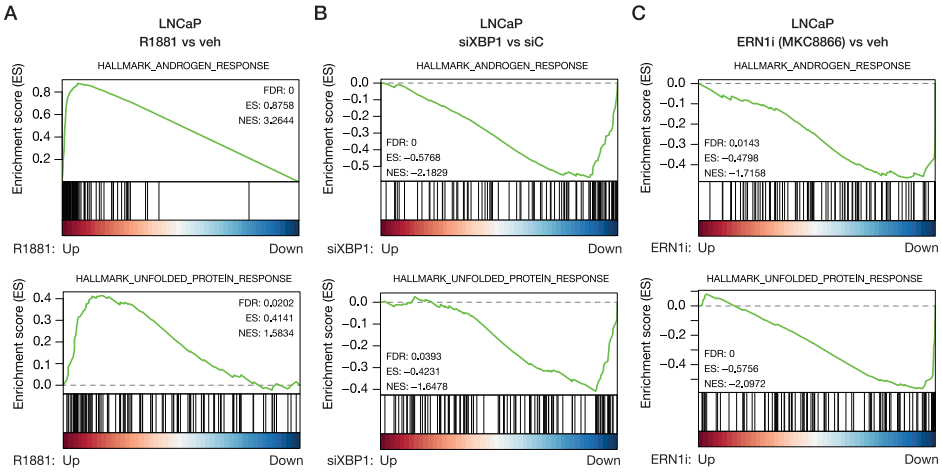

Figure 4: AR-XBP1 transcriptional regulation of androgen response and unfolded protein response genes. (**A**) GSEA on RNA-seq data from LNCaP cells treated with vehicle or R1881 for 24 hours. Shown are enrichment plots of the Hallmark pathways androgen response (top) and unfolded protein response (bottom). Genes are ranked by differential expression between treatment conditions. *Y*-axis indicates enrichment score (ES). GSEA statistics (FDR, ES, NES) are shown. (**B**) Same as (A) but depicting RNA-seq data from LNCaP cells upon XBP1 knockdown. Cells were either transfected with siXBP1 or siControl (siC). (**C**) Same as (A) but depicting RNA-seq data from LNCaP cells treated with the ERN1 inhibitor (ERN1i) MKC8866 or vehicle for 24 hours.

Discussion

Accumulating evidence has demonstrated that ER stress plays a crucial role in tumor growth and survival[26]. XBP1, a key transcription factor of the ER stress response, is often overexpressed in cancer and correlates with clinical outcome, as was previously reported for oral squamous cell carcinoma and hepatocellular carcinoma[27,28]. Here, we report that in five independent cohorts, high XBP1 expression associates with better biochemical recurrence outcome in patients with prostate cancer. Even though these data suggest a connection between ER stress and clinical outcome, the spliced form is the accurate biomarker for activated ER stress. Furthermore, since the unspliced form negatively regulates XBP1s[29], biological interpretation of the clinical data is challenging. As the spliced mRNA showed no association with biochemical recurrence in the RNA-seq cohort (TCGA), these data suggest that XBP1 isoforms are differently associated with recurrence. Future studies should be aimed to further elucidate the clinical implications of both XBP1 isoforms. Further, as biochemical recurrence is a poor indicator of survival outcome, the potential impact of both XBP1 variants on disease-specific survival as a stronger clinical endpoint should be tested.

Previously, we reported that XBP1 mRNA levels are markedly increased in primary prostate cancer as compared to benign tissues and metastasis[15]. The variable expression level of XBP1 at the different stages of the disease as well as decreased XBP1 upon hormone therapy[23] (**Fig. 1C**) may be AR signaling-dependent, as XBP1 is transcriptionally regulated by AR[1] (**Fig. 2**). In concordance, Sowalsky and colleagues showed a positive correlation between AR activity score and XBP1 expression[23]. Also, in our cohort of prostate cancer patients receiving neoadjuvant enzalutamide therapy as well as in an additional publicly available cohort, receiving ADT[22], XBP1 expression levels were decreased, further confirming the transcriptional dependency of XBP1 on AR action. As XBP1s levels were increased after neoadjuvant enzalutamide, cells may experience stress following AR inhibition, with a consequent induction of the UPR pathway. Further research should be aimed to investigate the physiological consequences of XBP1s induction after enzalutamide treatment, along with the potential clinical implications thereof.

Here we show, in agreement with previously published data, that both ERN1 as well as XBP1 are under direct transcriptional control of AR[1], and that ERN1 is critically involved in the splicing of XBP1, yielding increased XBP1s levels (**Fig. 2**). Interestingly, even though we observed AR binding proximal to the XBP1 locus in primary prostate cancers[15], XBP1s protein expression is primarily regulated at the

level of splicing through AR-induced ERN1. As AR activation led to increased XBP1 splicing – a biomarker for UPR signaling – future research should address whether misfolded proteins do indeed accumulate in AR-stimulated prostate cancer cells.

Besides increased expression of AR target genes upon androgen stimulation, androgens also regulate the expression of ER stress-associated genes (**Fig. 4**)[1,30]. Most likely, XBP1s controls the expression of these genes, as XBP1s primarily binds at promoters of UPR genes leading to increased expression of these genes as shown by overexpression of XBP1s. In the absence of hormones, XBP1s binds the chromatin largely at promoters. In contrast, upon UPR induction through physiological (R1881) or supraphysiological (Tg) cues the majority of XBP1s is bound to distal regulatory elements. This phenomenon is also observed upon liver damage (stress), where XBP1s occupies mostly promoters in sham-operated mice livers, while partial hepatectomy resulted in XBP1s binding mainly at distal elements[13]. At XBP1s binding sites, DNA binding motifs of the bZIP transcription factor family were enriched as well as many other transcription factor family motifs, suggesting that XBP1 cooperates with other transcription factors. In accordance with this, we found genomic overlap between AR and XBP1 binding sites, and permuting these signaling cascades in prostate cancer cells illustrated enrichment of the same gene sets, involved in AR signaling and UPR pathways (**Fig. 5**). AR stimulation resulted in the upregulation of androgen- as well as UPR-response pathways, while XBP1 knockdown showed, in effect, the exact opposite phenotype. As XBP1 acts downstream of AR, the XBP1 signaling cascade may provide a possible feedback mechanism to refine the activity for part of the canonical AR-responsive gene repertoire. However, XBP1 overexpression alone did not lead to upregulation of AR-target genes, suggesting that XBP1's supportive role at these sites remains dependent on AR activation. In addition, while most of our results point toward a functional role of XBP1s in AR biology, we cannot rule out potential involvement of the unspliced XBP1 isoform at this stage. Future studies should be undertaken to fully elucidate the relative contribution of each XBP1 variant in this process.

Taken together, we present a multi-step mechanism of gene regulation, in which androgen-induced expression of ERN1 enhances XBP1 splicing and transcriptional activity. This signaling cascade may prepare the cells for the increased translation, protein (mis)folding and mRNA decay that accompanies AR-regulated tumor cell proliferation.

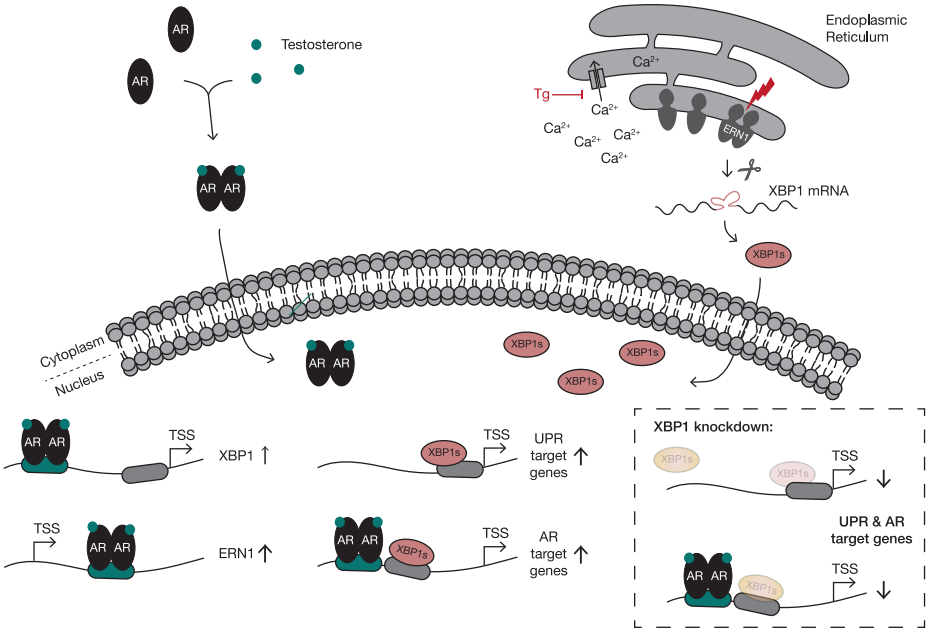

Figure 5: Androgen-induced modulation of AR and XBP1s transcriptional activity. Testosterone binds to the androgen receptor (AR). Upon binding, AR dimerizes and translocates to the nucleus where it binds the chromatin, mainly at androgen response elements (AREs, turquoise). AR binds an enhancer proximal to *XBP1* and an intron of the *ERN1* gene, ultimately leading to increased expression of XBP1 and ERN1. The AR-induced expression of ERN1, induces splicing of XBP1 (XBP1s). This subsequently leads to transcription of genes involved in, among others, the unfolded protein response (UPR) and canonical androgen response. Conversely, knockdown of XBP1 results in downregulation of UPR, but also androgen-responsive genes, showing that XBP1 is functionally supporting part of the AR transcriptional program.

Methods

Survival analysis

Gene expression as well as clinical data of five cohorts[20,21,31-33] were used. Expression data from Boormans et al., Gulzar et al. and Taylor et al. were downloaded from the Gene Expression Omnibus (GEO) database (https://www.ncbi.nlm.nih.gov/geo/; accession numbers are listed in Table 1). Clinical data from Boormans et al. was received directly from the authors, while the Gulzar and Taylor datasets were obtained from the respective publication (Gulzar, et al. 2013; Taylor, et al. 2010). Expression and clinical data from Glinsky et al. were received directly from the authors, while the TCGA data was downloaded using the UCSC Xena browser (https://xenabrowser.net). Samples were categorized in either high or low XBP1 expression using the median expression. Prognostic value of XBP1 expression was assessed using hazard ratios with confidence intervals of 95%, following the Cox's proportional hazard model (R package survival; https://cran.r-project.org/package=survival). Meta-analysis was performed using the R package rmeta (https://cran.r-project.org/package=rmeta). Hazard ratios were combined using the fixed effect model. Statistical relation between XBP1 expression and clinicopathological parameters, including Gleason Score, T-Stage, presence of lymph node metastasis and PSA level was tested using Pearson's C^2 test. For XBP1 splicing quantification, BAM files containing the XBP1 region were downloaded from the Genomics Data Commons (GDC) portal (https://portal.gdc.cancer.gov). Reads were converted to fastq format and aligned with hisat2 (version 2.0.4) using a bed file containing all splice variants of XBP1. The number of reads uniquely mapped to the complete gene region as well as only counts related to exon 4 were determined using Icount. Reads that exactly jumped from base position 1569 to 1595 within the XBP1 gene on chromosome 22 were determined using samtools. The number of reads were divided by the total number of reads per sample and XBP1s-specific reads were normalized to total XBP1 reads, providing relative XBP1s expression values.

DARANA patient samples

Pre- and post-enzalutamide treatment prostate cancer tissue of trial cases was acquired from the DARANA study[24] (Dynamics of androgen receptor genomics and transcriptomics after neoadjuvant androgen ablation; ClinicalTrials.gov NCT03297385). Patient characteristics prior to treatment are summarized in Supplementary Table S3. All trial patients received three months of neoadjuvant enzalutamide prior to radical prostatectomy. The study was approved by the IRB of the Netherlands Cancer Institute, informed consent was signed by all participants who entered the study and all research was performed in accordance with relevant guidelines and regulations. Biopsy (pre-treatment samples) and prostatectomy specimens (post-treatment samples) were

formalin-fixed and paraffin-embedded (FFPE). FFPE material was sectioned prior to RNA isolation (see below) and sections were pathologically assessed for tumor cell percentage. Only samples with a tumor cell percentage of ≥ 50% were used for further downstream analyses.

Cell culture

VCaP and LAPC4 cells were a kind gift from Dr. Wytske M. van Weerden (Erasmus MC) and Dr. Michiel van der Heijden (Netherlands Cancer Institute), respectively. Human prostate cancer cell lines were cultured in RPMI-1640 medium (LNCaP, VCaP) or IMDM medium (LAPC4) supplemented with 10% FBS. All cell lines were authenticated by STR profiling (BaseClear, Leiden, The Netherlands). In addition, cell lines were stocked at early passages and used at < 20-25 subcultures. For hormone deprivation, cells were cultured in medium containing 10% charcoal-treated FBS for three days, subsequently treated with 10 nM R1881 (synthetic androgen, PerkinElmer) or vehicle (DMSO) and harvested at the indicated time points. For Thapsigargin (Tg, Sigma) stimulations, cells were treated with 10 nM Tg for 3 hours. For ERN1 inhibitor (MKC8866, Mechem Express) treatment, cells were hormone-deprived as described above and subsequently treated with 10 nM R1881 supplemented with either vehicle (DMSO) or 10 μM ERN1 inhibitor for 24 hours.

Generation of ERN1 knockout cells with CRISPR-Cas9

Guide RNA targeting human ERN1 (TCGGGTTTTGGTGTCGTACA) was cloned into the PX330 CRISPR-Cas9 plasmid[34]. LNCaP cells were transiently transfected using Lipofectamine 2000 transfection reagent (Invitrogen) according to the manufacturer's instructions. After transfection, cells were selected using puromycin (0.5 ng/mL), single clones were picked and analyzed by TIDE (Tracking of Indels by Decomposition)[35] and Western blot. Finally, the clone with the best editing efficiency was selected.

Transient transfections

Lipofectamine 2000 was used for all transient transfections in LNCaP and LAPC4 cells. siRNA oligos targeting the Androgen Receptor (MU-003400-02), XBP1 (MU-009552-02), and the non-targeting control (D-001206-14) were purchased from Dharmacon. GFP and XBP1s expression plasmids were kindly provided by Dr. Sjaak Neefjes (Leiden University Medical Center) and Dr. Laurie H. Glimcher (Dana-Farber Cancer Institute), respectively. XBP1u containing expression plasmid was obtained from the CCSB-Broad Lentiviral Expression Library (https://horizondiscovery.com/en/products/gene-modulation/overexpression-reagents/orfs/pifs/CCSB-Broad-Lentiviral-Expression-Collection). In hormone deprivation experiments, 24 hours after switching to charcoal-treated FBS, cells were transfected and further hormone-deprived for additional 48-72 hours.

RNA isolation and mRNA expression analysis

Total RNA from cell lines was isolated with TRIzol according to the manufacturer's protocol (Invitrogen). RNA from FFPE material was isolated from 2-10 sections of 10 mm using the AllPrep DNA/RNA FFPE kit (Qiagen). cDNA was synthesized from ~2 mg (cell line) or 250 ng (FFPE samples) RNA using SuperScript III Reverse Transcriptase (Invitrogen) with random hexamer primers. qPCR was performed with SensiMix™ SYBR® No-ROX Kit (GC Biotech). Relative mRNA expression levels were normalized to TBP (cell lines) or to the average gene expression of the three housekeeping genes b-ACTIN, TBP and GAPDH (FFPE samples). Primer sequences are listed in Supplementary Table S4.

For RNA-seq, strand-specific libraries were generated with the TruSeq Stranded mRNA sample preparation kit (Illumina, Part # 15031047 Rev. E) and sequenced on a HiSeq2500. Sequencing data was aligned to hg38 using TopHat and number of reads per gene were measured with HTSeq count. Standard output of the Tophat was used to get the number of reads that span the 26-nt splice junction in exon 4 of XBP1. EdgeR-Limma workflow was used for gene expression analysis[36,37]. Genes with > 1 count per million in at least two samples were included. Gene set enrichment analysis (GSEA) was performed with the GSEA software (http://www.broad.mit.edu/gsea/index.jsp) using the MSigDB Hallmarks gene set collection. Ingenuity Pathway Analysis (IPA) software was used to identify upstream regulators of the differentially expressed genes (cutoff: absolute $\log_2$ fold change > 0.5).

Chromatin immunoprecipitation

Chromatin immunoprecipitations (ChIP) were performed as previously described[38]. Nuclear lysates were incubated with 7.5 µg of XBP1s antibody (Biolegend, 619502) prebound to 75 µl protein A beads. Immunoprecipitated DNA was processed for library preparation (Part# 0801-0303, KAPA biosystems kit). Samples were sequenced using an Illumina Hiseq2500 genome analyzer (65-bp reads, single end), and aligned to the Human Reference Genome (hg19, February 2009). Reads were filtered based on MAPQ quality (quality ≥ 20) and duplicate reads were removed. Peak calling over input control (input samples from publicly available datasets were merged and downsampled[38]) was performed using Dfilter and MACS peak callers[39,40]. MACS was run with the default parameters and $P = 10^{-5}$. DFilter was run with bs = 50, ks = 30, refine, nonzero. The peaks shared by both peak callers and both replicates were used for downstream analysis. Read counts and the number of aligned reads are shown in Supplementary Table S5. Genome browser snapshots, heatmaps and density plots were generated using EaSeq[41]. Genomic region enrichment analysis and motif analysis were performed with CEAS[42] and the SeqPos motif tool (http://cistrome.org/ap/), respectively. The Diffbind R package

was used to generate the correlation heatmap and PCA plot based on occupancy[43]. All ChIP-seq data generated in this study are deposited in the GEO database under the accession GSE121880. Publicly available AR (GSE94682), H3K4me3 (GSM503907) and H3K27ac (GSM686937) ChIP-seq data from LNCaP cells were used.

For ChIP-seq validations, qPCR analyses were performed using SensiMix™ SYBR® No-ROX Kit (GC Biotech). ChIP-qPCR enrichment was normalized to a negative control region. Primer sequences are listed in Supplementary Table S1.

Western blotting

Cells were lysed in Laemmli buffer supplemented with complete protease inhibitor cocktail. After protein separation via SDS-PAGE and protein transfer, membranes were incubated with antibodies against AR (sc-816, Santa Cruz Biotechnology), ACTIN (MAB1501R, Millipore), ERN1 (14C10, Cell Signaling Technology), total XBP1 (GTX113295, GeneTex) or XBP1s (619502, Biolegend).

Statistical analyses

For statistical analyses of survival data, Cox regression models were used. To test statistical association of XBP1 expression with clinicopathological parameters, Pearson's C^2 test was used. XBP1(s) expression in pre- vs. post-treatment samples were compared using a paired *t* tests. For qPCR data, unpaired *t* tests were used to compare normalized gene expression levels upon XBP1u/XBP1s overexpression to control-transfected samples (GFP) and to compare R1881-stimulated or siXBP1-transfected cells to vehicle or siC control samples, respectively. 2way ANOVAs followed by Tukey multiple comparisons tests were used to compare siC to siAR upon vehicle (DMSO) or R1881 stimulation. For RNA-seq, XBP1 knockdown-efficiency upon siRNA treatment was tested using a paired *t* test. All error bars represent standard deviation.

Conflict of interest

L.F.A. Wessels reports grants from Genmab outside the submitted work. H. van der Poel reports grants from Astellas outside the submitted work. A.M. Bergman reports grants and personal fees from Astellas Pharma outside the submitted work. W. Zwart reports grants and personal fees from Astellas Pharma, and grants from AstraZeneca outside the submitted work. No disclosures were reported by the other authors.

Author contributions

S. Stelloo: Conceptualization, Methodology, Software, Validation, Formal analysis, Investigation, Writing - Original Draft, Writing - Review & Editing, Visualization, Project administration. S. Linder: Conceptualization, Methodology, Software, Validation, Formal analysis, Investigation, Writing - Original Draft, Writing - Review & Editing, Visualization. E. Nevedomskaya: Methodology, Software, Formal analysis, Investigation, Resources, Data Curation, Writing - Review & Editing. E. Valle-Encinas: Methodology, Validation, Formal analysis, Investigation, Writing - Review & Editing. I. de Rink: Methodology, Software, Validation, Writing - Review & Editing. L.F.A. Wessels: Writing - Review & Editing, Supervision. H. van der Poel: Conceptualization, Methodology, Validation, Formal analysis, Writing - Review & Editing. A.M. Bergman: Conceptualization, Writing - Original Draft, Writing - Review & Editing, Visualization, Supervision, Project administration, Funding acquisition. W. Zwart: Conceptualization, Writing - Original Draft, Writing - Review & Editing, Visualization, Supervision, Project administration, Funding acquisition.

Acknowledgments

This work was supported by Movember (NKI01 to A.M. Bergman and W. Zwart), KWF Dutch Cancer Society (10084 ALPE to A.M. Bergman and W. Zwart), KWF Dutch Cancer Society/Alpe d'HuZes Bas Mulder Award (NKI 2014-6711 to W. Zwart), Netherlands Organization for Scientific Research (NWO-VIDI-016.156.401 to W. Zwart). The authors would like to acknowledge the NKI-AVL Core Facility Molecular Pathology & Biobanking (CFMPB) for supplying NKI-AVL Biobank material and/or lab support; the NKI Genomics Core Facility for Illumina sequencing and bioinformatics support; and the NKI Research High Performance Computing (RHPC) facility for computational infrastructure. We also thank all Zwart/Bergman lab members for fruitful discussions and technical advice.

Supplementary tables

Supplementary Table S1: Relation of XBP1 mRNA expression with clinical pathological parameters.

	Taylor			TCGA			
	low XBP1	high XBP1	*P*-value	low XBP1	high XBP1	*P*-value	low XBP1
	N = 66	*N* = 65		*N* = 250	*N* = 248		*N* = 44
Gleason Score			0.13			1.9E-06	
<7	21	20		17	28		4
7	33	41		102	146		31
>7	11	4		131	74		8
NA	1	0		0	0		1
T Stage			0.10			0.00	
T1	0	0		0	0		0
T2	37	48		69	119		32
T3	25	15		171	122		10
T4	4	2		6	4		1
NA	0	0		4	3		1
Lymph node metastasis			0.21			0.02	
No	49	53		153	174		39
Yes	5	1		50	30		4
NA	12	11		47	44		1
PSA			0.56			0.84	
<4 ng/mL	10	12		10	9		7
4-10 ng/mL	42	36		23	36		27
>10 ng/mL	13	17		42	67		8
NA	1	0		175	136		2

Gulzar			**Glinsky**			**Boormans**	
high XBP1	*P*-value	low XBP1	high XBP1	*P*-value	low XBP1	high XBP1	*P*-value
N = 41		*N* = 40	*N* = 40		*N* = 24	*N* = 24	
	0.06			0.90			0.29
9		8	9		14	16	
30		23	21		4	6	
2		9	10		6	2	
0		0	0		0	0	
	0.62			0.97			0.75
0		17	18		0	0	
31		22	21		7	8	
9		1	1		11	10	
0		0	0		5	6	
1		0	0		1	0	
	0.40			0.24			0.12
39		37	40		20	24	
1		3	0		4	0	
1		0	0		0	0	
	0.05			0.97			0.95
10		3	3		0	0	
29		23	22		11	12	
1		14	15		13	12	
1		0	0		0	0	

Supplementary Table S2: Relation of XBP1s expression with clinical pathological parameters.

	TCGA		
	low XBP1s *N* = 202	high XBP1s *N* = 200	*P*-value
Gleason Score			0.3932
<7	22	14	
7	96	99	
>7	84	87	
T Stage			0.28
T2	85	2	
T3	108	70	
T4	4	123	
NA	5	2	
Lymph node metastasis			0.64
No	138	128	
Yes	31	34	
NA	33	38	
PSA			0.71
<4 ng/mL	6	8	
4-10 ng/mL	26	21	
>10 ng/mL	50	46	
NA	120	125	

Supplementary Table S3: Baseline characteristics of patients enrolled in the DARANA study (NCT03297385).

DARANA cohort	*N* = 29
Age	67 (57-74)
PSA before treatment (ng/mL)	12.7 (2.8-41.9)
Gleason score	
7	16
8	7
9	6
T stage (cT)	
2	15
3	13
4	1
Lymph node status (cN)	
N0	28
N1	1

NOTE: Pretreatment measures are based on the histologic evaluation of biopsy material (clinical grading; c).

Supplementary Table S4: Primer sequences.

Primer	Gene	Forward (FW) / Reverse (RV)	5′-3′ sequence
mRNA expression primer	TBP	FW	GTTCTGGGAAAATGGTGTGC
		RV	GCTGGAAAACCCAACTTCTG
	ACTIN	FW	CCTGGCACCCAGCACAAT
		RV	GGGCCGGACTCGTCATACT
	GAPDH	FW	ATTTGGCTACAGCAACAGGG
		RV	TCAAGGGGTCTACATGGCA
	ERN1	FW	ATTGTGTACCGGGGCATGTT
		RV	CTCACGGTCTGCGAAGCTAA
	AR	FW	AGAGTGCCCTATCCCAGTCC
		RV	CAGTCTCCAAACGCATGTCC
	XBP1	FW	GAAGCCAAGGGGAATGAAGT
		RV	GCTGGCAGGCTCTGGGGAAG
	XBP1s	FW	TGCTGAGTCCGCAGCAGGTG
		RV	GCTGGCAGGCTCTGGGGAAG
	SEC11C	FW	GCGCCAGCTCTATTACCAGG
		RV	CATACTGCCACTCAGCACCA
	LARP1B	FW	CAGTTACCAGCTTTGGCTGC
		RV	AGGGAACCGAATTCTGGCG
	UFL1	FW	TCAGTGCTATTACCCGGCCT
		RV	CCTCGTAAGCGTCCGCTATT
	DNAJB9	FW	TAGTCGGAGGGTGCAGGATA
		RV	CGCTCTGATGCCGATTTTGG
	KLK3	FW	CCAGAGGAGTTCTTGACCCC
		RV	TCCAGCACACAGCATGAACT
	FKBP5	FW	AATCAAGGAGCTCAATCTCAAAAA
		RV	TATGCATATGGCTCGGCTGG
	TMPRSS2	FW	TCACTAGGTCGTTGAAAGTCAGA
		RV	TGGAGCCGGATACCAAGTAGA

Supplementary Table S4: Continued.

Primer	Gene	Forward (FW) / Reverse (RV)	5′-3′ sequence
ChIP-qPCR primer	Negative control	FW	CTAGGAGGGTGGAGGTAGGG
		RV	GCCCCAAACAGGAGTAATGA
	XBP1	FW	TTTCTACGGTCGTGGCCCTC
		RV	ATAGCCACGGTCCTGAAACG
	SEC11C	FW	ACCGCAGTCCATCTTTAGGC
		RV	TAACTCCCGCTCGCAAATCA
	DNAJB9	FW	GGGAAGCGTTTCGTGTAGGT
		RV	CTGGCACGCACCCTAATCTC
	CDK12	FW	GGACCTGATCTCGCGTTGTT
		RV	TAGCCTCTCGCGATGTTTCG
	R1881-induced 1	FW	GGTGTGGACTTACCGGTGTC
		RV	CCAGACCTACCCTTCACGTC
	ZRANB2-AS2	FW	TACAGGTGGGAGGACCCAAG
		RV	TTGATCAGTCACTTCCGCCT
	SNHG21	FW	TAACGATTCCCGGCCCTTTC
		RV	CAGGAGAATCGCGTTGGACT
	TRIP11	FW	GGGTTACTCCTGCCAACTCG
		RV	GCGGCGCTTTTCTATGATCC
	PRKCA	FW	TTGTCCAATTCAGCCACCCA
		RV	CAAAGGACTTGCTTCCTGCG
	Tg-gained 1	FW	CCTGTTGAAAGAATGCGGGC
		RV	GAGTTGGGAGGGATACGTGG
	HSD17B7P2	FW	GAAGTGTGAGTGCGCGAAGA
		RV	CAACACAAAGGAGCCTCACC
	RGS5	FW	TTGTTGCCAGCAGGGGTTTA
		RV	TATGGGCTGGTTGCCATGAG

Supplementary Table S5: Illumina sequencing data for ChIP-seq, number of sequenced and aligned reads and number of peaks.

Sample ID	Cell line	Factor	Treat-ment	Read count	Mapped reads	% mapped	Called peaks
wz48	LNCaP	XBP1s	veh	25108190	23514954	0.94	777
wz649	LNCaP	XBP1s	R1881	24051811	22096708	0.92	4927
wz823	LNCaP	XBP1s	veh	26830309	21952913	0.82	253
wz824	LNCaP	XBP1s	R1881	27013874	23822232	0.88	5391
wz1409	LNCaP	XBP1s	veh	26231808	24994936	0.95	521
wz1410	LNCaP	XBP1s	Tg	32364586	30576237	0.94	20166
wz1411	LNCaP	XBP1s	veh	26597313	25099722	0.94	963
wz1412	LNCaP	XBP1s	Tg	28533362	27055246	0.95	18481
wz1935	LNCaP_PX330	XBP1s	Tg	19883805	19003282	0.96	13689
wz1936	LNCaP_ERN1_KO	XBP1s	Tg	37126963	35461666	0.96	6
wz1937	LNCaP_PX330	XBP1s	Tg	35670081	34144440	0.96	9157
wz1938	LNCaP_ERN1_KO	XBP1s	Tg	18464789	17600476	0.95	1

Supplementary figures

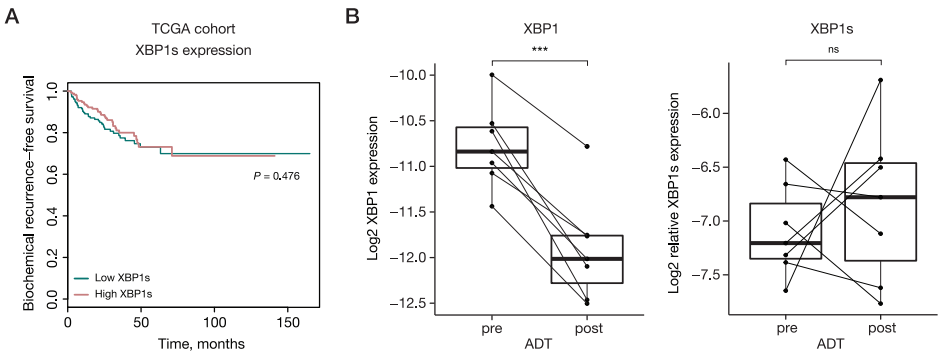

Supplementary Figure S1: XBP1s expression in clinical datasets. (**A**) XBP1s expression is not associated with biochemical recurrence-free survival in the TCGA cohort. Kaplan-Meier curve of biochemical recurrence-free survival between two groups is shown, where patient groups are separated on XBP1s expression using a median cut-off. (**B**) Log_2 XBP1 and relative XBP1s expression in samples from pre- and post-androgen deprivation therapy (ADT) treated patients (n = 7; GSE48403). The points indicate the samples and the lines connect the paired pre- and post-therapy samples. ns, $P > 0.05$; ***, $P < 0.001$ (paired t test).

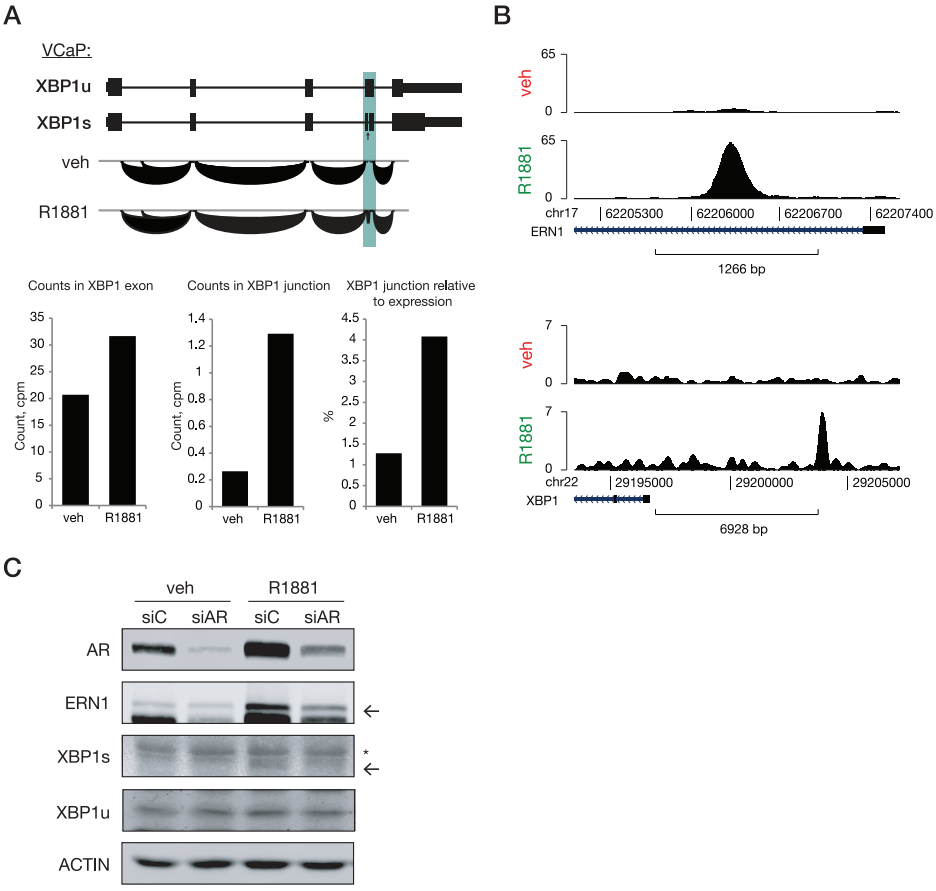

Supplementary Figure S2: R1881 induced XBP1 splicing in prostate cancer cells. (**A**) Hormone-deprived VCaP cells were stimulated with vehicle or 100 nM R1881 for 6 hours. RNA was isolated and sequenced. Splice junction tracks are shown (top). Exon-intron structure for XBP1u and XBP1s is given at the top. The arcs indicate splice junction reads and the height of the arc is proportional to the read counts in that area. The splicing region is highlighted. Quantification of XBP1 splicing (bottom; average of two biological replicates) is represented in the bar graphs. (**B**) Snapshots of AR chromatin binding in LNCaP cells at the *ERN1* and *XBP1* gene loci for vehicle and R1881 (4 hours) conditions (GSE94682). (**C**) Western blot analysis showing AR, ERN1, XBP1s and XBP1u expression in hormone-deprived LNCaP cells transfected with siControl (siC) or siAR. Cells were treated with vehicle (veh) or R1881 for 24 hours. ACTIN was used as a loading control, and a representative of three biological replicates is shown. The asterisk (*) indicates a non-specific band.

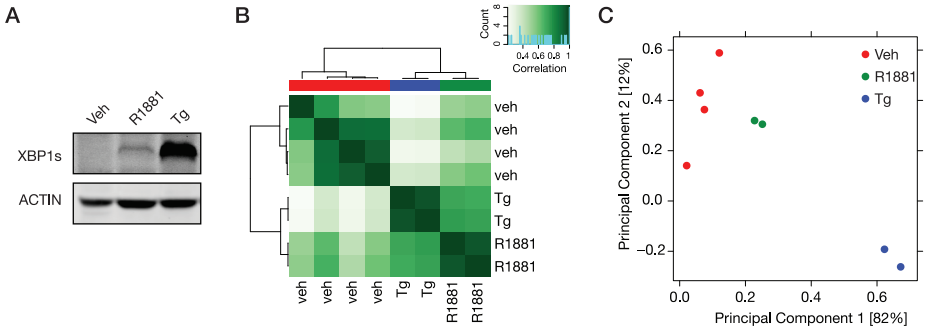

Supplementary Figure S3: XBP1s expression and ChIP-seq replicates. (**A**) Western blot analysis for XBP1s in hormone-deprived LNCaP cells treated with vehicle, R1881 (24 hours) or Tg (3 hours). ACTIN was used as a loading control, and a representative of three biological replicates is shown. (**B**) Unsupervised hierarchical clustering of the correlation between XBP1s peak occupancy in vehicle-, R1881- and Tg-treated LNCaP cells for both replicates. (**C**) Principal component analysis computed using the called XBP1s peaks across studied conditions and replicates.

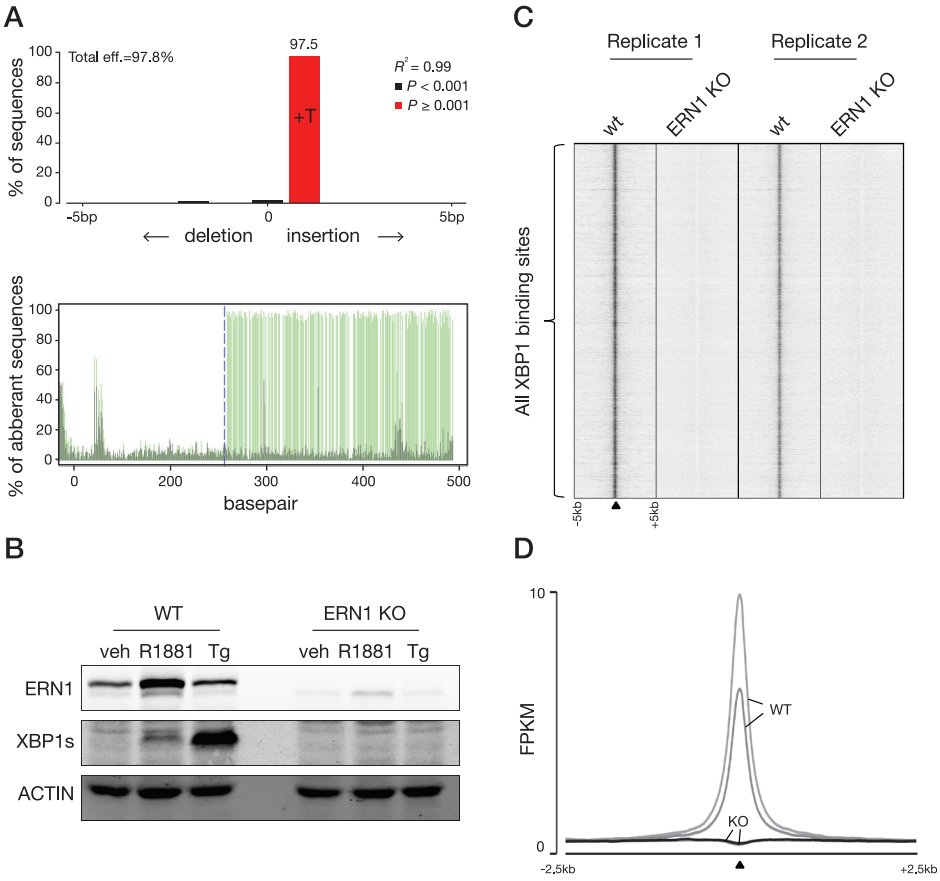

Supplementary Figure S4: XBP1s antibody specificity. (**A**) LNCaP cells were transfected with an empty PX330 CRISPR/Cas9 vector or with the PX330 sgRNA targeting *ERN1*. A single clone was made, and DNA was isolated, PCR-amplified and subjected to Sanger sequencing. Sequencing data was analyzed with TIDE (https://tide.nki.nl/). The indel spectrum around the PAM sequence for the ERN1 knockout (KO) clone used in this study is shown. (**B**) Western blot was performed with protein lysates from hormone-deprived wildtype LNCaP cells (WT) and ERN1 KO cells stimulated with either vehicle, R1881 (24 hours) or Tg (3 hours). Blots were stained for ERN1, XBP1s and ACTIN was used as loading control. (**C**) Heatmap visualizing XBP1s ChIP-seq signal [fragments per kilobase pair per million reads (FPKM)] in wildtype LNCaP cells and ERN1 KO cells for two biological replicates. Cells were treated with Tg for 3 hours. (**D**) Average XBP1s signal (FPKM) in wildtype LNCaP cells and ERN1 KO cells for two biological replicates. Data are centered at XBP1s peaks, depicting a 2.5-kb window around the peak.

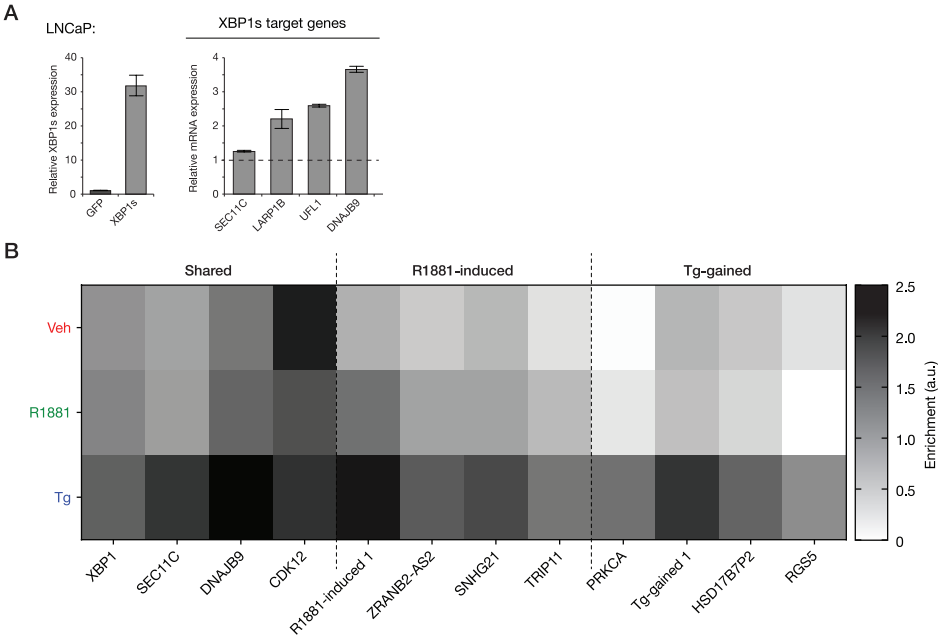

Supplementary Figure S5: Validation of XBP1s ChIP-seq analyses. (**A**) Relative mRNA expression levels of XBP1s and its target genes in LNCaP cells overexpressing XBP1s versus GFP. (**B**) Heatmap illustrating qPCR validation of shared, R1881-induced and Tg-gained binding sites identified in XBP1s ChIP-seq. Color intensity corresponds to ChIP-qPCR enrichment (see scale bar).

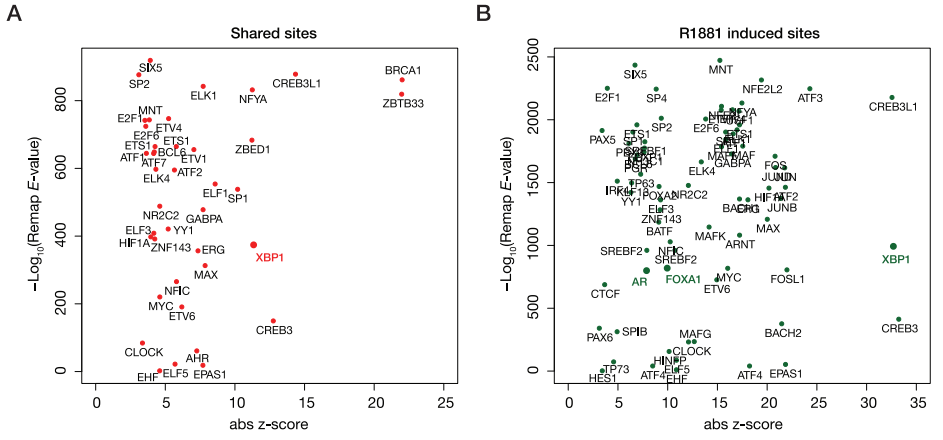

Supplementary Figure S6: ReMap tool analyses show overlap between XBP1s binding sites and those of other transcription factors. (**A**) Scatter plot of the motif enrichment (z-score) and ReMap overlap scores [-$\log_{10}$(*E*-value)] for transcription factor motifs found in XBP1s shared binding sites. (**B**) Scatter plot of the motif enrichment (z-score) and ReMap overlap scores [-$\log_{10}$(*E*-value)] for transcription factor motifs found in R1881-induced XBP1s binding sites.

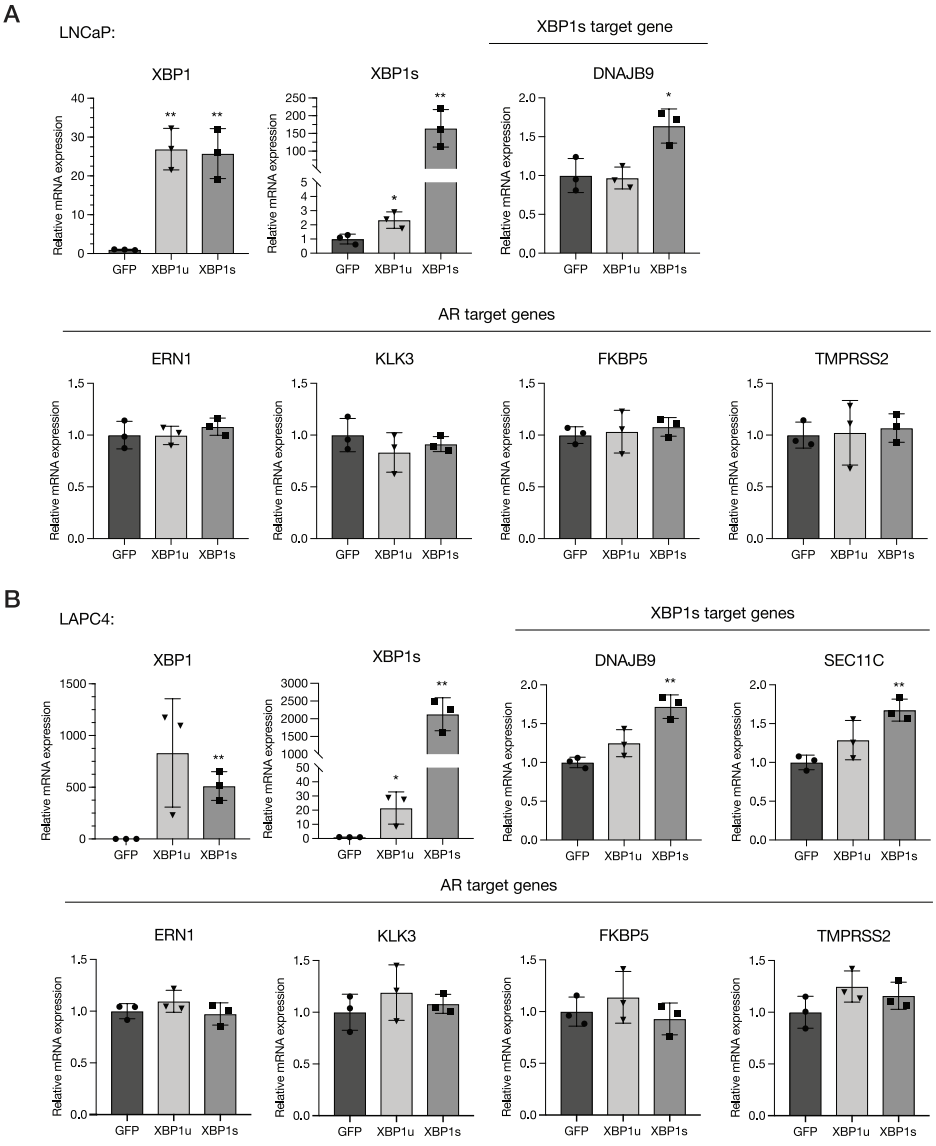

Supplementary Figure S7: XBP1s overexpression induces expression of its target genes, but no AR-responsive genes in multiple prostate cancer cell lines. (**A**) Relative mRNA expression of total *XBP1*, *XBP1s*, XBP1s target gene *DNAJB9* and AR target genes (*ERN1*, *KLK3*, *FKBP5*, *TMPRSS2*) in LNCaP cells overexpressing either XBP1u or XBP1s versus GFP control. Shown are individual datapoints and mean of three independent biological replicates. Error bars indicate standard deviation. *, $P < 0.05$; **, $P < 0.01$ (unpaired *t* test). (**B**) Relative mRNA expression of total *XBP1*, *XBP1s*, XBP1s target gene *DNAJB9* and AR target genes (*ERN1*, *KLK3*, *FKBP5*, *TMPRSS2*) in LAPC4 cells overexpressing either XBP1u or XBP1s versus GFP control. Shown are individual datapoints and mean of three independent biological replicates. Error bars indicate standard deviation. *, $P < 0.05$; **, $P < 0.01$ (unpaired *t* test).

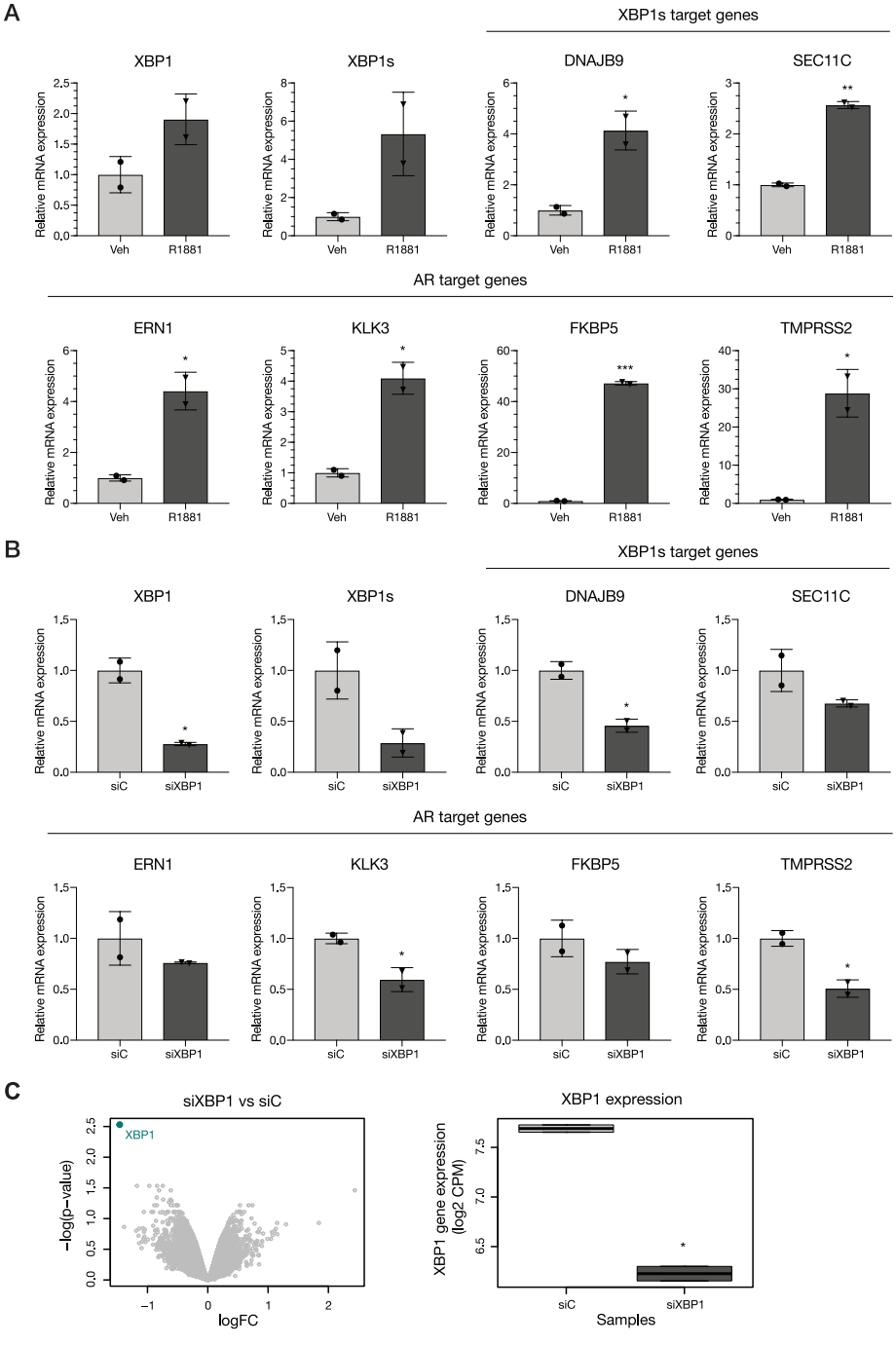
A
XBP1s target genes
XBP1
XBP1s
DNAJB9
SEC11C
Relative mRNA expression
Veh
R1881
AR target genes
ERN1
KLK3
FKBP5
TMPRSS2
B
XBP1s target genes
XBP1
XBP1s
DNAJB9
SEC11C
siC
siXBP1
AR target genes
ERN1
KLK3
FKBP5
TMPRSS2
C
siXBP1 vs siC
XBP1
−log(p−value)
logFC
XBP1 expression
XBP1 gene expression (log2 CPM)
Samples

◂ **Supplementary Figure S8:** Validation of RNA-seq analyses (I). (**A**) Relative mRNA expression of total *XBP1*, *XBP1s*, XBP1s target genes (*DNAJB9*, *SEC11C*) and AR target genes (*ERN1*, *KLK3*, *FKBP5*, *TMPRSS2*) in LNCaP cells treated with vehicle (Veh) or R1881 for 24 hours. Shown are individual datapoints and mean of two independent biological replicates. Error bars indicate standard deviation. *, $P < 0.05$; **, $P < 0.01$; ***, $P < 0.001$ (unpaired *t* test). (**B**) Relative mRNA expression of total *XBP1*, *XBP1s*, XBP1s target genes (*DNAJB9*, *SEC11C*) and AR target genes (*ERN1*, *KLK3*, *FKBP5*, *TMPRSS2*) in LNCaP cells transfected with siControl (siC) or siXBP1. Shown are individual datapoints and mean of two independent biological replicates. Error bars indicate standard deviation. *, $P < 0.05$ (unpaired *t* test). (**C**) XBP1-knockdown efficiency in RNA-seq experiment shown in **Fig. 4B**. Left: Volcano plot showing differential gene expression of LNCaP cells transfected with either siXBP1 or siControl (siC). XBP1 is depicted in turquoise. Right: Bar graph comparing XBP1 gene expression in LNCaP cells treated with siControl (siC) or siXBP1. *, $P < 0.05$ (paired *t* test).

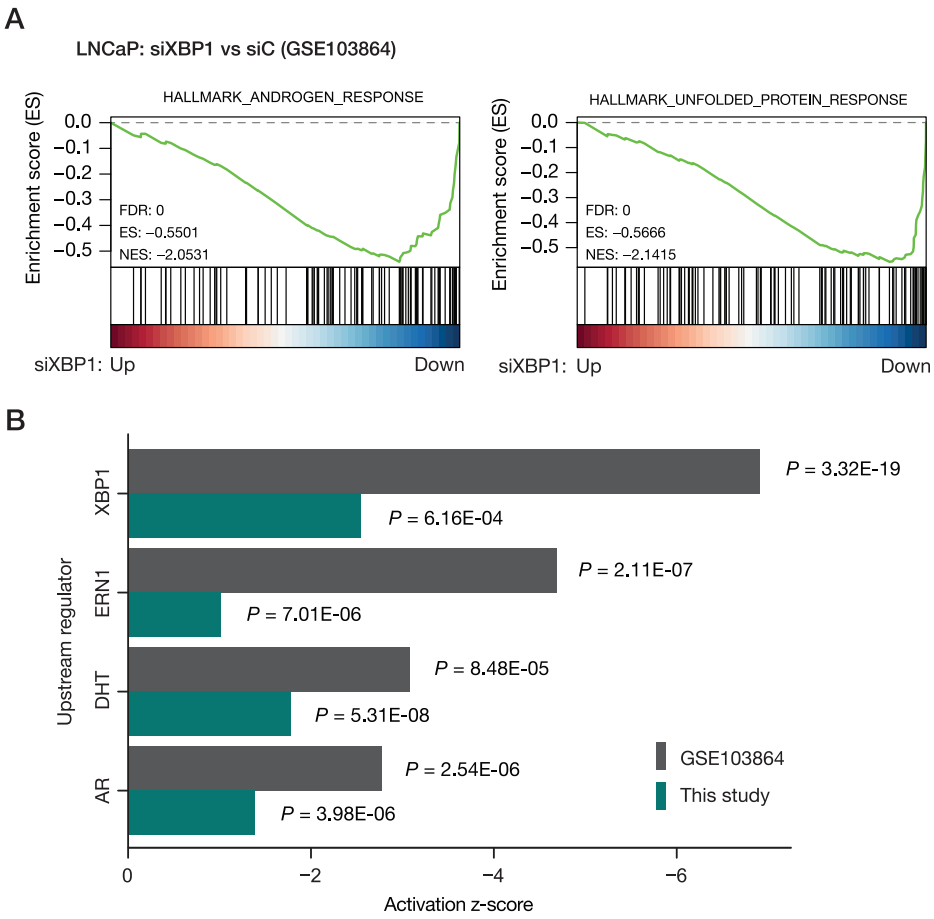

Supplementary Figure S9: Validation of RNA-seq analyses (II). (**A**) GSEA on RNA-seq data from LNCaP cells transfected with siControl (siC) or siXBP1 (GSE103864). Shown are enrichment plots of the Hallmark pathways androgen response (left) and unfolded protein response (right). Genes are ranked by differential expression between treatment conditions. *Y*-axis indicates enrichment score (ES). GSEA statistics (FDR, ES, NES) are shown. (**B**) Upstream regulators predicted by ingenuity pathway analysis (IPA) of differentially expressed genes upon XBP1 knockdown. The regulation *z*-score and the overlap *P*-value are shown for AR, dihydrotestosterone, ERN1 and XBP1.

References

1 Sheng, X. *et al.* Divergent androgen regulation of unfolded protein response pathways drives prostate cancer. *EMBO Mol Med* **7**, 788-801 (2015). https://doi.org:10.15252/emmm.201404509

2 Erzurumlu, Y. & Ballar, P. Androgen Mediated Regulation of Endoplasmic Reticulum-Associated Degradation and its Effects on Prostate Cancer. *Sci Rep* **7**, 40719 (2017). https://doi.org:10.1038/srep40719

3 Hetz, C., Chevet, E. & Harding, H. P. Targeting the unfolded protein response in disease. *Nat Rev Drug Discov* **12**, 703-719 (2013). https://doi.org:10.1038/nrd3976

4 Zambelli, A. *et al.* Transcription factor XBP-1 is expressed during osteoblast differentiation and is transcriptionally regulated by parathyroid hormone (PTH). *Cell Biol Int* **29**, 647-653 (2005). https://doi.org:10.1016/j.cellbi.2005.03.018

5 Huo, J. S. *et al.* Profiles of growth hormone (GH)-regulated genes reveal time-dependent responses and identify a mechanism for regulation of activating transcription factor 3 by GH. *J Biol Chem* **281**, 4132-4141 (2006). https://doi.org:10.1074/jbc.M508492200

6 Sengupta, S., Sharma, C. G. & Jordan, V. C. Estrogen regulation of X-box binding protein-1 and its role in estrogen induced growth of breast and endometrial cancer cells. *Horm Mol Biol Clin Investig* **2**, 235-243 (2010). https://doi.org:10.1515/HMBCI.2010.025

7 Calfon, M. *et al.* IRE1 couples endoplasmic reticulum load to secretory capacity by processing the XBP-1 mRNA. *Nature* **415**, 92-96 (2002). https://doi.org:10.1038/415092a

8 Yoshida, H., Matsui, T., Yamamoto, A., Okada, T. & Mori, K. XBP1 mRNA is induced by ATF6 and spliced by IRE1 in response to ER stress to produce a highly active transcription factor. *Cell* **107**, 881-891 (2001).

9 Duarte, M. *et al.* Rotavirus Infection Alters Splicing of the Stress-Related Transcription Factor XBP1. *J Virol* **93** (2019). https://doi.org:10.1128/JVI.01739-18

10 Lee, A. H., Iwakoshi, N. N. & Glimcher, L. H. XBP-1 regulates a subset of endoplasmic reticulum resident chaperone genes in the unfolded protein response. *Mol Cell Biol* **23**, 7448-7459 (2003).

11 Hassler, J. R. *et al.* The IRE1alpha/XBP1s Pathway Is Essential for the Glucose Response and Protection of beta Cells. *PLoS Biol* **13**, e1002277 (2015). https://doi.org:10.1371/journal.pbio.1002277

12 Chen, X. *et al.* XBP1 promotes triple-negative breast cancer by controlling the HIF1alpha pathway. *Nature* **508**, 103-107 (2014). https://doi.org:10.1038/nature13119

13 Argemi, J. *et al.* X-box Binding Protein 1 Regulates Unfolded Protein, Acute-Phase, and DNA Damage Responses During Regeneration of Mouse Liver. *Gastroenterology* **152**, 1203-1216 e1215 (2017). https://doi.org:10.1053/j.gastro.2016.12.040

14 Acosta-Alvear, D. *et al.* XBP1 controls diverse cell type- and condition-specific transcriptional regulatory networks. *Mol Cell* **27**, 53-66 (2007). https://doi.org:10.1016/j.molcel.2007.06.011

15 Stelloo, S. *et al.* Androgen receptor profiling predicts prostate cancer outcome. *EMBO Mol Med* **7**, 1450-1464 (2015). https://doi.org:10.15252/emmm.201505424

16 Cuperlovic-Culf, M., Belacel, N., Davey, M. & Ouellette, R. J. Multi-gene biomarker panel for reference free prostate cancer diagnosis: determination and independent validation. *Biomarkers* **15**, 693-706 (2010). https://doi.org:10.3109/1354750X.2010.511268

17 Takahashi, S. *et al.* Down-regulation of human X-box binding protein 1 (hXBP-1) expression correlates with tumor progression in human prostate cancers. *Prostate* **50**, 154-161 (2002).

18 Thorpe, J. A. & Schwarze, S. R. IRE1alpha controls cyclin A1 expression and promotes cell proliferation through XBP-1. *Cell Stress Chaperones* **15**, 497-508 (2010). https://doi.org:10.1007/s12192-009-0163-4

19 Sheng, X. *et al.* IRE1alpha-XBP1s pathway promotes prostate cancer by activating c-MYC signaling. *Nat Commun* **10**, 323 (2019). https://doi.org:10.1038/s41467-018-08152-3

20 Cancer Genome Atlas Research, N. The Molecular Taxonomy of Primary Prostate Cancer. *Cell* **163**, 1011-1025 (2015). https://doi.org:10.1016/j.cell.2015.10.025

21 Glinsky, G. V., Glinskii, A. B., Stephenson, A. J., Hoffman, R. M. & Gerald, W. L. Gene expression profiling predicts clinical outcome of prostate cancer. *J Clin Invest* **113**, 913-923 (2004). https://doi.org:10.1172/JCI20032

22 Rajan, P. *et al.* Next-generation sequencing of advanced prostate cancer treated with androgen-deprivation therapy. *Eur Urol* **66**, 32-39 (2014). https://doi.org:10.1016/j.eururo.2013.08.011

23 Sowalsky, A. G. *et al.* Neoadjuvant-intensive androgen deprivation therapy selects for prostate tumor foci with diverse subclonal oncogenic alterations. *Cancer Res* (2018). https://doi.org:10.1158/0008-5472.CAN-18-0610

24 Linder, S. *et al.* Drug-Induced Epigenomic Plasticity Reprograms Circadian Rhythm Regulation to Drive Prostate Cancer toward Androgen Independence. *Cancer Discov* **12**, 2074-2097 (2022). https://doi.org:10.1158/2159-8290.CD-21-0576

25 Cheneby, J., Gheorghe, M., Artufel, M., Mathelier, A. & Ballester, B. ReMap 2018: an updated atlas of regulatory regions from an integrative analysis of DNA-binding ChIP-seq experiments. *Nucleic Acids Res* **46**, D267-D275 (2018). https://doi.org:10.1093/nar/gkx1092

26 Yadav, R. K., Chae, S. W., Kim, H. R. & Chae, H. J. Endoplasmic reticulum stress and cancer. *J Cancer Prev* **19**, 75-88 (2014). https://doi.org:10.15430/JCP.2014.19.2.75

27 Sun, Y. *et al.* XBP1 promotes tumor invasion and is associated with poor prognosis in oral squamous cell carcinoma. *Oncol Rep* **40**, 988-998 (2018). https://doi.org:10.3892/or.2018.6498

28 Wu, S. *et al.* The role of XBP1s in the metastasis and prognosis of hepatocellular carcinoma. *Biochem Biophys Res Commun* **500**, 530-537 (2018). https://doi.org:10.1016/j.bbrc.2018.04.033

29 Yoshida, H., Oku, M., Suzuki, M. & Mori, K. pXBP1(U) encoded in XBP1 pre-mRNA negatively regulates unfolded protein response activator pXBP1(S) in mammalian ER stress response. *J Cell Biol* **172**, 565-575 (2006). https://doi.org:10.1083/jcb.200508145

30 Murray, J. I. *et al.* Diverse and specific gene expression responses to stresses in cultured human cells. *Mol Biol Cell* **15**, 2361-2374 (2004). https://doi.org:10.1091/mbc.e03-11-0799

31 Taylor, B. S. *et al.* Integrative genomic profiling of human prostate cancer. *Cancer Cell* **18**, 11-22 (2010). https://doi.org:10.1016/j.ccr.2010.05.026

32 Gulzar, Z. G., McKenney, J. K. & Brooks, J. D. Increased expression of NuSAP in recurrent prostate cancer is mediated by E2F1. *Oncogene* **32**, 70-77 (2013). https://doi.org:10.1038/onc.2012.27

33 Boormans, J. L. *et al.* Identification of TDRD1 as a direct target gene of ERG in primary prostate cancer. *Int J Cancer* **133**, 335-345 (2013). https://doi.org:10.1002/ijc.28025

34 Harmsen, T., Klaasen, S., van de Vrugt, H. & Te Riele, H. DNA mismatch repair and oligonucleotide end-protection promote base-pair substitution distal from a CRISPR/Cas9-induced DNA break. *Nucleic Acids Res* **46**, 2945-2955 (2018). https://doi.org:10.1093/nar/gky076

35 Brinkman, E. K., Chen, T., Amendola, M. & van Steensel, B. Easy quantitative assessment of genome editing by sequence trace decomposition. *Nucleic Acids Res* **42**, e168 (2014). https://doi.org:10.1093/nar/gku936

36 Robinson, M. D., McCarthy, D. J. & Smyth, G. K. edgeR: a Bioconductor package for differential expression analysis of digital gene expression data. *Bioinformatics* **26**, 139-140 (2010). https://doi.org:10.1093/bioinformatics/btp616

37 Ritchie, M. E. *et al.* limma powers differential expression analyses for RNA-sequencing and microarray studies. *Nucleic Acids Res* **43**, e47 (2015). https://doi.org:10.1093/nar/gkv007

38 Stelloo, S. *et al.* Endogenous androgen receptor proteomic profiling reveals genomic subcomplex involved in prostate tumorigenesis. *Oncogene* **37**, 313-322 (2018). https://doi.org:10.1038/onc.2017.330

39 Kumar, V. *et al.* Uniform, optimal signal processing of mapped deep-sequencing data. *Nat Biotechnol* **31**, 615-622 (2013). https://doi.org:10.1038/nbt.2596

40 Zhang, Y. *et al.* Model-based analysis of ChIP-Seq (MACS). *Genome Biol* **9**, R137 (2008). https://doi.org:10.1186/gb-2008-9-9-r137

41 Lerdrup, M., Johansen, J. V., Agrawal-Singh, S. & Hansen, K. An interactive environment for agile analysis and visualization of ChIP-sequencing data. *Nat Struct Mol Biol* **23**, 349-357 (2016). https://doi.org:10.1038/nsmb.3180

42 Shin, H., Liu, T., Manrai, A. K. & Liu, X. S. CEAS: cis-regulatory element annotation system. *Bioinformatics* **25**, 2605-2606 (2009). https://doi.org:10.1093/bioinformatics/btp479

43 Ross-Innes, C. S. *et al.* Differential oestrogen receptor binding is associated with clinical outcome in breast cancer. *Nature* **481**, 389-393 (2012). https://doi.org:10.1038/nature10730

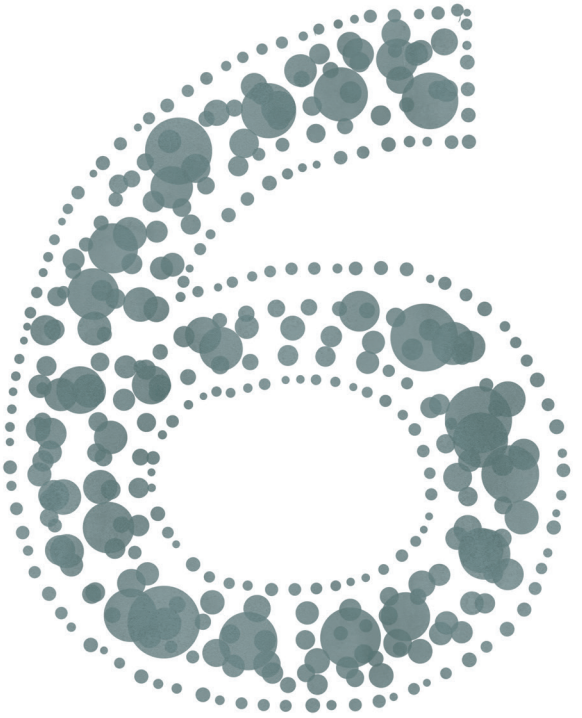

General discussion and perspectives

Ever since the direct critical link between androgens and prostate cancer progression was first described[1], scientists have sought ways to effectively block AR-mediated signaling (**Chapter 1**), ranging from surgical castration (orchiectomy) to chemical castration (androgen deprivation therapy) and finally to the development of next generation androgen biosynthesis and direct AR inhibitors known as antiandrogens[2,3]. Although most patients initially respond to AR-targeted interventions, treatment resistance inevitably occurs because sooner or later cancer cells have found ways to adapt under drug-induced evolutionary selection pressure (**Chapter 2**). The underlying resistance mechanisms are, however, not yet fully understood. While *in vitro* studies revealed various mechanisms how prostate cancer cells can acquire hormone therapy resistance[4] (such as intratumoral androgen production or AR compensation through glucocorticoid receptor action), in the clinic mainly somatic amplification of the *AR* gene[5] itself and/or an upstream *AR* enhancer[6,7] are observed, both of which are thought to have the potential to reactivate the AR signaling axis. This clearly illustrates the lack of *in vivo* datasets that can help us understand how prostate cancer cells adapt upon hormonal intervention. The main focus of this thesis is therefore to identify acquired molecular dependencies in prostate cancers that may help them evade AR-targeted therapies and to test whether these dependencies represent cellular vulnerabilities that could be exploited therapeutically (**Chapter 3**). The identification of novel drug targets in the treatment-resistant disease setting represents one of the greatest unmet medical needs in prostate cancer care and would clearly help solve the drug resistance dilemma we currently face. Furthermore, the work presented in this thesis aimed to improve our overall understanding of hormonal signaling in prostate cancer – not only to identify novel AR dependencies (**Chapter 5**), but also to gain more insights into AR signaling in different prostate cancer subtypes (**Chapter 4**) to ultimately ensure that each patient receives the best possible treatment in the future.

Lessons learned: identifying novel therapeutic targets for treatment-resistant prostate cancer requires thinking outside the box

Although prostate cancer screening and treatment have made great strides in recent decades, therapeutic options, particularly in later stages of the disease, remain limited, and improving clinical management of patients with refractory disease represents a major unmet medical need[8]. To address this, we need to gain insights into the cellular adaptation mechanisms in response to drug exposure to identify treatment-induced dependencies that allow prostate cancer cells to escape the evolutionary selection pressure imposed by hormone therapy. *In vitro* systems, particularly cell line models,

have significantly improved our understanding of AR biology in prostate cancer over the past decades[9-16]. Cell lines are great tools for mechanistically disentangling different components of the AR signaling axis, but also for directly investigating which of these components have the potential to promote drug resistance. In recent years, multiple genome-wide loss-of-function[17-21] and gain-of-function[22,23] screens have been performed in prostate cancer cell lines, which identified treatment-, cell line- and context-dependent drivers of hormone therapy resistance that represent new potential drug targets in prostate cancers with acquired resistance, but also highlight the importance of selecting the most appropriate cell line model to test the scientific hypothesis[24]. In addition, several treatment-resistant cell line clones have been generated by long-term drug exposure of hormone-sensitive cells either grown in culture dishes[25,26] or xenografted in animal models[27], which allow to profile how these cells molecularly evolved to become treatment resistant[28]. Although a number of success stories in prostate cancer research began with *in vitro* studies[27,29], the complexity of tumors *in situ* presents a major problem in translating cell line data directly to an *in vivo* setting[30,31]. Thus, targeting identified potential drivers of resistance *in vivo* does not always appear to be as effective as initially expected, underscoring the urgent need to think outside the box and generate data based on models that most closely resemble human prostate cancer or, ideally, are based directly on tumor biopsies. Such *in vivo* (or *ex vivo*[32]) datasets can help elucidate molecular adaptations in tumors, but require thorough and innovative study design to obtain the most comprehensive data possible, ideally including tissue samples collected at multiple time points (e.g., before and after a therapeutic intervention) that allow molecular profiling using multiple omics techniques. The data presented in **Chapter 3** represent, to our knowledge, the first multi-omics study embedded in a prostate cancer clinical trial that allowed simultaneous cistromic, transcriptomic, genomic, and proteomic profiling of high-risk prostate cancers before and after neoadjuvant enzalutamide therapy. In particular, the addition of cistromic profiling makes this study design unique and allowed us to identify a massive drug-induced transcription factor reprogramming and transcriptional rewiring, and ultimately led to the identification of ARNTL as an acquired vulnerability of prostate cancers after enzalutamide therapy (**Chapter 3**). This finding was completely unexpected given the canonical role of ARNTL in regulating the circadian clock[33], but demonstrates how normal physiological pathways or components thereof can be hijacked by cancer cells to maintain proliferative potential and facilitate cell survival. Whether this acquired ARNTL dependency in the localized disease setting is enzalutamide-specific or applicable to other AR-targeting agents (such as androgen deprivation therapy or treatment with other second-generation antiandrogens) remains to be tested. In addition, it would be interesting to examine whether ARNTL expression is similarly increased by hormone therapy in other hormone-dependent cancers, such as breast or endometrial

cancer, and to investigate whether ARNTL is also a vulnerability in these cancer types. Furthermore, direct ARNTL inhibitors or degraders need to be developed, as there are currently no small molecules available to (pre-)clinically test inhibition of this transcriptional regulator. Since our data suggest that ARNTL functions independently of the circadian clock as a rescue mechanism for tumor cells to escape AR blockade, available circadian modulators[34], such as compounds that block heterodimerization of ARNTL and CLOCK[35], may not be sufficient to block the action of ARNTL in this clinical setting. Transcription factors, with the exception of nuclear hormone receptors, have historically been considered undruggable due to the difficulty of targeting protein-DNA or protein-protein interactions, in contrast to the more accessible active sites of kinases or other enzymes[36,37]. Recently, however, several successful approaches for targeting transcription factors have emerged, including proteolysis targeting chimeras (PROTACs) that result in proteasome-mediated degradation of their target, which may be suitable for therapeutic development of a selective ARNTL-targeting agent[36,38].

On the one hand, our data illustrate that we must think outside the box if we are to identify new therapeutic targets that ultimately have the potential to cure patients with lethal prostate cancer – including innovative study designs, thorough multi-omics analyses, appropriate disease models, and rapid therapeutic drug development. On the other hand, they illustrate that we must expect the unexpected when it comes to therapeutic drug resistance in cancer, as even normal physiological processes can be hijacked by tumors to enable their survival.

Cistromic reprogramming and enhancer addiction: potential vulnerabilities in prostate cancer

In addition to identifying ARNTL as an acquired dependency after treatment with hormone therapy, **Chapter 3** also revealed a second dependency of prostate cancer disease progression: cistromic reprogramming. The genomic repositioning of key disease drivers such as FOXA1 from epigenetically inactivated developmental enhancers to *cis*-regulatory regions controlling essential genes that initiate prosurvival signaling and thus maintain proliferative capacities despite therapeutic intervention clearly demonstrates the dependence of prostate cancer on the gene regulatory activity of transcription factors. Primarily, this dependency has been studied for AR (**Chapter 1**) which binds to specific sets of regulatory elements at distinct stages of the disease – N-ARBS in normal prostate epithelium, T-ARBS in primary tumors, and Met-ARBS in metastatic lesions – that not only help us better understand cistromic AR activity in different prostate cancer subtypes (**Chapter 4**), but also harbor context-dependent

prognostic information that correlate with patient outcome[39]. However, the functional consequences of AR reprogramming depend on the activity of cofactors, especially pioneer factors such as FOXA1, which can remodel condensed chromatin, making it accessible to transcription factors[10,40,41]. In this way, AR, as well as other disease-promoting transcription factors – such as ARNTL – can bind *cis*-regulatory elements that would otherwise be inaccessible to drive tumorigenesis[42], therapy resistance (**Chapter 3**), or metastatic spread[43]. Despite the initial reprogramming of FOXA1 during prostate tumorigenesis, its enhancer repertoire was also found to be massively altered in neuroendocrine disease[44], suggesting an AR-independent role in prostate cancer progression – consistent with our findings in **Chapter 3**. Therefore, therapeutic targeting of this upstream AR regulator is very promising to advance the treatment of prostate cancer, and efforts to discover drugs that allow either direct or indirect[45] targeting of FOXA1 should be intensified, especially since other FOXA1-expressing tumor types such as breast cancer[46], pancreatic cancer[47], and thyroid cancer[48] could also benefit massively from such agents. In addition to upstream regulators that enable transcription factor binding, enhancer activity is also highly dependent on downstream players that collectively orchestrate the expression of transcription factor target genes. In particular, transcription coactivators (e.g., P300/CBP) and other cofactors, such as chromatin readers (e.g., BRD4) and remodelers (e.g., SWI/SNF) are essential for prostate cancer drivers to create or maintain a prosurvival chromatin state. Consistently, therapeutic targeting of all of the above-mentioned cofactors has been shown to successfully inhibit tumor growth in advanced disease models with persistent AR signaling[49-51]. This clearly indicates that enhancer addiction, and thus the need for an active epigenetic machinery to drive target gene expression, is a vulnerability of prostate cancers – but potentially of many other cancers as well.

State-of-the-art cistromics approaches for simultaneous profiling of multiple regulatory nodes

Transcriptional rewiring resulting from transcription factor reprogramming is mediated by the collective activity of several regulatory factors. However, the study of their combined mode of action in a single sample or preferably in a single cell is not trivial. Over the past decade multiple methodical refinements of chromatin immunoprecipitation sequencing (ChIP-seq) protocols[52] have been proposed, including the addition of carriers[53] or additional fixation steps[54] that decrease off-target signals and increase the on-target ChIP efficiency. These optimizations allowed us to study the *cis*-regulatory landscape and its surrounding epigenetic environment in limited amount of tissue culture cells (**Chapter 3** and **Chapter 5**), but also limited amounts

of tumor tissue (**Chapter 4**) and even in 18-gauge (1.27 mm in diameter) core needle biopsy material (**Chapter 3**). Nevertheless, these ChIP-seq protocols and the data obtained from them have intrinsic limitations. One limitation is that currently only one chromatin-binding protein can be profiled at a time, which is suboptimal when studying the interconnectivity of regulatory factors in gene regulation. This is particularly constraining in settings with limited sample material, such as tissue biopsies, which doesn't allow for multiple ChIP-seq experiments in parallel. Instead, sequential ChIPs of multiple factors from the same cellular lysate can be used for genomic profiling of transcription factors and histone modifications, which has been shown to be very successful in several studies[43,55-57]. This strategy has also been used in **Chapter 3**, in which we assessed how neoadjuvant hormone therapy in primary prostate cancers affected the *cis*-regulatory landscape of disease driver and drug target AR, its pioneer factor FOXA1 and the active histone modification H3K27ac. It enabled us to identify drug-induced cistromic reprogramming of FOXA1 and AR, away from inactive developmental enhancers toward active regulatory regions that drove tumor cell survival. In this study, we derived information on chromatin states not only from our H3K27ac ChIP-seq data, but also by integrating our binding sites of interest with a published cistromic dataset of additional histone marks that matched our experimental conditions[56]. However, a method that allows simultaneous genomic profiling of multiple histone modifications and chromatin-binding proteins in the same sample would be most ideal, as it could capture the genomic distribution and interconnectivity of different transcription factors and any associated changes in the epigenetic state of active and inactive chromatin. Recently, two multifactorial epigenome profiling techniques (Multiple Target Identification by Tagmentation, MulTI-tag[58]; Multiplexing Antibodies by barcode Identification, MAbID[59]) have been developed that enable simultaneous profiling of multiple epigenome targets, with which up to three histone modifications (MulTI-tag) or even up to six chromatin-associated proteins (MAbID) could be profiled successfully in limited input material. Given that both techniques allow comprehensive characterization of cell-specific gene regulatory landscapes at single-cell resolution, this may address yet another limitation of classical ChIP-seq experiments. ChIP-seq, like any other omics approach performed on bulk material, provides data that represents an average profile of all cells in a sample. Single-cell methods, especially in combination with (spatial) transcriptomic readouts, would therefore allow multi-omic profiling at much greater resolution to study whether epigenomic reprogramming and transcriptomic plasticity are seen uniformly across all profiled cells, or if these effects are more heterogeneous and cell- or even cell type-specific. While all studies in this thesis focus on the intrinsic cistromic features of tumor cells, single-cell methodologies would also allow to investigate how tumor-adjacent cells in the microenvironment or tumor-infiltrating immune cells are affected by AR-targeted interventions, as immune cells can promote therapy resistance and

disease progression, as recently shown in prostate cancer bone metastases[60]. Overall, multimodal single-cell sequencing methods[61-65] have advanced rapidly over the past decade and promise to comprehensively characterize the *cis*-regulatory enhancer repertoire and downstream transcriptomic programs in prostate cancer, as well as in tumor-adjacent normal or immune cells, to ultimately understand how these landscapes change during tumorigenesis or disease progression and how and when to most successfully intervene in a given patient.

Classifiers for prostate cancer risk stratification: preventing over-treatment and improving patient survival

The integration of state-of-the-art multi-omics techniques into innovative study designs involving clinical samples from patients at different disease stages (healthy tissue vs. primary tumor vs. metastatic lesions) or after therapeutic interventions (pre- vs. post-therapy) would also allow the identification of novel classifiers for cancer risk stratification and drug response prediction. Since approximately 30% of patients with primary prostate cancer relapse after prostatectomy or radiotherapy, prognostic or ideally predictive biomarkers are urgently needed to identify patients with very high risk at an early stage who would potentially benefit from more intensive adjuvant treatment regimens, as well as those with low-risk disease who would not benefit from such interventions. Previously, we identified a prognostic gene classifier through integrative AR-focused cistromic analyses comparing only a handful of therapy-naïve primary tumors (n = 5) with tumors exhibiting acquired therapy resistance (n = 3)[66]. These analyses revealed reprogramming of the AR-chromatin interactome between these two clinical stages, leading to AR regulation of a distinct set of genes, the expression of which has the prognostic potential to stratify prostate cancer patients on outcome, independent of classical clinicopathological parameters (such as Gleason grading[67]) and clinical risk classifiers (D'Amico[68]). Altogether, these analyses clearly demonstrate that genome-wide cistromic profiling has the potential to provide novel signatures with strong prognostic power, a strategy that should be further refined in future studies. In addition, our studies identified single-gene biomarkers for biochemical relapse (*XBP1* in **Chapter 5**) and for response to enzalutamide in primary disease (*ARNTL* in **Chapter 3**). The latter needs to be further validated in additional cohorts, ideally including patients treated with androgen deprivation therapy or other antiandrogens, to assess whether ARNTL upregulation is observable in localized prostate cancer independent of the AR-targeting agent. Moreover, future studies should include many more samples collected at different biological disease stages, but also after different systemic therapeutic interventions (AR-targeted and non-AR-targeted). This would not only help to better

model and capture the inherent heterogeneity of prostate cancer[69], but also help to identify more robust classifiers that will ultimately allow us to optimize and personalize treatment sequencing and efficacy – an unmet medical need thoroughly discussed in **Chapter 2**. For this reason, future research should aim at advancing precision medicine for prostate cancer, which can help determine the most appropriate treatment regimen for each patient, thereby avoiding overtreatment and ultimately improving patient survival and quality of life.

Low-risk prostate tumors: precancerous lesions or bona fide adenocarcinomas?

While identifying high-risk patients is paramount to improving survival, identifying patients with very low-risk disease that either has indolent features or can be cured through locoregional intervention is equally important to prevent overtreatment of this patient population. Ever since prostate-specific antigen (PSA)-based population screening was introduced in the late 1980s, prostate cancer mortality decreased whereas the incidence increased sharply[70,71]. Many men are, however, diagnosed with low-risk grade group 1 cancers[72] (Gleason score ≤6) that have an overall negligible risk of disease progression and distant metastases, which is why overtreatment is a key concern, as most patients will likely not die of the disease, even if left untreated. For this reason, there is much controversy in the prostate cancer community as to whether these lesions should be reclassified as "non-cancerous"[73-77], similar to ductal carcinoma in situ (DCIS) in breast cancer[78] . Over the last decade, a lot of resources went into DCIS research, which helped to identify challenges in DCIS diagnosis, allowed comparative omics analyses between DCIS and invasive breast cancer, and facilitated the generation of adequate disease models, all of which ultimately helped to better understand DCIS[79,80]. However, low-risk prostate cancer has not yet been thoroughly profiled, and much remains to be learned about its underlying biology to gain insight into what makes GG1 lesions clinically less aggressive compared with higher-grade tumors. To shed some light on this, we set out to study the activity of prostate cancer disease driver AR (**Chapter 4**), which revealed that AR's tumor-specific cistromic and transcriptomic activity in low-grade lesions is not enriched for normal prostate epithelium-specific signaling, but rather shows high concordance with high-grade prostate cancer. This clearly separates GG1 lesions from benign prostate epithelium and positions them as *bona fide* cancers from an epigenetic perspective. Our transcriptomic analyses identified, however, certain pathways to be differentially regulated in high- vs. low-risk disease (**Chapter 4**), including epithelial-mesenchymal transition, proliferation-related pathways, immune response, and signaling cascades such as IL2-STAT5, IFN-g and KRAS. Nonetheless, it remains elusive how these

pathways contribute to an overall more aggressive disease state, which should be further investigated by proteomic and phosphoproteomic analyses to obtain a better picture of the landscape of active oncogenic signaling pathways. The enrichment of inflammatory response pathways in high-grade disease, also point toward an active role of the tumor microenvironment in regulating prostate cancer aggressiveness. While our analyses solely focused on the characterization of tumor-intrinsic signaling, future studies should exploit single-cell technologies to gain insights into the crosstalk between prostate cancer and immune cells. Overall, it seems premature to remove the label of "cancer" from a low-risk disease at this stage, when so many variables are still unknown, especially since even GG1 tumors appear to progress to higher-grade carcinomas[81], in a small percentage of patients, highlighting that leaving the tumor *in situ* without adequate surveillance could result in a missed opportunity for cure[73]. But what determines if a GG1 lesion progresses or not? Although biochemical recurrence occurs in less than 5% of patients with GG1 prostate cancer[73,82,83], it would still be extremely helpful to have biomarkers to identify these individuals early in order to offer them therapeutic interventions with curative intent. In **Chapter 4** we showed that not only AR signal intensity at tumor- and metastases-specific AR binding sites (T-ARBS and Met-ARBS), but also the gene expression of the corresponding T-ARBS and Met-ARBS gene sets[39] were significantly increased in cases with future relapse and could help stratify low-risk prostate cancer patients on outcome. Undoubtedly, additional supervised analyses between GG1 cases and controls will allow the identification of additional signatures or biomarkers for recurrence prediction that are ideally compatible with current clinical routine and thus easily detectable via histology or immunohistochemistry. In addition, machine learning models that allow integration of radiomic magnetic resonance imaging features with digital pathology and gene expression data could help predict patient outcome and thus refine clinical decision making and treatment planning, as recently demonstrated for the prediction of upstaging in DCIS[84]. Taken together, ultra-low-risk lesions represent a largely understudied subset of prostate cancers that surprisingly share many AR-driven epigenetic features with higher-grade tumors, underscoring the need for future research to decipher the underlying oncogenic signals of their primarily indolent clinical phenotype.

AR and its targets: how new insights into hormonal signaling can help identify prostate cancer dependencies

In addition to studying hormonal signaling in low-grade disease (**Chapter 4**), we have also discovered how prosurvival signaling in prostate cancer cells can be achieved through activation of stress response pathways (**Chapter 5**). In particular, we identified an unexpected interplay between the unfolded protein response pathway and the AR

signaling axis, in which AR modulates the expression of key players of the UPR, such as ERN1 and XBP1(s), which in turn drive part of the AR transcriptional program. The UPR is a tightly regulated process that helps cells maintain homeostasis between protein production and degradation in response to transcriptional and translational stimuli[85,86]. The androgen-dependent activation of UPR signaling – which is observed not only in prostate cancer cell line models (**Chapter 5**), but also in clinical specimens (**Chapter 3**) – may help prostate cancer cells cope with increased translation and protein (mis) folding after AR-activated gene transcription. Therefore, the stress sensor ERN1 and its downstream transcriptional regulator XBP1s may represent novel therapeutic targets, especially since these factors also have a direct effect on AR activity, which should be further investigated in future preclinical studies. Whether other stress response pathways are similarly hijacked or exhibit similar dependencies remains elusive at this time, but once again underscores the importance of thinking outside the box to improve and advance prostate cancer therapies.

Concluding remarks

In recent years, we have made significant progress in improving our understanding of hormonal signaling in prostate cancer. Since all advanced prostate cancers sooner or later develop resistance to currently available AR-targeted therapies, it is of utmost importance to better model the activity of this disease driver to eventually identify novel prostate cancer dependencies. The data presented in this thesis demonstrate how the integration of tissue cistromics with other omics datastreams can not only help us gain new insights into AR signaling in prostate cancers, but also enable the identification of thus far unknow and – given their canonical role in normal physiological processes – surprising, prostate cancer dependencies whose therapeutic targeting could ultimately improve the efficacy of current AR-targeted therapies. It will be exciting to see what will be discovered in the coming years with all the cutting-edge multi-omics technologies that are now available. These undoubtedly have the potential to further improve current prostate cancer therapies and reveal new therapeutic strategies, and will ultimately bring us one step closer to our goal of curing (prostate) cancer - *it's about time*!

References

1 Huggins, C. & Hodges, C. V. Studies on prostatic cancer. I. The effect of castration, of estrogen and androgen injection on serum phosphatases in metastatic carcinoma of the prostate. *CA Cancer J Clin* **22**, 232-240 (1972). https://doi.org:10.3322/canjclin.22.4.232

2 Desai, K., McManus, J. M. & Sharifi, N. Hormonal Therapy for Prostate Cancer. *Endocr Rev* **42**, 354-373 (2021). https://doi.org:10.1210/endrev/bnab002

3 Helsen, C. *et al.* Androgen receptor antagonists for prostate cancer therapy. *Endocr Relat Cancer* **21**, T105-118 (2014). https://doi.org:10.1530/ERC-13-0545

4 Prekovic, S. *et al.* Molecular underpinnings of enzalutamide resistance. *Endocr Relat Cancer* **25**, R545-R557 (2018). https://doi.org:10.1530/ERC-17-0136

5 Robinson, D. *et al.* Integrative clinical genomics of advanced prostate cancer. *Cell* **161**, 1215-1228 (2015). https://doi.org:10.1016/j.cell.2015.05.001

6 Takeda, D. Y. *et al.* A Somatically Acquired Enhancer of the Androgen Receptor Is a Noncoding Driver in Advanced Prostate Cancer. *Cell* **174**, 422-432 e413 (2018). https://doi.org:10.1016/j.cell.2018.05.037

7 Viswanathan, S. R. *et al.* Structural Alterations Driving Castration-Resistant Prostate Cancer Revealed by Linked-Read Genome Sequencing. *Cell* **174**, 433-447 e419 (2018). https://doi.org:10.1016/j.cell.2018.05.036

8 Mateo, J. *et al.* Accelerating precision medicine in metastatic prostate cancer. *Nat Cancer* **1**, 1041-1053 (2020). https://doi.org:10.1038/s43018-020-00141-0

9 Shang, Y., Myers, M. & Brown, M. Formation of the androgen receptor transcription complex. *Mol Cell* **9**, 601-610 (2002). https://doi.org:10.1016/s1097-2765(02)00471-9

10 Lupien, M. *et al.* FoxA1 translates epigenetic signatures into enhancer-driven lineage-specific transcription. *Cell* **132**, 958-970 (2008). https://doi.org:10.1016/j.cell.2008.01.018

11 Wang, Q. *et al.* Androgen receptor regulates a distinct transcription program in androgen-independent prostate cancer. *Cell* **138**, 245-256 (2009). https://doi.org:10.1016/j.cell.2009.04.056

12 Yu, J. *et al.* An integrated network of androgen receptor, polycomb, and TMPRSS2-ERG gene fusions in prostate cancer progression. *Cancer Cell* **17**, 443-454 (2010). https://doi.org:10.1016/j.ccr.2010.03.018

13 Nadal, M. *et al.* Structure of the homodimeric androgen receptor ligand-binding domain. *Nat Commun* **8**, 14388 (2017). https://doi.org:10.1038/ncomms14388

14 Stelloo, S. *et al.* Endogenous androgen receptor proteomic profiling reveals genomic subcomplex involved in prostate tumorigenesis. *Oncogene* **37**, 313-322 (2018). https://doi.org:10.1038/onc.2017.330

15 Huang, C. F. *et al.* Functional mapping of androgen receptor enhancer activity. *Genome Biol* **22**, 149 (2021). https://doi.org:10.1186/s13059-021-02339-6

16 Davies, A. *et al.* An androgen receptor switch underlies lineage infidelity in treatment-resistant prostate cancer. *Nat Cell Biol* **23**, 1023-1034 (2021). https://doi.org:10.1038/s41556-021-00743-5

17 Fei, T. *et al.* Genome-wide CRISPR screen identifies HNRNPL as a prostate cancer dependency regulating RNA splicing. *Proc Natl Acad Sci U S A* **114**, E5207-E5215 (2017). https://doi.org:10.1073/pnas.1617467114

18 Palit, S. A. *et al.* TLE3 loss confers AR inhibitor resistance by facilitating GR-mediated human prostate cancer cell growth. *Elife* **8** (2019). https://doi.org:10.7554/eLife.47430

19 Das, R. *et al.* An integrated functional and clinical genomics approach reveals genes driving aggressive metastatic prostate cancer. *Nat Commun* **12**, 4601 (2021). https://doi.org:10.1038/s41467-021-24919-7
20 Tang, S. *et al.* A genome-scale CRISPR screen reveals PRMT1 as a critical regulator of androgen receptor signaling in prostate cancer. *Cell Rep* **38**, 110417 (2022). https://doi.org:10.1016/j.celrep.2022.110417
21 Tsujino, T. *et al.* CRISPR screens reveal genetic determinants of PARP inhibitor sensitivity and resistance in prostate cancer. *Nat Commun* **14**, 252 (2023). https://doi.org:10.1038/s41467-023-35880-y
22 Hwang, J. H. *et al.* CREB5 Promotes Resistance to Androgen-Receptor Antagonists and Androgen Deprivation in Prostate Cancer. *Cell Rep* **29**, 2355-2370 e2356 (2019). https://doi.org:10.1016/j.celrep.2019.10.068
23 Rodriguez, Y. *et al.* A Genome-Wide CRISPR Activation Screen Identifies PRRX2 as a Regulator of Enzalutamide Resistance in Prostate Cancer. *Cancer Res* **82**, 2110-2123 (2022). https://doi.org:10.1158/0008-5472.CAN-21-3565
24 Domcke, S., Sinha, R., Levine, D. A., Sander, C. & Schultz, N. Evaluating cell lines as tumour models by comparison of genomic profiles. *Nat Commun* **4**, 2126 (2013). https://doi.org:10.1038/ncomms3126
25 Kregel, S. *et al.* Acquired resistance to the second-generation androgen receptor antagonist enzalutamide in castration-resistant prostate cancer. *Oncotarget* **7**, 26259-26274 (2016). https://doi.org:10.18632/oncotarget.8456
26 Handle, F. *et al.* Drivers of AR indifferent anti-androgen resistance in prostate cancer cells. *Sci Rep* **9**, 13786 (2019). https://doi.org:10.1038/s41598-019-50220-1
27 Bishop, J. L. *et al.* The Master Neural Transcription Factor BRN2 Is an Androgen Receptor-Suppressed Driver of Neuroendocrine Differentiation in Prostate Cancer. *Cancer Discov* **7**, 54-71 (2017). https://doi.org:10.1158/2159-8290.CD-15-1263
28 Taavitsainen, S. *et al.* Single-cell ATAC and RNA sequencing reveal pre-existing and persistent cells associated with prostate cancer relapse. *Nat Commun* **12**, 5307 (2021). https://doi.org:10.1038/s41467-021-25624-1
29 Tran, C. *et al.* Development of a second-generation antiandrogen for treatment of advanced prostate cancer. *Science* **324**, 787-790 (2009). https://doi.org:10.1126/science.1168175
30 Gillet, J. P. *et al.* Redefining the relevance of established cancer cell lines to the study of mechanisms of clinical anti-cancer drug resistance. *Proc Natl Acad Sci U S A* **108**, 18708-18713 (2011). https://doi.org:10.1073/pnas.1111840108
31 Ertel, A., Verghese, A., Byers, S. W., Ochs, M. & Tozeren, A. Pathway-specific differences between tumor cell lines and normal and tumor tissue cells. *Mol Cancer* **5**, 55 (2006). https://doi.org:10.1186/1476-4598-5-55
32 Centenera, M. M. *et al.* A patient-derived explant (PDE) model of hormone-dependent cancer. *Mol Oncol* **12**, 1608-1622 (2018). https://doi.org:10.1002/1878-0261.12354
33 Patke, A., Young, M. W. & Axelrod, S. Molecular mechanisms and physiological importance of circadian rhythms. *Nat Rev Mol Cell Biol* **21**, 67-84 (2020). https://doi.org:10.1038/s41580-019-0179-2
34 Tamai, T. K. *et al.* Identification of circadian clock modulators from existing drugs. *EMBO Mol Med* **10** (2018). https://doi.org:10.15252/emmm.201708724
35 Doruk, Y. U. *et al.* A CLOCK-binding small molecule disrupts the interaction between CLOCK and BMAL1 and enhances circadian rhythm amplitude. *J Biol Chem* **295**, 3518-3531 (2020). https://doi.org:10.1074/jbc.RA119.011332

36 Bushweller, J. H. Targeting transcription factors in cancer - from undruggable to reality. *Nat Rev Cancer* **19**, 611-624 (2019). https://doi.org:10.1038/s41568-019-0196-7

37 Darnell, J. E., Jr. Transcription factors as targets for cancer therapy. *Nat Rev Cancer* **2**, 740-749 (2002). https://doi.org:10.1038/nrc906

38 Bekes, M., Langley, D. R. & Crews, C. M. PROTAC targeted protein degraders: the past is prologue. *Nat Rev Drug Discov* **21**, 181-200 (2022). https://doi.org:10.1038/s41573-021-00371-6

39 Severson, T. *et al.* Androgen receptor reprogramming demarcates prognostic, context-dependent gene sets in primary and metastatic prostate cancer. *Clin Epigenetics* **14**, 60 (2022). https://doi.org:10.1186/s13148-022-01278-8

40 Hankey, W., Chen, Z. & Wang, Q. Shaping Chromatin States in Prostate Cancer by Pioneer Transcription Factors. *Cancer Res* **80**, 2427-2436 (2020). https://doi.org:10.1158/0008-5472.CAN-19-3447

41 Cirillo, L. A. *et al.* Opening of compacted chromatin by early developmental transcription factors HNF3 (FoxA) and GATA-4. *Mol Cell* **9**, 279-289 (2002). https://doi.org:10.1016/s1097-2765(02)00459-8

42 Pomerantz, M. M. *et al.* The androgen receptor cistrome is extensively reprogrammed in human prostate tumorigenesis. *Nat Genet* **47**, 1346-1351 (2015). https://doi.org:10.1038/ng.3419

43 Pomerantz, M. M. *et al.* Prostate cancer reactivates developmental epigenomic programs during metastatic progression. *Nat Genet* **52**, 790-799 (2020). https://doi.org:10.1038/s41588-020-0664-8

44 Baca, S. C. *et al.* Reprogramming of the FOXA1 cistrome in treatment-emergent neuroendocrine prostate cancer. *Nat Commun* **12**, 1979 (2021). https://doi.org:10.1038/s41467-021-22139-7

45 Gao, S. *et al.* Chromatin binding of FOXA1 is promoted by LSD1-mediated demethylation in prostate cancer. *Nat Genet* **52**, 1011-1017 (2020). https://doi.org:10.1038/s41588-020-0681-7

46 Carroll, J. S. *et al.* Chromosome-wide mapping of estrogen receptor binding reveals long-range regulation requiring the forkhead protein FoxA1. *Cell* **122**, 33-43 (2005). https://doi.org:10.1016/j.cell.2005.05.008

47 Roe, J. S. *et al.* Enhancer Reprogramming Promotes Pancreatic Cancer Metastasis. *Cell* **170**, 875-888 e820 (2017). https://doi.org:10.1016/j.cell.2017.07.007

48 Nucera, C. *et al.* FOXA1 is a potential oncogene in anaplastic thyroid carcinoma. *Clin Cancer Res* **15**, 3680-3689 (2009). https://doi.org:10.1158/1078-0432.CCR-08-3155

49 Welti, J. *et al.* Targeting the p300/CBP Axis in Lethal Prostate Cancer. *Cancer Discov* **11**, 1118-1137 (2021). https://doi.org:10.1158/2159-8290.CD-20-0751

50 Asangani, I. A. *et al.* Therapeutic targeting of BET bromodomain proteins in castration-resistant prostate cancer. *Nature* **510**, 278-282 (2014). https://doi.org:10.1038/nature13229

51 Xiao, L. *et al.* Targeting SWI/SNF ATPases in enhancer-addicted prostate cancer. *Nature* **601**, 434-439 (2022). https://doi.org:10.1038/s41586-021-04246-z

52 Schmidt, D. *et al.* ChIP-seq: using high-throughput sequencing to discover protein-DNA interactions. *Methods* **48**, 240-248 (2009). https://doi.org:10.1016/j.ymeth.2009.03.001

53 Zwart, W. *et al.* A carrier-assisted ChIP-seq method for estrogen receptor-chromatin interactions from breast cancer core needle biopsy samples. *BMC Genomics* **14**, 232 (2013). https://doi.org:10.1186/1471-2164-14-232

54 Singh, A. A. *et al.* Optimized ChIP-seq method facilitates transcription factor profiling in human tumors. *Life Sci Alliance* **2**, e201800115 (2019). https://doi.org:10.26508/lsa.201800115

55 Severson, T. M. *et al.* Characterizing steroid hormone receptor chromatin binding landscapes in male and female breast cancer. *Nat Commun* **9**, 482 (2018). https://doi.org:10.1038/s41467-018-02856-2

56 Stelloo, S. *et al.* Integrative epigenetic taxonomy of primary prostate cancer. *Nat Commun* **9**, 4900 (2018). https://doi.org:10.1038/s41467-018-07270-2

57 Mazrooei, P. *et al.* Cistrome Partitioning Reveals Convergence of Somatic Mutations and Risk Variants on Master Transcription Regulators in Primary Prostate Tumors. *Cancer Cell* **36**, 674-689 e676 (2019). https://doi.org:10.1016/j.ccell.2019.10.005

58 Meers, M. P., Llagas, G., Janssens, D. H., Codomo, C. A. & Henikoff, S. Multifactorial profiling of epigenetic landscapes at single-cell resolution using MulTI-Tag. *Nat Biotechnol* (2022). https://doi.org:10.1038/s41587-022-01522-9

59 Lochs, S. J. A. *et al.* Combinatorial single-cell profiling of all major chromatin types with MAbID. *bioRxiv*, 2023.2001.2018.524584 (2023). https://doi.org:10.1101/2023.01.18.524584

60 Li, X. F. *et al.* Macrophages promote anti-androgen resistance in prostate cancer bone disease. *J Exp Med* **220** (2023). https://doi.org:10.1084/jem.20221007

61 Hu, Y. *et al.* Simultaneous profiling of transcriptome and DNA methylome from a single cell. *Genome Biol* **17**, 88 (2016). https://doi.org:10.1186/s13059-016-0950-z

62 Stoeckius, M. *et al.* Simultaneous epitope and transcriptome measurement in single cells. *Nat Methods* **14**, 865-868 (2017). https://doi.org:10.1038/nmeth.4380

63 Clark, S. J. *et al.* scNMT-seq enables joint profiling of chromatin accessibility DNA methylation and transcription in single cells. *Nat Commun* **9**, 781 (2018). https://doi.org:10.1038/s41467-018-03149-4

64 Cao, J. *et al.* Joint profiling of chromatin accessibility and gene expression in thousands of single cells. *Science* **361**, 1380-1385 (2018). https://doi.org:10.1126/science.aau0730

65 Swanson, E. *et al.* Simultaneous trimodal single-cell measurement of transcripts, epitopes, and chromatin accessibility using TEA-seq. *Elife* **10** (2021). https://doi.org:10.7554/eLife.63632

66 Stelloo, S. *et al.* Androgen receptor profiling predicts prostate cancer outcome. *EMBO Mol Med* **7**, 1450-1464 (2015). https://doi.org:10.15252/emmm.201505424

67 Gleason, D. F. & Mellinger, G. T. Prediction of prognosis for prostatic adenocarcinoma by combined histological grading and clinical staging. *J Urol* **111**, 58-64 (1974). https://doi.org:10.1016/s0022-5347(17)59889-4

68 D'Amico, A. V. *et al.* Biochemical outcome after radical prostatectomy, external beam radiation therapy, or interstitial radiation therapy for clinically localized prostate cancer. *JAMA* **280**, 969-974 (1998). https://doi.org:10.1001/jama.280.11.969

69 Kneppers, J. *et al.* Extensive androgen receptor enhancer heterogeneity in primary prostate cancers underlies transcriptional diversity and metastatic potential. *Nat Commun* **13**, 7367 (2022). https://doi.org:10.1038/s41467-022-35135-2

70 Welch, H. G. & Albertsen, P. C. Prostate cancer diagnosis and treatment after the introduction of prostate-specific antigen screening: 1986-2005. *J Natl Cancer Inst* **101**, 1325-1329 (2009). https://doi.org:10.1093/jnci/djp278

71 Fenton, J. J. *et al.* Prostate-Specific Antigen-Based Screening for Prostate Cancer: Evidence Report and Systematic Review for the US Preventive Services Task Force. *JAMA* **319**, 1914-1931 (2018). https://doi.org:10.1001/jama.2018.3712

72 Egevad, L., Delahunt, B., Srigley, J. R. & Samaratunga, H. International Society of Urological Pathology (ISUP) grading of prostate cancer - An ISUP consensus on contemporary grading. *APMIS* **124**, 433-435 (2016). https://doi.org:10.1111/apm.12533

73 Carter, H. B. *et al.* Gleason score 6 adenocarcinoma: should it be labeled as cancer? *J Clin Oncol* **30**, 4294-4296 (2012). https://doi.org:10.1200/JCO.2012.44.0586

74 Burke, H. B. Gleason 6 prostate cancer: That which cannot be named. *Front Oncol* **12**, 1073580 (2022). https://doi.org:10.3389/fonc.2022.1073580

75 Eggener, S. E. *et al.* Low-Grade Prostate Cancer: Time to Stop Calling It Cancer. *J Clin Oncol* **40**, 3110-3114 (2022). https://doi.org:10.1200/JCO.22.00123
76 Zhou, M. *et al.* Should grade group 1 prostate cancer be reclassified as "non-cancer"? A pathology community perspective. *Urol Oncol* **41**, 62-64 (2023). https://doi.org:10.1016/j.urolonc.2022.09.028
77 Baboudjian, M., Roupret, M. & Ploussard, G. Redefining Gleason 6 Prostate Cancer Nomenclature: The Surgeon's Perspective. *J Clin Oncol* **41**, 1492-1493 (2023). https://doi.org:10.1200/JCO.22.01621
78 van Seijen, M. *et al.* Ductal carcinoma in situ: to treat or not to treat, that is the question. *Br J Cancer* **121**, 285-292 (2019). https://doi.org:10.1038/s41416-019-0478-6
79 Casasent, A. K. *et al.* Learning to distinguish progressive and non-progressive ductal carcinoma in situ. *Nat Rev Cancer* **22**, 663-678 (2022). https://doi.org:10.1038/s41568-022-00512-y
80 Lips, E. H. *et al.* Genomic analysis defines clonal relationships of ductal carcinoma in situ and recurrent invasive breast cancer. *Nat Genet* **54**, 850-860 (2022). https://doi.org:10.1038/s41588-022-01082-3
81 Sheridan, T. B., Carter, H. B., Wang, W., Landis, P. B. & Epstein, J. I. Change in prostate cancer grade over time in men followed expectantly for stage T1c disease. *J Urol* **179**, 901-904; discussion 904-905 (2008). https://doi.org:10.1016/j.juro.2007.10.062
82 Khan, M. A., Partin, A. W., Mangold, L. A., Epstein, J. I. & Walsh, P. C. Probability of biochemical recurrence by analysis of pathologic stage, Gleason score, and margin status for localized prostate cancer. *Urology* **62**, 866-871 (2003). https://doi.org:10.1016/s0090-4295(03)00674-5
83 Donin, N. M., Laze, J., Zhou, M., Ren, Q. & Lepor, H. Gleason 6 prostate tumors diagnosed in the PSA era do not demonstrate the capacity for metastatic spread at the time of radical prostatectomy. *Urology* **82**, 148-152 (2013). https://doi.org:10.1016/j.urology.2013.03.054
84 Hou, R. *et al.* Prediction of Upstaging in Ductal Carcinoma in Situ Based on Mammographic Radiomic Features. *Radiology* **303**, 54-62 (2022). https://doi.org:10.1148/radiol.210407
85 Hetz, C., Chevet, E. & Harding, H. P. Targeting the unfolded protein response in disease. *Nat Rev Drug Discov* **12**, 703-719 (2013). https://doi.org:10.1038/nrd3976
86 Hetz, C., Zhang, K. & Kaufman, R. J. Mechanisms, regulation and functions of the unfolded protein response. *Nat Rev Mol Cell Biol* **21**, 421-438 (2020). https://doi.org:10.1038/s41580-020-0250-z

Addendum

English summary,
Nederlandse samenvatting,
Deutsche Zusammenfassung,
Curriculum Vitae,
List of publications,
Acknowledgments

English summary

Prostate cancer is the second most common cancer in men and a frequent cause of cancer-related death. In general, prostate cancer is considered hormone-dependent, as the development and progression of the tumor is highly dependent on the action of male sex hormones, called androgens. These hormones are able to activate their direct downstream receptor, the androgen receptor (AR), a master transcription factor that regulates the expression of numerous genes involved in various biological pathways, ultimately leading to the growth and survival of prostate cancer cells. Given the importance of this signaling axis, multiple therapeutic strategies have been developed over the years to effectively block the activity of this hormone-driven regulatory pathway. Despite these recent advances, hormone therapy inevitably results in treatment resistance, and available therapeutic options – particularly in late-stage disease – remain very limited, making the identification of novel drug targets in the treatment-resistant setting a serious unmet medical need.

The studies presented in this thesis therefore focus on improving our current understanding of hormonal signaling in prostate cancer and on gaining new insights into the cellular adaptation mechanisms leading to acquired hormone therapy resistance. In particular, so-called "multi-omics" approaches were used, which allow for gaining precise insights into the interrelationships between different signaling pathways in prostate cancer cells by collective analyses of several macromolecules (DNA, RNA, proteins).

The biological relevance of AR signaling in prostate cancer is described in detail in the general introduction (**Chapter 1**), which also highlights how multi-omics profiling of transcription factors can help further characterize and decipher the gene regulatory circuits they control and how they rewire during therapeutic interventions.

All currently available prostate cancer therapies are reviewed in **Chapter 2**, with a clear focus on the clinical history of enzalutamide – the most frequently used hormone therapy that directly targets the AR. Despite the variety of treatment options, these therapies prolong the survival of prostate cancer patients for only a few months. Therefore, current research efforts are focused on determining the optimal sequence of therapies; discovering new drugs that are effective in metastatic castration-resistant prostate cancer; and defining patient subpopulations that will ultimately benefit from these treatments. Molecular *in vitro* studies using prostate cancer cell line models have identified several signaling pathways that have the potential to mediate treatment resistance, but what happens in a patient during hormone therapy *in vivo* remains unknown.

Thus, in **Chapter 3**, we examined how prostate tumor cells adapt to evade AR suppression to identify novel drug targets that could improve the clinical management of patients with treatment-resistant disease. We performed integrative multi-omics analyses on tissues isolated before and after 3 months of AR-targeting enzalutamide monotherapy from patients with high-risk prostate cancer enrolled in a neoadjuvant clinical trial. Transcriptomic analyses demonstrated that AR inhibition drove practically all tumors toward a neuroendocrine-like disease state. Additionally, epigenomic charting revealed massive enzalutamide-induced reprogramming of pioneer factor FOXA1 from inactive chromatin sites toward active *cis*-regulatory elements that dictate pro-survival signals. Notably, these treatment-induced FOXA1 sites were enriched for the circadian clock component ARNTL, whose expression was elevated upon hormone therapy in our patient cohort. In addition, high posttreatment ARNTL levels were associated with poor clinical outcomes, and ARNTL knockout could restore enzalutamide sensitivity in treatment-resistant cell line and xenograft models. These data highlight a remarkable cistromic plasticity of FOXA1 following AR-targeted therapy and revealed an unexpected biological interplay between hormonal resistance and circadian rhythm regulator ARNTL, a novel candidate therapeutic target.

While the identification of factors driving hormone resistance in high-risk disease has rightly received considerable research attention, low-risk tumors remain understudied and even the role of AR in low-grade lesions is poorly understood. Nevertheless, there has long been debate among experts as to whether low-grade lesions are actually cancerous or rather benign, given their overall low risk of metastasis. In **Chapter 4**, we therefore set out to characterize the AR chromatin binding landscape in a specific subset of low-risk grade group 1 (GG1) prostate cancers. Our analyses showed that GG1 tumors don't harbor a distinct AR cistrome and, similar to higher-grade lesions, AR preferentially binds to tumor-defining *cis*-regulatory elements. Furthermore, the enhancer activity of these regions and the expression of their respective target genes were not significantly different in GG1 tumors, which – from an epigenetic perspective – supports the cancer designation currently given to these low-grade tumors and clearly distinguishes them from noncancerous benign tissue.

Since AR's activity in tumors is massively altered as compared to healthy prostate epithelium, AR consequently depends on additional cofactors and pathways that ultimately enable prostate cancer growth and survival. We mechanistically characterized one of these dependencies in **Chapter 5**, where we report an unexpected interplay between the AR signaling pathway and the unfolded protein response (UPR) in prostate cancer. AR binds to thousands of sites throughout the human genome to regulate expression of directly responsive genes, including pro-survival genes that enable tumor

cells to cope with increased cellular stress, such as ERN1 and XBP1 – two key players of the UPR. We could show that low expression of XBP1 was consistently associated with biochemical recurrence in five independent cohorts. Through integrative cistromic and transcriptomic analyses, we could further demonstrate that AR activation triggers UPR signaling through the ERN1/XBP1 axis leading to elevated XBP1 transcriptional activity, which not only results in expression of UPR genes but also functionally drives part of the AR transcriptional program. This signaling cascade may prime prostate cancer cells for the increased protein folding, mRNA decay, and translation associated with AR-regulated tumor cell proliferation, underscoring how the identification of AR dependencies may lead to novel therapeutic targets.

In **Chapter 6** all data are jointly discussed in the context of the current literature while highlighting some of the remaining questions and unmet medical needs. In recent years, we have made significant strides in improving our understanding of hormonal signaling in prostate cancer. Since acquired endocrine therapy resistance has unfortunately been inevitable in advanced disease to date, it is of utmost importance to better chart the activity of prostate cancer drivers to eventually identify novel therapeutic vulnerabilities. The results presented in this thesis demonstrate how the integration of multiple omics data streams can help to provide new insights into the biology of prostate cancer. In addition, it enables the identification of previously unknown prostate cancer dependencies, the therapeutic targeting of which could ultimately improve the efficacy of currently used therapies. This would bring us a big step closer to our goal of curing this deadly disease – *it's about time*!

Nederlandse samenvatting

Prostaatkanker is de tweede meest voorkomende vorm van kanker bij mannen en een frequente oorzaak van sterfte door kanker. In het algemeen wordt prostaatkanker gezien als een hormoonafhankelijke kanker, aangezien de ontwikkeling en het verloop van de tumor sterk afhankelijk zijn van de werking van mannelijke geslachtshormonen, genaamd androgenen. Deze hormonen kunnen hun directe doelreceptor, de androgeenreceptor (AR), activeren. AR is een transcriptiefactor die een sleutelrol speelt bij prostaatkanker, aangezien het de expressie regelt van talrijke genen die betrokken zijn bij diverse biologische signaalwegen, hetgeen uiteindelijk leidt tot de groei en overleving van prostaatkankercellen. Gezien het belang van deze signaleringsas zijn er in de loop der jaren verschillende therapeutische strategieën ontwikkeld om de activiteit van deze hormonaal gestuurde reguleringsroute effectief te blokkeren. Ondanks deze recente vooruitgang leidt hormoontherapie onvermijdelijk tot behandelingsresistentie en blijven de beschikbare therapeutische opties – vooral bij gevorderde ziekte – zeer beperkt. Daarom is de identificatie van nieuwe doelwitten voor de behandeling van therapieresistente prostaatkankercellen van groots belang om de overlevingskansen van prostaatkankerpatiënten te vergroten.

De in dit artikel gepresenteerde studies richten zich daarom op het verbeteren van ons huidige begrip van hormonale signalering in prostaatkankercellen en op het verkrijgen van nieuwe inzichten in de cellulaire aanpassingsmechanismen die leiden tot verworven hormoontherapieresistentie. Daarbij is vooral gebruik gemaakt van zogenaamde "multi-oom" benaderingen, die ons in staat stellen om via verscheidene analyses van verschillende macromoleculen (DNA, RNA, eiwitten) nauwkeurig inzicht te krijgen in de verbanden tussen verschillende signaalwegen in prostaatkankercellen.

De biologische relevantie van AR-signalering bij prostaatkanker wordt uitvoerig beschreven in de algemene inleiding (**hoofdstuk 1**). Daarin wordt ook belicht hoe multi-oom profilering van transcriptiefactoren kan bijdragen tot het verder ontrafelen van de genregulatiecircuits die zij controleren en tot het karakteriseren van de wijze waarop zij zich bij therapeutische interventies aanpassen.

Hoofdstuk 2 beschrijft alle momenteel beschikbare prostaatkankertherapieën, met een duidelijke nadruk op de klinische ontwikkeling van enzalutamide – de meest gebruikte hormoontherapie die AR rechtstreeks remt. Helaas verlengen deze therapieën, ondanks de verscheidenheid aan behandelingsmogelijkheden, de overleving van prostaatkankerpatiënten momenteel slechts met enkele maanden. Daarom zijn de huidige onderzoeksinspanningen gericht op het bepalen van de optimale

behandelingsvolgorde; het ontdekken van nieuwe geneesmiddelen die effectief zijn bij uitgezaaide castratieresistente prostaatkanker; en het definiëren van patiënten subpopulaties die uiteindelijk het meeste baat bij deze behandelingen kunnen hebben. Moleculaire *in vitro* studies met prostaatkanker cellijn modellen hebben verscheidene signaalwegen geïdentificeerd die mogelijk zorgen voor therapie-resistentie, maar wat er in patiënten (*in vivo*) gebeurt tijdens hormoontherapie blijft onbekend.

Daarom hebben wij in **hoofdstuk 3** onderzocht hoe prostaattumorcellen zich aanpassen om AR-inhibitie te omzeilen, om nieuwe doelwitten voor geneesmiddelen te identificeren die de klinische behandeling van patiënten met een behandelingsresistente ziekte zouden kunnen verbeteren. Wij voerden integratieve multi-oom analyses uit op weefsels geïsoleerd voor en na drie maanden AR-gerichte enzalutamide monotherapie van patiënten met hoog-risico prostaatkanker die onderdeel waren van een neoadjuvante klinische studie. Transcriptomische analyses toonden aan dat AR-remming in vrijwel alle tumoren resulteerde in een neuroendocrien-achtige ziektetoestand. Verder bleek uit epigenomische kartering dat enzalutamide voor een massale herprogrammering van de pioniersfactor FOXA1 zorgde, van inactieve plaatsen in het chromatine naar actieve *cis*-regulerende elementen die pro-overlevingssignalen kunnen dicteren. Opmerkelijk is dat deze door behandeling veroorzaakte FOXA1-plaatsen verrijkt waren voor ARNTL, een belangrijke component van het circadiaanse ritme (slaap-waak ritme), waarvan de expressie onder hormoontherapie in ons patiënten cohort verhoogd was. Bovendien correleerden hoge ARNTL-niveaus met een verhoogd risico op een recidief na hormoontherapie, en het genetische stilleggen van het *ARNTL*-gen kon de gevoeligheid voor enzalutamide herstellen in behandelingsresistente cellijn- en xenograft-modellen. Deze gegevens wijzen op een opmerkelijke genomische plasticiteit van FOXA1 na AR-gerichte behandeling en onthullen verder een onverwacht biologisch verband tussen resistentie tegen hormonale therapie en de circadiaanse ritmecomponent ARNTL, die een nieuw therapeutisch doelwit vormt bij prostaatkanker.

Terwijl de identificatie van factoren die leiden tot resistentie tegen behandeling bij hoog-risico prostaatkanker terecht veel onderzoek aandacht heeft gekregen, blijven laag-risico tumoren slecht begrepen, en zelfs de rol van AR is slecht ontrafeld in laaggradige laesies. Desalniettemin bestaat er onder deskundigen al geruime tijd discussie over de vraag of laaggradige laesies daadwerkelijk kankerachtig zijn of eerder goedaardig, aangezien hun totale risico op metastase zeer laag is. In **hoofdstuk 4** hebben wij daarom het AR chromatine-bindende landschap gekarakteriseerd in een specifieke subset van zeer laag-risico graad 1 (GG1) prostaatkankers. Onze analyses toonden aan dat AR bij voorkeur bindt aan tumor specifieke *cis*-regulerende elementen, zowel in GG1 tumoren als in laesies van hogere graad. Bovendien verschilde de activiteit van

deze regulerende DNA-sequenties en de expressie van hun respectieve doelgenen niet significant in GG1-tumoren, hetgeen – vanuit epigenetisch oogpunt – de huidige aanduiding van deze laaggradige laesies als kanker ondersteunt en ze duidelijk onderscheidt van gezond of zelfs goedaardig weefsel.

Aangezien de AR-activiteit in tumoren sterk veranderd is in vergelijking met gezond prostaatepitheel, is AR daarom afhankelijk van bijkomende cofactoren en signaalwegen die uiteindelijk de groei en overleving van prostaatkanker mogelijk maken. Een van deze afhankelijkheden hebben we mechanistisch gekarakteriseerd in **hoofdstuk 5**, waarin we een onverwachte wisselwerking melden tussen de hormoonafhankelijke AR-signaleringsroute en de *unfolded protein response* (UPR) in prostaatkankercellen. AR bindt aan duizenden plaatsen in het menselijk genoom om de expressie van doelgenen te reguleren. Daartoe behoren pro-overlevingsgenen die tumorcellen in staat stellen weerstand te bieden aan verhoogde cellulaire stress, zoals *ERN1* en *XBP1* – twee belangrijke spelers in de UPR. Wij hebben nu aangetoond dat een lage expressie van XBP1 geassocieerd was met een verhoogd risico op een biochemisch recidief in vijf onafhankelijke cohorten van prostaatkanker. Door integratieve multi-oom analyses hebben we ook aangetoond dat AR activatie UPR-signalering in gang zet via de ERN1/XBP1 as, wat leidt tot verhoogde XBP1 transcriptionele activiteit die niet alleen UPR-genexpressie bevordert maar ook functioneel een deel van het AR transcriptie programma aanstuurt. Deze signaalcascade kan prostaatkankercellen voorbereiden op de toegenomen eiwitvouwing, mRNA-verval en translatie die gepaard gaan met AR-gereguleerde tumorcelproliferatie, en laat zien hoe de identificatie van AR-afhankelijkheid kan leiden tot nieuwe therapeutische doelen.

In **hoofdstuk 6** worden alle in dit proefschrift gepresenteerde gegevens besproken en in de context van de huidige literatuur geplaatst. De laatste jaren is er aanzienlijke vooruitgang geboekt bij het verbeteren van het inzicht in de hormonale signalering bij prostaatkanker. Aangezien verworven resistentie tegen endocriene therapie helaas onvermijdelijk is bij gevorderde ziekte, is het van groots belang de activiteit van prostaatkanker drivers beter te begrijpen om uiteindelijk nieuwe therapeutische kwetsbaarheden te identificeren. De in dit artikel gepresenteerde resultaten laten zien hoe de integratie van diverse multi-oom gegevensstromen kan helpen om nieuwe inzichten te verkrijgen in de biologie van prostaatkanker. Bovendien hebben zij de identificatie mogelijk gemaakt van voorheen onbekende afhankelijkheden van prostaatkankercellen, die de doeltreffendheid van de nu gebruikte behandelingen sterk zouden kunnen verbeteren door middel van gerichte therapeutische benaderingen. Dit zou ons een zeer grote stap dichter brengen bij ons doel om deze dodelijke ziekte te kunnen genezen – het wordt tijd (*it's about time)*!

Deutsche Zusammenfassung

Prostatakrebs ist die zweithäufigste Krebserkrankung bei Männern und eine häufige Ursache für krebsbedingte Todesfälle. Im Allgemeinen gilt Prostatakrebs als hormonabhängig, da die Entwicklung und das Fortschreiten des Tumors in hohem Maße von der Wirkung männlicher Sexualhormone, der so genannten Androgene, abhängig ist. Diese Hormone sind in der Lage ihren Zielrezeptor, den Androgenrezeptor (AR), zu aktivieren. AR ist ein Transkriptionsfaktor, der eine Schlüsselrolle in Prostatakarzinomen einnimmt, da dieser die Expression zahlreicher Gene reguliert, die an verschiedenen biologischen Signalwegen beteiligt sind, was letztlich zum Wachstum und Überleben von Prostatakrebszellen führt. In Anbetracht der Bedeutung dieser Signalkaskade wurden im Laufe der Jahre diverse therapeutische Strategien entwickelt, um die Aktivität dieses hormonell gesteuerten Signalweges wirksam zu blockieren. Trotz dieser jüngsten Fortschritte führt die Hormontherapie unweigerlich zu einer Behandlungsresistenz, und die verfügbaren therapeutischen Optionen – insbesondere im fortgeschrittenen Stadium der Erkrankung – sind nach wie vor sehr begrenzt. Daher ist die Identifizierung neuer Zielmoleküle für die Behandlung therapieresistenter Prostatakrebszellen von größter Bedeutung, um die Überlebenschancen von Prostatakrebspatienten zu erhöhen.

Die in dieser Arbeit vorgestellten Studien konzentrieren sich daher auf die Verbesserung unseres derzeitigen Verständnisses der hormonellen Signalübertragung in Prostatakrebszellen und auf die Gewinnung neuer Erkenntnisse über die zellulären Anpassungsmechanismen, die zu einer erworbenen Hormontherapieresistenz führen. Im Zuge dessen wurden insbesondere sogenannte „Multi-Om" Ansätze verwendet, die es erlauben durch kollektive und integrative Analysen mehrerer Makromoleküle (DNA, RNA, Proteine) einen präzisen Einblick in die Zusammenhänge zwischen verschiedenen Signalwegen in Prostatakrebszellen zu gewinnen.

Die biologische Relevanz der AR-Signalübertragung in Prostatakrebs wird in der allgemeinen Einleitung (**Kapitel 1**) ausführlich beschrieben. Darin wird auch hervorgehoben, wie die Erstellung von Multi-Om-Profilen von Transkriptionsfaktoren dazu beitragen kann, die von ihnen kontrollierten Genregulationskreisläufe weiter zu entschlüsseln und zu charakterisieren, wie sie sich bei therapeutischen Eingriffen neu verschalten.

In **Kapitel 2** werden alle derzeit verfügbaren Prostatakrebstherapien beschrieben, wobei der Schwerpunkt auf der klinischen Entwicklung von Enzalutamid liegt – der am häufigsten verwendeten Hormontherapie, die AR direkt hemmt. Trotz der Vielfalt an Behandlungsmöglichkeiten verlängern diese Therapien das Überleben von Prostatakrebspatienten derzeit leider nur um wenige Monate. Daher konzentrieren

sich die aktuellen Forschungsanstrengungen auf die Bestimmung der optimalen Therapiesequenz; die Entdeckung neuer Medikamente, die bei metastasiertem kastrationsresistentem Prostatakrebs wirksam sind; und die Definition von Patientensubpopulationen, die letztendlich am meisten von diesen Behandlungen profitieren könnten. Molekulare „*in vitro*"-Studien unter Verwendung von Prostatakrebs-Zelllinienmodellen haben mehrere Signalwege identifiziert, die das Potenzial haben eine Therapieresistenz zu vermitteln, aber was in Patienten (*in vivo*) während einer Hormontherapie passiert, ist nach wie vor unbekannt.

Daher untersuchten wir in **Kapitel 3**, wie sich Prostatatumorzellen anpassen, um die AR-Hemmung zu umgehen, um neuartige Arzneimittelziele zu identifizieren, die die klinische Behandlung von Patienten mit behandlungsresistenter Erkrankung verbessern könnten. Wir führten integrative Multi-Om-Analysen an Geweben durch, die vor und nach einer dreimonatigen Enzalutamid-Monotherapie von Patienten mit Hochrisiko-Prostatakrebs isoliert wurden, welche an einer neoadjuvanten klinischen Studie teilnahmen. Transkriptomische Analysen zeigten, dass die AR-Hemmung bei praktisch allen Tumoren zu einem neuroendokrin-ähnlichen Krankheitszustand führte. Darüber hinaus zeigte die epigenomische Charakterisierung eine massive Enzalutamid-induzierte Umprogrammierung des Pionierfaktors FOXA1 von inaktiven Chromatinstellen zu aktiven *cis*-regulatorischen Elementen, die überlebensfördernde Signale diktieren können. Bemerkenswert ist, dass diese behandlungsinduzierten FOXA1-DNA Regionen eine hohe Bindungsaffinität für den Transkriptionsfaktor ARNTL, eine Hauptkomponente des zirkadianen Schlaf-Wach-Rhythmus, aufwiesen. Die ARNTL Genexpression wurde durch Enzalutamid Hormontherapie in unserer Patientenkohorte deutlich erhöht und darüber hinaus korrelierten hohe ARNTL-Level nach der Behandlung mit einem erhöhten Risiko eines Rezidivs. Dies lässt auf eine potenzielle Rolle dieses Transkriptionsfaktors bei der Entstehung einer Hormontherapieresistenz schließen, welche wir anschließend experimentell getestet haben. In diesen Experimenten führte die genetische Ausschaltung des *ARNTL*-Gens zur Wiederherstellung der Empfindlichkeit gegenüber Enzalutamid in behandlungsresistenten Zelllinien und Xenotransplantat-Mausmodellen. Diese Daten unterstreichen eine bemerkenswerte genomische Plastizität von FOXA1 nach einer AR-hemmenden Behandlung und enthüllen des Weiteren einen unerwarteten biologischen Zusammenhang zwischen hormoneller Therapieresistenz und der zirkadianen Rhythmuskomponente ARNTL, die einen neuen therapeutischen Angriffspunkt in Prostatakrebs darstellt.

Während die Identifizierung von Faktoren, die zu Therapieresistenzen bei Hochrisiko-Prostatakrebs führen, zu Recht große Aufmerksamkeit in der Forschung erhalten hat, sind Tumore mit niedrigem Risiko nach wie vor unzureichend erforscht, und selbst

die Rolle des AR ist bei niedriggradigen Läsionen nur unzureichend entschlüsselt. Dennoch wird in Fachkreisen seit langem darüber diskutiert, ob niedriggradige Läsionen tatsächlich krebsartig oder eher gutartig sind, da ihr Metastasierungsrisiko insgesamt sehr gering ist. In **Kapitel 4** haben wir uns daher vorgenommen, die AR-Chromatin-Bindungslandschaft in einer spezifischen Untergruppe von Prostatakrebsen mit sehr geringem Risiko der Gradgruppe 1 (GG1) zu charakterisieren. Unsere Analysen zeigten, dass AR genomweit in GG1-Tumoren, sowie in höhergradigen Läsionen, bevorzugt an tumorspezifische *cis*-regulierende Elemente bindet. Darüber hinaus unterschieden sich die Aktivität dieser regulatorischen DNA-Sequenzen und die Expression ihrer jeweiligen Zielgene in GG1 Tumoren nicht signifikant, was – aus epigenetischer Sicht – die derzeitige Bezeichnung dieser niedriggradigen Läsionen als Krebs unterstützt und sie eindeutig von gesundem oder auch gutartigem Gewebe unterscheidet.

Da die Aktivität von AR in Tumoren im Vergleich zum gesunden Prostataepithel massiv verändert ist, ist AR demzufolge von zusätzlichen Kofaktoren und Signalwegen abhängig, die letztlich das Wachstum und Überleben von Prostatakrebs ermöglichen. Eine dieser Abhängigkeiten haben wir in **Kapitel 5** mechanistisch charakterisiert, in welchem wir von einem unerwarteten Zusammenspiel zwischen dem hormonabhängigen AR-Signalweg und der Signalkaskade, die durch fehlgefaltete Proteine aktiviert wird (auf Englisch: *unfolded protein response*; UPR), in Prostatakrebszellen berichten. AR bindet an Tausende von Stellen im gesamten menschlichen Genom, um die Expression von Zielgenen zu regulieren. Darunter sind auch überlebensfördernde Gene, die es Tumorzellen ermöglichen, mit erhöhtem zellulärem Stress fertig zu werden, wie beispielsweise *ERN1* und *XBP1* – zwei Schlüsselakteure der UPR. Wir konnten nun zeigen, dass eine niedrige Expression von XBP1 in fünf unabhängigen Prostatakrebs-Kohorten mit einem erhöhten Risiko für ein biochemischen Rezidiv verbunden war. Durch integrative Multi-Om Analysen konnten wir außerdem zeigen, dass die AR-Aktivierung die UPR-Signalübertragung über die ERN1/XBP1-Achse auslöst, was zu einer erhöhten XBP1-Transkriptionsaktivität führt, die nicht nur die Expression von UPR-Genen fördert, sondern auch einen Teil des AR-Transkriptionsprogramms funktionell antreibt. Diese Signalkaskade könnte Prostatakrebszellen auf die erhöhte Proteinfaltung, den mRNA-Zerfall und die Translation vorbereiten, die mit der AR-regulierten Tumorzellproliferation einhergehen, und unterstreicht, wie die Identifizierung von AR-Abhängigkeiten zu neuen therapeutischen Zielen zur Verbesserung der Prostatakrebsbehandlung führen kann.

In **Kapitel 6** werden alle in dieser Thesis vorgestellten Daten erörtert und in den Kontext der aktuellen Fachliteratur gestellt, wobei auch einige der noch offenen Fragen und unerfüllten medizinischen Bedürfnisse hervorgehoben werden. In den letzten Jahren wurden erhebliche Fortschritte bei der Verbesserung des

Verständnisses der hormonellen Signalübertragung bei Prostatakrebs gemacht. Da eine erworbene endokrine Therapieresistenz bei fortgeschrittener Erkrankung bisher leider unvermeidlich war, ist es von größter Bedeutung, die Aktivität von Prostatakrebs-Treibern besser zu erfassen, um schließlich neue therapeutische Schwachstellen zu identifizieren. Die in dieser Arbeit vorgestellten Ergebnisse zeigen, wie die Integration verschiedenster Multi-Om Datenströme dazu beitragen kann, neue Erkenntnisse über die Biologie von Prostatakrebs zu gewinnen. Darüber hinaus ermöglichten sie die Identifizierung von bisher unbekannten Abhängigkeiten von Prostatakrebszellen, welche durch gezielte Therapieansätze die Wirksamkeit der derzeit eingesetzten Behandlungen stark verbessern könnten. Dies würde uns unserem Ziel, diese tödliche Krankheit heilen zu können, einen sehr großen Schritt näher bringen – es ist an der Zeit (*it's about time)*!

Curriculum Vitae

Simon Linder was born on October 28th, 1990, in Ludwigshafen am Rhein, Germany, and grew up in Neuhofen. He graduated high school from "Integrierte Gesamtschule Mutterstadt" in 2010, majoring in Biology, English, Geography, and Chemistry. In 2014, he graduated with a Bachelor of Science degree in Biomolecular Engineering at the Technical University of Darmstadt, Germany, where he worked on *in vitro* analyses of methyl-CpG binding domain protein 2 DNA binding and base flipping under the supervision of Prof. dr. M. Cristina Cardoso. He continued with the master's program Biomolecular Engineering at Darmstadt University of Technology, with majors in Molecular Cell Biology and Epigenetics, Applied Biochemistry, and Radiation Biophysics. He completed his research internship and master's thesis at the Netherlands Cancer Institute in Amsterdam, the Netherlands, where he conducted research on the exploitation of chromosomal instability for the treatment of triple-negative breast cancer in the group of Prof. dr. René H. Medema. In 2017, he obtained his Master of Science degree *cum laude* and started as a PhD student under the supervision of Prof. dr. Wilbert Zwart and Dr. Andries M. Bergman in the department of Oncogenomics at the Netherlands Cancer Institute. During his PhD studies, he investigated hormone-dependent gene regulatory circuits in prostate cancer tissue specimens and disease models using multi-omics approaches and integrative analysis strategies. The results of his research to improve and personalize prostate cancer therapies are described in this thesis.

List of publications

Linder S, Severson TM, van der Mijn JCK, Nevedomskaya E, Siefert JC, Stelloo S, Pomerantz MM, Freedman ML, van der Poel H, Jerónim C, Henrique R, Bergman AM, and Zwart W. Grade Group 1 Prostate Cancers Exhibit Tumor-defining Androgen Receptor-Driven Programs. 2023; *submitted*.

Morel KL, Hamid AA, Falcón BG, Singh JN, Linder S, Bergman AM, van der Poel H, Hofland I, Bekers EM, Trostel S, Wilkinson S, Ku AT, Burkhart DL, Kim M, Kim J, Plummer JT, You S, Sowalsky AG, Zwart W, Sweeney CJ, and Ellis L. Loss of tristetraprolin activates NF-κB induced phenotypic plasticity and primes transition to lethal prostate cancer. bioRxiv 2022.08.05.500896. doi: https://doi.org/10.1101/2022.08.05.500896

Severson TM‡, Zhu Y‡, Prekovic S‡, Schuurman K, Nguyen H, Brown L, Hakkola S, Kim Y, Kneppers J, Linder S, Stelloo S, Lieftink C, van der Heijden MS, Nykter M, van der Noort V, Sanders J, Morris B, Jenster G, van Leenders G, Pomerantz MM, Freedman ML, Beijersbergen R, Urbanucci A, Wessels LFA, Corey E, Zwart W, and Bergman AM. Enhancer profiling identifies epigenetic markers of endocrine resistance and reveals therapeutic options for metastatic castration-resistant prostate cancer patients. medRxiv 2023.02.24.23286403. https://doi.org/10.1101/2023.02.24.23286403

Linder S‡, Hoogstraat M‡, Stelloo S, Eickhoff N, Schuurman K, de Barros H, Alkemade M, Bekers EM, Severson TM, Sanders J, Huang C-CF, Morova T, Altintas UB, Hoekman L, Kim Y, Baca SC, Sjöström M, Zaalberg A, Hintzen DC, de Jong J, Kluin RJC, de Rink I, Giambartolomei C, Seo J-H, Pasaniuc B, Altelaar M, Medema RH, Feng FY, Zoubeidi A, Freedman ML, Wessels LFA, Butler LM, Lack NA, van der Poel H, Bergman AM, and Zwart W. Drug-Induced Epigenomic Plasticity Reprograms Circadian Rhythm Regulation to Drive Prostate Cancer toward Androgen Independence. Cancer Discov 2022;12(9):2074-97. https://doi.org/10.1158/2159-8290.CD-21-0576

Baca SC, Singler C, Zacharia S, Seo J-H, Morova T, Hach F, Ding Y, Schwarz T, Huang C-CF., Anderson J, Fay AP, Kalita C, Groha S, Pomerantz MM, Wang V, Linder S, Sweeney CJ, Zwart W, Lack NA, Pasaniuc B, Takeda DY, Gusev A, and Freedman ML. Genetic determinants of chromatin reveal prostate cancer risk mediated by context-dependent gene regulation. Nat Genet 2022;54(9):1364-1375. https://doi.org/10.1038/s41588-022-01168-y

Manjon AG, Linder S, Teunissen H, Friskes A, Zwart W, de Wit E, and Medema RH. Unexpected gene activation following CRISPR-Cas9-mediated genome editing. EMBO Rep 2022;23(2):e53902. https://doi.org/10.15252/embr.202153902

Long MD‡, Jacobi JJ‡, Singh PK, Llimos G, Wani SA, Rowsam AM, Rosario SR, Hoogstraat M, Linder S, Kirk J, Affronti HC, Bergman AM, Zwart W, Campbell MJ, and Smiraglia DJ. Reduced NCOR2 expression accelerates androgen deprivation therapy failure in prostate cancer. Cell Rep 2021;37(11):110109. https://doi.org/10.1016/j.celrep.2021.110109

Davies A, Nouruzi S, Ganguli D, Namekawa T, Thaper D, Linder S, Karaoğlanoğlu F, Omur ME, Kim S, Kobelev M, Kumar S, Sivak O, Bostock C, Bishop J, Hoogstraat M, Talal A, Stelloo S, van der Poel H, Bergman AM, Ahmed M, Fazli L, Huang H, Tilley W, Goodrich D, Feng FY, Gleave M, He HH, Hach F, Zwart W, Beltran H, Selth L, and Zoubeidi A. An androgen receptor switch underlies lineage infidelity in treatment-resistant prostate cancer. Nat Cell Biol 2021;23(9):1023-34. https://doi.org/10.1038/s41556-021-00743-5

Palit SAL, van Dorp J, Vis D, Lieftink C, Linder S, Beijersbergen R, Bergman AM, Zwart W, and van der Heijden MS. A kinome-centered CRISPR-Cas9 screen identifies activated BRAF to modulate enzalutamide resistance with potential therapeutic implications in BRAF-mutated prostate cancer. Sci Rep 2021;11(1):13683. https://doi.org/10.1038/s41598-021-93107-w

Huang CF‡, Lingadahalli S‡, Morova T‡, Ozturan D‡, Hu E, Yu IPL, Linder S, Hoogstraat M, Stelloo A, Sar F, van der Poel H, Altintas UB, Saffarzadeh M, Le Bihan S, McConeghy B, Gokbayrak B, Feng FY, Gleave ME, Bergman AM, Collins C, Hach F, Zwart W, Emberly E, and Lack NA. Functional mapping of androgen receptor enhancer activity. Genome Biol 2021;22(1):149. https://doi.org/10.1186/s13059-021-02339-6

Bernasocchi T‡, El Tekle G‡, Bolis M‡, Mutti A, Vallerga A, Brandt LP, Spriano F, Svinkina T, Zoma M, Ceserani V, Rinaldi A, Janouskova H, Bossi D, Cavalli M, Mosole S, Geiger R, Dong Z, Yang C-G, Albino D, Rinaldi A, Schraml P, Linder S, Carbone GM, Alimonti A, Bertoni F, Moch H, Carr SA, Zwart W, Kruithof-de Julio M, Rubin MA, Udeshi ND, and Theurillat J-PP. Dual functions of SPOP and ERG dictate androgen therapy responses in prostate cancer. Nat Commun 2021;12(1):734. https://doi.org/10.1038/s41467-020-20820-x

Stelloo S‡, Linder S‡, Nevedomskaya E, Valle-Encinas E, de Rink I, Wessels LFA, van der Poel H, Bergman AM, and Zwart W. Androgen modulation of XBP1 is functionally driving part of the AR transcriptional program. Endocr Relat Cancer 2020;27(2):67-79. https://doi.org/10.1530/ERC-19-0181

Singh AA‡, Schuurman K‡, Nevedomskaya E, Stelloo S, Linder S, Droog M, Kim Y, Sanders J, van der Poel H, Bergman AM, Wessels LFA, and Zwart W. Optimized ChIP-seq method facilitates transcription factor profiling in human tumors. Life Sci Alliance 2019;2(1):e201800115. https://doi.org/10.26508/lsa.201800115

Linder S, van der Poel HG, Bergman AM, Zwart W, and Prekovic S. Enzalutamide therapy for advanced prostate cancer: efficacy, resistance and beyond. Endocr Relat Cancer 2018;26(1):R31-R52. https://doi.org/10.1530/ERC-18-0289

Prekovic S, van den Broeck T, Linder S, van Royen ME, Houtsmuller AB, Handle F, Joniau S, Zwart W, and Claessens F. Molecular underpinnings of enzalutamide resistance. Endocr Relat Cancer 2018;25(11):R545-R57. https://doi.org/10.1530/ERC-17-0136

Maia ARR, Linder S, Song JY, Vaarting C, Boon U, Pritchard CEJ, Velds A, Huijbers IJ, van Tellingen O, Jonkers J, and Medema RH. Mps1 inhibitors synergise with low doses of taxanes in promoting tumour cell death by enhancement of errors in cell division. Br J Cancer 2018;118(12):1586-95. https://doi.org/10.1038/s41416-018-0081-2

‡ These authors contributed equally to this work as co-first authors.

Acknowledgments

I would like to thank **everyone** who has helped me in one way or another to complete this work. Over the past six years, I have met so many amazing individuals who have helped me grow, not only as a scientist, but also as a person. Thank you to those I have learned from, those who have supported me from afar, and those who have been there for me on a daily basis – you have truly made this PhD journey unforgettable.

First of all, I would like to say dankjewel to my mentors **Wilbert** and **André** for giving me the opportunity to work in their labs. Thank you for the daily supervision, scientific discussions, and for believing in me as the right person to lead the DARANA project. **Wilbert**, your enthusiasm and positive attitude are truly contagious and make working in your lab an absolute pleasure. Thank you for your guidance, for helping me develop my scientific skills, and for bringing me together with so many expert scientists from around the world. **André**, I admire your calm demeanor – it really is the perfect counterpart to Wilbert's ultra-high energy level. Your oncology expertise and medical input really helped me become a better translational scientist, which is exactly what I wanted to accomplish during my PhD studies. Thank you so much for helping me achieve this goal. Thanks to both of you and the amazing group of people you have hired over the years, I have enjoyed every single day at the NKI, and I will be forever grateful for your endless support.

I would also like to thank my PhD committee – **Charlotte Bevan**, **Stefan Fröhling**, **Jop Kind**, **Henk Verheul**, and **Luc Brunsveld** – for their feedback and time invested in the evaluation of this thesis. I'm also very grateful to my PhD committee at the NKI – **Thijn Brummelkamp**, **Reuven Agami**, and **Henk van der Poel** – for their helpful comments and suggestions on my PhD projects over the years. **Henk**, there is not a single article in this thesis in which you were not involved. Thank you so much for all your critical and constructive feedback, and for the constant supply with tissue samples which were absolutely instrumental for my research.

My dear paranymphs **Isa** and **Anniek**. Thank you so much for accepting my little paranymph proposal and for standing by my side – not only on the day of the defense, but also during my entire PhD period. I can't imagine how my PhD would have gone without you two. There would definitely have been a lot less laughter in the lab, less guilty pleasures on the lab playlist, less GIFs/stickers shared in various WhatsApp groups, less empty bottles in the seminar room, (even) less Friday night memories, less epic road trips across the US, and most importantly, less moments I got to share with two amazing people. **Isa**, my office partner from day one. You have the most infectious

&

laugh of anyone I know, and I'm really going to miss hearing it every day. I will even miss the noises you make when you are clumsy, when you trip while trying to casually walk down the hall, which only endears you more, or when you run and scream because of a wasp while eating lunch. Having been on this PhD journey together and watching you grow each day into the strong and independent person you are today makes me super happy and very proud! **Anniek**, my sports partner in crime. I will definitely miss our Wednesday morning padel sessions (especially the VV speciaal), your enthusiasm when you showed us a new, really dumb but incredibly funny reel you found, my near-death experiences when I tried to run with you (and failed miserably), your raccoon-like appearance when you came back from skiing, your funny sneezes (which I hardly ever saw but often heard from the other office), and most of all, your caring, selfless, and genuinely endearing personality. I love how hard it is for you to say no (especially to social events), and I'm really looking forward to seeing "your" shot and beer glass collection in all its beauty one day. Muchas gracias and dankjewel again for everything the two of you have done for me (and everyone else in the lab), and I'm super grateful for our friendships and excited about what is to come for the three of us in the future. Mucho liefde!

I thank all past and present members of the **Agami**, **Jacobs**, and **Faller** groups in the Oncogenomics division for their feedback and suggestions during department meetings, and our office managers **Lisa D** and **Elise M** for helping me with all the bureaucratic hurdles – you all make H5 such a fun place to do science.

Over the past six years, I have learned that being a PhD is much more than just pipetting and splitting ridiculous amounts of cells, especially when you are surrounded by amazing colleagues. Therefore, I would like to thank all current and past members of the Zwart and Bergman labs. **Emma**, although you didn't join the team too long ago, I couldn't imagine the lab without you anymore. Dankjewel for teaching me the strangest sayings in Dutch (that even a Dutchy would never say), for the fun nights out, for the various lifts back home to Leiden, for sharing my love for bouldering and padel, and for being the kindest and sweetest soul – I will dearly miss you. **Nils**, my German buddy and "little" Padawan. Danke vielmals for all your help in the lab, for sharing your love for various sports with me, for playing German hip-hop in cell culture, for being at least as competitive as me in sports, and for being a super nice and supportive person. I hope we will play (and win) many more padel tournaments in the future. **Emira**, I greatly admire your creativity and kindness, and I will definitely miss our bouldering sessions. I'm super happy that you joined our lab and I think it's mega that you will defend your PhD in the very same week – I'm sure you will be absolutely great (as always). **Seb**ab, grazie mille for

always answering my (sometimes rather dumb) bioinformatics questions, for all the fun moments at various conferences (and, of course, for sharing the honeymoon suite), for showing me that you can drink beer at the speed of light, for spicing up every single foosball match ("expect the unexpected"), and for being such a nice human being. **Nuno**, obrigado for inviting us for lekker Francesinha, for showing us (and the fridges) the sexiest dance moves of all time, for always being yourself, and for your ability to make everyone around you smile and laugh. And again, sorry for stalking you and Steven in Leiden back then. **Jeroen**, congratulations again on your PhD and dankjewel for a great and fun time in the office and at the various PhD conferences. Good luck with your new job – I'm very happy for you. **Stefan**, Хвала for all your feedback and suggestions on my PhD projects, for the unforgettable time in the US, and for bringing some sarcastic humor to the office (which I love). Good luck with starting your own lab in Utrecht – I'm sure you'll excel. **Karianne**, dankjewel for all your help in the lab, for teaching me how to ChIP, for keeping the lab running, and for the constant supply of drops, nuts and fried seaweed (= mega lekker!). **Tesa**, thank you so much for all your bioinformatics support over the years and for keeping some of my previous projects going – it's wonderful to know they are in very good hands. **Kim**, it was a lot of fun to "cast" you. Dankjewel for the great time in the office and good luck with all your exciting PhD projects. **Suzanne**, dankjewel for all your support in the lab and for being such a kind and caring person. **Koen vdM**, dankjewel for all your innovative project ideas and for your feedback and suggestions. **Yanis**, although we only shared a month in the lab, I want to say merci for changing your mind and not hating me after all. You are a clever and super nice person and I wish you all the best in your postdoc. **Chayenne**, **Merel** and **Zhanna**, I wish you good luck in your PhDs and I am sure you guys will be very successful. I would also like to thank all the former members of the Zwart/Bergman labs that I worked with: **Alex**, **Maria**, **Yanyun**, **Stacey**, **Bianca**, **Rebecca**, and **Koen F**. A big thank you to **Yongsoo**, **Joe**, and **Abhishek** for all your bioinformatics support and for teaching me how to run my own analyses. Finally, I would like to thank **Marlous** and **Suz**; it was a great pleasure sharing projects and working with you – I really learned a lot, for which I will be forever grateful.

Big thank you to all the people I have collaborated with over the years. **Elise B**, dankjewel for all your help and support in various projects – your uropathology expertise was extremely helpful. **Hilda**, dankjewel for helping us with the clinical data of all our cohorts. I really appreciate your support and I wish you all the best for the last steps in your PhD studies. **Sanne L**, **Cat** and **Danielle**, it was a lot of fun to work and collaborate with you. I wish you the best of luck as you complete your exciting projects (I'm sure each of them will be very well received) and PhDs.

When I joined the NKI for my master's internship, I got to know an amazing bunch of people (= NKI mafia <3) from all around Europe, and I was lucky enough that most of them stayed in the Netherlands as well. I'm super thankful for all these friendships and look forward to sharing many more unforgettable memories with you all. **Ale**, ciao ragazza! Grazie mille for all the mega lekker (Italian) food, and for always being your amazing self – you're an incredibly nice and caring person. **Louise**, I love your competitive nature with board games, and there is no one I would rather be a saboteur with than you. Dankjewel for all the fun evenings and days we spent together, and for being such a sweet soul. I'm really going to miss living in the same city with you two, but I'm sure many more fun evenings/trips await us. **Anna GM**, I totally admire your confidence and willpower, and I would like to say muchas gracias for being such a nice and big-hearted human being. **Jeremy**, mon amour. Merci beaucoup for being such an easy-going, spontaneous and super kind person, and for teaching me how to belay and climb lead. **Antonio**, muchas gracias for your constant positivity and the biggest smile in the world. Training camp in HD was one of the most fun weeks in my PhD and there is no one I would rather have spent it with. To many more padel sessions, chupitos, fun nights out and parties before parties – I'll miss you! **Mathias** (aka Matatitis), du alter Schlawiner. I don't think I know anyone who is more fun than you. Danke for all the reels you shared with me that either made me laugh out (very) loud or even brought me to tears. You know where to find Holy Günter – go get him. **Alberto** (cip***!) and **Clara**, you're both such kind and sweet individuals – a match made in heaven. Muchas gracias for letting me be part of your wedding – this whole weekend in Madrid was just amazing and something to remember forever. **Živa**, hvala for being such a good friend, and for trusting me with booking a random trip for you and Anna. You have a really big heart and even your grumpy face is pretty adorable – will definitely miss seeing it! **Eric**, **Mariana**, **Roel**, **Ruben**, **Lisa K**, **Soufiane**, **Xabi**, **Miriam**, **Mar**, **Ronak**, **João**, **Marjon**, **Julia Y**, **Angela**, **Celia**, thank you all for being part of my PhD journey and for all the fun moments that I'll never forget.

Also a big thank you to **Mercedes**, **Iris**, **Zowi**, **Felipe**, **Rebeca, Ana**, **Alberto GJ**, **Davinia**, **Dorine**, **Jonne**, **Mila**, **Anoek**, **Michael**, **Apostolos**, **Claire**, **Judith**, **Joana**, **Ferro**, **Sofia**, **Rob**, **Anna D**, **Inés**, **Matheus**, **Sander P**, and everyone else I met during my time at the NKI for making lab-life, borrels, PhD retreats and conferences so much fun. Special thanks to **Tim**(my boy) – groβes Dankeschön for all the fun bouldering sessions, the perfect excuse not to go home too early on Friday's (@**Ezgi**: I'm very sorry), the fun nights out, the "memorable" train rides back to Leiden, and for literally always being in a good mood. **Henri**, dankjewel for all you have done over the years to make the NKI such a fun place to work and do science, but don't forget to take a day or two off now and then.

Thank you also to everyone I met while living in Leiden. **Sanne R**, **Jorren**, **Julia M**, **Mikhail**, **Tassilo**, **Wieke**, **Sam**, **Miles** (aka Milo), **Nienke**, and **Joost**, thank you guys for all the fun nights out, the nice trips within the Netherlands or through Europe. Special thanks also to the whole wildflower climbing crew – **Tiba**, **Jørg**, **Matthijs**, **Paul**, **Noa**, **Marloes**, **Eddie**, **Dirk**, **Charlotte** and **Lizzie** – I will definitely miss our boulder training and moonboard seshs, and especially all the good vibes and psych in the gym.

Danke auch an meine Zweitfamilie (aka La Familia) in good old Deutschland. Egal ob Boulder- oder Klettersessions, epische Spikeballduelle, Wandertouren (samt Schorlegewitter), Novemberfest, Putenfest, Geburtstagsfeten oder Skiurlaube – mit euch ist man immer in allerbester Gesellschaft und ich freue mich schon darauf ab Sommer bei noch mehr Festivitäten am Start sein zu können. Danke **Tschani**, **Alica**, **David B**, **Paul vR**, **Julia**, **Nadja**, **Philip**, **Sari**, **Carsten**, **Yannic**, **Axi**, **Markusen**, **Nadine**, **Marius**, **Zabrina**, **Sebi**, **Wiebke**, **Paul S**, **Annika**, **Carla**, **Baptiste**, **Svenja A**, **Marcel**, **Svenja P**, **Dancel**, **Teddy**, **David K**, **Martina**, **Flo**, **Tamara**, **Isi** – ihr seid mega!

Danke **Michi** und **Maike** für die zahlreichen Surf, Boulder 'n Chill Urlaube – mit euch ist's einfach immer mega spaβig und ich freu mich schon jetzt auf unsere nächsten Trips. **Andi**, **Simon**, **Lena**, **Jana** – ohne euch wären Heimatbesuche definitiv nicht dasselbe gewesen. Danke für all die schnieken Abende und ich freu mich euch bald wieder viel öfter zu Gesicht zu bekommen.

Zu guter Letzt möchte ich mich bei meiner Familie bedanken – **Mama**, **Papa**, **Margot**, **Mira**, **Michi**, **Matilda**, **Luca**, **Oma Hilde**, **Opa Adolf**, **Markus**, **Leslie**, **Nick**, **Liz**. Danke für eure unendliche Unterstützung und dass ihr immer für mich da seid – ohne euch hätte ich es niemals so weit geschafft und dafür bin ich euch ewig dankbar. Gleiches gilt für die gesamt **Familie Kissel** – danke, dass ihr mich mit offenen Armen in eurer Familie aufgenommen habt.

And last, but definitely not least, **Theresa**! Danke, dass du trotz anfänglich relativ geringer Begeisterung mit mir in dieses Abenteuer gestartet bist. Du bist DIE Person in meinem Leben, auf die ich mich immer verlassen kann, und ich bin dir ewig dankbar für all deine Unterstützung und für alles, was du für mich getan hast. Zu sehen wie sehr du in den letzten Jahren „gewachsen" und wie selbstbewusst du geworden bist macht mich unglaublich stolz und ich freue mich unheimlich auf alles, was für uns beide noch kommt!

&